The study of allostery in aminoglycoside *N*-6'-acetyltransferase through the use of calorimetry and spectroscopy

Lee A. Freiburger

Degree of Doctor of Philosophy
Department of Chemistry
McGill University
Montreal, Quebec, Canada
H3A 2K6

August 2011

A Thesis submitted to McGill University in partial fulfillment of the requirements for the degree of Doctor of Philosophy

Abstract

Allostery is the change in structure, dynamics and/or function in biological macromolecules upon binding to a target molecule. Since its initial proposal, allostery has been shown to be essential to cellular function. One result of allostery is the cooperative binding of identical ligands to the same macromolecule. One enzyme which has shown interesting kinetic behaviour is Aminoglycoside *N*-6'-acetyltransferase-Ii (AAC(6')-Ii), an antibiotic resistance causing enzyme chromosomally encoded in *Enterococcus faecium*. This enzyme is responsible for the low level resistance to aminoglycosides found in these bacteria. AAC(6')-Ii belongs to the GCN5-related *N*-acetyltransferase (GNAT) super family, and its known function is to acetylate most known aminoglycosides at the 6' position. It is constitutively active as a homo dimer and has previously shown cooperative behaviour between the subunits.

A technique utilized in the studying of the cooperative binding observed with AAC(6')-Ii is isothermal titration calorimetry. However, studying allosteric cooperativity can be quite challenging due to the difficulty in identifying the correct binding model. Chapter 2 of this thesis describes a protocol to address this problem through performing multiple ITC experiments at different concentrations and globally fitting the dataset to a single set of binding parameters. This technique has been labelled Variable-c ITC.

Many allosteric interactions occur through the change of structure. Chapter 3 describes an approach which combines ITC with circular dichroism spectroscopy to identify a linked folding event. In addition, we developed a novel fitting approach for a multiple temperature ITC dataset by introducing the *van 't* Hoff isochore as a restriction.

The protocol developed in Chapter 3 was then used in Chapter 4 and 5 to identify allosteric events in the binding of Acetyl coenzyme A (AcCoA) and aminoglycosides to AAC(6')-Ii, respectively. Nuclear magnetic spectroscopy (NMR) was combined with the thermodynamic data to develop a model to explain the observed cooperativity. When AAC(6')-Ii binds AcCoA one subunit folds into a bound conformation which is reminiscent to a KNF folding model. This destabilizes the interactions between the two subunits and reduces the unbound subunits stability, causing it to unfold at lower temperatures. This produces to separate opposing cooperative events which causes AcCoA to bind with positive cooperativity at lower temperatures and negative cooperativity at higher temperatures. Intriguingly, when AAC(6')-Ii binds aminoglycosides it appear that both subunits undergo a conformational change with the first binding event. This likely stabilizes the unbound subunit, causing to unfold at a higher temperature. This behaviour suggests that AAC(6')-Ii has ligand dependent allosteric processes and behaves quite differently depending on which ligand it binds.

Résumé

L’allostérie est définie par le changement de la structure, de la dynamique et/ou de la fonction des macromolécules biologiques lors de la liaison à une molécule cible. Depuis sa proposition initiale, l’allostérie a été démontré d’être une contribution essentielle pour le fonctionnement cellulaire. Un des résultats de l'allostérie est la liaison coopérative de ligands identique à la même macromolécule. Une enzyme qui a demontré des comportements cinétiques intéressants est aminoglycoside N-6'-acétyltransférase-Ii (AAC(6 ')-Ii), une enzyme qui provoque une résistance aux antibiotiques et encodé dans les chromosomes de *Enterococcus faecium*. Cette enzyme est responsable de la résistance de bas niveau aux aminoglycosides trouvés dans ces bactéries. AAC (6 ')-Ii appartient à la super-famille des GCN5 N-acétyltransférase (GNAT), et sa fonction connu est d’acétyler les aminoglycosides les mieux décrits à la position 6 '. Il est constitutivement actif sous forme d’homodimère et a déjà montré un comportement de coopération entre les sous-unités.

Une technique utilisée dans l'étude de la liaison coopérative observée par AAC(6')-Ii est la calorimétrie de titration isothermique (ITC). Cependant, l'étude de la coopérativité allostérique peut être assez difficile en raison de la difficulté d'identifier le modèle de liaison approprié. Le chapitre 2 de cette thèse décrit un protocole pour traiter ce problème par l'exécution de multiples expériences ITC à

différentes concentrations et par l’ajustement global de l'ensemble de données à un ensemble unique de paramètres de liaison. Cette technique a été nommé Variable-c ITC.

Plusieurs interactions allostériques se produisent par le changement de structure. Le chapitre 3 décrit une approche qui combine la ITC avec la spectroscopie de dichroïsme circulaire pour identifier un événement de pliage lié. De plus, nous avons développé une nouvelle approche d’ajustement pour un ensemble de données de ITC à multiples températures en introduisant le isochore de van't Hoff en tant que restriction.

Le protocole présenté dans le chapitre 3 a ensuite été utilisé dans les chapitres 4 et 5 pour identifier les événements allostériques de la liaison de la coenzyme Acetyl A (AcCoA) et des aminoglycosides à AAC (6 ')-II, respectivement. La spectroscopie par résonance magnétique nucléaire (RMN) a été combinée avec les données thermodynamiques pour développer un modèle pour expliquer la coopérativité qui est observée. Lorsque AAC (6 ')-Ii se lie à AcCoA, une sous-unité se replie dans une conformation liée qui est semblable au modèle de pliage KNF. Ceci déstabilise les interactions entre les deux sous-unités et réduit la stabilité des sous-unités non liées, les amenant à se déplier à des températures plus basses. Ceci produit la séparation d’événements coopératifs opposants qui provoque AcCoA à se lier avec une coopérativité

positive à des températures plus basses et une coopérativité négative à hautes températures. Curieusement, lorsque AAC (6 ')-Ii lie les aminoglycosides, il semblerait que les deux sous-unités subissent un changement de conformation avec le premier événement de liaison. C'est probablement ce qui stabilise la sous-unité non liée, l'amenant à se déplier à une température plus élevée. Ce comportement suggère que AAC (6 ')-Ii est allostériquement dépendant au ligand et se comporte très différemment selon le ligand auquel il se lie.

Acknowledgements

First and foremost I would like to thank my supervisors, Dr Karine Auclair and Dr Anthony Mittermaier, for their continual guidance, and support. Their continual efforts helped to shape the scientist which I am today. They took a chance on me and I can only thank them for the opportunities I have been given.

Secondly I wish to express my thanks to Professor Paul Wiseman, Professor Masad Damha, Professor Gonzalo Cosa, Professor James Gleason, Professor Amy Blum, Professor Chao-Jun Li, and many other professors throughout the department for their wonderful teaching and helpful advice.

I would also like to express my thanks to the professors I have collaborated with throughout my studies: Professor Gerry Wright at McMaster University for providing the plasmids, Professor Albert Berghuis at McGill University for providing X-ray crystal structures and NMR peak assignments, and Professor John Blanchard at Albert Einstein College of Medicine.

I thank Dr Tara Sprules with her constant help in the NMR facility. For her dedicated work to keeping the NMR spectrometers in working order, in addition to her helpful advice, problem solving and obtaining spectral assignments.

I would like to thank the support staff in the chemistry department with special recognition to Chantal Marotte.

I would like to acknowledge my lab mates Pat Farber and Teresa Milletti for their help with NMR theory and general talks we had about our projects in the lab or over a drink. I also thank my other lab mates both past and present, Aaron, Amelie, Kenward, Erick, Ang, Kayode, Eric, Amandine, Harry, Jason, JP, Feng, Xuxu, and Jin for providing an enjoyable working atmosphere.

I would like to thank my friends Paul, Kraig, Jen, Graydon, Heather, Vishya, Mitch, Kylie, Matt, Jason, Jess, Carla, Rae and many others not listed here for making my experience over the last 6 years memorable. There are too many fond memories to count, and as we travel the world I hope we can continue to meet up and create new memories.

I wish to thank all members of the McGill Figure Skating Team for providing me with the opportunity to have an outlet for my stress.

I would like to thank my family for their constant support, and patience through all my years of study.

Finally I wish to thank Eva Dias, the most important person in my life. Your constant support and encouragement helped me through the difficult times. And your presence has given me someone with which to share the good times. I look forward to the future and what surprises it has in store.

Table of Contents

List of Figures

List of Tables

Abbreviations

A	alanine
A_{280}	absorbance at 280 nm
AAC	aminoglycoside acetyltransferase
AAC(6')-Ii	aminoglycoside *N*-6'-acetyltransferase-Ii
AcCoA	acetyl coenzyme A
ANT	aminoglycoside nucleotidetransferase
APH	aminoglycoside phosphotransferase
B	bound enzyme state
B	magnetic field strength
CD	circular dichroism
CoA	coenzyme A
DF	degrees of freedom
G	Gibbs free energy
f	fraction populated
HSQC	heteronuclear single quantum coherence correlation
EDTA	ethylenediaminetetraacetic acid
ESI	enzyme-substrate-inhibitor complex
EXSY	exchange spectroscopy
F	folded enzyme state
GNAT	GCN5 related *N*-acetyltransferase
HEPES	4-(2-hydroxyethyl)-1-piperazineethanesulfonic acid
HT	Hilser-Thompson
I	peak intensity
IPTG	isopropyl-β-D-thiogalactoside
iNOS	inducible nitric oxide synthase
ITC	isothermal titration calorimetry
k	rate constant
K	equilibrium constant
KNF	Koshland-Némethy-Filmer

LB	Luria-Bertani
m	molar ellipticity temperature dependence
M	molar
M	external magnetic field
MC	monte carlo
mol	mole
mRNA	messenger ribonucleic acid
MW	molecular weight
MWC	Monod-Wyman-Changeux
NMR	nuclear magnetic resonance
OD	optical density
pI	isoelectric point
PP5	protein phosphatase 5
Q	heat function
R	gas constant
R_2	transverse relaxation rate
rf	radio frequency
RSS	residual sum of squares
T_m	melting temperature
TPR	tetratricopeptide repeat
rRNA	ribosomal ribonucleic acid
tRNA	transfer ribonucleic acid
U	unfolded enzyme state
W	tryptophase
α	cooperativity coefficient
γ	gyromagnetic ratio
μ	magnetic moment
Δδ	change of chemical shift
[Θ]	molar elliptcity
ω	chemical shift

1 Introduction

1.1 The importance of aminoglycoside *N*-6'-acetyltrasferase-Ii

Aminoglycosides are broad spectrum antibiotics which produce rapid and concentration dependent bacteriostatic and bactericidal activity.[1-2] Unfortunately, due to the appearance of resistance in the clinical environment, the utility of aminoglycosides has been drastically reduced.[3-5] One of the most common methods of resistance is through enzymatic modification of the aminoglycoside. One such enzyme is aminoglycoside *N*-6'-acetyltransferase-Ii (AAC(6')-Ii). The method of activity for (AAC(6')-Ii) is through transfer of an acetyl group from acetyl coenzyme A to a free amine at the 6' location on aminoglycosides. A description of antibiotics, their resistance, aminoglycosides, Coenzyme A, and AAC(6')-Ii is provided below.

1.1.1 Antibiotics

The understanding of infectious disease has undergone an extensive transformation in the past 150 years. In 1878 Louis Pasteur introduced Germ Theory which proposed that microorganisms are the cause of disease and began the true understanding of the field.[6] This idea was pursued and expanded upon by Joseph Lister with the development of antiseptic techniques. The work of Robert Koch's on isolating *Bacillus anthracis* conclusively demonstrated that microorganisms are the cause of many diseases.[7] This work led the way for Paul

Ehrlich and Sahachiro Hata to develop Arsphenamine in 1908, the first modern chemotherapeutic agent for bacteria.[8] The development of this compound, commonly known as salvarsan, gave the first effective treatment against syphilis, and proof that antimicrobial agents can be developed in the lab.[8-9] The subsequent discovery of penicillin in 1928[10] and streptomycin in 1943[11] provided for the first time treatment for almost all forms of bacterial infection. This started the beginning of the golden age of antibiotic discovery, which lasted until the 1970's. During this period was the discovery of the majority of antibiotics.[12-14] The discovery of these compounds also shifted the focus of antibiotic drug discovery away from the synthetic approach to screening natural products.[14] Most antibiotic classes used today were originally discovered during this time frame.

There are currently 16 classes of antibiotics approved for clinical use. Most classes have several derivatives available giving rise to over 100 different antimicrobial agents clinically available. Even with this plethora of compounds the targets for the antimicrobial effect is quite narrow. There are only five bacterial systems which are targeted: protein synthesis, cell wall synthesis, folate biosynthesis, DNA replication and transcription, and the cell membrane stability.[15]

1.1.2 Background of aminoglycosides

Aminoglycosides are one of the oldest antibiotics used clinically. Streptomycin was the first aminoglycoside to be discovered, originally isolated in 1943 by Albert Schatz under the supervision of Selman Waksman. Aminoglycosides were the first known antibiotics which could effectively treat gram-negative bacterial infections.[11] Even though they were discovered over 60 years ago aminoglycosides are still relevant and have clinical activity. They are used in the treatment of serious Gram-negative nosocomial infections, and streptomycin (the first discovered aminoglycoside) is still used in the treatment of tuberculosis, brucellosis and tularaemia.[16] Aminoglycosides are sugar molecules which contain amino groups and are very diverse. Most aminoglycosides which exhibit antibiotic activity have similar structures. They are highly cationic molecules with most consisting of a central aminocyclitol ring linked to one or more aminosugars. For most antibiotic aminoglycosides the aminocyclitol ring is deoxystreptamine, however some, for example streptomycin, have streptidine instead, shown in Fig. 1.1.

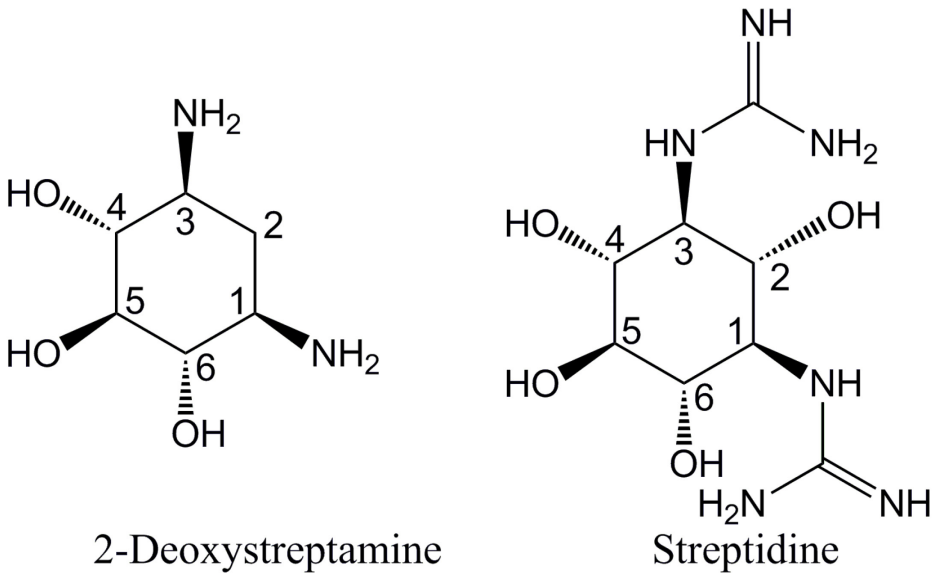

Fig. 1.1: Typical central ring of aminoglycosides

The smallest active aminoglycoside contains a single substitution at the aminocyclitol at the 4 position. However most are di-substituted at the 4,5 (neomycin class) or 4,6 position (kanamycin class) with amino-sugars.[17] The nomenclature for the position of each functional group is dependent upon the ring in which it is located. The numbering, shown in Fig. 1.2, begins on the central aminocyclitol ring I, the ring attached at the 4 position, ring II, is then labelled as "prime" and the rings at either 5 or 6 position, ring III, are labelled "double prime". If there is an additional ring, ring IV, it is labelled "triple prime".[18] There are a few examples of antibiotic aminoglycosides which have structures different from typical active aminoglycosides; these are shown in Fig. 1.3

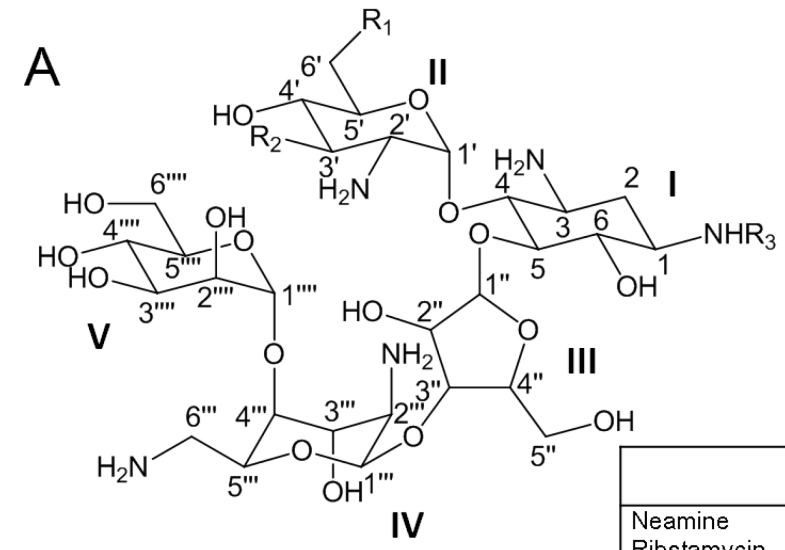

	R_1	R_2	R_3	Rings Present
Neamine	NH_2	OH	H	II
Ribstamycin	NH_2	OH	H	III
Neomycin	NH_2	OH	H	IV
Paromomycin	OH	OH	H	IV
Livdomycin	OH	H	H	V
Butirosin B	NH_2	OH	AHB	III

	R_1	R_2	R_3	R_4	R_5	R_6	R_7	R_8	R_9	R_{10}
Kanamycin A	H	NH_2	OH	OH	OH	H	H	OH	H	CH_2OH
Kanamycin B	H	NH_2	OH	OH	NH_2	H	H	OH	H	CH_2OH
Kanamycin C	H	OH	OH	OH	NH_2	H	H	OH	H	CH_2OH
Tobramycin	H	NH_2	OH	H	NH_2	H	H	OH	H	CH_2OH
Dibekacin	H	NH_2	H	H	NH_2	H	H	OH	H	CH_2OH
Amikacin	H	NH_2	OH	OH	OH	AHB	H	OH	H	CH_2OH
Isepamicin	H	NH_2	OH	OH	OH	AHB	CH_3	CH_3	OH	H
Gentamicin C_1	CH_3	$NHCH_3$	H	H	NH_2	H	CH_3	CH_3	OH	H
Gentamicin C_2	CH_3	NH_2	H	H	NH_2	H	CH_3	CH_3	OH	H
Gentamicin C_{1A}	H	NH_2	H	H	NH_2	H	CH_3	CH_3	OH	H
Genticin	CH_3	OH	OH	OH	NH_2	H	CH_3	CH_3	OH	H

Fig. 1.2: Structure of Aminoglycosides. There are two major classes A) 4,6 position kanamycin class and B) 4,5 position on the 2 deoxystamine ring neomycin class.

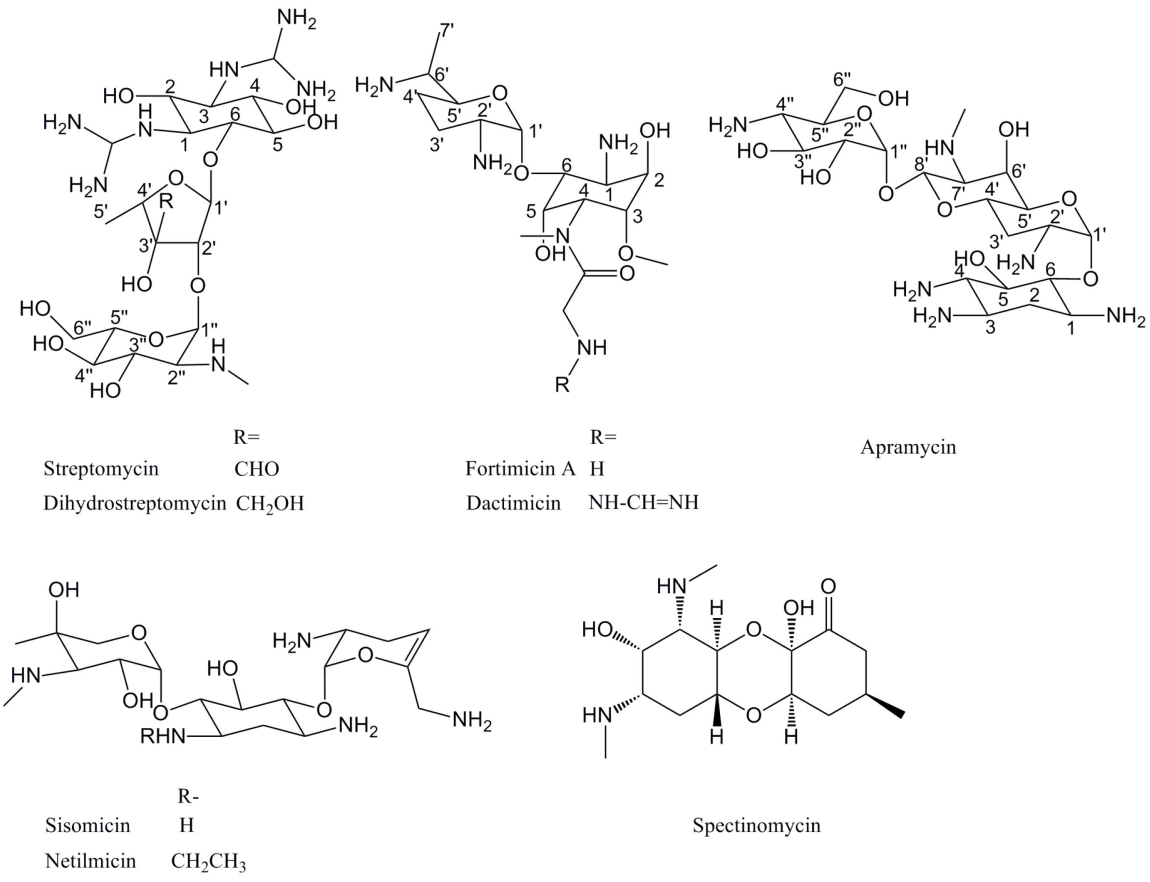

Fig. 1.3: Structure of unusual aminoglycosides

The antibacterial activity of aminoglycosides is caused by the disruption of protein synthesis leading to mistranslated proteins which disrupt the cell membrane.[4] There have been many studies performed which detail aminoglycosides' mechanism of action against bacteria.[19-29] Aminoglycosides bind to the negatively charged cell wall of the bacteria. The aminoglycoside is transported inside the cell through an oxygen dependent uptake process. Once in the cell, the aminoglycoside binds to the A site of the bacterial 30S ribosomal RNA subunit (rRNA). The A site is known as the decoding site and plays an

important role in maintaining the high fidelity of protein translation (Fig. 1.4). The correct match between the messenger RNA (mRNA) codon and tRNA anticodon is signalled through the bases A1492 and A1493. These bases are in a dynamic equilibrium between an intrahelical, 'off', state and an extrahelical, 'on' state. When no tRNA is present or an incorrect tRNA is bound to the mRNA, the conformational equilibrium for bases A1492 and A1493 favours the intrahelical 'off' state. This prevents the addition of any new amino acids to the growing polypeptide chain. When the correct tRNA binds, the mRNA adopts a conformation which favours the interactions with the bases A1492 and A1493. This alters the equilibrium of the two bases to favour an extrahelical conformation and promotes the rRNA to incorporate the amino acid from the bound tRNA to the growing polypeptide chain, shown in Fig. 1.4.[19,30] It has been shown when the aminoglycosides bind the ribosomal A site the mobility of A1492 and A1493 is decreased. This reduces the energetic barrier required for the bases to adopt an extrahelical conformation and interact with the mRNA.[31] This stabilizes the interaction in the presence of any tRNA and allows incorrect amino acids to be incorporated into the growing polypeptide chain. This causes extensive protein mistranslation.[19] These mistranslated proteins are believed to sequester in the bacterial membrane, and destabilize it.[32-33]

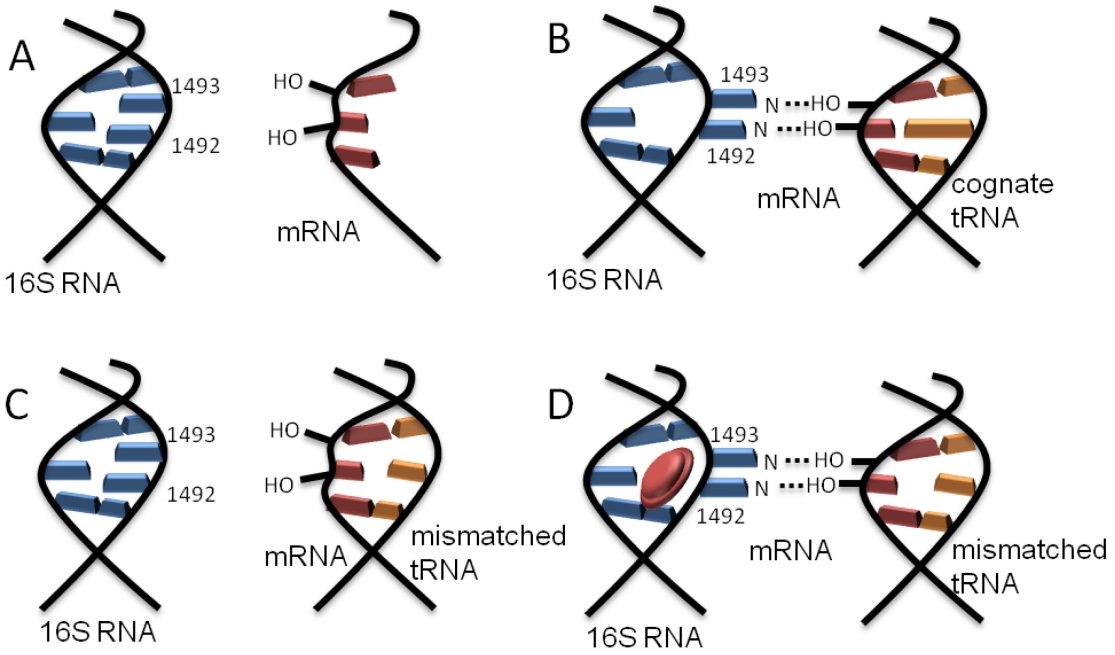

Fig. 1.4: Schematic model of the ribosome mRNA-tRNA interaction in the A site: A) When no tRNA is bound the equilibrium favours the intrahelical conformation B) when the correct tRNA binds, the mRNA adopts a conformation which promotes the interaction with bases A1492 and A1493. These two bases adopt an extrahelical conformation C) incorrect tRNA binding disrupts the mRNA conformation so bases A1492 and 1493 favour an intrahelical conformation D) in the presence of an aminoglycoside (red disk) the mobility of the bases A1492 and A1493 are reduced so the interaction with the mRNA is favoured regardless of the tRNA present.

Due to small structural differences in the rRNA, aminoglycosides have roughly 10 fold greater affinity for the prokaryotic ribosome over the eukaryote ribosome[34]. A major difference is located at position 1408, which is an A in prokaryotes and a G in eukaryotes, shown in Fig. 1.5. Additionally, position 1491 is a G in prokaryotes and an A in eukaryotes. Mutation of A1408 to G in

prokaryotes confers resistance to some aminoglycosides, which suggests position 1408 is important for specificity of aminoglycosides.[34]

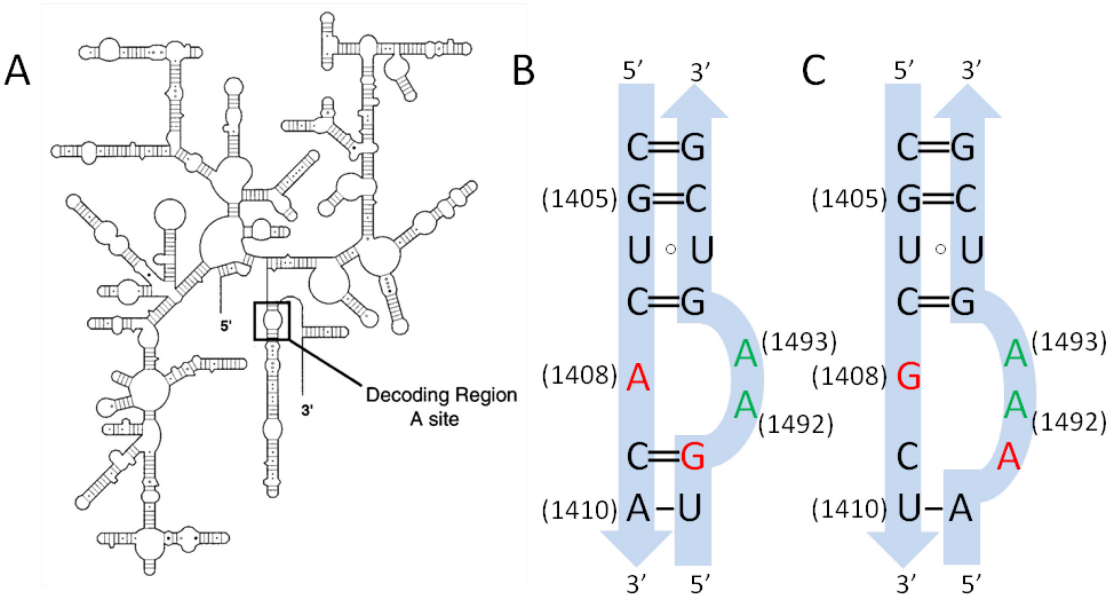

Fig. 1.5: Secondry structure of Ribosomal A-site. A) Prokaryote 16S RNA subunit. Aminoglycoside binding site located in the decoding region A site. B) A-site of prokaryotic 16S ribosomal subunit; C) A-site of eukaryotic 18S ribosomal subunit. The *Escherichia coli* (*E. coli*) numbering is used for both A-sites. The conserved adenines A1492 and A1493 are in green. Bases 1408 and 1491 which differ between prokaryotes and eukaryotes are shown in red.

1.1.3 Antibiotic resistance

With the use of antibiotics comes the spread of resistance. Alexander Flemming originally predicted the rise of resistance before it was a problem clinically.[35] Resistance was investigated as early as 1945 by Demerec,[36] and it was identified that antibiotic resistance originated genetically from the bacteria.[37] It was understood that bacteria became increasingly resistant in a stepwise

process through mutations. In the presence of antibiotics, susceptible bacteria are killed off, and those that are resistant will survive longer to propagate. This redistributes the population of the bacteria to be more resistant to the antibiotic. As the bacteria continue to reproduce, random mutation will occur and some mutations will increase the resistance to the antibiotic. If the antibiotic is still present then the newer more resistant bacteria will out-compete the less resistant bacteria and the cycle will continue, selectively pressuring the bacteria to become increasingly resistant to the antibiotic. In order to combat the growing resistance, new antibiotics were developed, and older antibiotics were modified to reintroduce potency.[14]

Through the development of more advanced techniques (i.e. cloning, transformation, protein purification, X-ray crystallography, NMR, site directed mutagenesis, and PCR) the mechanisms of antibiotic resistance have been identified. There are six resistance classes identified so far: drug modification, target modification, by-pass systems, drug efflux, intrinsic resistance and membrane impermeability[15]. There is a resistant mechanism available for every known antibiotic and for many there are multiple resistant mechanisms identified.[38]

One of the most studied resistant mechanisms in aminoglycosides is drug inactivation. Inactivation occurs through enzymatic modification of the

aminoglycoside which in turn alters the affinity of the drug for the ribosome. These enzymes attach a small chemical group to the aminoglycoside. These are the most widespread and clinically problematic forms of resistance for aminoglycosides.[39] There are three main classes of drug-modifying enzymes, based on the chemical group transferred: aminoglycoside *O*-phosphotransferase (APH), *O*-adenylyltransferase (ANT) and *N*-acetyltransferase (AAC).[40] In 1993 Shaw *et al.* developed a standardized nomenclature for these enzymes.[40] 'AAC', 'APH' or 'ANT' are use to refer to the type of modification. The location of modification on the aminoglycoside antibiotic by the modifying enzyme gives a number: (1), (3), (6), (9), (2'), (3'), (4'), (6'), (2''), and (3''). The resistant profile produced by the enzyme is referred to by a roman numeral: I,II, III, IV, IV, etc. For example AAC(6')-I and AAC(6')-II can acetylate tobramycin, netilmicin, sisomycin, dibekacin and 2'-*N*-ethylnetimicin. However, AAC(6')-I enzymes can also acetylate amikacin, gentamicin C_{1A} and gentamicin C_2, while AAC(6')-II enzymes cannot modify amikacin but can modify all gentamcin C compounds. There can be multiple isoforms of enzymes which perform identical chemical modifications to identical substrates. To differentiate among these enzymes, the specific proteins are labelled by a letter: a, b, c, d, e, etc.[40] Through using AAC(6')-Ii as an example, this system works as follows: AAC(6')-Ii is an *N*-acetyltransferase and modifies 6' position on aminoglycosides. It modifies

tobramycin, dibekacin, amikacin, 5-episisomicin, netilmicin, 2'-N-ethylnetilmicin, and sisomicin. The specific isoform of this enzyme is referred to as 'i'. There have been many reviews describing the different modifying enzymes in great detail[40-42]. A list of many of the known aminoglycoside modifying enzymes is shown on Table 1.1 and Fig. 1.6 shows the locations of modification on aminoglycosides.

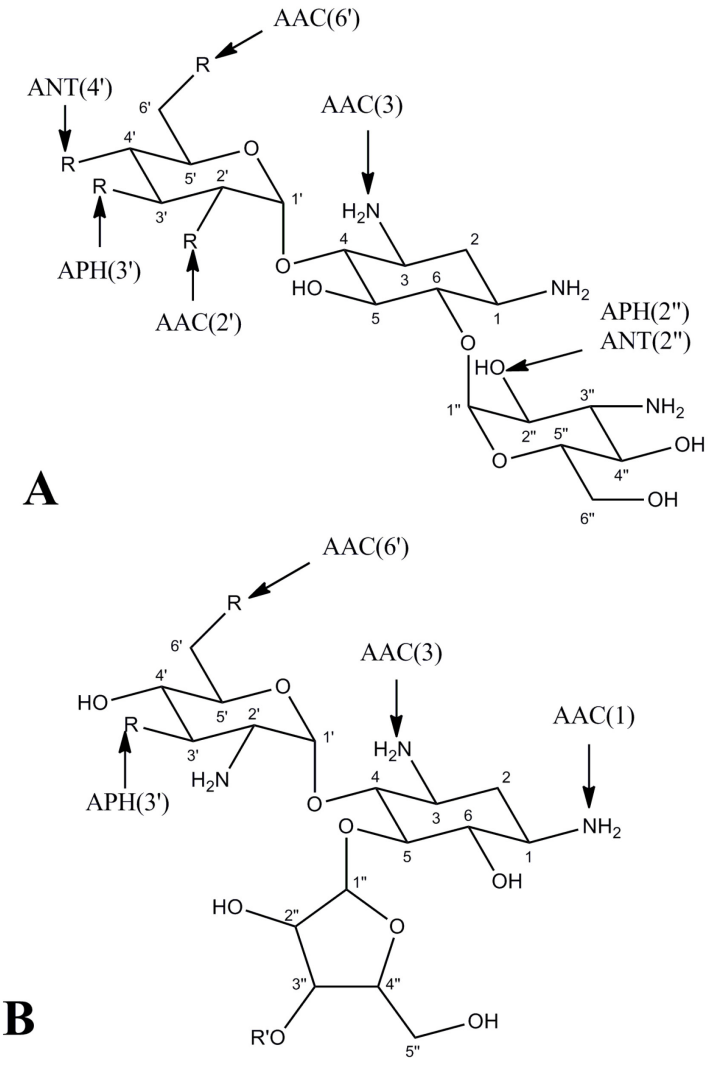

Fig. 1.6: Modification sites of aminoglosides for A) 4,6 disubstituted kanamycin class or B) 4,5 disubstituted neomycin class.

Table 1.1: List of Example Aminoglycoside Modifying Enzymes

Enzyme		Isoform	Substrate
AAC(6')-	I	a-z	A, Dbk, I, K, N, S, T
	II	a-b	Dbk, G, K, N, S, T
	III	c	A, I, K, N, T
	IV		A, G, K, N, T
AAC(2')-	I	a	Dbk, G, N, Ne, T, S
AAC(3)-	I	a-b	G, S
	II	a-c	Dbk, G, N, S, T
	III	a-c	Dbk, G, K, L, N, P, S, T
	IV	a	A, Dbk, N, S, T
	VI	a	G, N, S, T
	VII	a	G
AAC(1)			Ap, L, P, R
APH(3')-	I	a-c	G, K, L, Ne, P, R
	II	a	A, B, G, K, Ne, P, R
	III	a	A, B, G, I, K, L, Ne, P, R
	IV	a	A, B, I, K, Ne, P, R
	V	a-c	Ne, P, R
	VI	a-b	A, B, G, I, K, Ne, P, R
	VII	a	A, K, Ne
APH(2")-		a, b, d	Dbk, G, K, N, T
APH(2")-AAC(6')			A, Dbk, G, I, K , N, S, T
ANT(4')-	I	a	A, Dbk, G, K, I, S, T
	II	a	A, I, K, T
ANT(2")	I	a-c	Dbk, G, K, S, T
ANT(3")	I	a	S, Sp, St

A, amikacin; B, butirosin; Dbk, dibekacin; G, gentimicn; I, isepamicin; K, kanamycin; L, lividomycin; N, netilmicin; Ne, neomycin; P, paromomycin; R, ribostamycin; S, sisomicin; Sp, spectinomycin; St, streptomycin; T, tobramycin

1.1.4 Aminoglycoside N-6'-acetyltransferase-Ii

1.1.4.1 Background

AAC(6')-Ii is a chromosomally encoded enzyme isolated from *Enterococcus faecium* and was first characterized by Costa *et al.* in 1993.[43] Their studies showed that this 182 amino acid, 20.7 kDa, protein was responsible for the natural low level resistance to aminoglycoside antibiotics found in *E. faecium*. The initial cloning of the *aac*(6')-Ii gene and three step purification procedure of the AAC(6')-Ii enzyme was developed in 1997 by Wright *et al.* who also performed the initial enzymatic assays.[44] These initial studies revealed that AAC(6')-Ii exists as a stable homodimer in solution and has a broad spectrum of aminoglycoside substrates.[44] AAC(6')-Ii transfers an acyl group from AcCoA to the 6' amine of most aminoglycosides, shown in Fig. 1.7. A series of steady state dead-end and product inhibitions experiments determined that AAC(6')-Ii proceeds via a bi-bi sequential ordered mechanism. The order of the steps, shown in Fig. 1.7, are as follows 1) binding of the cofactor AcCoA; 2) binding of the aminoglycoside; 3) attack of the 6' NH_2 of the aminoglycoside onto the thioester of the AcCoA to form a tetrahedral intermediate; 4) collapse of the tetrahedral intermediate and breaking of the thioester bound; 5) release of the acetylated aminoglycoside; 6) release of the CoA. Solvent viscosity studies showed that the final step of releasing CoA is the rate limiting step in the catalytic

cycle.[45] The kinetic parameters determined for this reaction are K_m ≈ 5-20 μM for aminoglycosides, K_m ≈ 20 μM for AcCoA and the k_{cat} ≈ 0.4 s^{-1}. The computed k_{cat}/K_m is on the order of 10^4 M^{-1} s^{-1}, which is relatively low compared to other aminoglycoside-modifying enzymes.[45] This suggests that AAC(6')-Ii may be involved in other biochemical processes in *E. faecium*.[44] This is further supported through the extensive substrate base of AAC(6')-Ii. For example AAC(6')-Ii has been shown to acetylate poly-L-Lys and histones.[46] Also AAC(6')-Ii knockout comparisons of crude cell extracts of *E. faecium* showed several proteins were acetylated only in the presence of AAC(6')-Ii.[47]

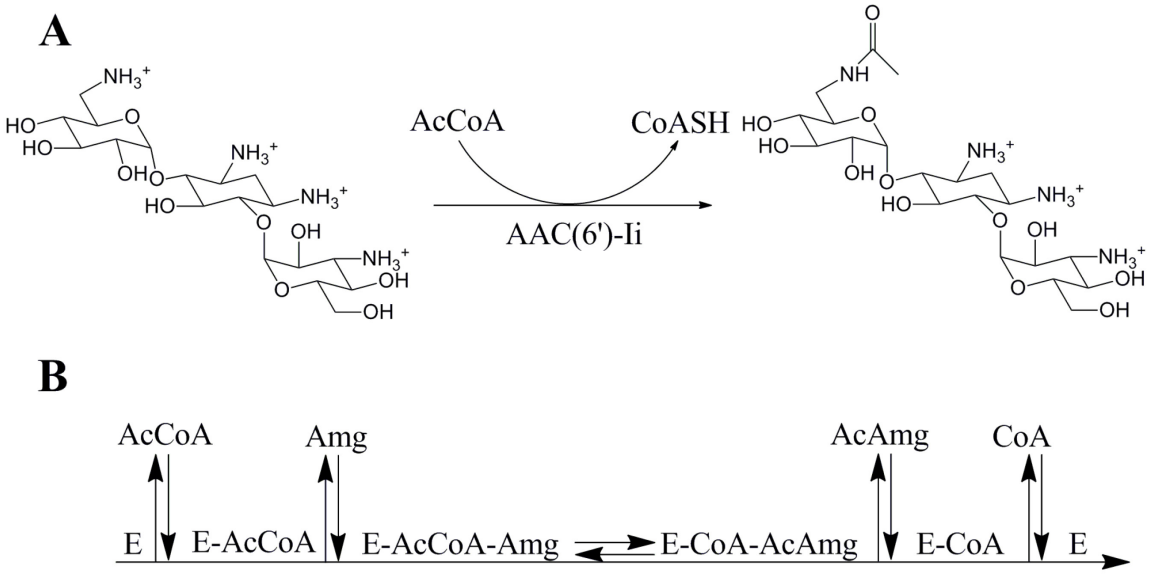

Fig. 1.7: A) Enzymatic Reaction of AAC(6')-Ii on the aminoglycoside kanamycin B) The kinetic reaction scheme of AAC(6')-Ii

1.1.4.2 AAC(6')-Ii structure

The first crystal structures were obtained by Wybenga-Groot *et al.* in 1999. There have been several crystal structures published of AAC(6')-Ii binding either CoA or AcCoA..[46,48-49] There have been several additional unpublished crystal structures obtained by the Berghuis lab of AAC(6')-Ii in its Apo form and bound to a series of bisubstrate inhibitors which consist of CoA molecule connected to an aminoglycoside via a small linker. The crystal structure showed that AAC(6')-Ii belongs to the GCN5-related N-acetyltransferase (GNAT) superfamily.[46] This group of enzymes is found in all forms of life and comprises dozens of families.[50] Even though the sequence similarity of these proteins can be quite low, they all contain a similar structural fold, consisting of a four stranded mixed beta-sheet with two alpha helices on either side of the sheet, shown in Fig. 1.9.[48,50] Each monomer contains a V-like structure, with the active site is located inside this cleft, and the C-terminus forming one arm and the N-terminus forming the second arm.[46] AAC(6')-Ii is constituently active as a homo dimer, shown through X-ray crystal structures[48] and supported with analytical gel filtration experiments.[45] Each monomeric subunit adopts the GNAT fold and contains a single active site, as shown in Fig 1.8.[48] The interface is composed of interactions of both the N and C regions of each subunit[48] and there has been no evidence of the AAC(6')-Ii subunits dissociating at any concentrations[44].

Intriguingly, even though the wild type enzyme is such a stable dimer, a single mutation at tryptophan 164 to alanine causes the enzyme to be a monomer in solution.[45] This mutant is still active but its function is impaired with a 10 fold reduction in k_{cat} and a 10-fold increase in K_m.[45]

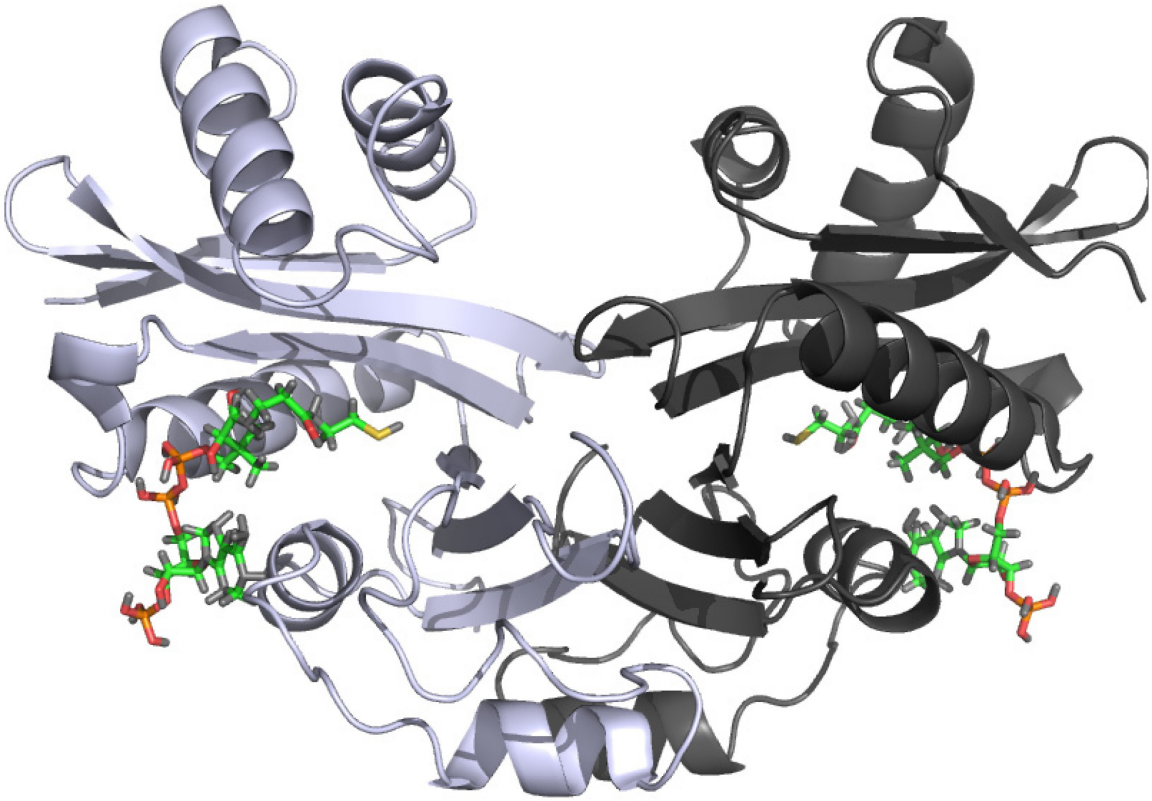

Fig. 1.8: Structure of aminoglycoside 6'-*N*-acetyltransferase-Ii complexed to Coenzyme A. Each subunit is coloured separately with chain A pale blue, and chain B dark grey. Generated from pdb code 2A4N[49] and PyMOL molecular graphics software (DeLano Scientific, ver 1,2r1, 2009).

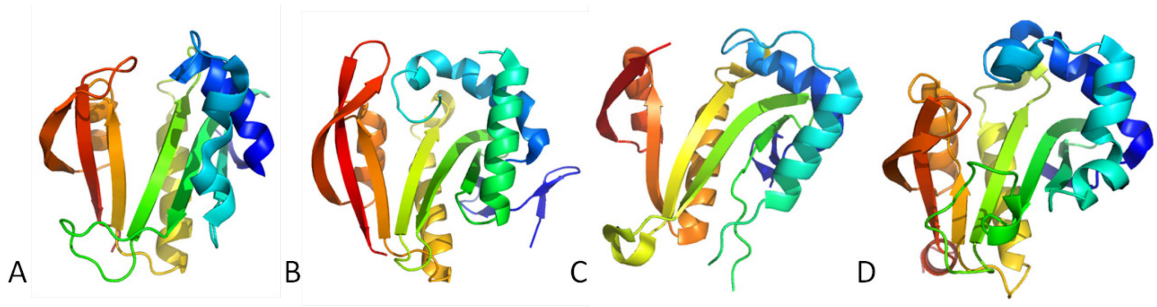

Fig. 1.9: Tertiary structure of example proteins with a GNAT fold: A) Glyphosphate-N-acetyltransferase,[51] B) RimL,[52] C) yeast GNA1,[53] and D) AAC(6')-Ib[54]

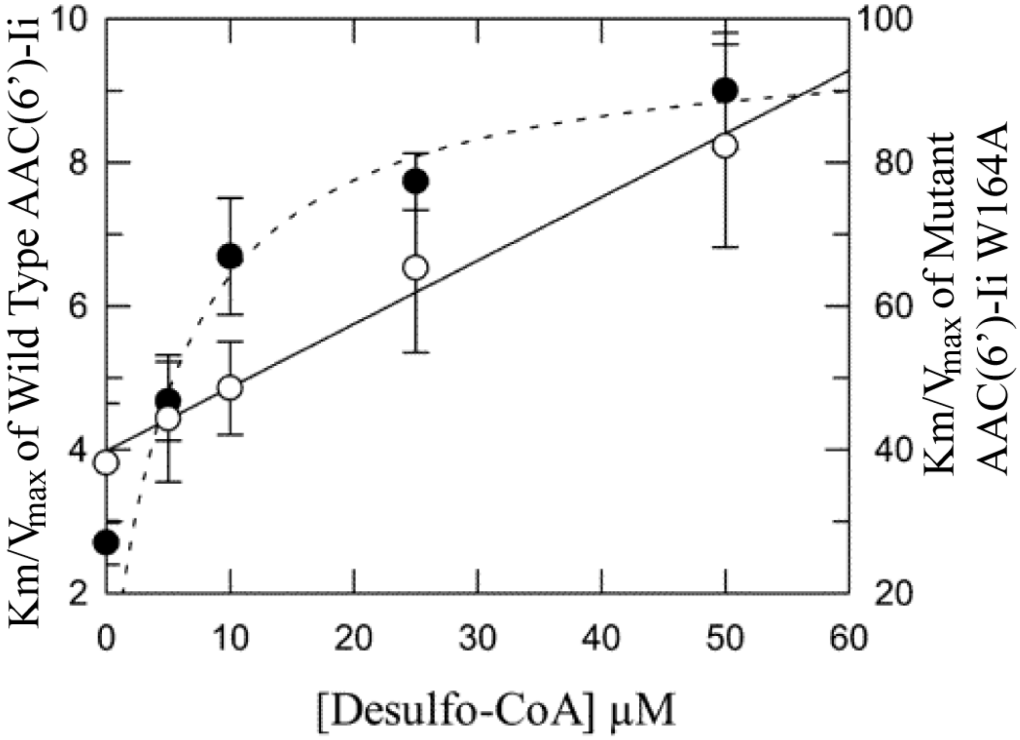

Fig. 1.10: Change of Km/V_{max} with increasing inhibitor. Wild type enzyme (●) shows a hyperbolic dependence which suggests partial competitive inhibition. Mutant enzyme (○) shows a linear dependence which suggests competitive inhibition. Reprinted with permission from Draker, K., Northrop, D. B. & Wright, G. D. *Biochemistry* **42**, 6565-6574 (2003) copyright 2003 American Chemistry Society. [45]

Observed cooperativity in AAC(6')-Ii

As mentioned above, AAC(6')-Ii is present in solution as a homodimer. Experiments performed by Draker *et al.* suggest that the homodimer acts as a functional unit and the two binding sites present in this unit behave cooperatively.[45] Dead end inhibition studies were performed using desulfo-CoA as an inhibitor. Desulfo-CoA is a dead end inhibitor as it competes directly for the active site with AcCoA.[45] Partial competitive inhibition was observed with the dead-end inhibitor, and gives a distinct hyperbolic shape for the dependence of K_m/V_{max} vs inhibitor concentration, shown in Fig. 1.10. [45] AAC(6')-Ii still retained activity when desulfo-CoA is bound, but the activity is reduced. Therefore the enzyme can form a catalytically active enzyme-substrate-inhibitor (ESI) complex. This suggests that the wild type AAC(6')-Ii binds multiple ligands with different affinities. There are two identical subunits; therefore this suggests that the subunits interact in a cooperative manner. [48] In the case of the W164A mutant monomer the dependence of K_m/V_{max} vs desulfo-CoA concentration is linear. This indicates that desulfo-CoA behaves as a competitive inhibitor, and no there is no cooperative binding. Therefore cooperativity is believed to be from interactions between the two subunits. This was further confirmed through isothermal titration studies (ITC), where aminoglycosides were shown to bind

with two non-equivalent binding sites. This asymmetric binding was abolished in the W164A mutant monomer.[45,55]

1.1.4.3 Coenzyme A

AAC(6')-Ii requires coenzyme A (CoA) as a second substrate to function. CoA is an important molecule found in all forms of life with over 4% of all known enzymes requiring CoA to function.[56] In *E. coli* the concentration of CoA varies from 100-400 μM,[57] and in *S. aureus* the concentration can reach the millimolar levels.[58] It is a requirement in many aspects of metabolism: the tricarboxylic acid cycle, protein acetylation, fatty acid synthesis, etc.[59] CoA consists of pantetheine moiety linked to adenosine 3'-phosphate by a pyrophosphate as shown in Fig. 1.11. A major function of CoA is to act as an acyl group carrier. The acyl group is bonded to the free thiol on the pantetheine portion forming a highly reactive thioester. These acyl groups can be different lengths, from short acetyl groups to long-chain fatty acids.[60] When an acetyl group is bonded to CoA, it is designated as AcCoA.[61]

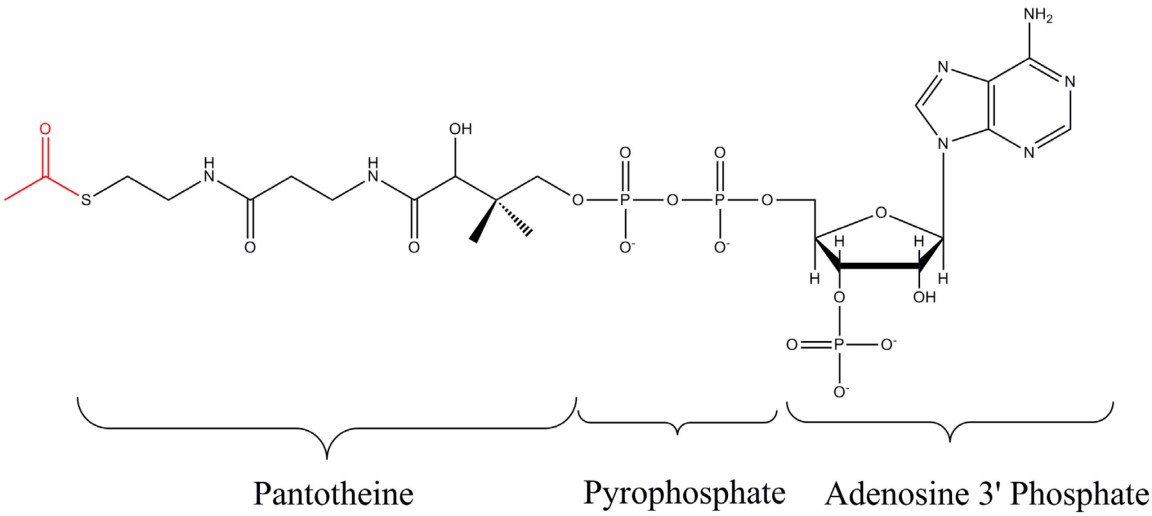

Fig. 1.11: Structure of acetyl coenzyme A. The acetyl group which is transferred is highlighted in red.

1.2 Allosteric cooperativity

1.2.1 Discription of allostery

At the molecular level cooperativity can occur through the interaction of discrete binding sites on a protein. Through cooperativity, an enzyme or substrate from metabolic pathway can modulate the activity of a second pathway or affect the binding of additional ligands.[62] Bohr first observed cooperativity in enzymes with the sigmoidal binding curve of oxygen associated with hemoglobin at increasing concentrations and postulated that binding of the first O_2 makes it easier for the next O_2 to bind and could be called 'cooperative'. [63]

Cooperativity which occurs at the molecular realm is known as 'allosteric cooperativity' or allostery.[64-65] Allostery is a ligand-macromolecule interaction which induces conformational or dynamic changes in proximal and distal regions

of the macromolecule.[62,66-67] Simply stated, allostery is control at a distance. Allostery does not necessarily lead to cooperative binding. Membrane pores can have allosteric regulation with no additional binding.[68-69] The change in conformation simply opens or closes the pore. Conversely the allosteric change in conformation in hemoglobin results in the cooperative binding of oxygen, hence the term allosteric cooperativity. The term allostery was first introduced by Jacques Monod in 1961 to explain the experiments of François Jacob, a student of his at the time, on end-product inhibition of the enzyme, L-theonine deaminase.[70-71] Since then, allostery has gained increasing interest to the scientific community, and has been used as a source for new drug targets.[72-74] Foster *et al.* developed compounds which recover the activity of mutant P53, a protein involved in DNA repair which has strong anticancer activity.[75] In another example, McMillan *et al.* identified an allosteric inhibitor of inducible nitric oxide synthase (iNOS) which prevents dimerization of iNOS, a required step for activity.[76] Many proteins have multiple active sites, and binding at a one site can elicit a change in binding or activity in the subsequent sites. There are two types of allosteric cooperativity. The first, heterotropic allostery, involves multiple sites with different ligands (for example signal transduction in tyrosine protein kinase receptors).[77-80] The affinity of one of the ligands is altered in the presence or absence of the second ligand, shown in Fig. 1.12A. The second, homotropic

allostery, has multiple sites with identical ligands (for example the aspartate receptor[81] or oxygen binding in hemoglobin[79]). The binding affinity of the protein for the ligand depends on the current ligation state of the protein, i.e. the first ligand binds with a different affinity from the second, etc, shown in Fig. 1.12B.

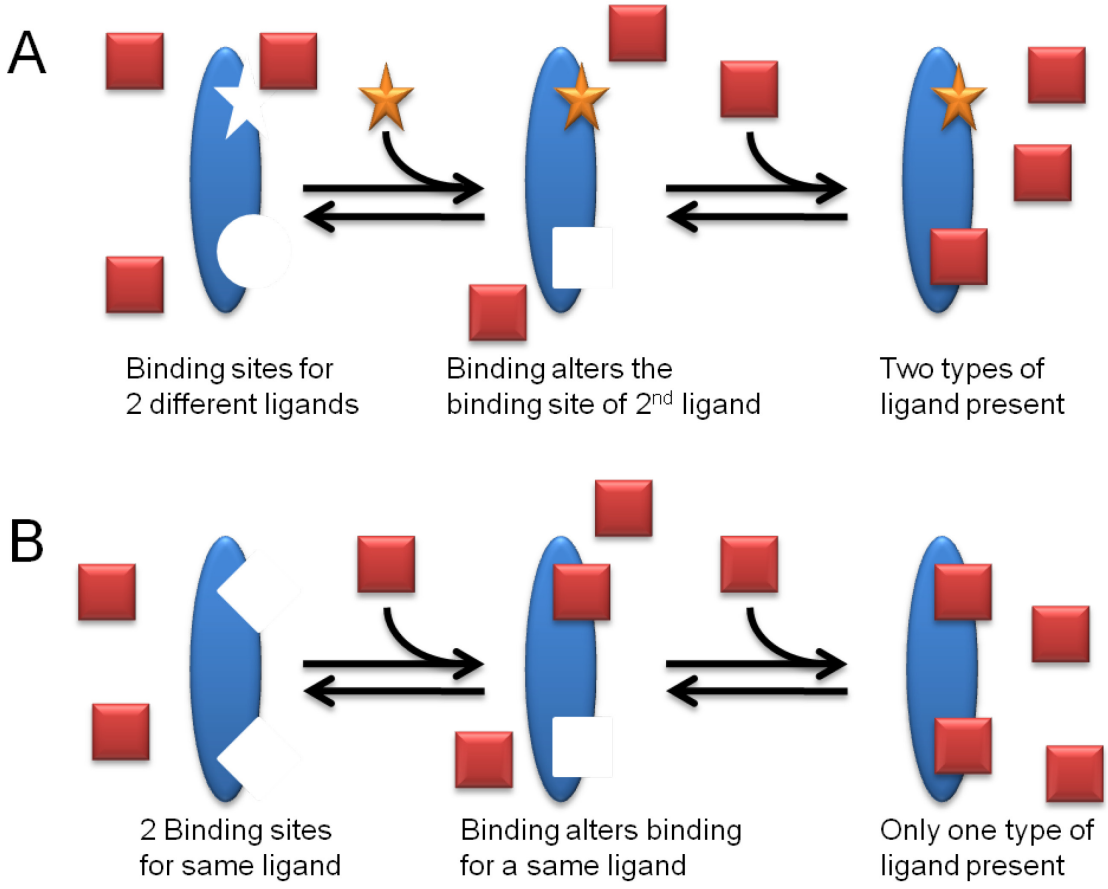

Fig. 1.12: Schematic representation of allosteric cooperativity. A) Heterotropic allostery - two different ligands involved. Binding at type of ligand alters the affinity for the second type. B) Homotropic allostery - multiple sites for the identical compounds. Binding at one site alter the affinity at the remaining sites

Cooperativity can be either positive or negative. In the case of positive cooperativity, the first binding events promotes additional binding events, while in

the case of negative cooperativity, the first binding inhibits additional binding events. The magnitude of cooperativity is often expressed as the Hill Coefficient, n_H, which is given by[82]

$$\log \frac{\bar{Y}}{1-\bar{Y}} = \log K + n_H \log S \qquad 1.1$$

where $\bar{Y}$ is the fractional saturation, S is the concentration of the free ligand, K is the apparent binding constant, and n_H is the Hill coefficient. Systems with positive cooperativity have a $n_H > 1$, and systems with negative cooperative have an $n_H < 1$. Non cooperative binding curves are hyperbolic; however cooperativity produces an interesting effect on the binding curve, shown in Fig. 1.13. For example, Hemoglobin is known to bind oxygen with positive cooperativity and gives a sigmoidal binding curve. A requirement for hemoglobin is maximum uptake of oxygen in oxygen rich areas and complete unloading in oxygen deficient regions. Hemoglobin requires a 3-fold change in oxygen concentration to alter its saturation from 10% to 90%.[62,83] Under normal Langmuir adsorption, the system has to change its ligand concentration by 81 fold for the same response. Positive cooperativity causes the saturation state of the enzyme to be much more sensitive to the ligand concentration. Meanwhile negative cooperativity decreases the sensitivity to substrate concentration. This allows the enzyme to behave at an intermediate rate over a larger concentration range

of its ligand.[62] Cooperativity is likely used as a mechanism to control protein activity.[84-86]

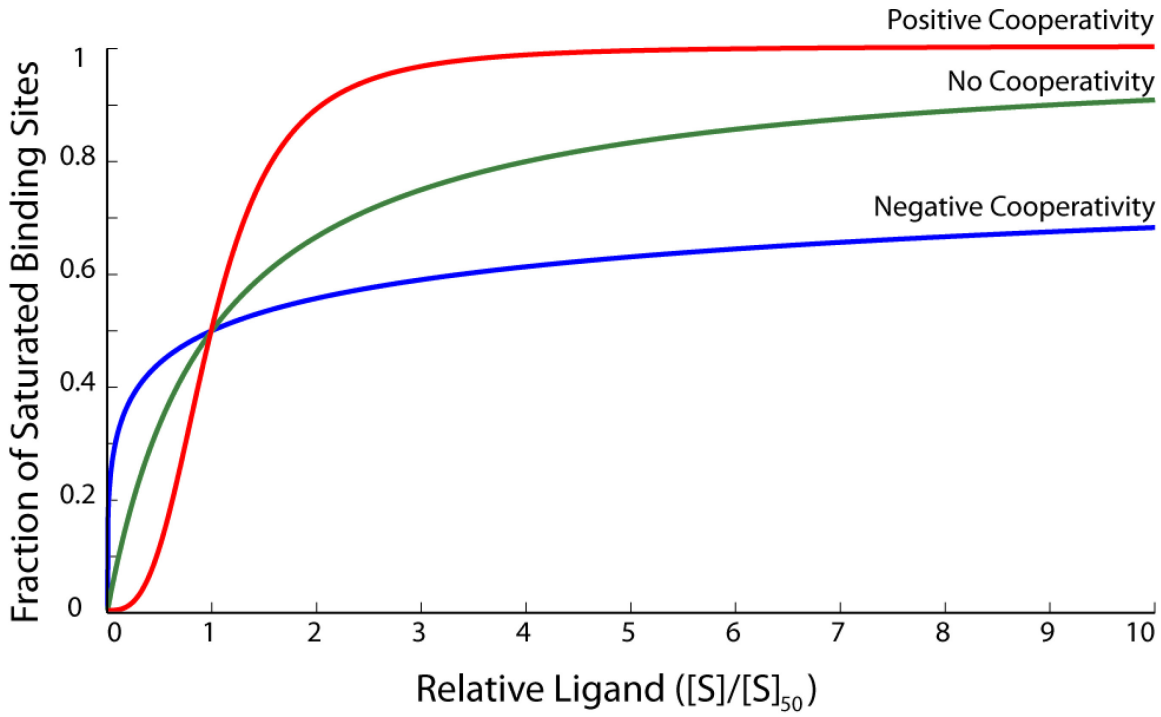

Fig. 1.13: Theoretical binding profiles of a system with positive (red), no cooperativity (green), and negative (blue). The concentration at which the binding sites are 50% saturated is given by $[S]_{50}$.

As explained above, the term allostery was coined in 1961 and explains cooperativity through changes in conformation and dynamics. However, 25 years earlier in 1935 Pauling proposed a mathematical model to explain the positive cooperativity observed in binding of oxygen by hemoglobin.[87] The determination of the X-ray crystal structure of hemoglobin bound and unbound to oxygen inspired two physical models: The Monod-Wyman-Changeux model (MWC model) and the Koshland-Nemethy-Filmer model (KNF model).[64-65,78]

These two models are the most well known and commonly used to explain allostery observed in proteins. Additional models have been developed to explain systems which behave differently. One such model was recently proposed by Hilser and Thompson.[88] Each of these model are explained in detail below.

1.2.2 The MWC model - concerted or two state

One of the first models proposed was the MWC model in 1965, also known as the concerted or two-state model, shown in Fig. 1.14.[62,65] This model proposes that allostery occurs in oligomeric proteins and that the protein is symmetric. In this model the enzyme can be in one of two different states: a low affinity **A** state and high affinity **B** state. These two states are in equilibrium. When the protein undergoes a conformational change all subunits change in a concerted manner so that symmetry is retained. The equilibrium between these two states is determined by the differences in free energy (ΔG). The equilibrium is perturbed by the difference in free energy of binding between the **A** state and the **B** state and causes the protein to adopt the high affinity **B** state. Subsequent binding events occur with a higher population of protein in the high affinity **B** state which will cause the ligand to bind with a higher affinity.[65] If this is looked at in terms of free energy (ΔG), the free energy of binding (ΔG_B) is the same for the

first binding event and the second binding event. However, in the first binding event there is also a conformational transition. The assumption is that the free energy from this transition (ΔG_F) is positive because the binding competent conformation is at a higher energy level. Therefore the total free energy is more negative in binding the second event compared to the first binding event. This gives a higher binding affinity.

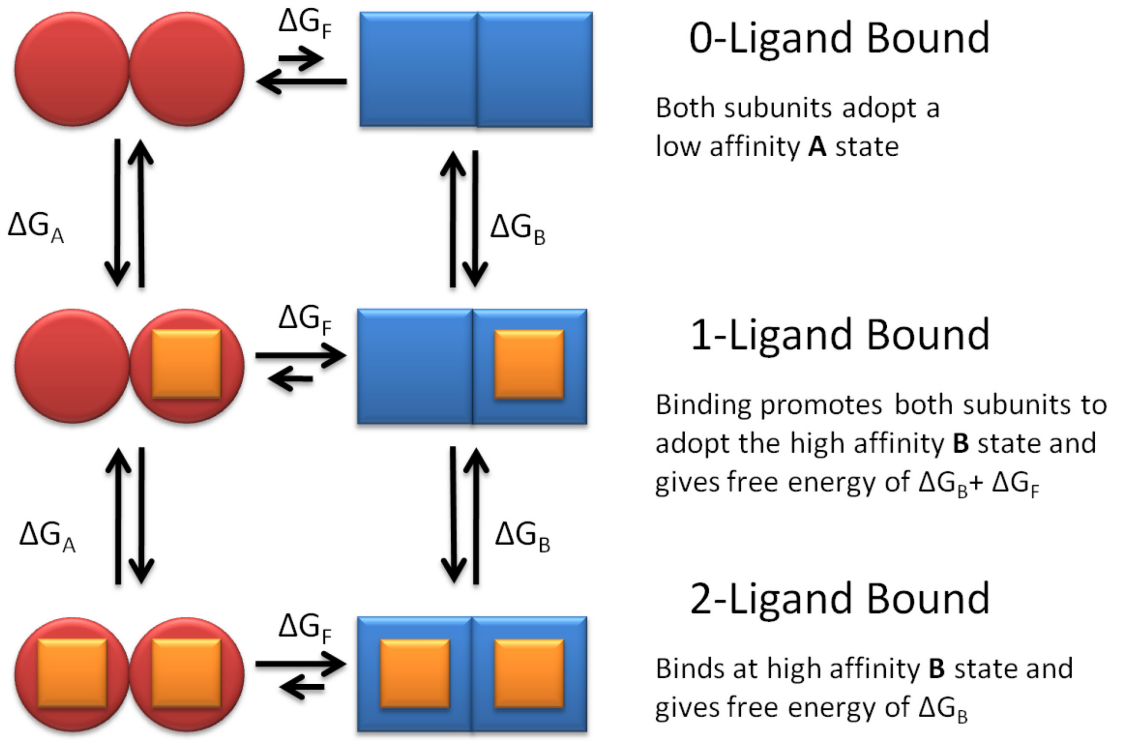

Fig. 1.14: Schematic representation of the MWC model. The protein is present in two states, a low affinity **A** state (red circle) and high affinity **B** state (blue square). Ligand (orange squares) binding promotes the individual subunit to adopt the **B** state.

Equilibrium constants for binding a substrate, S, can be derived for binding to give[65]

$$[\mathbf{AS_1}] = [\mathbf{A}]n\frac{[S]}{K_A} \quad 1.2$$

$$[\mathbf{A}\mathrm{S}_2] = [\mathbf{A}\mathrm{S}_1]\frac{n-1}{2}\frac{[S]}{K_A} \quad 1.3$$

$$\vdots$$

$$[\mathbf{A}\mathrm{S}_n] = [\mathbf{A}\mathrm{S}_{n-1}]\frac{1}{n}\frac{[S]}{K_A} \quad 1.4$$

for the **A** state where K_A is the dissociation constant for the ligand and the **A** state, n is the number of binding sites. In addition we get

$$[\mathbf{BS_1}] = [\mathbf{B}]n\frac{[\boldsymbol{S}]}{\boldsymbol{K_B}} \quad 1.5$$

$$[\mathbf{B}\mathrm{S}_2] = [\mathbf{B}\mathrm{S}_1]\frac{n-1}{2}\frac{[S]}{K_B} \quad 1.6$$

$$\vdots$$

$$[\mathbf{B}\mathrm{S}_\mathrm{n}] = [\mathbf{B}\mathrm{S}_{n-1}]\frac{1}{n}\frac{[\mathrm{S}]}{K_B} \quad 1.7$$

for the **B** state where K_B is the association constant for the ligand and the **B** state.

The transition between the **A** and **B** state is given by

$$\frac{[\mathbf{B}]}{[\mathbf{A}]} = L \quad 1.8$$

The fraction of sites bound to ligand, $\bar{P}_S$, is given by the following expression

$$\bar{P}_S = \frac{([\mathbf{A}\mathrm{S}_1] + [2\mathbf{A}\mathrm{S}_2] + \cdots + [n\mathbf{A}\mathrm{S}_n]) + ([\mathbf{B}\mathrm{S}_1] + [2\mathbf{B}\mathrm{S}_2] + \cdots + [n\mathbf{B}\mathrm{S}_n])}{n\big(([\mathbf{A}] + [\mathbf{A}\mathrm{S}_1] + [\mathbf{A}\mathrm{S}_2] + \cdots + [\mathbf{A}\mathrm{S}_n]) + ([\mathbf{B}] + [\mathbf{B}\mathrm{S}_1] + [\mathbf{B}\mathrm{S}_2] + \cdots + [\mathbf{B}\mathrm{S}_n])\big)} \quad 1.9$$

By defining the ratios

$$\alpha = \frac{[\mathrm{S}]}{K_A} \quad 1.10$$

and

$$c = \frac{K_A}{K_B} \tag{1.11}$$

and substituting the equilibrium constants 1.10 and 1.11 into 1.9 and simplifying we get

$$\bar{P_S} = \frac{Lc\alpha(1 + c\alpha)^{n-1} + \alpha(1 + \alpha)^{n-1}}{L(1 + c\alpha)^n + (1 + \alpha)^n} \tag{1.12}$$

From this equation cooperativity is determined by both the relative stabilities of **A** and **B**, and the ratio of their binding strengths. If L is very small or c = 1 then equation 1.12 simplifies to

$$\bar{P_S} = \frac{\alpha}{1 + \alpha} = \frac{[\mathrm{S}]}{K_A + [\mathrm{S}]} \tag{1.13}$$

which is the Langmuir isotherm. The MWC model has been used extensively since its inception to describe various biological systems, from hemoglobin[89] to signal transduction.[90] However useful, this model does have its limitations. The original MWC model fails to explain cooperativity observed in monomeric proteins, which counters the first assumption in which allostery occurs only in oligomeric proteins. The second requirement of symmetry is also not always followed with allosteric proteins. Finally, this model assumes that ligand binding drives the conformational equilibrium of the protein to the high affinity **B** state, so additional binding will always be at a higher affinity. Therefore it fails to explain negative cooperativity and an alternative model must be used.[78]

1.2.3 The KNF model - sequential model

The next model proposed was by Koshland *et al.*, in 1966, and was based on the original proposal of Pauling.[64] The KNF model is known as the sequential model, shown in Fig. 1.15.[62] Similar to the MWC model, the subunits in the KNF model are present in two states: a low affinity **A** state and high affinity **B** state. In this model each subunit changes conformation independently of the other when a ligand binds specifically to that subunit. In a system which contains only identical subunits, the protein then has n+1 states where n is the number of subunits. For example, in a 2 subunit protein there are 3 possible states: **AA**, **AB**, and **BB**. As the subunits are identical **AB** and **BA** are degenerate. The subunits interact with each other, and this energy is dependent on which state the subunits are in (ΔG_{IAA}, ΔG_{IAB}, ΔG_{IBB}). Each binding event involves a conformational transition from one state to another **AA** to **AB** to **BB**, so the total ΔG is dependent on ΔG_{B} and the difference in ΔG between the two states ($\Delta\Delta G_{\mathrm{I}}$). This can be shown through equilibriums folding and binding constants. If we assume that the substrate binding constant, K_{S}, is the same for every event then

$$K_S = \frac{[\mathbf{B}S]}{[\mathbf{B}][S]} \qquad 1.14$$

where [B] is the concentration of protein which binds the substrate and [S] is the concentration of substrate. The enzyme undergoes a conformational change from **A** to **B** giving

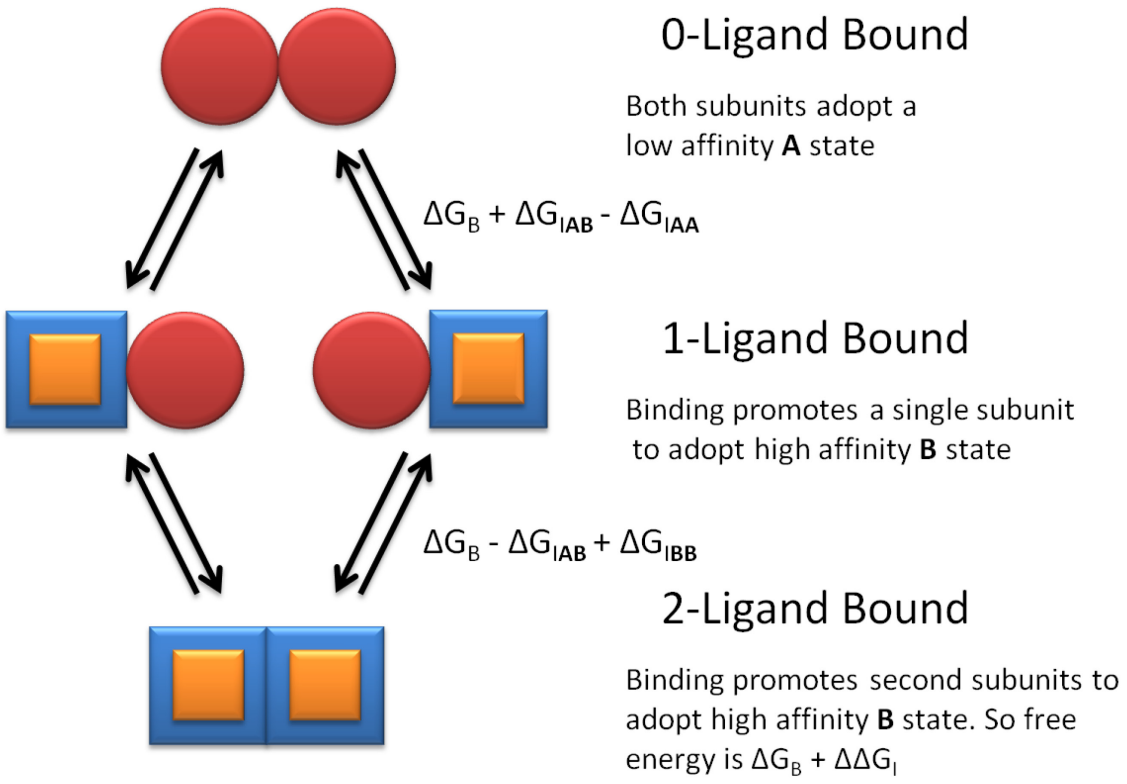

Fig. 1.15: Schematic representation of the KNF model. The protein is present in two states, a low affinity **A** state (red circle) and high affinity **B** state (blue square). Ligand (orange squares) binding promotes the individual subunit to adopt the **B** state.

$$K_r = \frac{[\mathbf{B}]}{[\mathbf{A}]} \qquad 1.15$$

and it is assumed that $K_r \ll 1$. Equilibrium constants can be introduced to give the relative stability of **AB** (K_{AB}) and **BB** (K_{BB}) to the initial state **AA**. Combining these constants we can determine the concentration of each bound state

$$[\mathrm{ES}] = 2K_{AB}[\mathrm{E}]([\mathrm{S}]K_S K_r) \qquad 1.16$$

$$[\mathrm{ES}_2] = K_{BB}[\mathrm{E}]([\mathrm{S}]K_S K_r)^2 \qquad 1.17$$

Any observed cooperativity is determined by the difference in the stability between the **AB** state and **BB**. When $K_{AB} > K_{BB}$ the system will behave with negative cooperativity and the reverse will produce positive cooperativity. Therefore, it is the change in the interactions between the subunits that drives the cooperativity.[64] Koshland *et al.* give a thorough description of how this can be applied to multimeric systems in which the different subunits adopt in several different orientations.[64] Even though this model is often referred to as 'induced fit',[62] Koshland *et al.* never explicitly stated a mechanism for ligand uptake. In fact Koshland *et al.* clearly state that the KNF model can be explained through induced fit or conformational selection.[64] The models are described with greater detail below. When there is a ligand-induced conformational change this model is able to explain all forms of allosteric effects: positive, negative, or no cooperativity.

1.2.3.1 Induced fit vs conformation selections

Originally enzyme catalysis was thought to occur through a 'lock and key' model. The enzymatic active site was rigid and was a mould for the substrates to fit. When the substrates bound they would be in the precise orientation to react. However there have been several example of ligand binding coupled to a conformational change. The two possible scenarios are 'induced fit' and

'conformational selection'. The induced fit was originally proposed by Koshland, and proposed that a substrate would first bind to the macromolecule in its ligand free conformation, and then the macromolecule would undergo a conformational change to a higher affinity conformation.[91-92] The conformational selection model proposes the macromolecule is present in multiple different exchanging states. One of the states present is the high affinity conformation, but this state is present as the minority. The substrate preferentially binds to the active conformation and this drives the conformational equilibrium from the low affinity state to the high affinity state. In the conformational selection model, the conformational change event occurs before the ligand binds to the active site.

The dependence on which pathway system follows can be describe by the flux through each pathway shown in Fig. 1.16.[93] Which for conformational selection is given by

$$F_{CS} = \left(\frac{1}{k_{\mathrm{W-T}}[\mathrm{P_{weak}}]} + \frac{1}{{k_{\mathrm{on}}}^{\mathrm{T}}[\mathrm{P_{tight}}][\mathrm{L}]}\right)^{-1}, \quad 1.18$$

and for induced fit is given by

$$F_{IF} = \left(\frac{1}{{k_{\mathrm{on}}}^{\mathrm{W}}[\mathrm{P_{weak}}][\mathrm{L}]} + \frac{1}{{k_{\mathrm{W-T}}}^{\mathrm{L}}[\mathrm{P_{weak}} \cdot \mathrm{L}]}\right)^{-1} \quad 1.19$$

where ${k_{\mathrm{on}}}^{\mathrm{W}}$ and ${k_{\mathrm{on}}}^{\mathrm{T}}$ is the rate constant for ligand binding to the low and high affinity state, $k_{\mathrm{W-T}}$ and ${k_{\mathrm{W-T}}}^{\mathrm{L}}$ is the rate constant for the conformational transition between the low and high affinity states free and bound to ligand (L)

respectively. The concentration of macromolecule in the low affinity and high affinity states is given by [P_{weak}] and [P_{tight}].

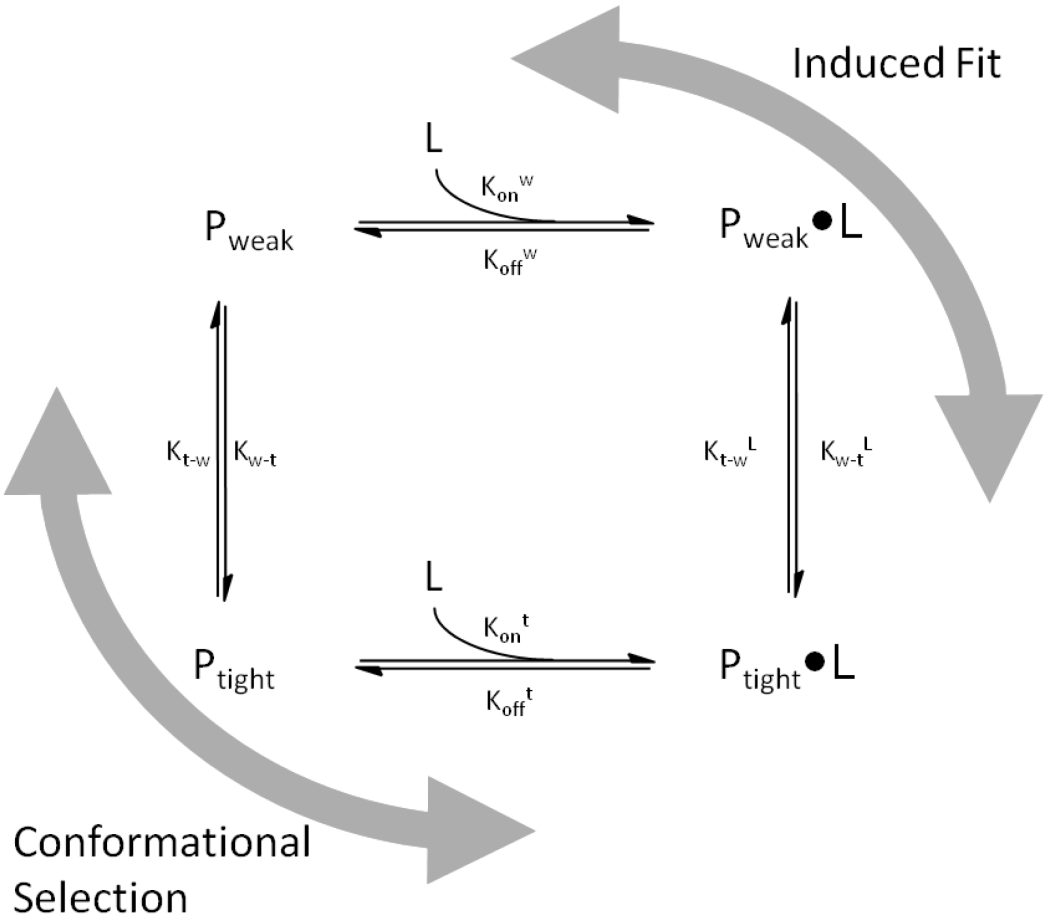

Fig. 1.16 Graphical differences between conformational selection and induced fit. P_{weak} and P_{tight} are the macromolecule in the low and high affinity conformations for the ligand (L).

1.2.4 Hisler and Thompson Model - intrinsic disorder

In 2007 Hilser and Thompson (HT) proposed a model to showed that intrinsic disorder can lead to allostery.[88] In this model, subunits in a protein are

allowed to independently fold and unfold, shown in Fig. 1.17. Like the previous two models, the subunits can be present in one of two states: a binding incompetent unfolded **A** state and a binding competent folded **B** state. This unfolding can be full or partial disordering, but the subunits must remain associated. The subunits interact with one another and the total free energy is composed of the energy of folding (ΔG_{F}) and the energy of interactions (ΔG_{I}) present only when both of the subunits are folded. The protein can only bind a ligand in the folded state. The first binding event requires only a single subunit to fold so the total free energy is from the energy of binding (ΔG_{S}) and the energy of folding (ΔG_{A}). A transition to the folded state requires energy, so the total free energy (ΔG_{App}) is greater than the energy of binding. However the second binding event requires both subunits to fold so the additional interaction energy is present so the total free energy is $\Delta G_{\mathrm{F}} + \Delta G_{\mathrm{S}} + \Delta G_{\mathrm{I}}$.[88] Whether ΔG_{I} is positive or negative determines whether the cooperativity is positive or negative. This model may appear similar to the KNF model, but it is different in one major aspect. In the KNF model the conformational transitions only occur in the presence of ligand, in the HT model the folded and unfolded forms are present in the absence of any bound ligand.

The equilibrium constant given for binding (K_{s}) is given by

$$K_s = e^{-\frac{\Delta G_S}{RT}} = \frac{[\mathbf{B}\mathrm{S}]}{[\mathbf{B}][S]} \qquad 1.20$$

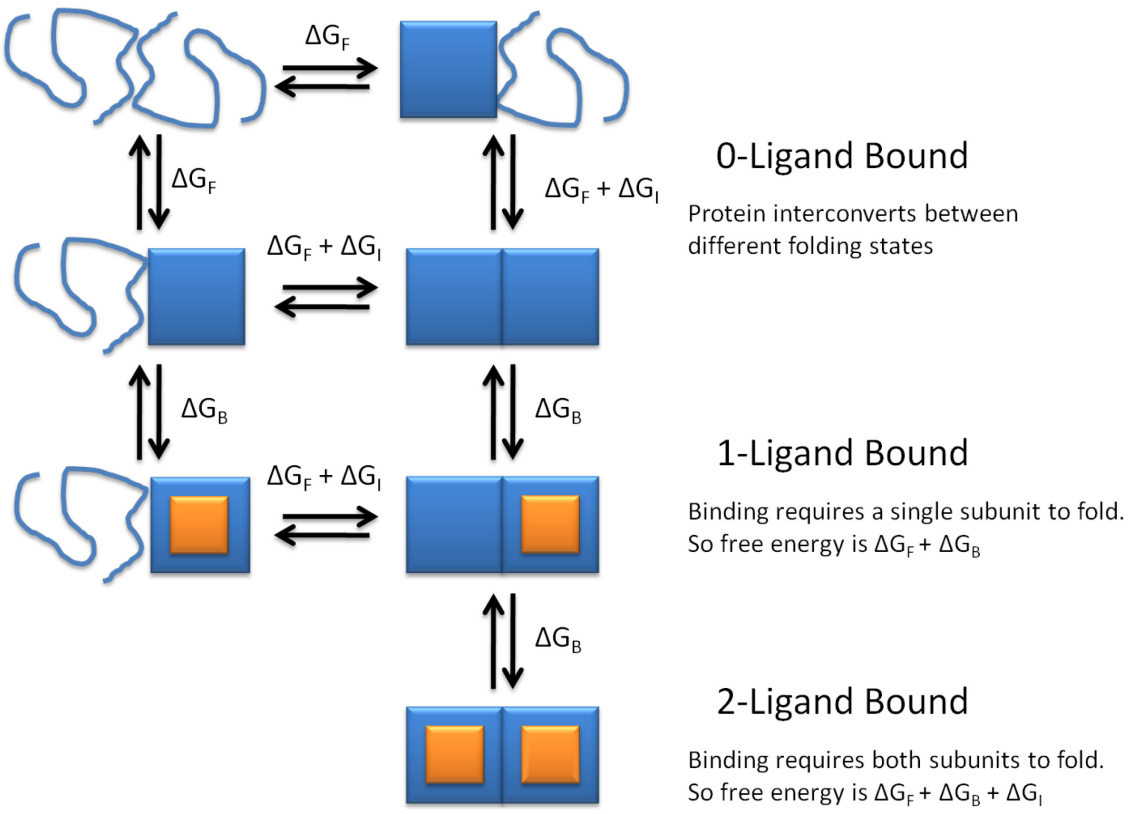

Fig. 1.17 Schematic representation of the HT model. Protein in the unfolded state is shown as blue line, and folded state is given by blue squares. Bound ligand is shown as orange squares.

Hisler and Thompson explain cooperativity through a partition function, Q, which is the sum of the statistical weights of all folded/unfolded states. For a dimer in the absence of ligand this is given by

$$Q = 1 + K_A\phi_I + K_B\phi_I + K_AK_B\phi_I \qquad 1.21$$

where $K_B = e^{-\Delta G_B/\mathrm{RT}}$, $K_B = e^{-\Delta G_B/\mathrm{RT}}$, and $\phi_I = e^{-\Delta G_I/\mathrm{RT}}$. K_A and K_B are the unfolding constants and ΔG_I is the interaction between the two subunits. When

$\Delta G_I \neq 0$, i.e. $\phi_I \neq 0$, the subunits are coupled. In homotropic allostery K_A=K_B so the partition function simplifies to

$$Q = 1 + 2K_A\phi_I + {K_A}^2\phi_i \quad 1.22$$

Only subunits in the **AB**, **BA**, or **BB** is able to bind ligand S. Therefore the partition function for the folded and unfolded states (Eq 1.22) in the presence of ligand S becomes

$$Q = 1 + 2K_S[\mathrm{S}] + {K_S}^2[\mathrm{S}]^2 + 2K_S[\mathrm{S}]K_A\phi_I + 2K_A\phi_I + {K_A}^2\phi_I \quad 1.23$$

Note that at concentration of [S] << $1/K_s$ Eq 1.23 reduces to Eq 1.22. The ratio of the protein in its different folded states is dependent on the concentration of ligand present. The ratio of protein in the **AB** or **BA** state is given by

$$\overline{P_1} = \frac{2K_S[\mathrm{S}]K_A\phi_I + 2K_A\phi_I}{Q}, \quad 1.24$$

and the ratio of protein in the **BB** state is given by

$$\overline{P_2} = \frac{1 + 2K_S[\mathrm{S}] + {K_S}^2[\mathrm{S}]^2}{Q}. \quad 1.25$$

At increased concentrations of S, there is more protein bound to S and shifts the equilibrium of the protein from the **A** state to the **B** state. The concentration of the zero bound can be given by

$$[\mathbf{BB}] = \frac{1 + 2K_A\phi_I + {K_A}^2\phi_I}{Q} \quad 1.26$$

while the singly bound state can be given by

$$[\mathbf{BB}\mathrm{S}] = 2K_S[\mathrm{S}][\mathrm{PP}]\frac{1 + K_A\phi_I}{Q} \quad 1.27$$

and the concentration of the doubly bound state is given by

$$[\mathrm{S}\mathbf{BB}\mathrm{S}] = \frac{{K_S}^2[\mathrm{S}]^2[\mathrm{PP}]}{Q} \quad 1.28$$

where

$$[\mathrm{PP}] = [\mathbf{AA}] + [\mathbf{AB}] + [\mathbf{BA}] + [\mathbf{BB}] \quad 1.29$$

The apparent affinity constants ($K_{S,app1}$ and $K_{S,app2}$) for the binding of S is given by the expressions

$$K_{S,app1} = 2K_S \frac{1 + K_A\phi_I}{1 + 2K_A\phi_I + {K_A}^2\phi_I} \quad 1.30$$

and

$$K_{S,app2} = \frac{{K_S}^2}{1 + 2K_A\phi_I + {K_A}^2\phi_I} \quad 1.31$$

Cooperativity is determined by the energetic coupling between the two subunits. In cases where ΔG_{I} is positive, it is favourable for the two subunits to interact. As the complete folding of both subunits is required for the second binding event, this interaction reduces the total free energy of the system. This results in positive cooperativity. In the cases where ΔG_{I} negative, the reverse occurs.

1.2.5 Comparing MWC, KNF and HT models

All three models use a change in protein conformation as a mechanism to explain cooperativity. Both of the MWC and the KNF models detail the enzyme in two folded states: A low affinity state, and a high affinity state. Binding promotes the protein to adopt a higher affinity conformation. The MWC model requires the subunits to remain symmetrical and undergo a conformational

change together. The energy required to change the conformation is need only in the first binding event which induces the observed cooperativity. Meanwhile the KNF model allows the two subunits to undergo a conformational change independently. There are interactions between the two subunits which are affected by the conformational state of each subunit. The interaction between the subunits induces the cooperativity in the system. The HT model proposes that the two states are in equilibrium in the absence of ligand. One of the states is either partially or completely unfolded and cannot bind the ligand. There is interaction energy between the two subunits which is present only when both subunits are folded. It is this equilibrium which causes cooperativity in the system.

1.2.6 Other explanations of allostery and the difficulty in studying allostery

There have been several other physical models proposed in which the driving factor involves change in protein dynamics,[66,94] interacting amino acids residues,[95-96] and shifting binding populations.[97] These models give other specific explanations for observed allostery but will not be described in detail here. In some cases multiple contributions are required in a model to describe the observed allostery.[98-99]

Studying cooperativity in homotropic systems is a very challenging task. As the free and fully bound states are often symmetrical only the intermediate state can give detailed information about the mechanism of cooperativity. In negative cooperativity the second ligand binds more weakly than the first. This allows situations when the partially saturated state is present as the major population. This has allowed the singly bound intermediate state in negatively cooperative systems to be isolated.[81,100] In systems with positive cooperativity the intermediate state is typically at a low population. This makes structural studies very difficult, if not impossible, in most cases. Binding studies and kinetic assays can be performed to study positive cooperativity, but it is often difficult to deconvolute the multiple binding events. A technique which has been useful for studying cooperativity is ITC.[101] In cooperativity, the binding events occur with different enthalpies and association constants. ITC directly measures the enthalpy released during binding, and because each binding event may have a different enthalpy, deconvoluting the binding curve becomes much easier.[102]

1.3 Isothermal Titration Calorimetry

1.3.1 Background

ITC is a technique which directly measures the heat released or absorbed throughout a titration experiment. The measurement of this heat from a single

experiment allows for the accurate determination of dissociation constants (K_d) and stoichiometry (n) as well as the binding thermodynamics: enthalpy (ΔH), entropy (ΔS), and Gibbs free energy (ΔG).[103] Additionally the change in heat capacity (ΔC_p) can be ascertained through performing experiments at a series of temperatures.[104-105] ITC does not require any modification of the protein or secondary reporter molecules since the absorption or production of heat is a property of almost all biochemical reactions.[105] ITC works through periodically titrating a small amount of one reactant into a sample containing a second reactant. As the two interact, heat is released or absorbed. The amount of heat released/absorbed at the i^{th} injection (q_i) is dependent on the volume of the cell (v), the change in ligand bound (ΔL_i), and the enthalpy of binding (ΔH_B). According to[106]

$$q_i = v \cdot \Delta L_i \cdot \Delta H_B \qquad 1.32$$

The system measures the heat released and maintains the system at a constant temperature through a thermocouple. The heat signal is dependent on the interaction of the macromolecule with the ligand of interest. As the titration progresses the amount of the free macromolecule decreases until no free macromolecule is present. This causes the magnitude of the peaks to decrease until each injection produces similar peaks which correspond only to the heat of dilution of the injected ligand and the saturation point of the experiment, as shown in Fig. 1.18.[106] The amount of heat released for each injection, q_i, is given

by integrations of the heat signal under the baseline between two injection points. This value is dependent on the ΔH_B, K_A and the particular binding model the system follows. In the simplest case where the macromolecule of interest has only one binding site, q_i at the i^{th} injection is given by

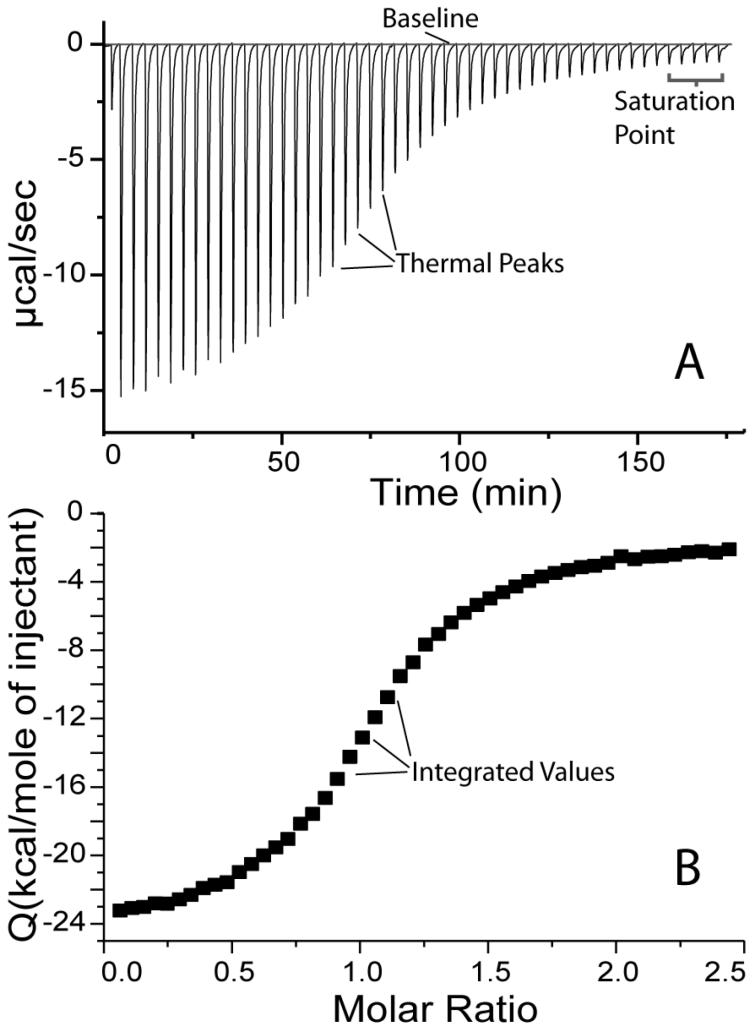

Fig. 1.18: A) Standard ITC isotherm. The negative heat peaks correspond to injection of ligand into sample cell. B) Integrated values from the ITC thermal peaks.

$$q_i = v \cdot \Delta H_B \cdot [P] \cdot \left(\frac{K_A[L]_i}{1 + K_A[L]_i} - \frac{K_A[L]_{i-1}}{1 + K_A[L]_{i-1}} \right) \quad 1.33$$

where $[L]_i$ is the concentration of the free ligand and $[P]$ is the concentration of the macromolecule. Non-linear regression of Eq 1.33 to the experimental data yields ΔH_B, and K_A. Entropy (ΔS) can then be calculated from

$$\Delta S = \frac{\Delta H}{\mathrm{T}} - R \ln\{K_A\} \quad 1.34$$

where R is the gas constant, 8.314 J mol^{-1} K^{-1} and T is the temperature at which ΔH and K_A were obtained. When several experiments are performed at different temperatures the heat capacity (ΔC_p) can be obtained by the slope of the enthalpy vs temperature curve

$$\Delta C_P = \frac{\Delta H_2 - \Delta H_1}{\Delta \mathrm{T}} \quad 1.35$$

Like many techniques, the utility of ITC was restricted by the technology available. In the 1970's, only systems which produce heats on the order of 10^{-3} cal or greater per injection could be reliably measured. In order to produce large enough signals, experiments were performed at high concentration (mM). Full binding isotherms could only be obtained for systems with K_A under 10^4 M. Any system with a K_A above 10^4 could only have the enthalpic component determined.[104,107] It was not until 1980's, when sensitive calorimeters able to measure heat effects of 10^{-6} cal were developed, that ITC could be used for most biological systems.[104]

As the instrumentation sensitivity of the instruments improved so did the development of the theory. In 1989, Wiseman *et al.* show that a parameter 'c' must be between 1-1000 during ITC experiments so the thermodynamic parameters could be reliably determined.[108] This value is determined by the concentration of the macromolecule in the sample cell, [P], the binding constant, K_A, and the number of binding sites, n. Through the following expression

$$c = n \times [P] \times K_A \qquad 1.36$$

Even with modern instruments this sets the upper limit of 10^8-10^9 M^{-1} for the binding constant which can be measured through conventional means. One method which is used to overcome this limitation is a competitive binding assay. In these experiments, a weaker binding ligand is competitively displaced by the titration of a stronger binding ligand. The apparent binding constant (K_A^{app}) is given by

$$K_A^{app} = \frac{K_A}{1 + K_B[\mathrm{B}]} \qquad 1.37$$

where K_A is the association constant of the tight binding ligand of interest and K_B and [B] is the association constant and concentration of the weaker binding ligand. The affinity of the weaker binding ligand can be obtained through separate titrations, so K_A can be calculated from equation 1.37. Over the past decade there has been an explosion of literature describing different methods to address possible limitations of ITC. If one wishes to go into detail there have

been a large number of reviews which describe these techniques in great detail.[105-106,109-114]

1.3.2 Observing linked folding/binding events

The idea that conformational changes in proteins can be induced from ligand binding has been around for over 50 years. In 1958, Koshland introduced the concept of induced fit to explain the substrate specificity he observed with a 5'-nucleotidase.[115] This proposed that a ligand induces a conformational change in the macromolecular structure after it binds. Since then, the idea of induced fit has become increasingly popular and generally accepted. A quantitative approach to link folding and binding was later address by Eftink and Biltonen. The model they proposed would account for the changes observed in heat capacity, enthalpy and entropy.[116] In this model there are two states for the protein, a binding competent state and a binding incompetent state. In order to bind a ligand the protein must first switch to a binding competent state, Scheme 1.1.

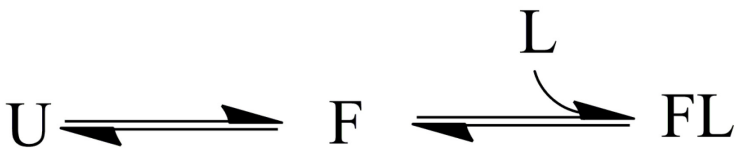

Scheme 1.1: Linked binding/folding event

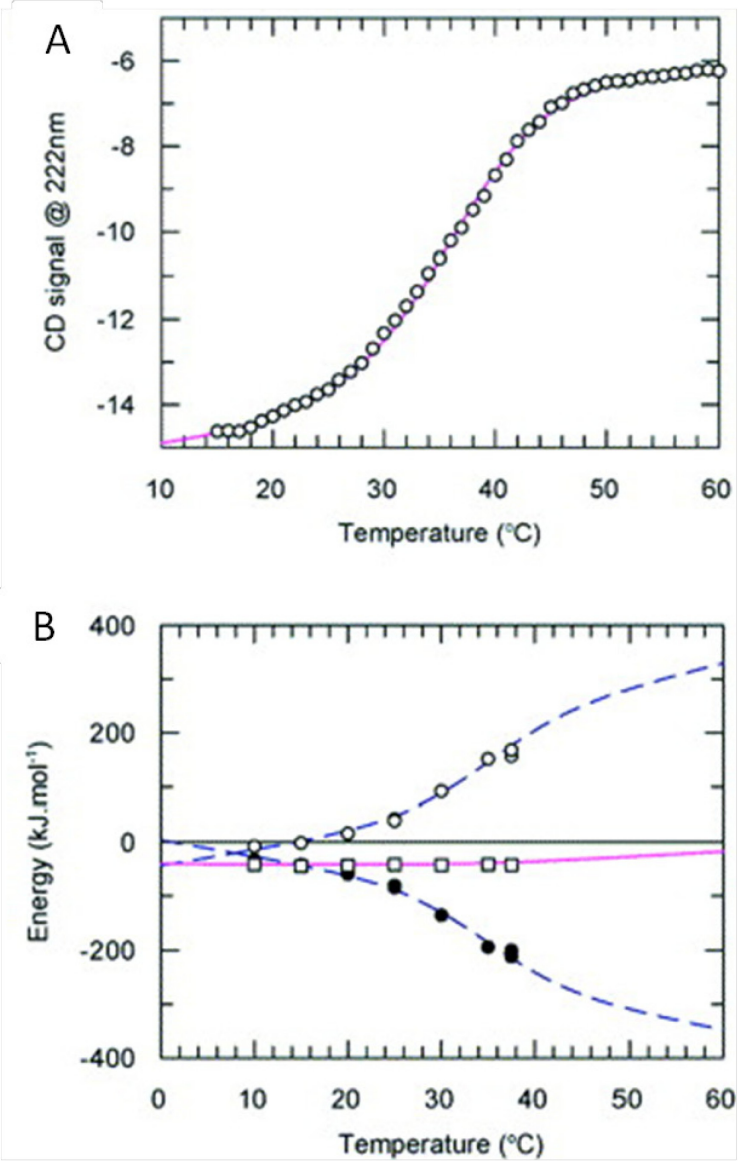

Fig. 1.19: A) CD melting curves and B) temperature-dependence of the thermodynamic parameters of PP5 TPR binding Hsp90 peptide, together with fitted curves from the global analysis. (Obtained from Cliff 2005)[102]

The association of **F** and L to form **F**L is temperature independent provided that the differences heat capacity between the bound and free states remain constant.[117] Therefore, the enthalpy of binding (ΔH_A) will vary linearly with

temperature with the slope equal to the difference in heat capacity between the free and bound form of the protein. If the protein undergoes a temperature dependent event like thermal melting, a temperature dependent component will be added to the ΔH_A which can create a large change in heat capacity with increasing temperature.[102] If this transition occurs over the temperature range studied, then ΔH_A will exhibit strongly curvilinear temperature dependence. As ITC observes all the heat changes associated with binding, this additional enthalpy will be included in the measurements.

Ladbury and coworkers applied this to a tetratricopeptide repeat (TPR) domain of protein phosphatase 5 (PP5).[102] The TPR domain was shown to have non-linear temperature dependence of enthalpy which is indicative of a temperature dependent event coupled to binding. These linked events can vary greatly: protonation/deprotonation, additional binding ligands, change of aggregation, or a conformational change.[116] ITC is able to measure the energetics of these systems but does not give any structural information. Therefore, in order to confirm that a conformational change was linked to binding, Ladbury and coworkers combined nuclear magnetic resonance and circular dichroism (CD) spectroscopy with their studies.[102] Both of these give structural details about the protein structure. The NMR spectra showed that the TPR domain is partially unfolded at physiological temperatures and upon binding

chaperone protein Hsp90 it undergoes a conformational change and becomes more structured. CD was used as a quantitative measurement to determine the extent of unfolding. This could then be used to determine the binding component and the folding component of the measured enthalpy, shown in Fig. 1.19.

1.4 Nuclear magnetic resonance (NMR) spectroscopy

1.4.1 Nuclear spin

NMR is a very useful technique to study large complex bio-macromolecules like proteins, DNA and RNA, as it can provide structural information of bio-macromolecules at the atomic scale. NMR takes advantage of the nuclear spin present in atomic nuclei. Nuclear spin is a quantum phenomenon conventionally described by the quantum number I, nuclear spin angular momentum. A particle with a nuclear spin of I can exist in $2I$+1 different states. Spin ½ nuclei (^{1}H, ^{13}C, and ^{15}N) have 2 different states (spin up and spin down). Nucleii also possess an intrinsic magnetic moment ($\boldsymbol{\mu}$). In the absence of external fields the particles can orient in any direction with equal probabilities. However, if a magnetic field, **B**, is applied then the particles interact with the magnetic field. This produces interaction energy known as magnetic energy (E_{mag}). This energy is dependent on the strength of **B** and the orientation of both **B** and $\boldsymbol{\mu}$,

$$E_{\mathrm{mag}} = -\boldsymbol{\mu} \cdot \mathbf{B} \qquad 1.38$$

This induces a preferential orientation of the magnetic moments with the energy level dependent on the direction of alignment. Both magnetization and spin are closely related. The magnetic moment of a nucleii ($\hat{\boldsymbol{\mu}}$) is proportional to the nuclear spin angular momentum of the particle given by

$$\boldsymbol{\mu} = \gamma \cdot I \tag{1.39}$$

where γ is the gyromagnetic ratio of the nucleus of interest. Under standard conditions **B** is aligned with the Z-axis, with inserting 1.39, 1.38 can be rewritten as

$$E = -\gamma I_Z B^0 \tag{1.40}$$

A nucleus does not behave in a classical manner. When a magnetic field of **B** is applied, the nuclei do not align with the magnetic field, but the spin magnetic moment begins to precess about the magnetic field. As the magnetic moment precesses it maintains a constant angle to the magnetic field. The rate at which the nucleus precesses is known as the Larmor frequency (ω^0) and is given by,

$$\omega^0 = -\gamma B^0 \tag{1.41}$$

An isolated atom will maintain this angle of precession indefinitely. However, Atoms are not in a static environment; instead they are constantly moving and colliding with surrounding atoms. These interactions cause the magnetic moment of a nucleus to constantly reorientate and sample all possible orientations. Mentioned above, in a magnetic field the energy levels of the

magnetic moments are different. This difference of energy drives the nucleus to favour one orientation in the magnetic field over another. This results in a higher population of nuclei orientating in a specific direction, and producing a net bulk magnetization (**M**) along the magnetic field which is aligned in the z-axis (M_z).

1.4.2 NMR magnetization

Particles can transition between two different energy states through the absorption of a photon. The photons energy must exactly match the energy difference between the ground state and the excited state, which is given by

$$\Delta E = \hbar \gamma B^0 \qquad 1.42$$

For NMR, these energies lie in the radio frequency (rf) range of the electromagnetic spectrum.

At the beginning of a NMR experiment, the magnetization is aligned with the external magnetic field (B^0) along the vertical axis, shown in Fig. 1.20A. An rf pulse is applied to the sample, transferring the magnetization into the transverse plane, M_{xy}, Fig. 1.20B. All nuclei which have a non-zero nuclear spin angular momentum precesses around B^0. This precession is measured and a FID signal is obtained. The rate at which nuclei precess is given by eq 1.41. Even though each nuclei (^{1}H, ^{13}C, ^{15}N, etc) precesses at a unique range of frequencies, the specific precession frequency is very sensitive to the chemical environment of the atom in question. The frequency which a specific nuclei precesses is known

as the chemical shift (ω). The differences in ω allow NMR spectroscopy to differentiate between different nuclei.

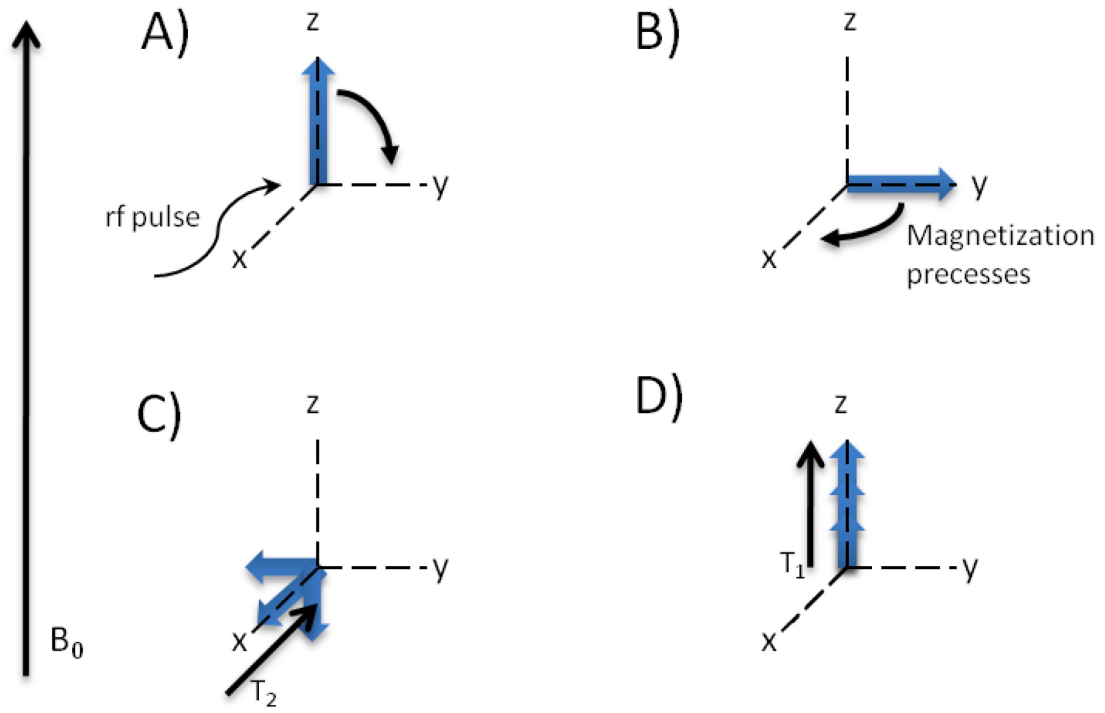

Fig. 1.20: Vector model of magnetization throughout an NMR experiment. A) At equilibrium as a rf pulse is applied. B) After rf pulse, magnitization precesses around z-axis. C) The transverse magnetization decreases due to T_2 relaxation. D) The M_z component returns to equilibrium due to T_1 relaxation.

As mentioned above, nuclei will precess at specific angle indefinitely if there were not additional interactions with the nuclei. Relaxation is the term given to describe the net magnetization returning equilibrium. There are two relaxation mechanisms, spin lattice and spin-spin relaxation. Spin-lattice relaxation, also known as longitudinal or T_1 relaxation, returns the net

magnetization of the M_z component of **M**, Fig. 1.20D. This occurs through the interactions and exchange of energy of the individual spin with the surrounding lattice. It is dependent on the physical and chemical properties of the spins' environment. Spin-spin relaxation, also known as transverse or T_2 relaxation, causes the gradual decay of the M_{xy} component of **M**, Fig. 1.20C. This occurs through the interactions with the spin lattice, exchanging between different chemical environments and more importantly interactions with neighbouring nuclei.

1.4.3 Exchange

Molecules exist is very dynamic environments. They are constantly tumbling, vibrating and rotating. Most motions (molecular rotations, vibrations and tumbling) tend to be very fast (μs-ps) and are too fast to directly measure through NMR, and only the average chemical environment is observed. There are some motions which can be directly observed through NMR (ligand binding, large conformational changes). If we consider a nucleus which exchanges between two different states, the process may be depicted as

where k_{AB} and k_{BA} are the corresponding rate constants. The chemical exchange rate constant (k_{ex}) is given by

$$k_{ex} = k_{AB} + k_{BA} \quad (1.43)$$

The effect on the NMR spectra from the exchange process is dependent on the rate of exchange, and the difference in chemical shift frequency (ω_Δ), denoted by

$$\Delta\omega = \omega_A^0 - \omega_B^0 \quad (1.44)$$

where ω_A^0 and ω_B^0 are the chemical shift frequencies of the A state and B state respectively. There are three different exchange regimes depending on the relation of $\Delta\omega$ to k_{ex}.[118-120]

$$k_{ex} \ll |\Delta\omega| \quad \text{(Slow Exchange)}$$

$$k_{ex} \gg |\Delta\omega| \quad \text{(Fast Exchange)} \quad (1.45)$$

$$2k_{ex}(p_A p_B)^{\frac{1}{2}} \approx |\Delta\omega| \quad \text{(Intermediate Exchange)}$$

Where p_A and p_B are the relative populations between two different exchanging states. In a situation which is under slow exchange ($k_{ex} \ll |\Delta\omega|$) two distinct sharp peaks are observed with their intensities dependent on the relative populations in each state. As the exchange rate increases the peaks begin to broaden due to dephasing of the signals from the nuclei jumping between the two states. This is labelled *chemical exchange broadening*. This broadening increases as the exchange rate increases until it reaches the intermediate exchange where the peaks coalesce.[118] At the coalescence point ($k_{ex} = |\Delta\omega|/\sqrt{2}$) the two peaks merge into a single peak with a chemical shift

determined by the population weighted average of the precession frequency of the two states, given by[118]

$$\omega_{obs} = \omega_A^0 + p_B \Delta\omega \quad 1.46$$

As k_{ex} increases the nuclei moves into the fast exchange regime and the peakwidth is reduced. This narrowing continues as k_{ex} increases. An idealized 1-dimensional spectrum of a system with 2 site exchange with a skewed population (p_A = 0.75, p_B = 0.25) is shown in Fig. 1.21. The change from fast exchange to slow exchange occurs over a narrow range, when the frequency of k_{ex} is within roughly 1 order of magnitude to the frequency $\Delta\omega$. The timescale for motions of macromolecules, such as proteins, often occur close to this timescale. The intermediate exchange regime is quite sensitive to the dynamics of the systems, so the experimental spectra can be used to obtain accurate estimates of exchange rate constants.[121]

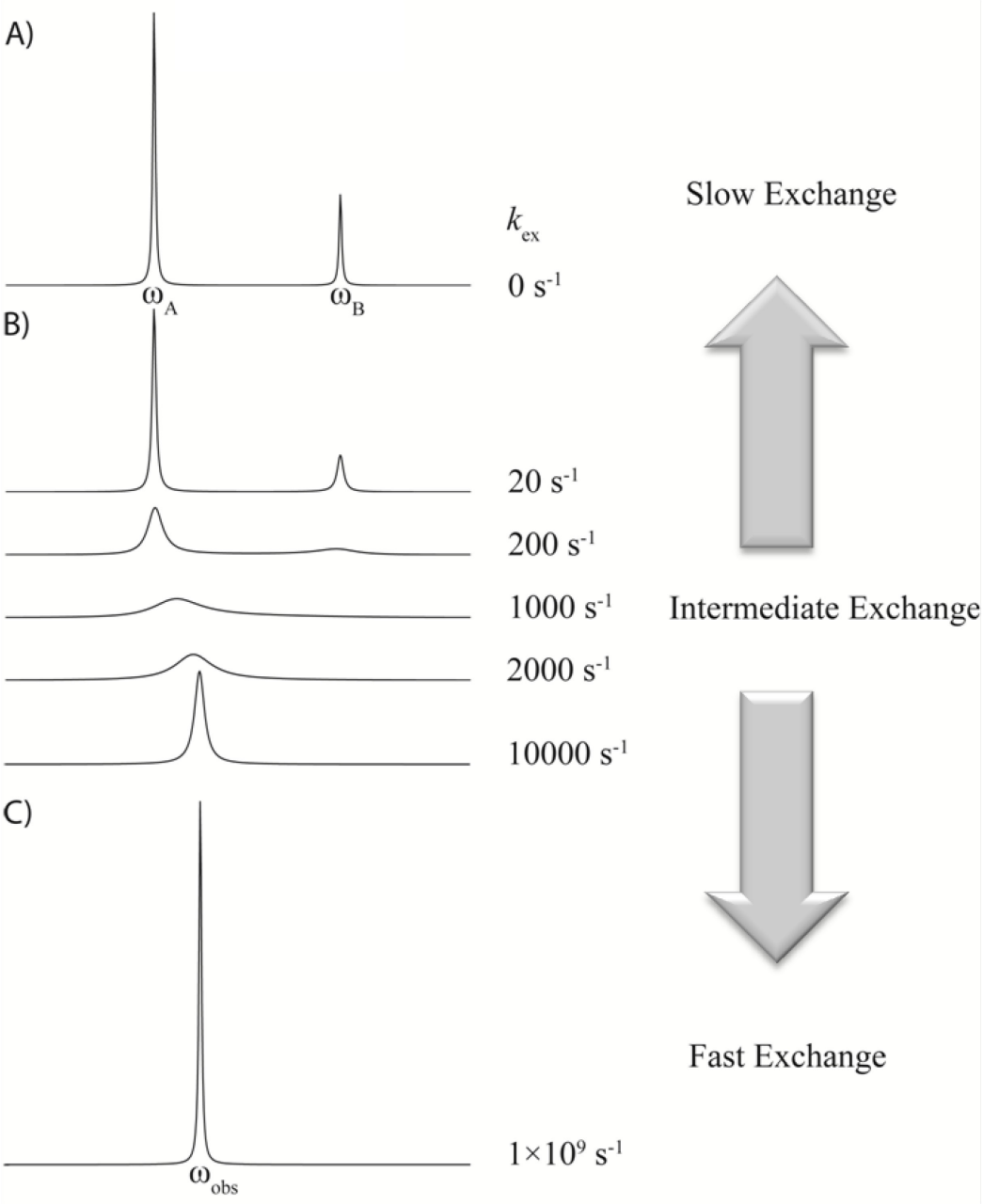

Fig. 1.21: Line shapes of a spectrum with 2 site exchange with a Δω of 1000 s^{-1}. A) Slow exchange produces two distinct sharp peaks. B) As the exchange rate increases the two peaks broaden until they coalesce. The single peak's width narrows as the exchange rate increases. C) Fast exchange produces a single sharp peak at the average chemical shift. (Adapted from Palmer *et al.* 2001[121])

1.5 Overall objectives

The goal of this thesis is to identify the physical binding model which explains AAC(6')-Ii binding to AcCoA or an aminoglycoside. This was achieved through a series of different biophysical techniques: ITC, NMR, and CD. This required the development of complex fitting protocols which link together the thermodynamic information from ITC to the structural information gathered from NMR and CD. The majority of this work is based on the work done by Ladbury and coworkers on the TPR domain.[102] The system presented herein is far more complex than that described by Ladbury and this required a development of global fitting protocols for ITC. TPR binds to its ligand in a 1:1 stoichiometry, whereas the AAC(6')-Ii quatinary structure contains two active sites which binds ligands with different binding parameters (ΔH, ΔS and K_A).

Chapter 2 first addresses the multiple binding sites observed with AcCoA binding to AAC(6')-Ii and determines the correct binding model. When ITC experiments were performed at a single concentration the isotherm could be fit to one of two binding models: 2-site sequential and 2-site independent. By performing multiple titrations at different concentrations of protein and globally fitting the ITC isotherms to a single set of binding parameters it was possible to elucidate the correct binding model which is a 2 site sequential binding model.

Once the correct binding model was determined, a variable temperature dataset can be used to identify additional physical process linked to binding such as: folding/unfolding, or protonation/deprotantion. Temperature dependence of the binding enthalpy and association constants can give thermodynamic information to these linked processes. However, a major problem arose during the ITC fitting. There is significant scatter in the physical parameters obtained between each isotherm. This scatter prevents the accurate analysis of the temperature dependence. To overcome this challenge, the data was fit globally linking the isotherms at different temperatures through the *van 't* Hoff relationship. This approach was labelled the *van 't* Hoff global fit. Chapter 3 describes this fit in detail using a simple model system of the AAC(6')-Ii W164A mutant monomer. The *van 't* Hoff global fitting procedure together with NMR spectroscopy and CD spectroscopy was applied to wild type AAC(6')-Ii, describe in Chapter 4. Through combining these multiple different techniques and employing the *van 't* Hoff restriction a model was developed which explains the observed cooperativity over all temperatures. AAC(6')-Ii contains two opposing allosteric events which alter the observed cooperativity from positive to negative with increasing temperature. There is a KNF like folding model which promotes positive cooperativity through the folding of a single subunit per binding event, and a HT like model which contains intrinsic disorder. The stability of the

unbound subunits is dependent on the temperature which alters the observed cooperativity from positive to negative.

In Chapter 5, paromomycin replaces AcCoA as a ligand and the differences with how it binds to AAC(6')-Ii is described in detail. AAC(6')-Ii follows the a MWC model instead of the KNF model when it binds paromomycin, additionally it structurally behaves differently. The enzyme adopts a different fold as suggested by NMR, and the dynamics of the intermediate state is much more complex. While the change from 0-bound to 1-bound is on the slow time scale, the change from 1-bound to 2-bound has regions which appear to change on the fast time scale. This shows that the unproductive complex contains much more dynamics compared to that of the binary complex.

The new methods developed for ITC described in this thesis will allow ITC to be used on increasingly complex systems. The new global fitting approaches described in this thesis help to gain accurate binding parameters in complex systems. Additionally, this thesis provides for the first time a thermodynamic description of multiple allosteric mechanisms to describe the control of binding events of a ligand to a protein. The understanding of allostery has been a great interest for decades. This thesis indentifies a system which contains multiple form of allostery and describes techniques which are able to quantify the contributions of these phenomena.

As is convention of the current literature we will express equilibrium constants with the units of concentration for dissociation constants and inverse concentration for association constants. However, equilibrium constants are in fact unitless so any mathematical expression detailed herein uses unitless values for any equilibrium constant.

2 Elucidating the AAC(6')-Ii binding mechanism through variable-*c* ITC

2.0 Preface

Isothermal titration calorimetry (ITC) can be used to measure molecular interactions of macromolecules with their ligands. However the correct model must be used to properly extract the thermodynamic parameters of the interaction. This chapter addresses the difficulties in determining the correct model to describe the binding of acetyl coenzyme A (AcCoA) to aminoglycoside *N*-6'-acetyltransferase-Ii (AAC(6')-Ii). As was mentioned in Chapter 1, the two subunits homodimeric AAC(6')-Ii appear to behave cooperatively. Results presented in these initial reports were determined using an independent binding model to fit the ITC data collected from AAC(6')-Ii titrations.[45] This chapter will show that the correct binding model is in fact a sequential binding model. Identification of the correct model can be challenging. We show that performing ITC experiments at a wide range of concentrations and globally fitting the results allows the identification of the correct binding model with reasonable accuracy. The majority of the work presented in this chapter is published and cited as:

Freiburger, L. A., Auclair, K. Mittermaier, A. K., "Elucidating protein binding mechanisms by variable-c ITC." *Chembiochem*. **2009**, 14, 2871-3.

The work presented in this chapter was performed by myself under the guidance of Dr. Auclair and Dr. Mittermaier.

2.1 Introduction

ITC is a very powerful technique to characterize the physical parameters involved in binding events. As described in the introduction, from ITC data, the entire thermodynamic signature, enthalpy, entropy and dissociation constants (ΔH, ΔS and K_d) can be extracted from a single experiment.[106] ITC is commonly used to measure 2-state ligand-host systems with a single binding mode. However, it can also provide important information about complicated systems that have multiple binding sites that are allosterically coupled.[114] Allostery is a ligand-macromolecule interaction which induces conformational, dynamic, or functional changes in a proximal and/or distal region of the macromolecule.[62,66-67] The two subunits can then interact and alter the binding of additional ligands, which is known as cooperativity.

Allostery and cooperativity are very important in biological systems and as mentioned before are involved in regulation, signal transduction, and enzymatic activities.[64-65,72-74] Thusly, it is of great interest to elucidate the underlying mechanisms of allostery.[78] Due to the high complexity of many allosteric systems, several models can often fit the same data equally well.[114,122] In this chapter, ITC data acquired during the binding of AcCoA to AAC(6')-Ii proved challenging to interpret using current methodology and led us to develop a simple method to discriminate between different potential binding models. Our

methodology uses the global analysis of ITC data obtained over a large range of macromolecule concentrations.

2.2 Interesting Behaviour in AAC(6')-Ii

As reported by Draker *et al.*, AAC(6')-Ii shows partial inhibition with the dead-end inhibitor desulfo-CoA, which suggests cooperative effects. A dead-end inhibitor is expected to block catalysis competitively. However, the partial inhibition observed with the dead-end inhibitor suggests that there is cooperativity between the two active sites of the homodimer. Initial ITC experiments performed by Draker *et al.* demonstrated the presence of two active sites in the AAC(6')-Ii dimer, each binding with different binding parameters (Fig. 2.1C).[45] Draker *et al.* showed that AcCoA is competitively inhibited by the CoA product and unaffected by high concentrations of the acetylated aminoglycoside product. Additionally, AAC(6')-Ii undergoes substrate inhibition under high concentration of aminoglycosides. It was therefore concluded that binding of AcCoA must occur before aminoglycosides to produce a catalytically competent complex. In light of these results we decided to study binding of AcCoA to AAC(6')-Ii to understand the first step of the catalytic mechanism.

In a simple two state system, the binding isotherm is sigmoidal, Fig. 2.1A. At the beginning of the titration the heat released/absorbed is at its maximum.

The signal decreases in a sigmoidal manner until it plateaus at its saturation point. The isotherm for AcCoA is different from that of a simple 2-state binding. As the titration progresses the heat released increases until it reaches a maximum at which point the enzyme begins to saturate. This is followed by a decrease in heat released to the saturation point. This suggests that the two subunits of the homodimer bind to AcCoA with different affinities and enthalpies.

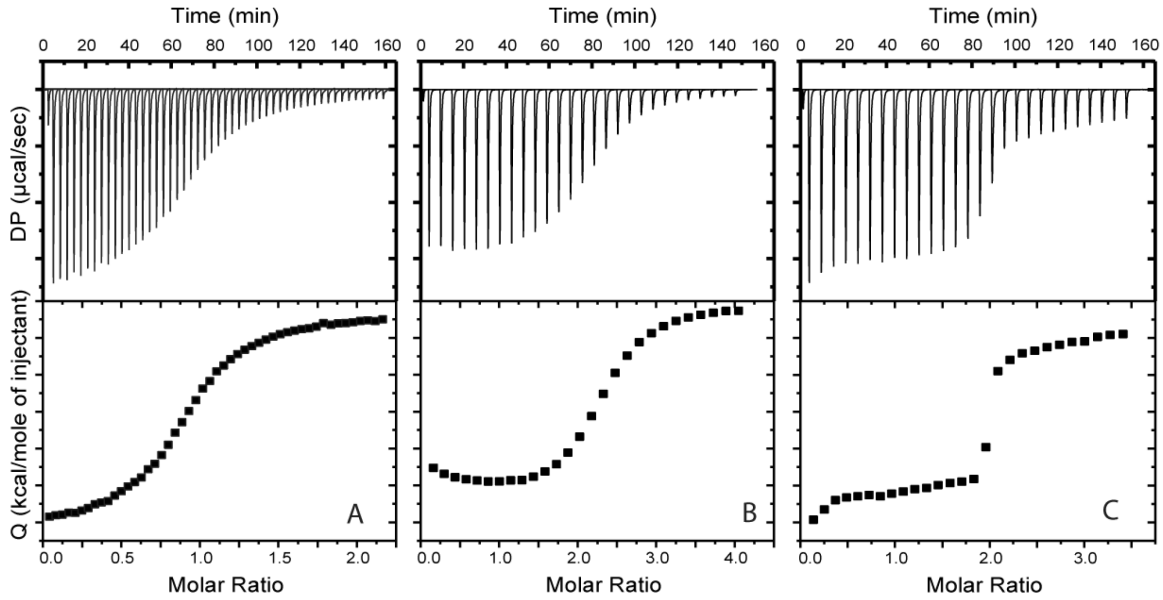

Fig. 2.1: Example Binding Isotherms at 20ºC of AAC(6')-Ii with A) simple 2 state binding B) AcCoA binding to AAC(6')-Ii and C) Paromomycin binding AAC(6')-Ii

When multiple binding sites are available in a host macomolecule, several binding models can potentially fit the data equally well. The two most likely models for this system involve either independent sites or cooperatives sites (Fig. 2.2). A model comprised of multiple independent binding sites consists of two

different classes of binding sites on the host that interact with ligand independently. Each macromolecule contains n_1 type 1 sites with affinity K_{A1} and binding enthalpy ΔH_{A1}, and n_2 type 2 sites with affinity K_{A2} and binding enthalpy ΔH_{A2}.

In the sequential binding site model, the binding sites are identical.[123] The first ligand molecule binds to either site of the apo-protein with an affinity K_{A1} and a binding enthalpy ΔH_{A1}. This alters the affinity of the subsequent binding sites, so the second ligand molecule binds a singly bound protein with an affinity K_{A2} and enthalpy ΔH_{A2}.

These two models appear similar but represent two significantly different binding mechanisms. In a two-site protein the independent model predicts that the host contains two structurally distinct and noninteracting binding surfaces for the ligand, shown in Fig. 2.2A. Meanwhile the sequential model predicts that the enzyme contains two binding sites that are energetically coupled, also known as cooperative binding sites. The binding at one site influences the thermodynamics of the second site, shown in Fig. 2.2B.

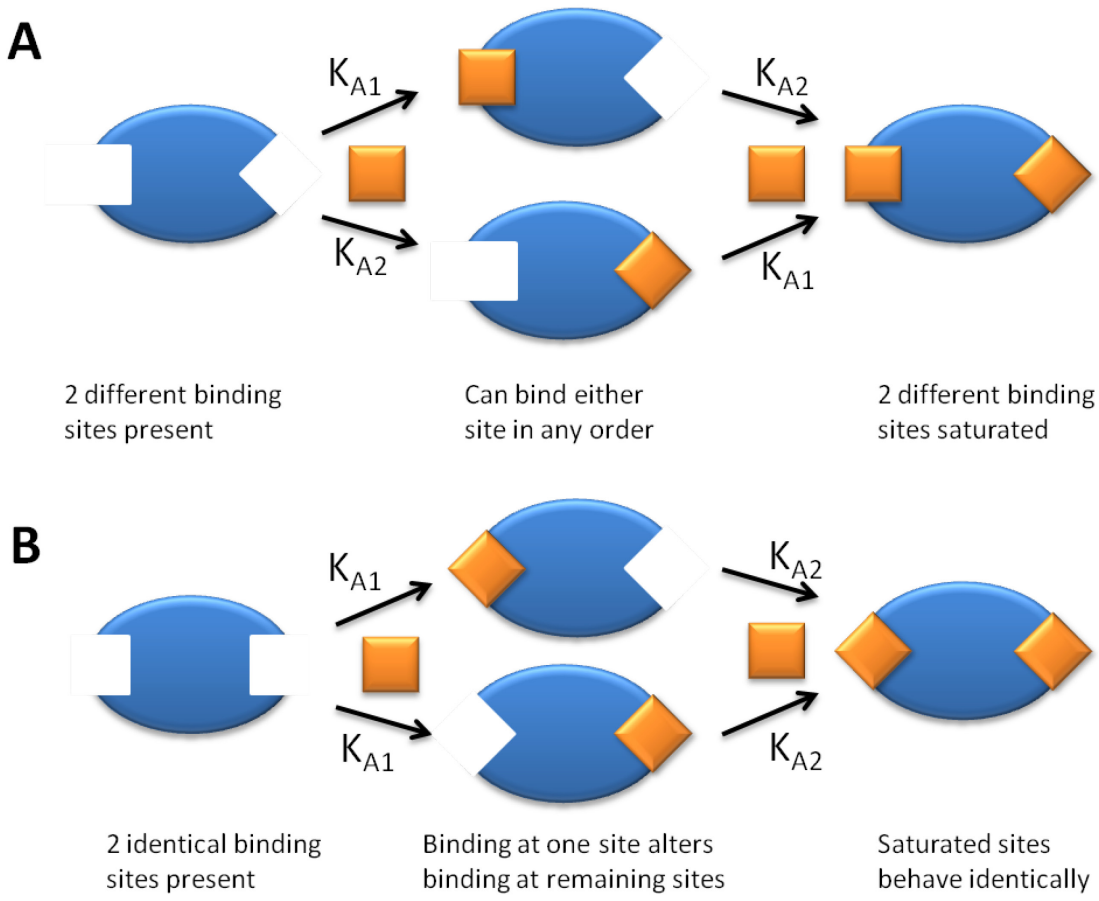

Fig. 2.2: Graphical representation of different binding models. A) Independent Model - binding sites are intrinsically different and can bind the ligand in any order. B) Seqential Binding Model - binding sites begin identical, binding at on site alters the affinity at second site. Sites at saturation point are again identical.

2.3 Applying models to AAC(6')-Ii

An example of a binding isotherm of AAC(6')-Ii with AcCoA is shown in Fig. 2.3. The experimental data were fit to both independent and sequential binding models, Fig. 2.3A and Fig. 2.3B respectively. The values for each fit are given in Table 2.1. As can be seen, both the independent and sequential binding

model agree well with the experimental data, and their residual sums of squares (RSS) = 4.11×10^4 vs 5.04×10^4 respectively. Although the multiple independent sites model has the number of type 1 binding sites as a small fraction even though the number of binding sites to a protein must be whole numbers, it cannot be eliminated for this reason alone. This problem can be resolved if there two non-exchangeable states of the protein present in solution, with a major state represented by type 2 sites and a minor state represented by type 1 sites. Regardless, it still provides a realistic model and has been used previously in studies of this enzyme.[45] The sequential model predicts that binding at the first site alters the binding at the second site. In this case $K_{A1} < K_{A2}$, so the sequential model predicts AAC(6')-Ii will bind AcCoA with positive cooperativity. From these initial results, both the independent and sequential binding models are possible. They both have physical descriptions to explain their results and fit the data equally well. To identify the correct model additional experiments must be performed.

Table 2.1: Comparisons of Independent and Cooperative Models

Model Type	K_{d1}[a](μM)	ΔH_{A1} [b] (kcal/mol)	n_1[c]	K_{d2}[a] (μM)	ΔH_{A2}[b] (kcal/mol)	n_2[c]	RSS[d]
Cooperative	11 ±1.9	-9.3 ±0.37	NA	5 ±1.2	-17 ±2.5	NA	5.04 ×10⁴
Independent	0.4 ±0.1	-4 ±1	0.29 ±0.05	4.2 ±0.1	-9.0 ±0.1	2.31 ±0.04	4.11 ×10⁴

[a] Equilibrium dissociation constant $1/K_A$. [b] Binding Enthalpy, $\Delta H = H_{occupied}-H_{free}$. [c] Effective number of binding sites. [d] Sum of squared residual differences between experimental and calculated data points.

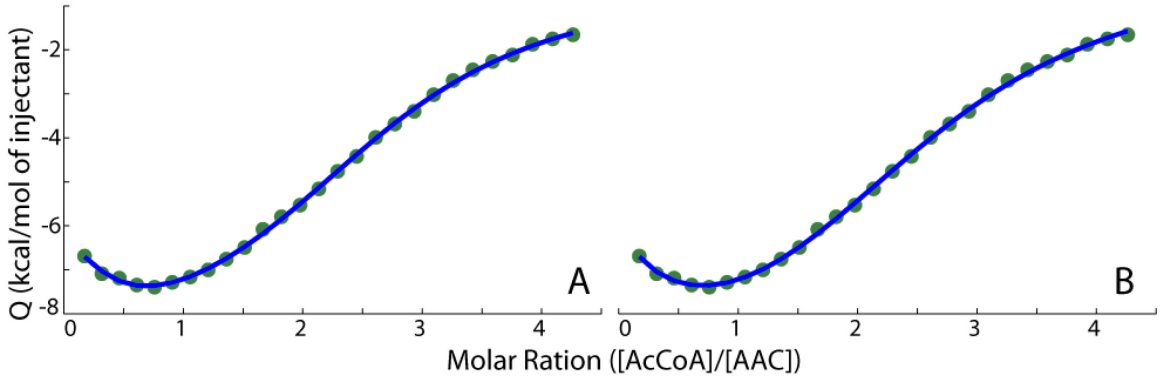

Fig. 2.3: ITC Isotherm of AAC(6')-Ii binding AcCoA at 20ºC fit to a A) multiple independent binding model and B) 2 site sequential binding model

2.4 ITC at Varying Concentrations

In the case of a single binding site, it is convenient to express the protein analyte concentration, $[P]_T$, in terms of the parameter $c \equiv [P]_T/K_d$. With ITC experiments performed with $[P]_T \gg K_d$ and thus high c values (>50) produce isotherms with sharp transitions occurring at$[X]_T = [P]_T$, in which $[X]_T$ is the total concentration of injected ligand. Data obtained with low $[P]_T$ and c values (<10)

produce isotherms with shallow slopes that extend to higher $[X]_T$: $[P]_T$ ratios.[108] This trend is also followed in more complicated systems with multiple binding sites. The shape of the ITC isotherm is dependent on the binding model, the physical binding parameters, and the c value. The binding model and the physical binding parameters should remain constant even when the protein concentration is altered. However the c value is directly related to the protein concentration. By adjusting the protein concentrations we can test the validity of both models, as the correct model should fit all concentration with the same binding parameters (i.e. ΔH_A and K_d). We find that the dependence of ITC isotherms on $[P]_T$ and c provides an effective criterion for selecting an appropriate binding model.

ITC experiments were performed on six different concentrations of AAC(6')-Ii ranging from 6-192 μM (Fig. 2.4). Each experiment was individually fit to both the independent and sequential models, and binding parameters were computed for each sample. The individual fits between the two models were then compared and shown on Table 2.2. The independent and sequential models fit each isotherm with a similar agreement, total RSS = 4.2×10^5 vs 5.5×10^5 respectively. The slightly lower RSS obtained from the independent model is due to the additional stoichiometric parameters (n_1 and n_2) not present in the cooperative model. This difference in not statistically significant with a $p = 0.11$.

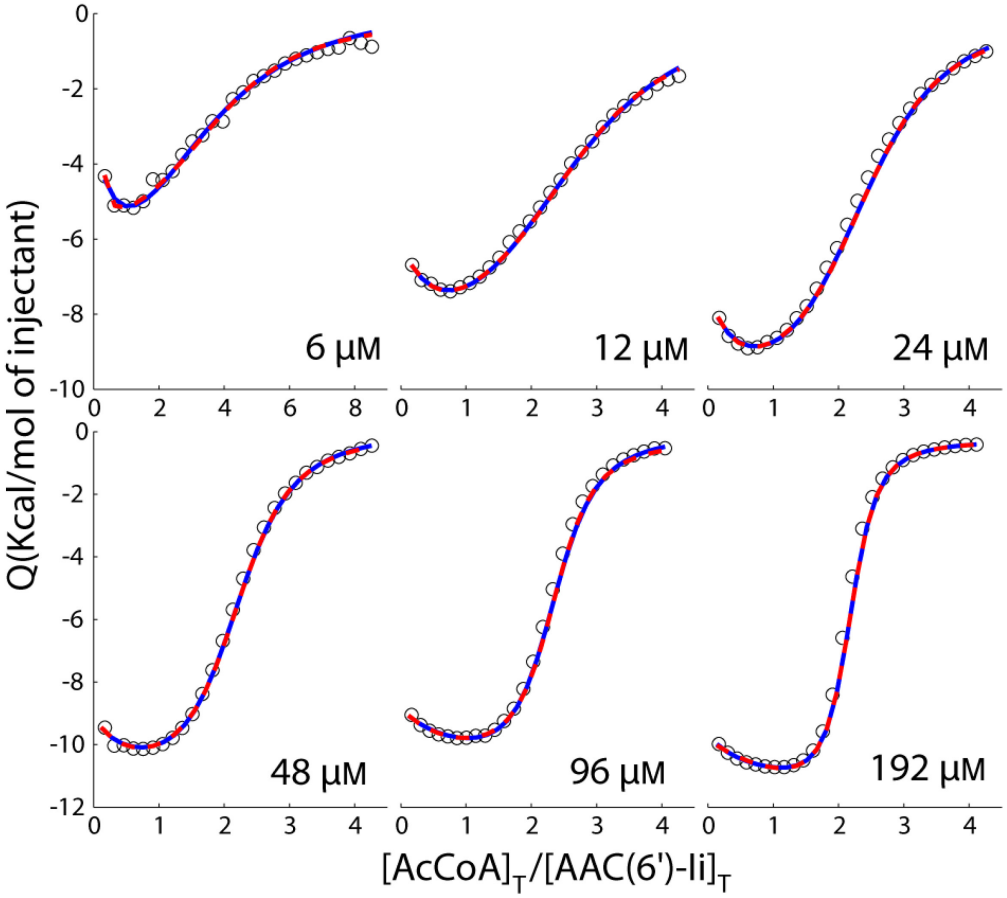

Fig. 2.4: Isotherm of AAC(6')-Ii at 6, 12, 24, 48, 96, and 192 µM titrated with AcCoA at 20ºC. Each isotherm is individually fitted to an independent (dashed red) and sequential (solid blue) models.

Table 2.2: Binding Parameters of Individual Fits

[AAC(6')-Ii] (μM)	Model Type	K_{d1}[a] (μM)	ΔH_{A1}[b] (kcal)	n_1[c]	K_{d2}[a] (μM)	ΔH_{A1}[b] (kcal)	n_2[c]	RSS[d]
6	Coop[e]	30 ±130	-17 ±89	-	5 ±12	-20 ±70	-	3.36×10^5
	Indep[f]	0.1 ±0.2	-3 ±6	0.3± 0.3	4.1 ±0.5	-6.3 ±0.4	3.5 ±0.5	2.50×10^5
12	Coop[e]	11 ±2	-9.3 ±0.4	-	5 ±1	-17 ±3	-	5.04×10^4
	Indep[f]	0.4 ±0.1	-4 ±1	0.29± 0.05	4.2 ±0.1	-9.0 ±0.1	2.31 ±0.04	4.11×10^4
24	Coop[e]	13 ±1	-9.7 ±0.1	-	4.5 ±0.4	-15.0 ±0.5	-	2.72×10^4
	Indep[f]	1.1 ±0.7	4×10^4 $\pm3\times10^{10}$	4×10^{-6} ±0.4	4.5 ±0.4	-11.00 ±0.04	2.30 ±0.04	2.10×10^4
48	Coop[e]	10 ±2	-10.00± 0.06	-	4.1 ±0.3	-14.0 ±0.2	-	5.49×10^4
	Indep[f]	2 ±3	6×10^3 $\pm3\times10^7$	3×10^{-4} ±1	5 ±2	-11.9 ±1.2	2 ±1	5.89×10^4
96	Coop[e]	9 ±1	-9.30 ±0.05	-	4.8 ±0.3	-13.2 ±0.2	-	6.21×10^4
	Indep[f]	2 ±1	7×10^3 $\pm2\times10^7$	3×10^{-4} ±1	4 ±1	-11.2 ±0.8	2 ±1	1.80×10^4
192	Coop[e]	4.2 ±0.4	-9.66 ±0.03	-	7.6 ±0.2	-12.3 ±0.06	-	1.51×10^4
	Indep[f]	2 ±3	800 $\pm5\times10^5$	4×10^{-3} ±4	4 ±3	-13 ±5	2 ±4	3.14×10^4

(a) Equilibrium dissociation constants. (b) Binding Enthalpy of association, $\Delta H = H_{occupied}-H_{free}$. (c) Effective number of binding sites. (d) Sum of squared residual differences between experimental and calculated data points (MATLAB). (e) Cooperative binding model comprising K_{d1}, ΔH_{A1}, K_{d2}, ΔH_{A2}, and a protein concentration correction factor. (f) Independent binding model comprising K_{d1}, ΔH_{A1}, n_1, K_{d2}, ΔH_{A2}, and n_2.

2.5 Global fitting approach

For individually fitting, the difference in the sum of RSS between the two models are not statistically significant, $p = 0.11$. As can be seen both fit the data with excellent agreement, RSS = 4.2×10^5 vs 5.5×10^5 respectively. However, when the ITC isotherms are subjected to a global fit with a single set of binding parameters the sequential model has better agreement with the data then the independent model, the RSS = 9.7×10^6 versus 2.4×10^7. This becomes noticeable in Fig. 2.5A and B, in which the sequential model and not the independent model follows the initial negative slope of the ITC isotherms. The improvement of the fit from the sequential to the independent binding model is statistically significant to a high level of confidence, $p = 2\times10^{-8}$. Analysis of the ITC data obtained from a single $[P]_T$ does not effectively discriminate between the two different binding models, while a global analysis of the variable-*c* dataset conclusively shows that the sequential model provides a better explanation of AcCoA binding to AAC(6')-Ii.

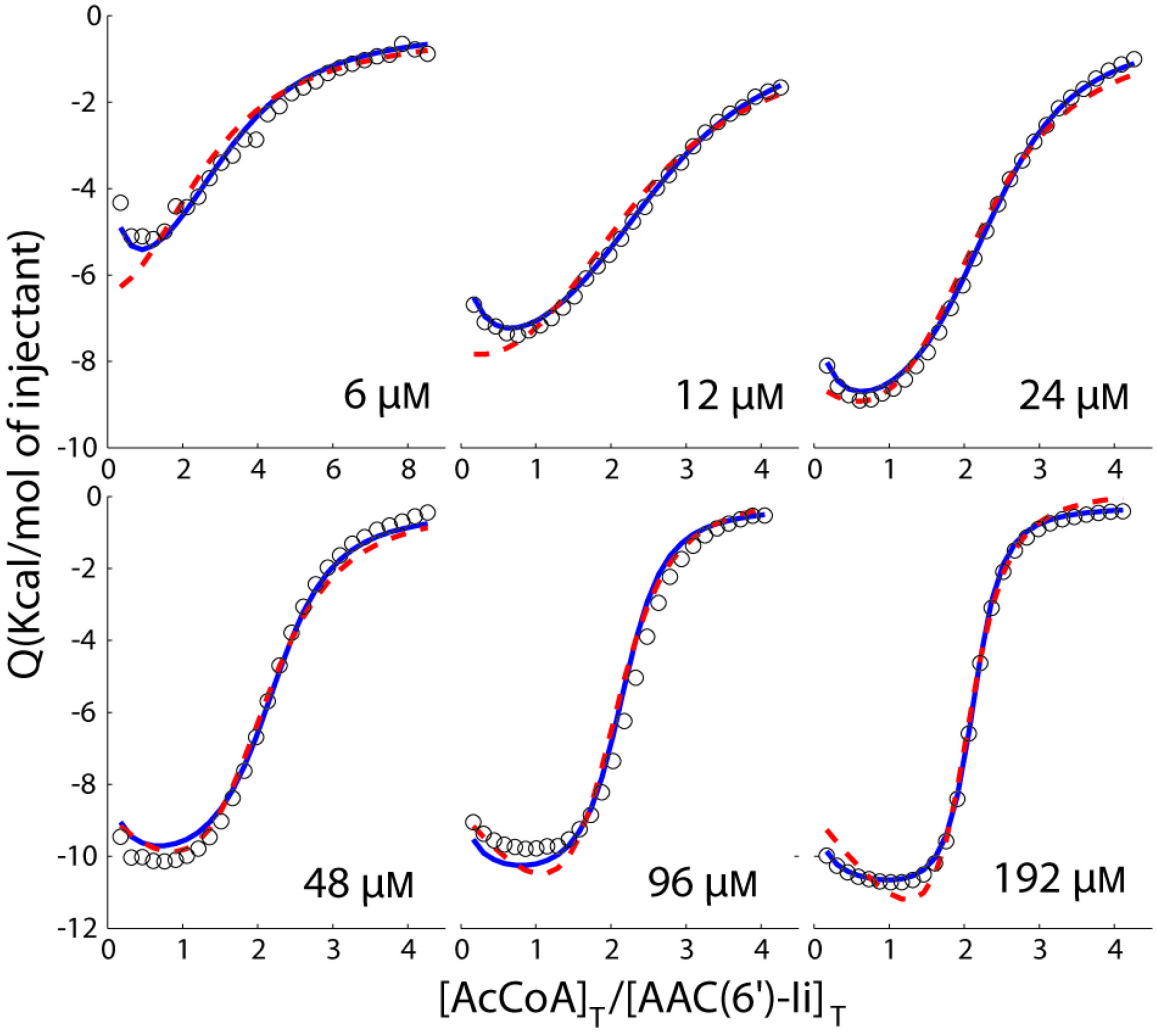

Fig. 2.5: ITC binding isotherms (circles) of AAC(6′)-Ii at 6, 12, 24, 48, 96, and192 µM titrated with AcCoA at 20 °C. Dashed red and solid blue lines correspond to global fits using the independent and cooperative models, respectively. Values of *c* range from 0.4–11 and 2–64 for the first and second binding events.

2.6 Binding Results

The sequential binding result is consistent with the structure of AAC(6')-Ii. The two binding sites are consistent with the two active sites of the homodimeric enzyme interacting cooperatively. These results also support previous reports of

kinetic analysis suggesting cooperativity.[45] The parameters extracted from either the cooperative or the independent fits are shown in Table 2.3. AAC(6')-Ii appears to bind AcCoA with positive cooperativity. This sixfold increase in affinity is mainly attributed to a difference in binding enthalpy, $\Delta H_{a2} - \Delta H_{a1} = -3.1$ kcal mol^{-1}. The difference in entropy between the first and the second binding event, $\Delta S_{a2} - \Delta S_{a1} = -6.8$ cal mol^{-1} K^{-1}, implies an additional exothermic event, likely disorder-to-order transitions in the protein and/or solvent, occuring during the binding to the second site. This event is investigated thoroughly in Chapter 4.

Table 2.3: Global Fitting Results

Model Type	K_{d1}[a] (μM)	ΔH_{A1} [b] (kcal/mol)	n_1[c]	K_{d2}[a] (μM)	ΔH_{A2}[b] (kcal/mol)	n_2[c]	RSS[d] ×10^6
Cooperative	17 ±1.4	-9.3 ±0.12	-	3.0 ±0.2	-13.0 ±0.18	-	9.7
Independent	7 ±4.1	-9×10^3 ±1.3×10^{10}	0.2 ±200	7 ±3.3	9×10^2 ±2.0×10^8	2 ±200	24

[a] Equilibrium dissociation constant. [b] Binding Enthalpy, $\Delta H = H_{occupied} - H_{free}$. [c] Effective number of binding sites. [d] Sum of squared residual differences between experimental and calculated data points.

The work of this chapter builds upon previous studies which employ global fitting of ITC datasets to elucidate complicated binding mechanisms.[124-126] When heterologous allostery is suspected in a multicomponent complex, ITC titrations

of one ligand may be performed at an array of different fixed concentrations of the second ligand.[124,126] However, this method cannot be applied to systems which exhibit homologous cooperativity. Alternatively, a titration and reverse titration datasets, where two titrations, ligand is titrated into the macromolecule and the macromolecule is titrated into the ligand, are globally fit.[124] This method can be problematic because high concentrations of both the host and ligand are needed.[124] The variable-c method described in this chapter can be applied to homologous systems and only requires one of the components to be present at high concentrations. A similar approach has been applied to a lipid-cholesterol interaction,[125] however this was the first use of this protocol to differentiate two different protein binding models.

2.7 Deriving Equations

The following equations describe the method to generate an ITC isotherm from either a 2-site independent or 2-site sequential binding model. The total heat released at any given point in a titration is expressed as Q. In a simple two state system, Q is expressed as[127]

$$Q = n\Theta[P]_T\Delta H_A V_c, \quad 2.1$$

where n is the number of sites, Θ is the fraction of sites occupied by the ligand, $[P]_T$ is the total protein concentration, ΔH_A is the enthalpy of binding, and V_c is the volume of the sample cell. The value of Θ is dependent of the concentration of

the ligand ($[X]_T$) and the association constant. In systems which there are more than one binding site, the expression for Q becomes much more complicated and will be described below. ITC isotherms were fitted using equations defining the change in the Q value for each injection, i, given by the expression[127]

$$\Delta Q(i) = Q(i) - Q(i-1)\left(1 - \frac{V_i}{V_c}\right) + Q_0 \qquad 2.2$$

which takes into account the displaced volume from the sample cell after each injection.[127] V_i is the volume of the i^{th} injection, $Q(i)$ is the value of the heat function after the i^{th} injection, and Q_0 is the heat which accounts for the heat released during mixing. The total heat released, $Q(i)$ is dependent on the concentrations of the ligand, $[X]_T$, and protein, $[P]_T$, present in the sample cell after n injections, with a total volume of V_i. This is given by the expression

$$[X]_T = [X]_0\left(1 - \left(1 - \frac{V_i}{V_c}\right)^n\right) \qquad 2.3$$

$$[P]_T = [P]_0\left(1 - \frac{V_i}{V_c}\right)^n \qquad 2.4$$

where $[X]_0$ is the concentration of ligand in the syringe and $[P]_0$ is the initial protein concentration. The value of Q is dependent on the binding model which the macromolecule follows. In a system with two different binding sites the simplest possible models involve either independent or sequential binding. The heat function for both models are calculated in terms of $[X]_T$, $[P]_T$ and the binding parameters as follows.

2.7.1 Independent binding model

The independent model describes a macromolecule which contains 2 independent binding sites each with n sites with a dissociation constant (K_d) for the ligand and the host, and enthalpy of binding (ΔH_A). There can be a different number of type 1 sites and type 2 sites so a n value given for each type of site. This gives a total of six variables: n_1, n_2, K_{d1}, K_{d2}, ΔH_{A1}, and ΔH_{A2}. The fraction of saturation of site 1 and site 2 is determined by[127]

$$\Theta_1 = \frac{[X]}{K_{d1} + [X]} \text{ and } \Theta_2 = \frac{[X]}{K_{d2} + [X]} \quad 2.5$$

where $[X]$ is the concentration of free ligand in solution. Θ_1 and Θ_2 are the fraction state of site 1 and site 2 respectively. The total concentration of ligand present is given by

$$[X]_T = [X] + [P]_T(n_1\Theta_1 + n_2\Theta_2) \quad 2.6$$

Substituting equation 2.5 into 2.6 gives the third order polynomial as follows

$$a + b[X] + c[X]^2 + [X]^3 = 0 \quad 2.7$$

where

$$a = -K_{d1}K_{d2}[X]_T$$
$$b = (K_{d2}n_1 + K_{d1}n_2)[P]_T - (K_{d1} + K_{d2})[X]_T + K_{d1}K_{d2}$$
$$c = K_{d1} + K_{d2} + (n_1 + n_2)[P]_T - [X]_T$$

The concentration of the free ligand, $[X]$, at any combination of $[X]_T$, $[P]_T$ and dissociation constants is the positive real root of equation 2.7 which can be determined numerically, in this case the bisection method was used.[128] By

substituting [X] into equation 2.5 the fractions of bound protein, Θ_1 and Θ_2, can be determined. Finally the heat function of the independent model is given by

$$Q(i) = [P]_T(i)V_c(n_1\Theta_1(i)\Delta H_{A1} + n_2\Theta_2(i)\Delta H_{A2}) \quad 2.8$$

where ΔH_{A1} and ΔH_{A2} are the binding enthalpies (H_{bound}-H_{free}) for site 1 and site 2, respectively. While $[P]_T(i)$, $\Theta_1(i)$ and $\Theta_2(i)$ are the total enzyme concentration and the fraction of the singly and doubly bound proteins after i injections respectively.

2.7.2 Sequential binding model

A simple sequential binding model describes a macromolecule which contains multiple binding sites which are affected by the ligation state of the other binding sites. These binding sites are coupled and binding at one site alters the binding parameters of the remaining site. Unlike the independent model, the macromolecule is assumed to have a fixed number of binding sites, in this case 2. For 2 sequential sites there are four adjustable parameters: K_{d1}, K_{d2}, ΔH_{A1}, and ΔH_{A2}. The first ligand can bind to the protein at either binding site of the free protein, P→PX, with a dissociation constant $K_{d1,}$[127]

$$K_{d1} = \frac{[P][X]}{[PX]} \quad 2.9$$

The second ligand binds to the remaining unoccupied site of the singly bound protein, PX→PX_2, with a dissociation constant $K_{d2,}$

$$K_{d2} = \frac{[PX][X]}{[PX_2]} \quad 2.10$$

The fractions of protein with a single ligand bound, Θ_1, and protein with two ligands bound, Θ_2, are given by the expressions

$$\Theta_1 = \frac{2K_{d2}[X]}{K_{d1}K_{d2} + 2K_{d2}[X] + [X]^2} \quad 2.11$$

and

$$\Theta_2 = \frac{[X]^2}{K_{d1}K_{d2} + 2K_{d2}[X] + [X]^2} \quad 2.12$$

while the concentration of the total ligand in solution is

$$[X]_T = [X] + [P]_T(\Theta_1 + 2\Theta_2) \quad 2.13$$

Through substituting 2.11and 2.12 into 2.13 the following cubic expression is obtained

$$a + b[X] + c[X]^2 + [X]^3 = 0 \quad 2.14$$

where

$a = -K_{d1}K_{d2}[X]_T$
$b = -K_{d1}K_{d2}([P]_T - [X]_T)$
$c = 2K_{d2} + 2[P]_T - [X]_T$

Similarly to the independent model, the positive real root of equation 2.14 gives the concentration of the free ligand, $[X]$. This value substituted into equation 2.11 and 2.12 gives Θ_1 and Θ_2. The total heat released from binding the ligand is dependent on the values for Θ_1 and Θ_2. The fraction of protein with a single ligand bound (Θ_1) will have released heat equivalent to the enthalpy from the first

binding event, ΔH_{A1}. However, the fraction of protein with two ligands bound (Θ_2) will have released heat equivalent to the enthalpy from the first binding event and the second binding event, ΔH_{A1} and ΔH_{A2}. Therefore the heat released from Θ_2 fraction is ΔH_{A1} + ΔH_{A2}. Therefore the heat function for the sequential model is given by

$$Q(i) = [P]_T(i)V_c\left(\Theta_1(i)\Delta H_{A1} + \Theta_2(i)(\Delta H_{A1} + \Delta H_{A2})\right) \quad 2.15$$

In this case ΔH_{A1}=H_{PX}-H_P and ΔH_{A2}=H_{PX2}-H_{PX}.

2.7.3 Obtaining the best fit

The best fit for both models was obtained through a non-linear regression of the binding parameters to obtain the minimum RSS between the experimental data points and those calculated in equation 2.1 ,

$$\mathrm{RSS} = \sum_i \left(\Delta Q(i)_{calc} - \Delta Q(i)_{exp}\right)^2, \quad 2.16$$

where in individual fits the sums include all the data points in a single ITC titration

In an attempt to differentiate between the two models, all six isotherms were fit to a single set of binding parameters. The best fit was again obtained through non linear regression to obtain the minimum RSS, equation 2.16, between the experimental data points and those calculated through equation 2.1. For the global fits the sums include all the data points from all the ITC titrations.

2.7.4 Statistical probability

The agreement of experimental ITC data with different binding models was analyzed by using F-statistics, according to the expression[129]

$$F = \frac{\mathrm{RSS}_1}{\mathrm{RSS}_2}\frac{v_2}{v_1} \tag{2.17}$$

in which RSS_1, RSS_2 and v_1, v_2 are the residual sum of squared deviations and the degrees of freedom for the two models, and $RSS_1 > RSS_2$. The probability that a value of F as large or larger than the one observed would be obtained if model 1 fit the data as well or better than model 2 was calculated as[130]

$$P = I\frac{v_2}{v_2 + v_1 F}\left(\frac{v_2}{2}, \frac{v_1}{2}\right) \tag{2.18}$$

in which I is the incomplete beta function.

2.7.5 Experimental error

Uncertainties in the fitted parameters were obtained from the covariance matrix, which is given by the expression[131-132]

$$V = \frac{\mathrm{RSS}}{v}(XWX^T)^{-1} \tag{2.19}$$

where

$$X = \begin{bmatrix} \frac{\partial F_1}{\partial K_{d1}} \cdots \frac{\partial F_i}{\partial K_{d1}} \\ \frac{\partial F_1}{\partial K_{d2}} \cdots \frac{\partial F_i}{\partial K_{d2}} \\ \frac{\partial F_1}{\partial \Delta H_{A1}} \cdots \frac{\partial F_I}{\partial \Delta H_{A1}} \\ \frac{\partial F_1}{\partial \Delta H_{A2}} \cdots \frac{\partial F_1}{\partial \Delta H_{A2}} \end{bmatrix}, \tag{2.20}$$

$$F_i = \Delta Q(i)_{calc} - \Delta Q(i)_{exp}, \quad 2.21$$

and the derivatives are evaluated numerically at the optimized values of the binding parameters. W is a diagonal matrix of the fitting weights, which in this case are equal to 1, and v is the number of degrees of freedom of the fit. The diagonal elements of V are the variances of the K_d and ΔH_d parameter estimates.

2.8 Discussion

The variable-c ITC method requires the ITC isotherms to vary as a function of protein concentration. To show the applicability of this method, arrays of different binding conditions were simulated (Fig. 2.6). Each panel consists of a different cooperative binding scenario with a series of ITC isotherms calculated with different protein concentrations and identical binding parameters. In all cases, the ITC isotherms varies greatly between the different values of $[P]_T$ and lend themselves toward global fitting. Interestingly, the greatest variations of the isotherms occur at low concentration of $[P]_T$, with a c value below 1 for the weaker binding site. This range of c is below the suggested value used for most ITC experiments, as was explained in the introduction, yet appears to be optimal for studying complex binding mechanisms. Accurate values for K_d can be obtained from isotherms with low c values but the enthalpy of binding component may be ill-defined.[133] Therefore it is important that isotherms with a higher c

*v*alue are included in the variable-*c* data set so the enthalpy of binding can be accurately determined.

To work at low c values requires very dilute protein concentrations. This can be a problem due to the relatively small amount of heat released or absorbed from a sample with a low concentration of protein. In systems with very high affinities, the concentrations required to reach a low *c* value may release too little heat to be measured by the instrument. The sensitivity of an experiment is determined by the parameter $h \equiv [P]_{\mathrm{T}}\Delta H_A$.[132] For the experiments described herein the lowest value of h measured was 0.06 cal L^{-1} which corresponds to the first binding event of the most dilute protein sample. This event would release about 3 µcal on average per injection. The sensitivity MicroCal VP-ITC used for these experiments requires the heat released from the injection to be at least 1 µcal.[134] This method should then tolerate systems with an h value threefold lower then used here, which in turns allows for systems with a 3 fold higher affinity (K_{A}) or a 3 fold lower binding enthalpy (ΔH_{A}). Through optimization of injection volumes the range could be extended to even lower h values.[132] The high concentration end of the variable-c dataset requires the solubilities of the protein and ligand to reach a c value of at least 10.

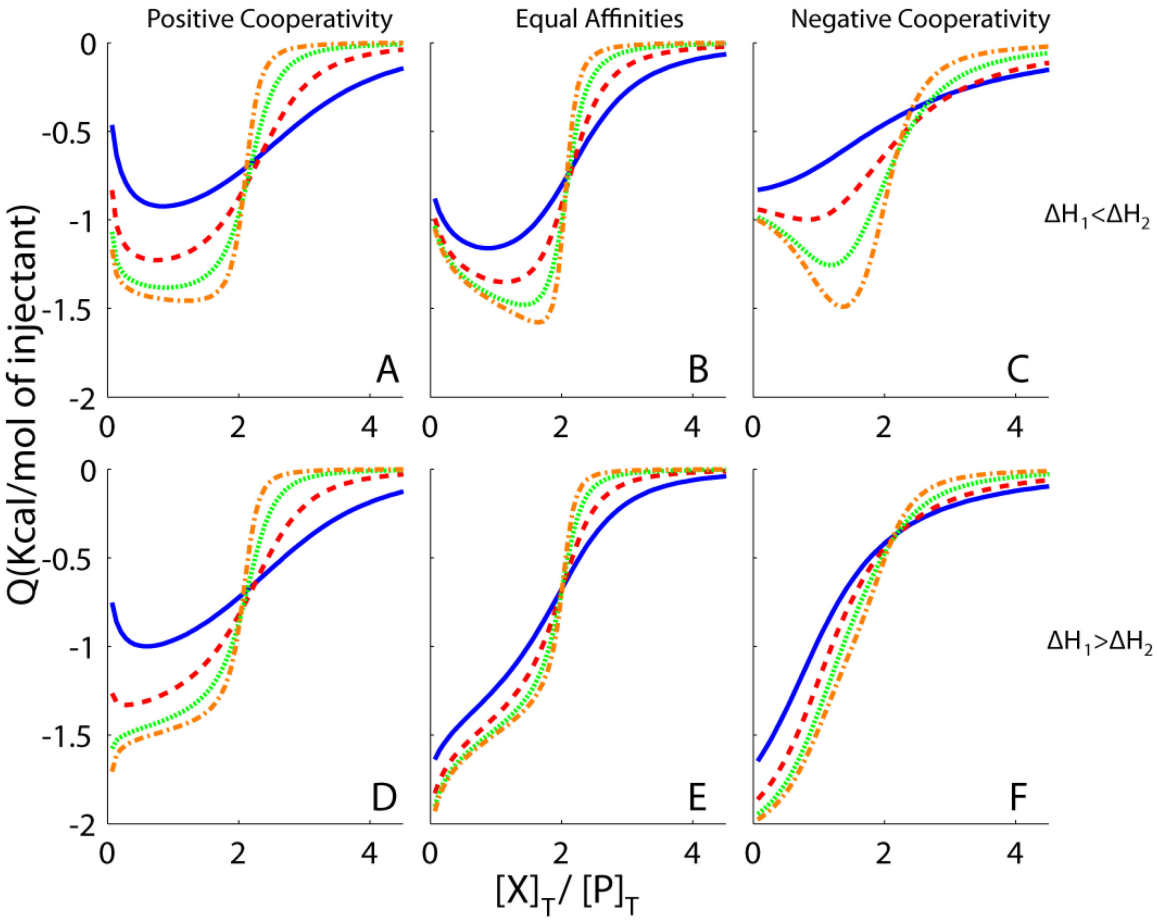

Fig. 2.6: Theoretical ITC isotherms generated according to a 2-site cooperative model, with $[P]_T$=0.5, 1.5, 4.5, 13.5 μM for the blue solid, red dashed, green dotted, and orange dash dotted lines respectively. A) and D) show positively cooperative, C) and F) show negatively cooperative datasets. B) and E) correspond to systems in which both ligands bind with equal affinities, but with different enthalpies. In A)–C), $|\Delta H_2|>|\Delta H_1|$. In D)–F), $|\Delta H_2|<|\Delta H_1|$. Values of K_{d1} (μM), K_{d2} (μM), ΔH_1(kcal mol^{-1}), ΔH_2(kcal mol^{-1}) employed are: A) 10, 1, −1, −2; B) 10, 10, −1, −2; C) 1, 10, −1, −2; D) 10, 1, −2 ,−1; E) 10, 10, −2, −1 F) 1, 10, −2, −1.

Typically, ITC studies of macromolecular interactions involve replicate experiments performed at near identical concentrations. It is proposed here that it would be advantageous to repeat ITC experiments at different c $v$alues and

globally fit the results. Systems which appear to behave with a 1:1 stoichiometry could have more complex binding mechanisms revealed through global analysis of variable-c ITC datasets. Additionally, variable-c ITC can help determine if apparent binding thermodynamics are influenced by protein self association. In situations where significant amount of protein self associates, a variable-c dataset would not likely fit to any simple model. Nevertheless, global fits can have concentration dependent effects incorporated into the model.[124] It should be noted that this method uses dilute protein concentrations and should not be affected by any additional concentration effects compared to standard experiments performed at a single c value. Finally, in systems like AAC(6')-Ii, where ITC isotherms collected at a single concentration are fit equally well with multiple different binding models, the variable-c ITC method clearly identifies the model which better represents the system. Thus, global fitting of variable-c ITC datasets provides simple and effective method to identify correct models to interpret data, and help improve our understanding of protein/ligand interactions.

3 Using the van't Hoff relation to globally fit a variable temperature isothermal titration calorimetry data set

3.0 Preface

In this chapter, the interactions between acetyl coenzyme A (AcCoA) and a monomeric mutant (ie. W164A) of the (normally dimeric) enzyme aminoglycoside *N*-6'-acetyltransferase-Ii (AAC(6')-Ii W164A) were studied. Tryptophan 164 is located at the dimer interface. Replacement of this tryptophan with alanine reduces the interactions between the subunits and results in the protein being present as a monomer in solution. Using isothermal titration calorimetry (ITC), the binding of AcCoA to AAC(6')-Ii W164A is shown to be quite weak at temperatures above 25°C. This results in a high level of uncertainty in the values of apparent binding enthalpy (ΔH_A^{app}) and the apparent association constants (K_A^{app}) extracted from individual ITC isotherms. Apparent curvature in the ΔH_A^{app} temperature profile for individual fits suggests that the mechanistic model for binding might involve coupled folding upon ligand binding. Circular dichroism (CD) data support this model, as suggested by a temperature dependent loss of secondary structure. There is a large amount of scatter in the binding parameters which makes it difficult to determine the level of agreement with this model. A global fitting approach was applied to the variable temperature data set which used the *van 't* Hoff relation as a physical constraint. The scatter in the ΔH_A^{app} and K_A^{app} values was significantly reduced, allowing the curvature in both temperature profiles to be precisely defined. Quantitative agreement was

obtained between CD and the globally-fit ITC data. This confirmed that binding is coupled to protein folding and allowed for the thermodynamics of both steps of the reaction to be clearly distinguished.

The work presented in this chapter was performed by me under the guidance of Dr. Mittermaier and Dr. Auclair.

3.1 Introduction

As seen in earlier chapters, ITC allows characterization of the thermodynamic parameters involved during molecular interactions. This is made possible via measurements of the heat which is released or absorbed as a ligand is titrated into a sample cell containing its binding partner.[134] In this chapter binding models are divided into two main classes; these will be referred to as phenomenological (macroscopic) binding models and mechanistic (microscopic) binding models. Phenomenological binding models make no assumptions about the underlying mechanisms of binding and rely only on the stoichiometry of interaction. From the binding polynomial, the phenomenological model which contains n identical ligand consists of exactly n+1 different themodynamic states (0 bound, 1 bound ... n bound) with 2n thermodynamic parameters (n enthalpies and n affinity constants).[135] For example, systems with a 1:1 binding stoichiometry can have their data explained with 2 different states (i.e. 0 bound, 1

bound) and 2 thermodynamics parameters, K_A^{app} and ΔH_A^{app}. While systems with a 2:1 binding stoichiometry can have their data explained with 3 states (i.e. 0 bound, 1 bound, 2 bound) and 4 thermodynamic parameters, the 2 binding affinities (K_{A1}^{app} and K_{A2}^{app}) and the 2 enthalpies of binding(ΔH_{A1}^{app} and ΔH_{A2}^{app}). The phenomenological model fits any system with the given stoichiometry. The thermodynamic parameters thus measured are also referred to as macroscopic or apparent binding parameters. However, these parameters do not describe how the binding occurs at the microscopic level, as they are a convolution of all events which occur during binding. The phenomenological model is able to describe which bound state the system is in, but not how it got there, or what changes have had to occur. Mechanistic models, in contrast, describe the binding event in detail and propose a specific hypothesis regarding the physical processes. This can involve an arbitrarily large number of physical states and microscopic thermodynamic parameters which describe the measurements in enthalpy, entropy, free energy, and heat capacity. Mechanistic models relate directly to the physical events which occur during binding, such as conformational changes or ionizations. Due to this additional information, mechanistic models are of greater interest then phenomenological models.

Typically ITC data are analyzed through a two step process.[135] First, the raw ITC isotherms are fitted using a phenomenological model. This produces

apparent ΔH_A^{app} and K_A^{app} of binding. These parameters are then fit to a specific mechanistic model and the corresponding model-specific thermodynamic parameters are obtained. A great deal of information can be gained through performing ITC experiments over a wide range of temperatures. Mechanistic models can be fitted to sets of ΔH_A^{app} and K_A^{app} values obtained at different temperatures, shedding light on the relationship between ligand binding and conformational changes in the protein or additional coupled equilibria.[102,116,136] In a simple two-state system (free and bound), ΔH_A^{app} varies linearly with temperature, provided that the difference in heat capacity between the free and bound states remain constant.[137] If a binding event is linked to additional equilibria, such as thermal denaturation, the dependence of ΔH_A^{app} on temperature can be curvilinear.[102] If several equilibria are involved which produce multiple binding competent states, the temperature dependence of ΔH_A^{app} can give highly complex profiles.[138] Many different physical events can influence the temperature dependence of ΔH_A^{app}, such as: folding/unfolding, ionization, dimerization.[139-140] By analyzing the temperature dependence of phenomenological binding parameters one can obtain important information to determine the correct mechanistic binding model and identify the underlying physical processes involved in binding. This approach requires precisely defined experimental data, and even fairly modest errors in ΔH_A^{app} and K_A^{app} can make it

very difficult or impossible to make quantitative conclusions about the physical processes involved. There are several possible experimental situations which can cause elevated errors in ΔH_A^{app} and K_A^{app} parameters. These include but are not limited to, low affinities[133], small changes in enthalpy, or the presence of multiple non-equivalent binding sites on the host (such is the case of AAC(6')-Ii).[140-141]

The previous chapter demonstrated that by fitting several ITC isotherms to a single set of binding parameters one can greatly increase the accuracy of the measured binding parameters. As mentioned previously, this global fitting has been applied to many different systems with successful results.[55,114,126,142-146] Using this approach, one could improve the accuracy of the experimental binding parameters which, in turn, can be used to elucidate the correct mechanistic model. To globally fit a data set, all isotherms must be related mathematically. A variable-*c* approach could be used to reduce errors. However, the standard phenomenological binding models do not include temperature variations, so they cannot be used to link a variable temperature dataset in a global fitting approach. Therefore each temperature would be fit independently of all other temperatures. In contrast, mechanistic binding models detail exact mechanisms of binding so they can address temperature dependence of binding parameters in ITC isotherms. Currently, all the variable temperature global fits have fit a

mechanistic model directly to the ITC isotherms,[143-145] but this forces a predetermined model onto the experimental data. This can be problematic when the binding parameters are poorly defined, as accurate binding ΔH_A^{app} and K_A^{app} values are important for determining which mechanistic binding model is appropriate.

This chapter explains a novel approach for the global analysis of a variable temperature dataset without the requirement of an a priori determined mechanistic model. This new method is referred here as the *van 't* Hoff global fit. All models regardless of their mechanism must follow the *van 't* Hoff relation

$$\frac{\partial \ln\{K_A^{app}\}}{\partial T} = \frac{\Delta H_A^{app}}{RT^2} \qquad 3.1$$

If a set of numbers do not follow this relationship they are not physically reasonable. The integrated form of the *van 't* Hoff equation was used to simultaneously analyze the raw ITC isotherms obtained at a variety of temperatures. This strategy constrains the extracted values of phenomenological binding parameters to a set of physically reasonable values and yields sets of binding ΔH_A^{app} and K_A^{app} values with improved accuracy compared to those obtained from fits of individual ITC isotherms. No prior binding information beyond the binding stoichiometry is required for analyzing the isotherms. The parameters thus computed can be used to design and test mechanistic binding models.

Chapter 2 showed that the wild type enzyme binds AcCoA with a 2 site sequential binding model. In this chapter, *van 't* Hoff global analysis was used on the model system of AAC(6')-Ii W164A with AcCoA. Trp164 is located at the dimer interface of the two subunits in AAC(6`)-Ii, and its substitution with Ala destabilizes the dimer and produces a monomeric protein with about 10% of the wild-type activity.[45] The monomeric mutant only binds a single molecule of AcCoA, and is therefore a much simpler system to study. The *van 't* Hoff global analysis is also utilized in later chapters to describe more complex binding interactions. Chapter 4 details wild type AAC(6')-Ii binding AcCoA and Chapter 5 details wild type AAC(6')-Ii binding the aminoglycoside paromomycin.

3.2 Variable temperature ITC

ITC experiments were performed on mutant AAC(6')-Ii W164A titrated with AcCoA at 10, 15, 20, 25, 30, 34, 37, and 40°C. The resulting isotherms are shown in Fig. 3.1. The ITC isotherms were initially fit individually to obtain the phenomenological binding parameters for ΔH_A^{app} and K_A^{app} (Fig. 3.2 and Table 3.1). There is a large varience in the values obtained between each experiment, in particular for K_A^{app}. This is likely due to the low affinity of AAC(6')-Ii W164A for AcCoA ($K_A^{app} \approx 3.2\times10^3$ M^{-1} at 40°C). The low K_A^{app} makes it challenging to achieve a high c-value and fully saturate the protein by the end of the titration

due to the high concentrations required for both the ligand and protein. However, it is apparent that there are some trends present. From 10 to 30°C the change in heat capacity (ΔC_p) remains constant; this results in ΔH_A^{app} of binding varying linearly with temperature (Fig. 3.2). Above 30°C the ΔH_A^{app} varies non-linearly with temperature resulting in a large increase in the ΔC_p. This behaviour is characteristic of coupling between a binding event and an additional conformational transition or ionization equilibrium.[116] As discussed below, CD spectroscopic measurements indicate that the protein undergoes a partial or complete unfolding around 30°C. This suggests that ligand binding is coupled to a protein conformational change under these conditions.

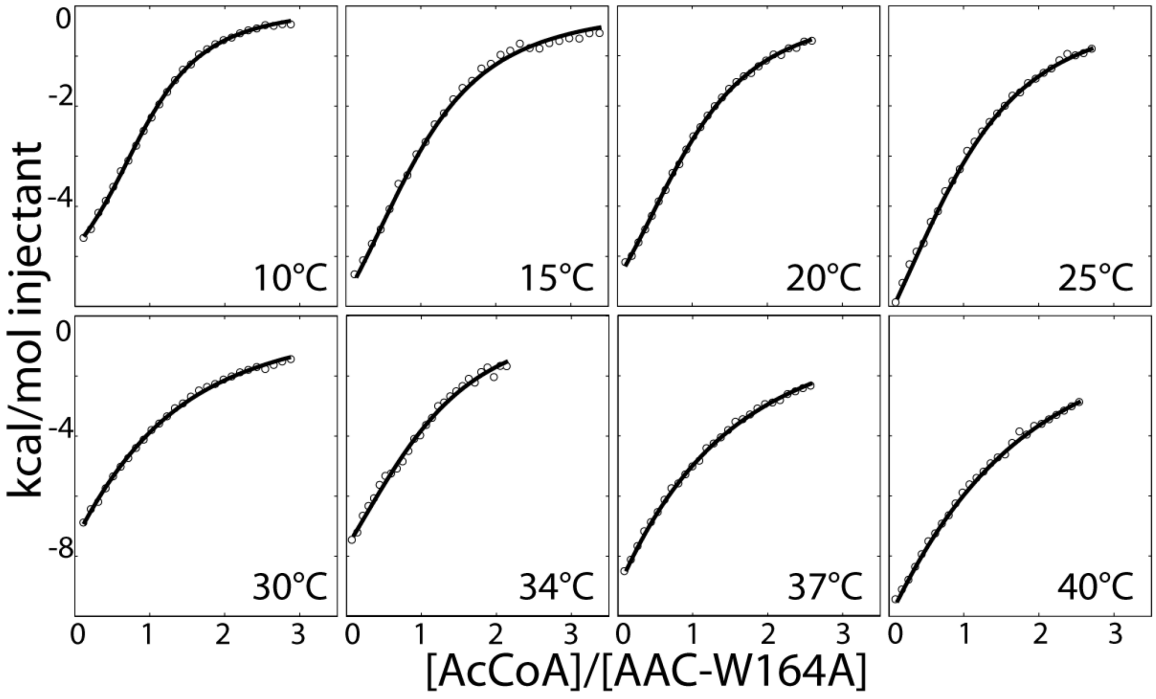

Fig. 3.1: ITC Isotherms of AcCoA binding to AAC(6')-Ii W164A at 10, 15, 20, 25, 30, 34, 37, and 40 ºC. Experimental data (open circles) is individually fit (black line) to a one site binding model.

3.3 Circular Dichroism

Circular dichroism (CD) is the difference of absorption of left-handed (negative) and right handed (positive) circularly polarized light. This occurs when a molecule contains a chiral chromophore. Proteins are chiral molecules and preferential absorb circular polarized light. For proteins, the direction of rotation absorbed is dependent on the structure that the protein adopts. The wavelength range of 220 to 230 nm gives a negative molar ellipticity for alpha helices and beta sheets (folded)[147-148] and a positive molar ellipticity for random coil (unfolded)[147-149]. This range is ideal to monitor the transition from defined

secondary structures (alpha helices and beta sheets) to an unfolded state (random coil). As mentioned above, a sudden change in ΔC_p can be linked to a folding/unfolding event. CD spectroscopy can detect changes in secondary structure through the change of molar ellipticity. CD spectra of AAC(6')-Ii W164A were measured from 0.1-70°C in increments of 1°C. At low temperatures, the molar ellipticity at 222 nm was on the order of -9000 deg cm^2 $dmol^{-1}$. As the temperature increases, the molar ellipticity in this range sigmoidally approaches zero. This suggests that AAC(6')-Ii W164A undergoes partial or complete thermal unfolding. This process is completely reversible up to ~50°C, so only data from 0.1 to 47°C will be used for further analysis.

3.4 Coupled folding and binding

The data from both ITC and CD suggest that the appropriate mechanistic binding model to describe the association of AcCoA with AAC(6')-Ii W164A is one in which a thermal unfolding event is linked to binding. In this model there are two unbound states, a folded state (**F**) and an unfolded state (**U**). Moreover, only the **F** state is binding-competent, and hence in order for the protein in the **U** state to bind ligand it must first fold to the **F** state. This suggests the following scheme[116,150]

$$U + L \underset{}{\overset{K_F, \Delta H_F, \Delta C_{p,F}}{\longleftrightarrow}} F + L \underset{}{\overset{K_A, \Delta H_A, \Delta C_{p,A}}{\longleftrightarrow}} FL$$

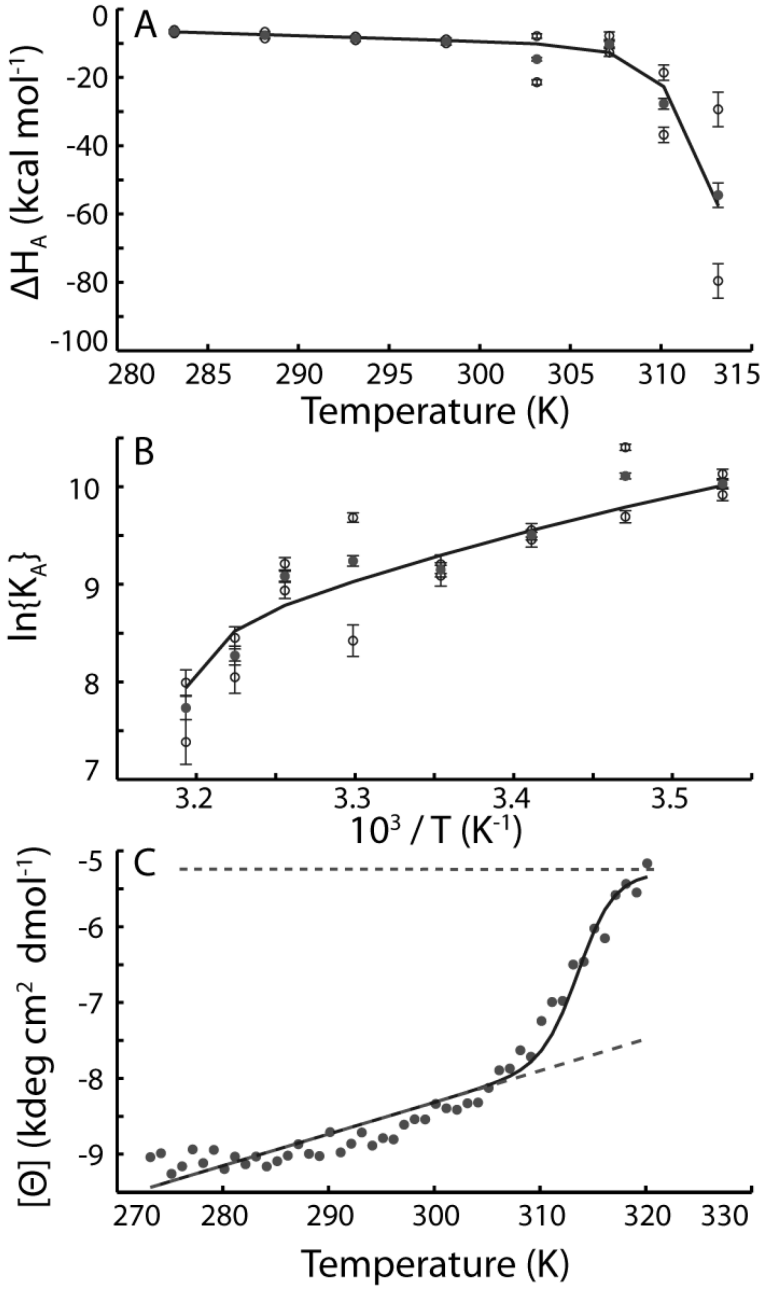

Fig. 3.2: Coupled folding/binding analysis of (A) ΔH_A^{app}, and (B) K_A^{app}, values obtained from fits of individual ITC isotherms, together with (C) circular dichroism spectroscopic data (222 nm). In A and B, open circles indicate the values obtained for individual replicate experiments (two per temperature), while the solid circles are the pair-wise averages (ΔH_A^{app}(indiv) and K_A^{app}(indiv)). In (C), the upper and lower dashed lines correspond to the unfolded and folded ellipticity baselines, respectively.

where ΔH_F, ΔH_A and $\Delta C_{p,F}$, $\Delta C_{p,A}$, are the changes in enthalpy and heat capacity for the folding and binding steps, while K_F = [**F**]/[**U**] and K_A = [**F**L]/([**F**][L]) are equilibrium constants. As with most folding events, the transition from the **U** to the **F** state is exothermic ($\Delta H_F < 0$) and entropically disfavoured. At low temperatures, the protein is mostly folded. At these temperatures, the macroscopic binding affinity and binding enthalpy are simply given by K_A and ΔH_A. At increased temperatures, there is an appreciable amount of unfolded protein (**U**). This requires transitions from **U** to **F**L. The macroscopic binding affinity and binding enthalpy from ITC will contain components from both folding and binding events. The phenomenological binding constants can be defined as:

$$K_A^{app}(T) = \frac{K_F(T)}{1 + K_F(T)} K_A(T) \quad 3.2$$

$$\Delta H_A^{app}(T) = \Delta H_A(T) + \frac{1}{1 + K_F(T)} \Delta H_F \quad 3.3$$

where

$$K_X(T) = K_X(T_0) \times e^{\left\{\frac{\Delta H_X(T_0)}{R}\left(\frac{1}{T_0} - \frac{1}{T}\right) + \frac{\Delta C_{p,X}}{R}\left(\ln\left\{\frac{T}{T_0}\right\} + \frac{T_0}{T} - 1\right)\right\}}, \quad 3.4$$

$$\Delta H_X(T) = \Delta H_X(T_0) + \Delta C_{p,X}(T - T_0) \quad 3.5$$

X = F or A, and T_0 is an arbitrary reference temperature, in this case 283.15 K. It is possible to extract the values of $K_F(T_0)$, $K_A(T_0)$, $\Delta H_F(T_0)$, $\Delta H_A(T_0)$, $\Delta C_{p,F}$, and $\Delta C_{p,A}$ from sets of K_A^{app} and ΔH_A^{app} values determined by ITC over a range of temperatures. However, due to the large covariance between the parameters this becomes difficult, and leads to unreliable estimates of their values based on

ITC data alone. Cliff *et al.* have shown that it is possible to combine CD measurements with ITC to overcome this problem.[102] As mentioned earlier in this chapter, CD measurements can detect changes in secondary structure of proteins. The **U** and **F** states contain different amounts of secondary structure, so CD measurements represent an independent measurement of the folding equilibrium constant, K_F. This allows for the determination of the other microscopic binding and folding parameters from the macroscopic parameters. This procedure can then be used to validate the *van 't* Hoff global fit which will be described later in the chapter.

A single wavelength for CD was chosen to measure the folding equilibrium. Alpha helices give a spectral minimum for the molar ellipticity at 222 nm. This wavelength was therefore monitored to determine the folding equilibrium.[102] The temperature dependence of the molar ellipticity was modeled through the following expression[102]

$$[\theta](T) = \frac{K_F(T)}{1 + K_F(T)}\left([\theta]_F + m_F(T - T_0)\right) + \frac{1}{1 + K_F(F)}\left([\theta]_U + m_U(T - T_0)\right), \qquad 3.6$$

which assumes that the overall signal is the population-weighted average of the folded and unfolded signals, and that both baselines are linear functions of temperature. The variables $[\theta]_F$ and $[\theta]_U$ are the molar ellipticities of the folded and unfolded states at the reference temperature, and m_F and m_U are the corresponding baseline slopes. Unfortunately, the unfolding baseline, m_U, is not

well defined, because the CD melts can only be obtained partway through the unfolding transition due to the irreversible unfolding. Fortuitously, CD studies of protein thermal denaturation typically yield approximately a horizontal baseline.[102,151-153] Therefore, analysis was performed by optimizing for $[\theta]_U$ while fixing m_U near zero. The final results were unaffected by the precise choice of m_U, and in the following analysis m_U =0.

CD data and ITC-derived values of ΔH_A^{app} and K_A^{app} were simultaneously fit to equation 3.2 - 3.6, to provide the data shown in Fig. 3.2. The best fit for the folding model was obtained through non-linear regression of the binding parameters to obtain the minimal residual squared differences (RSS) between the K_A^{app}, ΔH_A^{app} and [θ] and those calculated equations 3.2 - 3.6,

$$\mathrm{RSS} = \sum \left(\frac{\ln\{K_A^{app}\} - \ln\{K_A^{app}\}_{calc}}{\ln\{K_A^{app}\}} \right)^2 + \sum \left(\frac{\{\Delta H_A^{app}\} - \{\Delta H_A^{app}\}_{calc}}{\{\Delta H_A^{app}\}} \right)^2 + \sum \left(\frac{[\Theta]_{exp} - [\Theta]_{calc}}{[\Theta]_{exp}} \right)^2 . \quad 3.7$$

The overall agreement was reasonable, but the scatter in the data makes it difficult to judge the overall quality of the fits. Furthermore, there are small but systematic deviations between the calculated and CD data (Fig. 3.2C). Before this mechanistic model is rejected or accepted, the scatter in the ITC derived parameters must be addressed. In the next section, a global fitting procedure will be explained which link together ITC isotherms from different temperatures using the *van 't* Hoff relation.

3.5 *van 't* Hoff method for global fitting of ITC isotherms

To properly address the scatter observed in the ITC-derived values there can be no assumptions regarding the underlying mechanism of binding, as this could introduce bias into the fit and cause one to come to incorrect conclusions. A restriction should only be applied to a fit if it occurs in every possible physical model. One such restriction is the *van 't* Hoff relation. For any model to be physically possible it must follow the *van 't* Hoff expression

$$\frac{\partial \ln\{K\}}{\partial \mathrm{T}} = \frac{\Delta H}{\mathrm{R}T^2} \qquad 3.8$$

This expression can constrain the values of $\Delta H_{\mathrm{A}}^{\mathrm{app}}$ and $K_{\mathrm{A}}^{\mathrm{app}}$ within the global fits. This will ensure that the values obtain are physically possible and will greatly reduce the scatter in the obtained binding parameters. Thus, the binding enthalpy, $\Delta H_{\mathrm{A}}^{\mathrm{app}}(T_{\mathrm{n}})$, is optimized for each temperature, and only an association constant for a single temperature (K_{A,T_0}^{app}) is fitted. The remaining association constants are obtained from the set of $\Delta H_{\mathrm{A}}^{\mathrm{app}}(T_{\mathrm{n}})$ and the integrated form of equation 3.8

$$\ln\{K_A^{app}(T_n)\} = \ln\{K_A^{app}(T_0)\} + \frac{1}{R}\int_{T_0}^{T_n} \frac{\Delta H_A^{app}(T)}{T^2}\, dT. \qquad 3.9$$

The last term in equation 3.9 is evaluated by trapezoidal numerical integration, in which the function $\Delta H_{\mathrm{A}}^{\mathrm{app}}(T)/T^2$ is approximated by a series of straight lines connecting the experimental $\Delta H_{\mathrm{A}}^{\mathrm{app}}(T_{\mathrm{n}})/T_{\mathrm{n}}^2$ points (Fig. 3.3). This approach

greatly reduces the number of adjustable variables and improves the accuracy of the extracted parameters. Additionally, the approach does not restrict the possible mechanistic model, as every possible physical model must obey the *van 't* Hoff relation. The only assumption is that the numerical integral of $\Delta H_A^{app}(T)/T^2$ is evaluated accurately.

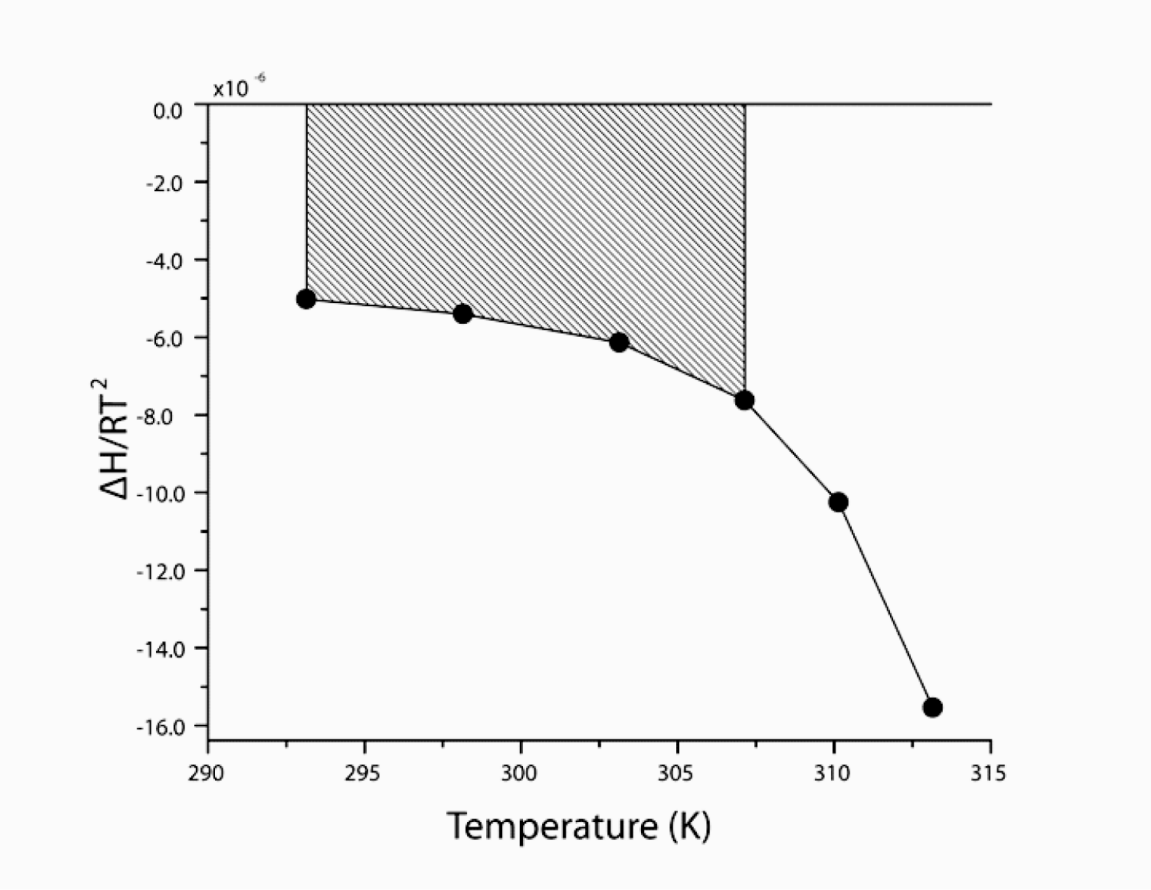

Fig. 3.3: Schematic representation of trapezoidal integration of $\Delta H_A/RT^2$. The points represent the fitted values of ΔH_A, divided by the corresponding values of RT^2. The difference in binding affinity between temperatures T_i and T_{ii} corresponds to the shaded area, i.e. K_A^{app}(ii) = K_A^{app}(i) + shaded area. Thus the $\Delta H_A^{app}/RT^2$ profile together with the single value of K_A^{app}(i) specifies the affinity constants at all other temperatures.

3.5.1 Application of *van 't* Hoff method to AAC(6')-Ii W164A

The experimental ITC isotherms obtained at all temperatures for the titration of AcCoA into AAC(6')-Ii W164A were refit simultaneously using the *van 't* Hoff global approach (Fig. 3.4, Table 3.1, and Appendix Figure A.1). This yielded a new set of values, denoted as ΔH_A^{app}(global) and K_A^{app}(global). The agreement between the predicted and the experimental isotherms are good (Fig. 3.4). The residual sum-of-squares only increases by a factor of 2.5 relative to the individual fits. Additionally, the temperature dependence of ΔH_A^{app}(global) and K_A^{app}(global) appear smoother than those of ΔH_A^{app}(indiv) and K_A^{app}(indiv). At many temperatures, the values from the *van 't* Hoff global approach and individual fits are similar. However, at higher temperatures, values from the two approaches deviate greatly, in particular for ΔH_A^{app} (Table 3.1). For example, at 40°C the average ΔH_A^{app}(indiv) and ΔH_A^{app}(global) differ by more than 20 kcal mol^{-1}. These deviations may explain why the folding model (equations 3.2-3.6) contained systematic deviations in the combined CD and individual ITC fit Fig. 3.2.

Table 3.1: Thermodynamic parameters from individual and global fits of ITC data[a].

	Individual Fits[b]		Global Fits	
T (°C)	ΔH_A^{app} (kcal mol $^{-1}$)	K_A^{app} ($\times 10^3$ M^{-1})	ΔH_A^{app} (kcal mol $^{-1}$)	K_A^{app} ($\times 10^3$ M^{-1})
10	-7.1±0.1	20±1	-6.89±0.06	21.5±0.3
	-6.1±0.1	25±1		
15	-8.6±0.2	16±1	-7.75±0.08	17.2±0.3
	-6.7±0.2	33±1		
20	-9.1±0.3	13±1	-8.5±0.1	13.5±0.2
	-8.0±0.3	14±1		
25	-10.0±0.5	1±1	-9.4±0.1	10.4±0.2
	-8.8±0.5	9±1		
30	-7.9±0.7	16.0±0.8	-11.1±0.2	7.9±0.2
	-21.4±0.7	4.5±0.8		
34	-13±1	7.6±0.7	-14.3±0.3	6.0±0.2
	-8±1	1.0±0.7		
37	-37±2	3.1±0.5	-19.2±0.6	4.6±0.2
	-19±2	4.7±0.5		
40	-29±5	3.0±0.4	-28±2	3.2±0.2
	-80±5	1.6±0.4		

[a] Errors are taken as the standard deviations of values extracted from Monte Carlo simulations.

[b] There are two isotherms for tempterature and each isotherm is fit individually so each temperature has two obtained values.

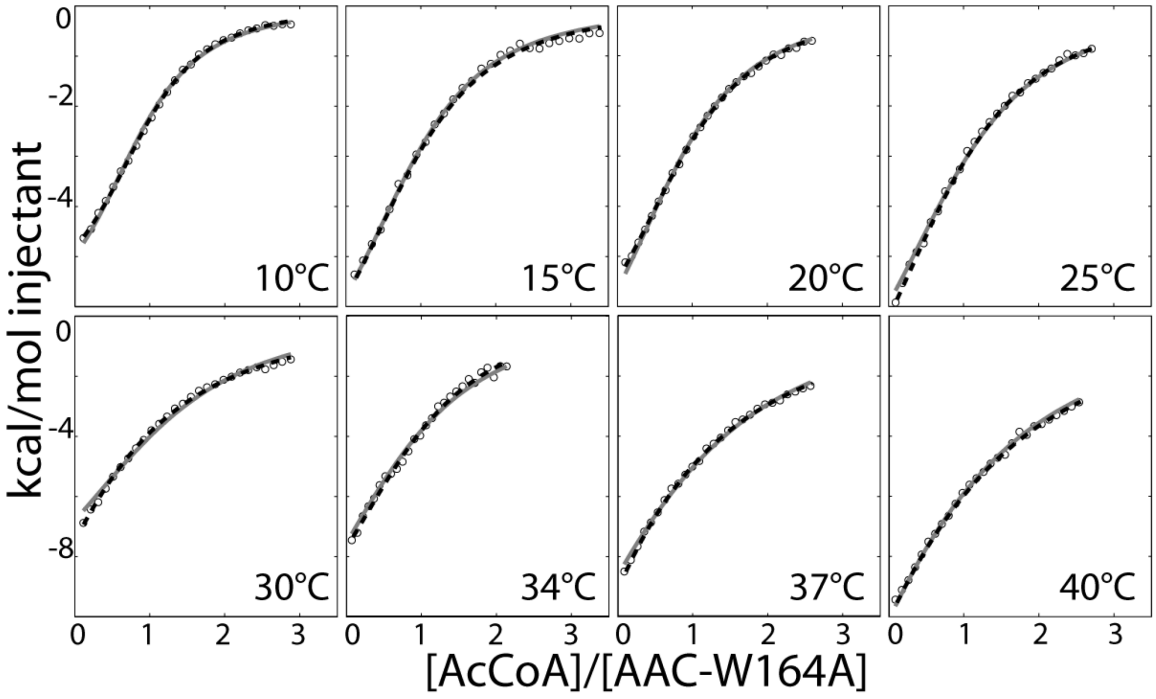

Fig. 3.4: ITC Isotherms of AcCoA binding to AAC(6')-Ii W164A at 10, 15, 20, 25, 30, 34, 37, and 40 ºC. Experimental data (open circles) is individually fit (black dashed) or globally fit (grey line) through the *van 't* Hoff approach to a one site binding model

The coupled folding and binding model used above to fit ΔH_A^{app}(indiv) and K_A^{app}(indiv) was used to fit the values ΔH_A^{app}(global) and K_A^{app}(global). Again equations 3.2 - 3.6 were used to optimize the fit with the same CD temperature melt data, shown in Fig. 3.5. Excellent agreement was obtained between the CD data and the globally-fit ITC values, which confirms that the coupled folding/binding model is an appropriate mechanistic binding model. The level of agreement obtained for the global values is far better than the individual fit ITC isotherms. The RSS deviations for ΔH_A^{app}(global) and K_A^{app}(global) for the

coupled folding/binding mechanistic model are 10 fold lower compared to the ΔH_A^{app}(indiv) and K_A^{app}(indiv). Additionally, the parameters obtained from *van 't* Hoff global fit differ greatly from the values from the individual fits (Table 3.2). The improved fits obtained through ΔH_A^{app}(global) and K_A^{app}(global) strongly suggest that *van 't* Hoff global fitting approach provides a clearer picture of the interactions between AAC(6')-Ii W164A with AcCoA.

Table 3.2: Coupled folding/binding parameters for individual and global fits of ITC data

	Individual Fits	Global Fits
$\Delta H_A(T_0)$ (kcal mol^{-1})	-6.8±0.1	-7.5±0.1
$K_A(T_0)$ ($\times 10^3$ M^{-1})	22±1	22.4±0.5
$C_{p,A}$ (kcal mol^{-1} K^{-1})	-0.02±0.03	-0.08±0.02
$\Delta H_F(T_0)$ (kcal mol^{-1})	-120±10	-53±3
$K_F(T_0)$	(1.38±0.08)$\times 10^6$	24±5
$C_{p,F}$ (kcal mol^{-1} K^{-1})	0±0.5	-2.1±0.2
$[\theta]_F$ (deg cm^2 dmol^{-1})	-7700±300	-8000±100
$[\theta]_U$ (deg cm^2 dmol^{-1})	-5300±200	-4500±200
m_F (deg cm^2 dmol^{-1} K^{-1})	41±8	42±3
RSS	0.299	0.011

T_0 = 283.15 K. Errors are taken as the standard deviations of parameters extracted from coupled folding/binding fits using $\Delta H_A^{app,MC}$(global & indiv) and $K_A^{app,MC}$(global & indiv) values obtained from global and individual analyses of synthetic Monte Carlo ITC datasets.

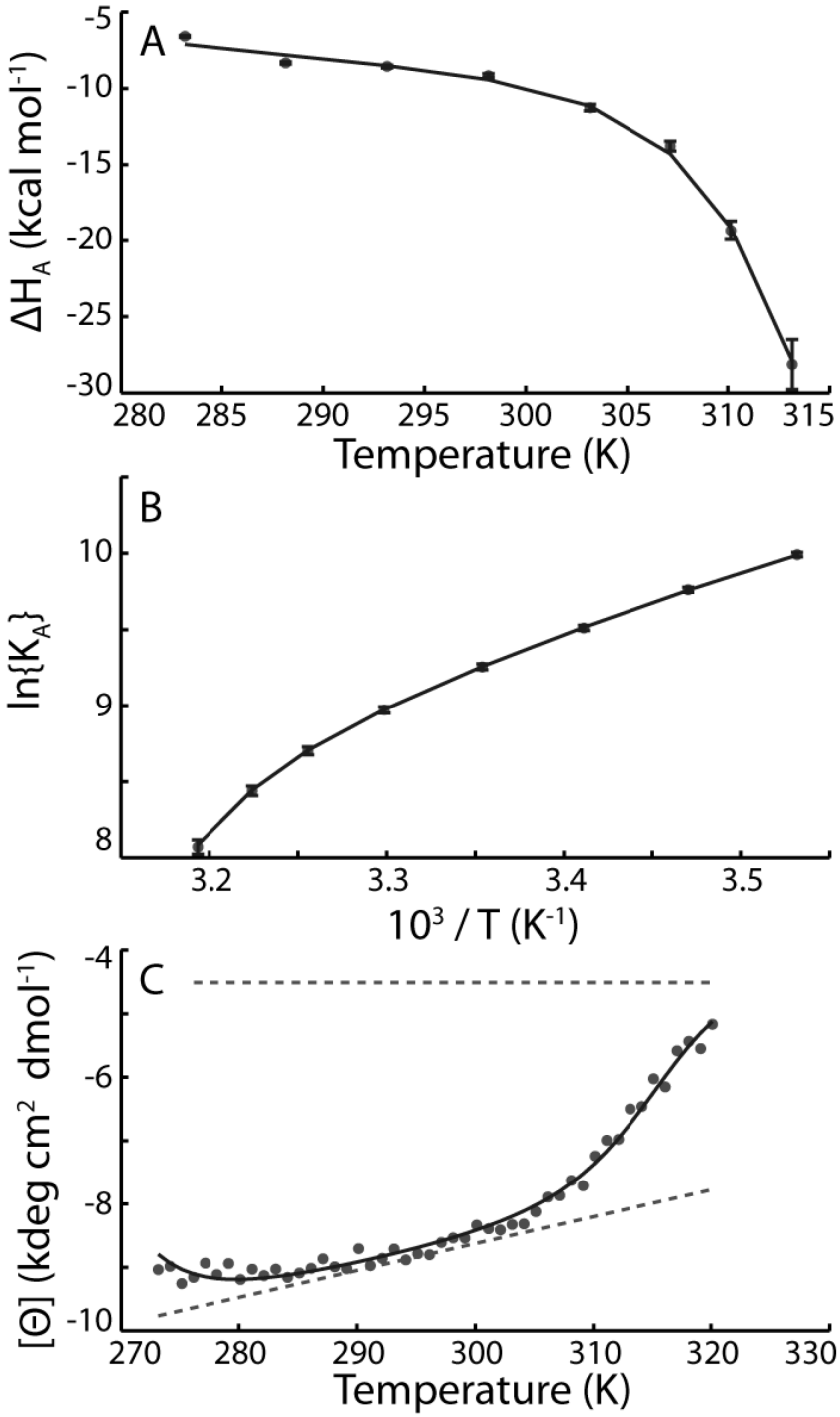

Fig. 3.5: Coupled folding/binding analysis of (A) ΔH_A^{app}(global) and (B) K_A^{app}(global) values obtained from a simultaneous fit of all 16 ITC isotherms, together with (C) circular dichroism spectroscopic data (222 nm). In (C), the upper and lower dashed lines correspond to the unfolded and folded ellipticity baselines, respectively.

The model predicts that the unfolding event linked to binding of AcCoA to AAC(6')-Ii W164A is 50% complete at 42°C, with a $\Delta C_{p,F}$ = -2.1 kcal mol^{-1} K^{-1} and ΔH_F = -52.9 kcal mol^{-1} at this temperature. These values are consistent with unfolding events in proteins the size of AAC(6')-Ii W164A (182 aa). Robertson and Murphy reported that the ΔC_p of globular proteins can be approximated by the relation -(N_{res}×14 cal mol^{-1} K^{-1}), while the ΔH (extrapolated to 100ºC) is given by -(N_{res}×1.26 kcal mol^{-1}), where N_{res} is the number of residues.[154] The experimental values, $\Delta C_{p,F}$ = -2.1 kcal mol^{-1} K^{-1} and ΔH_F(100ºC) = -176 kcal mol^{-1} are comparable, but smaller than those predicted by the empirical relationships, ΔC_p^{pred} =-2.5 kcal mol^{-1} K^{-1} and ΔH^{pred} =-229 kcal/mol. This reduction could be due to the **F** state being only slightly more stable then the **U** state. The CD traces also suggest that the enzyme undergoes cold denaturation at around 0 °C, and that at the most stable temperature of 17ºC only 3% of the enzyme is present in the unfolded **U** state. This increases to about 25% at 37ºC. The mutation at Trp 164 may play a role in the mutant's stability, as the unfolding transition for the mutant is broader (Fig. 3.6) compared to the wild type. In addition, the absolute molar ellipticity is lower in the mutant then the wild type enzyme, which suggests decreased secondary structure in the mutant. However, wild type protein does undergo thermal denaturation in the same

temperature range. Chapter 4 will further discuss the stability of the wild type enzyme.

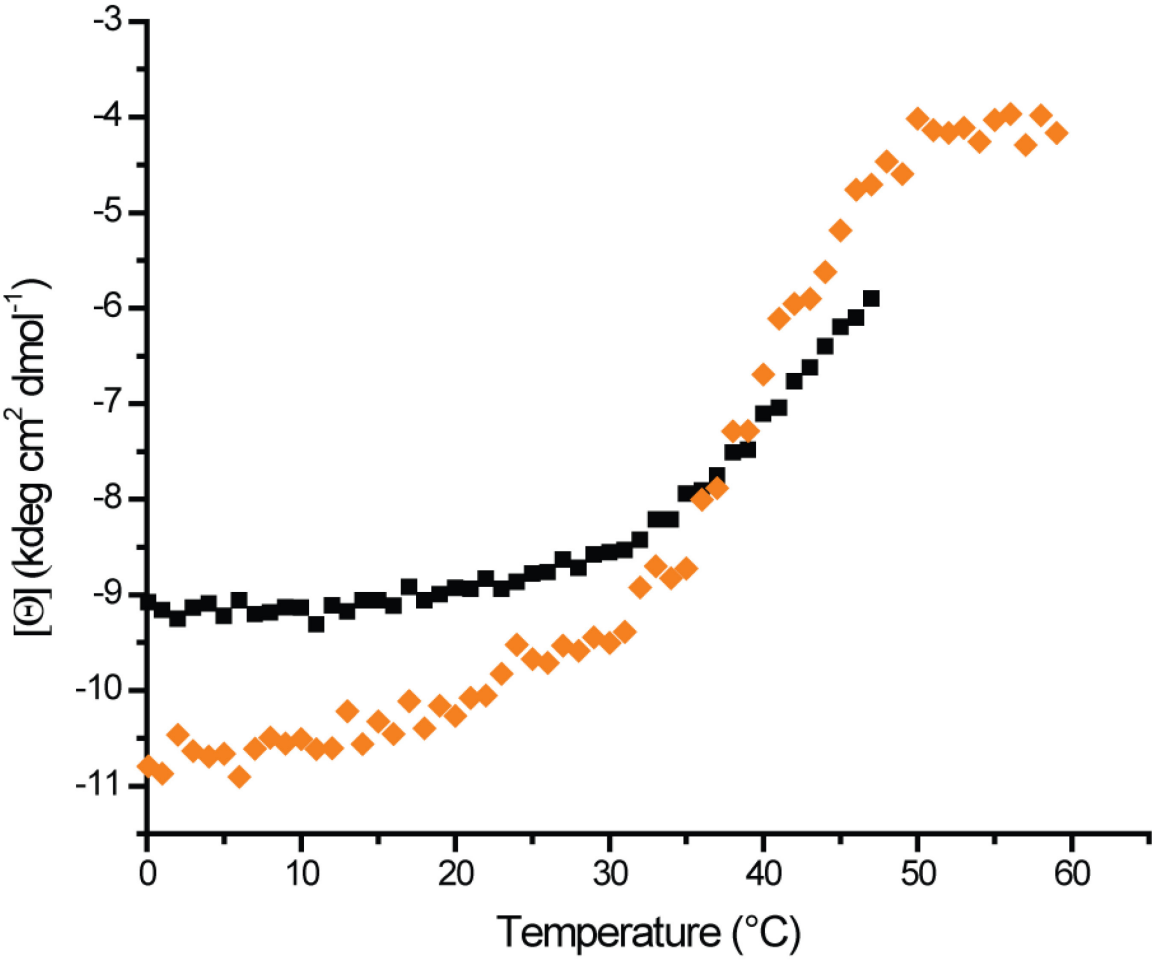

Fig. 3.6: CD molar ellipticities of the aminoglycoside 6'-N-acetyltransferase-Ii W164A mutant (■), and wild-type (◆) measured as a function of temperature at a wavelength of 222 nm. Unfolding of the W164A mutant is reversible up to about 47°C, so data beyond this temperature in not shown. Unfolding of the wild-type protein is reversible over the entire temperature range tested.

3.6 Monte Carlo error analysis

It is important to ensure that the *van 't* Hoff global fitting approach is a generally applicable as a method for improving accuracy of ITC data analysis. To test the utility of the *van 't* Hoff approach a series of Monte Carlo (MC) simulations were performed. All of the fits obtained through the MC analysis extracted the phenomenological binding parameters, ΔH_A^{app} and K_A^{app}.

The coupled folding/binding mechanistic model parameters obtained from the globally-fit ITC data were used to calculate theoretical ΔH_A^{app} and K_A^{app} values at 10, 15, 20, 25, 30, 34, 37, and 40°C (Fig. 3.7). From these values, 300 datasets were generated which consisted of 16 isotherms with random experimental errors (2 isotherms for each temperature). Each MC dataset was fit both individually and through the *van 't* Hoff global approach. The individual fitting yielded two ΔH_A^{app} and K_A^{app} values at each temperature and the van't Hoff analysis produced only a single value for each temperature, ΔH_A^{appMC}(global) and $K_A^{app,MC}$(global). The two individual values were averaged and these pair-wise averages will be referred to $\Delta H_A^{app,MC}$(indiv) and $K_A^{app,MC}$(indiv). The two fitting procedures produced 300 Monte Carlo ΔH_A^{app} and K_A^{app} temperature series, which are shown in Fig. 3.7.

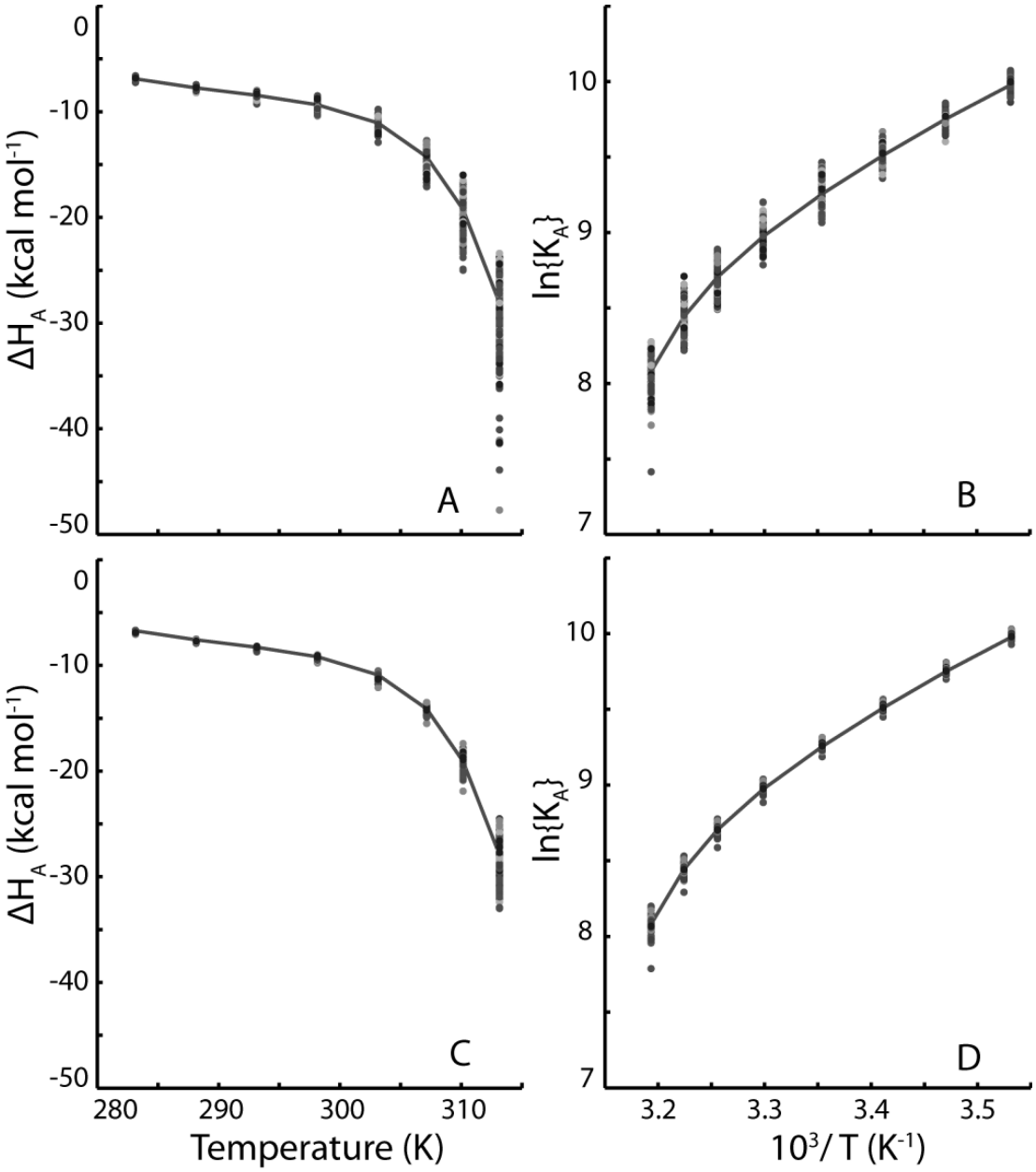

Fig. 3.7: Plots of $\Delta H_A^{app,MC}$ and $K_A^{app,MC}$ values extracted from fits of Monte-Carlo ITC datasets generated using the coupled folding/binding parameters obtained for AAC-W164A and AcCoA. In all panels, the fitted parameters are indicated by points, while the true values are shown as lines. (A,B) Results are pair-wise average for individual analyses, where the points correspond to fitted values of (A) $\Delta H_A^{app,MC}$(indiv) and (B) $K_A^{app,MC}$(indiv). (C,D) Results for *van 't* Hoff global analyses, where points correspond to fitted values of (C) $\Delta H_A^{app,MC}$(global) and (D) $K_A^{app,MC}$(global).

Individual fits produce $\Delta H_A^{app,MC}$(indiv) and $K_A^{app,MC}$(indiv) values with a large amount of scatter. Even with averaging two individual values, there appears to be broad distribution, especially at higher temperatures. This scatter is consistent with the experimental fits obtained with AAC(6')-Ii W164A data (Fig. 3.2). Meanwhile, the $\Delta H_A^{app,MC}$(global) and $K_A^{app,MC}$(global) values from the *van 't* Hoff fitting approach produce much less scatter. The error calculated in the individual fits is around 2 fold higher compared to the *van 't* Hoff fits. The relative errors for the individual fit are 2% at 10°C and 13% at 40°C compared to the *van 't* Hoff approach which produces errors of 1% at 10°C and 6% at 40°C. The relative errors are shown graphically on Fig. 3.8. A large amount of the uncertainty is likely due to the weakness of the interactions between AAC(6')-Ii W164A and AcCoA. This makes it difficult to saturate the protein. In these experiments, the injectant concentration was above 2 mM, yet even with this relatively high concentration of AcCoA, only 55% of the protein was saturated at the final injection at 40°C. Tellinghuisen has shown in detail, that greater than 90% saturation is required for optimal accuracy in the fitted parameters.[155] This is a common problem in weakly binding systems, as a high concentration (mM to M) of ligand is required to fully saturate the protein. Ligand solubility and aggregation, as well as availability and cost can place restrictions on the maximum concentrations that are experimentally accessible. Additional MC

simulations were performed at a 30 fold higher concentration of AcCoA. These simulations show that increasing the concentration of AcCoA does reduce the uncertainties in the calculated ΔH_A^{app} and K_A^{app}.

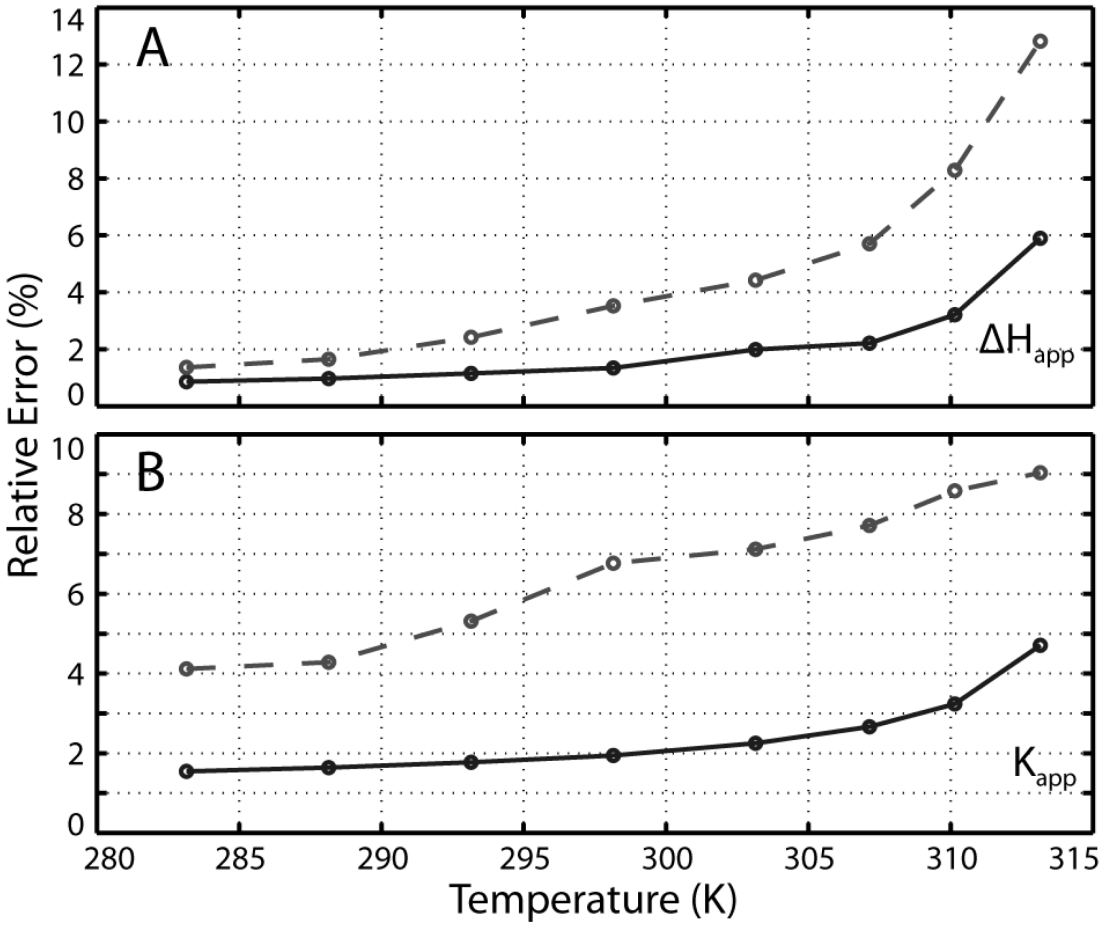

Fig. 3.8: Relative errors (standard deviation/true value × 100%) for (A) ΔH_A^{app} and (B) K_A^{app} values extracted from Monte Carlo ITC data sets by fitting pairs of individual isotherms (dashed line) or globally fitting all 16 synthetic isotherms (solid line).

As mentioned above, the *van 't* Hoff fitting approach clusters the extracted $\Delta H_A^{app,MC}$(global) and $K_A^{app,MC}$(global) values (points) closer to the true values.

Additionally, these values are evenly distributed about the true values. This is important, as it shows that the fitting method does not introduce bias into the extracted thermodynamic parameters, and that the numerically integration of $\Delta H_A^{app}/T^2$ in Equation 3.9 does not lead to systematic errors. The two fold improvement observed in the accuracy of fitted ΔH_A^{app} and K_A^{app} values implies that the *van 't* Hoff approach produces accuracy which would be expected for an ITC dataset 4 times larger (8 replicates instead of 2 for each temperature). This improvement occurs due to the restriction of parameter-space available. The *van 't* Hoff relation as a constraint allows only values which are physically realistic since the set of ΔH_A^{app} and K_A^{app} produced by any physical model must obey the *van 't* Hoff relationship.

3.7 Application to other systems

The binding of AcCoA to AAC(6')-Ii W164A represents a system where low affinity prevents complete saturation, which leads to high uncertainties in the apparent ΔH_A^{app} and K_A^{app} values computed from ITC isotherms. The *van 't* Hoff fitting approach has been shown to produce significant improvements in the uncertainties of the extracted phenomenological binding parameters. Chapter 4 and 5 will detail additional situations where the *van 't* Hoff fitting approach can improve the accuracy of the phenomenological binding parameters and lead to a

gain of insight on microscopic binding models. MC analysis was performed on other theoretical binding systems to test the utility of the *van 't* Hoff fitting approach at improving the accuracy of the ΔH_A^{app} and K_A^{app} values in systems different from the one studied in this chapter. There were two scenarios tested: 1) systems with low heats of binding that lead to poor signal-to-noise ratios in ITC data and consequently poorly defined ΔH_A^{app} and K_A^{app} values; and 2) systems with two non-equivalent binding sites, for which it is difficult to separate the overall heat signals into contributions from the different sites.[141] The results of the simulations are shown on Fig. 3.9. In both of these situations the uncertainties for the extracted ΔH_A^{app} and K_A^{app} values are decreased when using the *van 't* Hoff global fit. The hypothetically low-enthalpy interactions have the uncertainties in both ΔH_A^{app} and K_A^{app} reduced by a factor of 2. In systems with two non-equivalent binding sites, uncertainties in K_A^{app} are reduced by up to 4 fold and ΔH_A^{app} are reduced by up to 1.5 fold. These simulations show that the *van 't* Hoff approach will work well to improve the accuracy of the ΔH_A^{app} and K_A^{app} for the wild type AAC(6')-Ii, as we have shown in Chapter 2 that AAC(6')-Ii binds AcCoA with 2 non-equivalent binding sites.

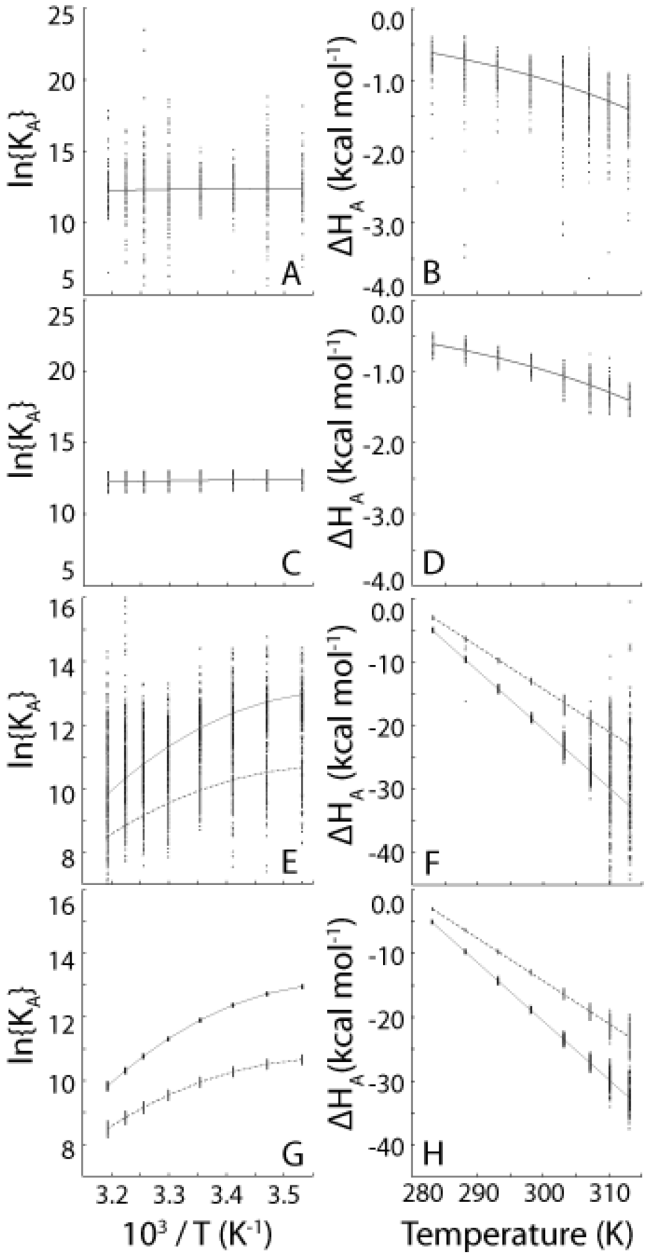

Fig. 3.9: Plots of ΔH_A^{app} and K_A^{app} values extracted from fits of Monte-Carlo ITC datasets generated for (A-D) a system with a low binding enthalpy, and (E-H) a molecule with two non-equivalent binding sites.[55] Lines indicate the true values, while points indicate the parameters obtained from (A,B,E,F) fits of individual isotherms and (C,D,G,H) global fits of isotherms over the temperature range. In (E-H), the dashed and solid lines correspond to binding of the first and second ligand molecules

3.8 Discussion

ITC data collected over a range of temperatures can provide uniquely detailed information on how ligand binding to a macromolecule occurs at a molecular level. However, the interpretation of variable temperature ITC data sets is not always straightforward. Ideally, each ITC isotherm can be analyzed using a phenomenological binding model to yield values for ΔH_A^{app} and K_A^{app}. These, in turn, help to indicate which mechanistic model best corresponds to the actual ligand binding process. Analysis of the phenomenological ΔH_A^{app} and K_A^{app} values using the selected mechanistic model yields thermodynamic parameters that explicitly describe molecular events associated with binding. However there are situations in which this approach becomes problematic. When binding is weak, saturation can be difficult to achieve during the titration experiment and errors in the extracted parameters are elevated.[133] When binding enthalpies are low, the amount of heat released or absorbed during the experiment is small and the signal-to-noise ratio is reduced. When the binding stoichiometry is greater than 1:1, phenomenological binding models contain larger numbers of adjustable parameters that can suffer from covariation.[141] In addition, analyte impurities or incorrect estimates of the injectant concentration or the can lead to errors in ΔH_A^{app} and K_A^{app}.[156] Deviations in extracted ΔH_A^{app} and

K_A^{app} values due to any of these factors can make it difficult to determine which mechanistic binding model best describe the system under study.

The *van 't* Hoff global fitting method, presented in this chapter, provides a simple and effective way to reduce uncertainties in phenomenological ΔH_A^{app} and K_A^{app} values for binding. Unlike previous methods reported, the *van 't* Hoff method does not fit a mechanistic model directly to the experimental ITC isotherms. Also it requires no prior assumptions regarding the thermodynamic equilibria beyond the binding stoichiometry. This method can be applied to any variable temperature dataset and can be used to determine accurate phenomenological ΔH_A^{app} and K_A^{app} values in systems where the underlying mechanics of binding are unknown. The values obtained can be used to test possible mechanistic binding models. Additionally, the *van 't* Hoff global fitting method can be used on any system, because any model, regardless of the complexity of the underlying coupled equilibria, must obey the *van 't* Hoff relation.

4 Competing allosteric mechanisms modulate substrate binding in a dimeric enzyme

4.0 Preface and contributions

Allostery is a key feature of biological systems in which covalent modification or ligand binding at one site influences the activity at distant sites in a macromolecule or macromolecular assembly. Allosteric regulation plays a central role in metabolism and cell signaling, and has been identified as a source of new drug targets.[157-161] Thus, detailed descriptions of allostery have far reaching implications. A number of systems have been explained in terms of mechanistic models, yet allostery takes a variety of forms and many details of this phenomenon remain unresolved.[162-165] This chapter expands upon Chapter 2 and Chapter 3 to develop an allosteric model to describe acetyl coenzyme A (AcCoA) binding to the antibiotic resistance causing aminoglycoside *N*-6'-acetyltransferase-Ii (AAC(6')-Ii). Isothermal Titration Calorimetry (ITC) is used to obtain thermodynamic details, whereas nuclear magnetic resonance spectroscopy (NMR) and circular dichroism spectroscopy (CD) are used to gain structural insights. The majority of the work presented in this chapter has been published and cited as:

> Freiburger, L. A. Baettig, O. M. Sprules, T. Berghuis, A. M. Auclair, K.; Mittermaier, A. K. "Competing allesteric mechanisms modulate substrate binding in a dimeric enzyme."*Nature: Structure and Molecular Biology* **2011**, 18, 288-294.

Except for the assignments of the NMR spectra with AcCoA bound, the work presented in this chapter was performed by myself. The assignment was completed by Oliver Baettig, a graduate student in Dr Albert Berghuis's lab, with the assistance of Dr Tara Sprules, Ph.D. These assignments were instrumental in determining changes in specific regions of AAC(6')-Ii upon binding AcCoA and in partially assigning the spectra of the apo-enzyme.

4.1 Introduction

In Chapter 2, the binding of AcCoA to AAC(6')-Ii was shown to fit a sequential binding model. Since AAC(6')-Ii contains two identical subunits, both of which are able to bind AcCoA,[48] the difference between the 2 binding events was expected to arise from homotropic allosteric cooperativity. Homotropic allostery involves interactions between a macromolecular system and two or more identical ligands. Cooperativity implies that binding depends on the ligation state, i.e. the first ligand is bound with a different affinity than the second, etc. These behaviours are frequent in oligomeric proteins and many theoretical models have aims at describing them. For example, as was explained in the introduction, in the Monod-Wyman-Changeux (MWC) model, ligand binding leads to simultaneous conformational changes in all subunits of a oligomeric protein, thereby altering their binding affinities for the next ligand(s).[158] In the Koshland-

Nemethy-Filmer (KNF) model, free and bound subunits adopt different conformations, and cooperativity results from inter-subunit interactions.[161] Recently, Hilser and Thompson (HT) have proposed a model in which allostery is mediated by coupled folding and binding of adjacent protein domains or subunits.[166] A key difference between these last two paradigms is that the KNF model assumes that conformational changes occur only upon ligand binding, while the HT model explicitly includes conformational equilibria in the unbound subunits. The MWC, KNF, and HT models are illustrated schematically in Fig. 4.1. Other allosteric models have also involved coupled folding and binding,[167] changes in protein flexibility,[168-170] networks of interacting amino acid residues,[96,171] or shifting populations within conformational ensembles.[172-175] A detailed description of the KNF, MWC, and HT models can be found in the introduction, sections 1.2.2-1.2.4.

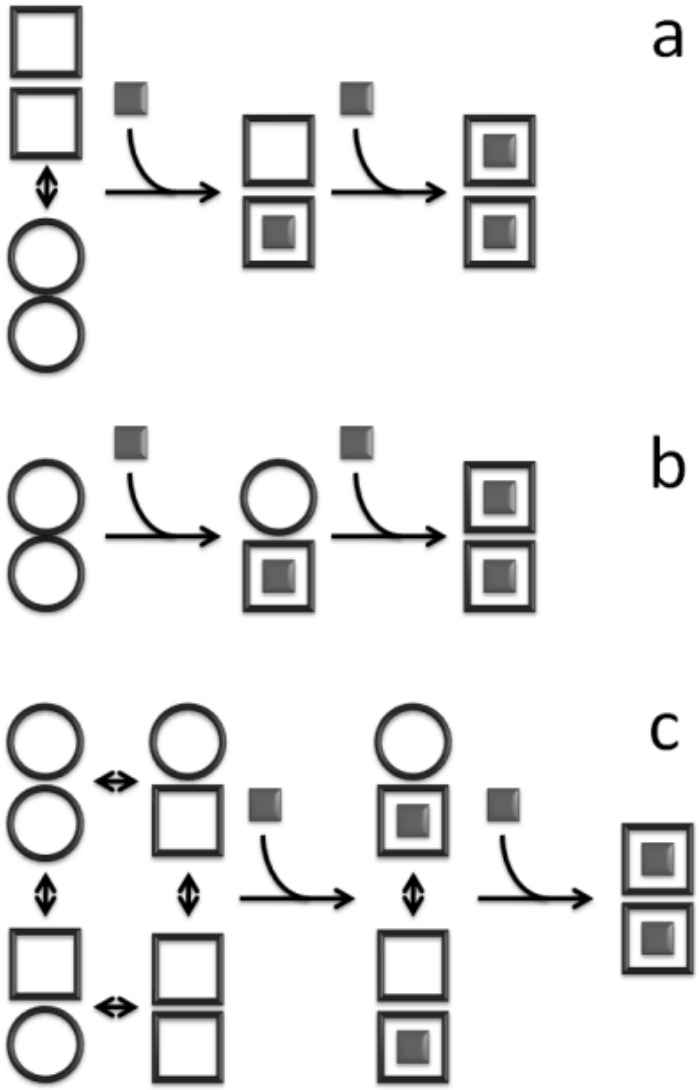

Fig. 4.1: Schematic representation of homotropic allosteric models for a dimeric protein. ○ and □ correspond to subunits in binding-incompetent, and binding-competent states, respectively. **(a) Monod-Wyman-Changeux (MWC):** Symmetry of the dimer is preserved, so that only ○○ and □□ states are permitted. In the absence of ligand, both states are populated, while ligand binding forces the dimer into the □□ state. **(b) Koshland-Nemethy-Filmer (KNF):** Each subunit converts from the ○ to the □ state only upon binding ligand. **(c) Hilser-Thompson (HT):** ○ and □ correspond to the unfolded and folded states, respectively. Each unbound subunit can populate either the folded or unfolded state, and the folding equilibrium is influenced by the state of the adjacent monomer.

Chapter 3 described a global fitting approach which used the *van 't* Hoff relation as a restriction in fitting a variable temperature dataset. This approach linked a series of isothermal titration calorimetry (ITC) binding isotherms of acetyl coenzyme A (AcCoA) with the mutant variant aminoglycoside *N*-(6')-acetyltransferase-Ii (AAC(6')-Ii) W164A at a variety of temperatures to a single set of binding enthalpies (ΔH_A) and association constants (K_A). Also, a combination of isothermal titration calorimetry (ITC) and circular dichroism (CD) spectroscopy was shown to describe a linked folding/binding event in AAC(6')-Ii W164A. In this chapter these techniques were applied to the wild type AAC(6')-Ii to characterize the allosteric mechanism of AcCoA binding to this enzyme. This homo-dimeric enzyme confers bacterial resistance to aminoglycoside antibiotics by transferring an acetyl group from AcCoA to the 6'-*N* position of the drugs.[44] The structure of AAC(6')-Ii has been solved by X-ray crystallography, with CoA, AcCoA,[46,176-177] or inhibitors[178] bound in the two active sites of the homo-dimeric enzyme. Chapter 2 showed that AAC(6')-Ii binds two molecules of AcCoA with positive cooperativity, likely reflecting energetic coupling between the active sites.[55] Chapter 3 showed that folding was linked to binding. This chapter shows that the cooperative interactions vary unexpectedly with temperature, shifting from positive to negative cooperativity as the temperature is raised. Data from nuclear magnetic resonance (NMR) spectroscopy is coupled with the

experimental data gained from ITC and CD to gain additional structural and mechanistic information. Together these data suggest a novel arrangement in which an HT-type coupled folding and binding mechanism is superposed onto a classical KNF-type interaction. This finding provides experimental validation for the recently-proposed HT paradigm, and to our knowledge, represents the first example of a hybrid allosteric mechanism.

4.2 Isothermal Titration Calorimetry.

A total of 28 ITC experiments were performed at 8 temperatures ranging from 10 to 40ºC, titrating AcCoA into solutions of AAC(6')-Ii (Fig. 4.2 and Appendix Figure A.2) in 25 mM 4-(2-hydroxyethyl)-1-piperazineethanesulfonic acid (HEPES), 2 mM ethylenediaminetetraacetic acid (EDTA), pH 7.5. Chapter 3 showed the utility of simultaneously fitting experimental isotherms using a *van 't* Hoff global fit. This approach was used here with the ITC data to improve the accuracy of extracted binding parameters. In summary, the ΔH_A and K_A of binding at a variety of temperatures are linked through the *van 't* Hoff equation.

$$\frac{\partial \ln\{K_A\}}{\partial T} = \frac{\Delta H_A}{RT^2}, \qquad 4.1$$

where T is the temperature for the measured ΔH_A and K_A. As was done in Chapter 3, the ΔH_A is fit for all the temperatures used for each titration (10, 15,

20, 25, 30, 34, 37, and 40°C). Only a single K_A is fit at reference temperature (20 °C). The remaining K_A are determined through an integrated form of eq 4.1.

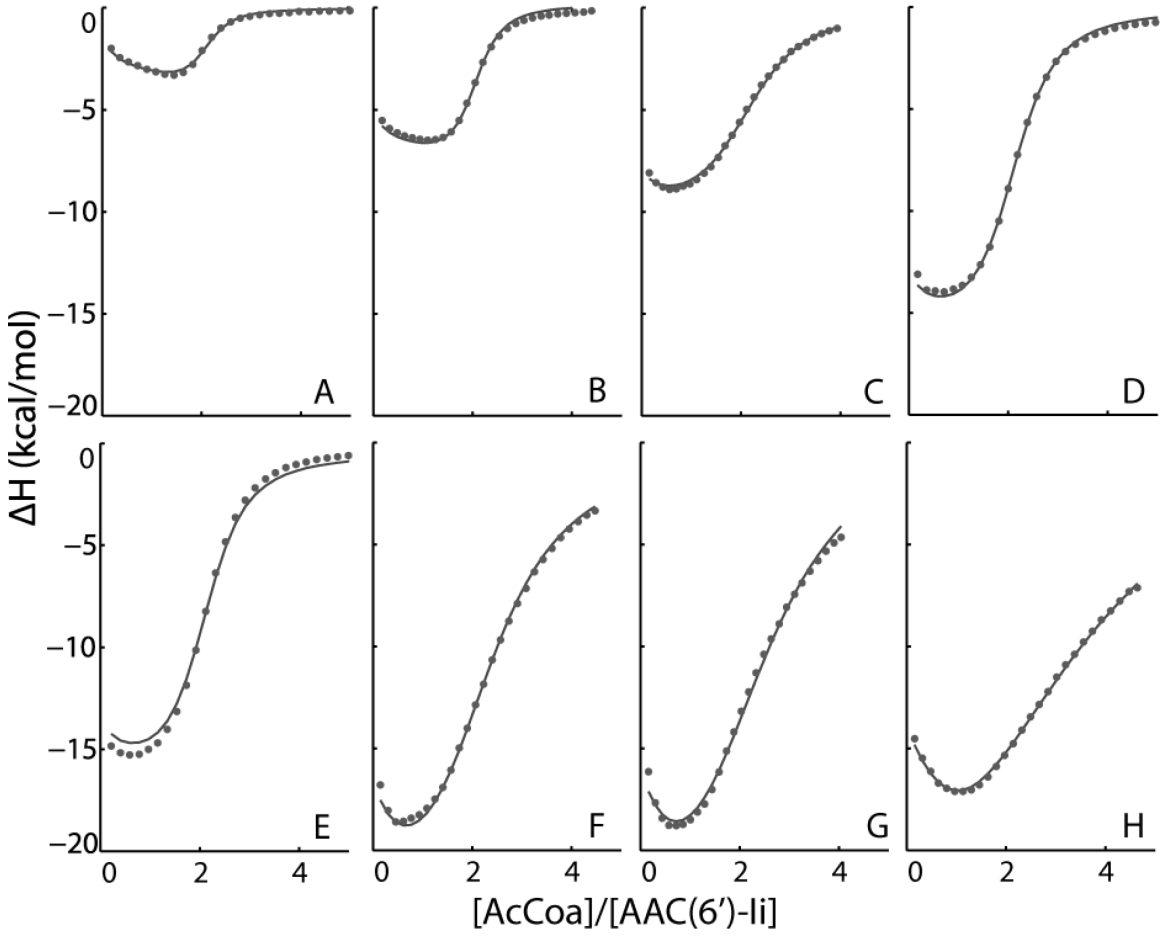

Fig. 4.2: ITC isotherms of AcCoA binding to AAC(6')-Ii with the experimental data (•) fit using the van 't Hoff global appoach (–) at a) 10, b) 15, c) 20, d) 25, e) 30, f) 34, g) 37, and h) 40°C.

$$\ln\{K_A(T_n)\} = \ln\{K_A(T_0)\} + \frac{1}{R}\int_{T_0}^{T_n} \frac{\Delta H_A(T)}{T^2}\, dT \qquad 4.2$$

This method yields apparent equilibrium association constants (K_{A1}^{app}, K_{A2}^{app}) and enthalpy changes (ΔH_{A1}^{app}, ΔH_{A2}^{app}) for binding of the first and

second molecules of AcCoA to the enzyme as functions of temperature (Fig. 4.3 A,B,Table 4.1). At 10ºC, K_{A2}^{app} > K_{A1}^{app}, indicating that the second molecule of AcCoA binds more tightly than the first and the interaction is positively cooperative. The difference between K_{A2}^{app} and K_{A1}^{app} decreases as the temperature increases and the situation reverses to negative cooperativity, K_{A2}^{app} < K_{A1}^{app}, at around 37ºC and above.

Table 4.1: ITC-derived association constants and enthalpies of AcCoA binding to AAC(6')-Ii

Temperature (ºC)	ΔH_{A1}^{app} (kcal mol^{-1})	ΔH_{A2}^{app} (kcal mol^{-1})	K_{A1}^{app} ($\times 10^4$ M^{-1})	K_{A2}^{app} ($\times 10^4$ M^{-1})
10	-1.6±0.2	-4.8±0.2	13.3±0.3	33.2±0.7
15	-6.0±0.3	-8.2±0.6	11.9±0.3	27.2±0.5
20	-9.5±0.2	-12.2±0.3	9.5±0.2	20.1±0.3
25	-15.3±0.4	-17±1	6.6±0.2	13.1±0.2
30	-15.6±0.1	-28.3±0.3	4.3±0.1	6.9±0.1
34	-21.5±0.3	-31±2	2.89±0.08	3.65±0.06
37	-21.7±0.2	-46.7±0.2	2.05±0.06	1.97±0.04
40	-20.4±0.5	-84.1±0.4	1.48±0.05	0.71±0.02

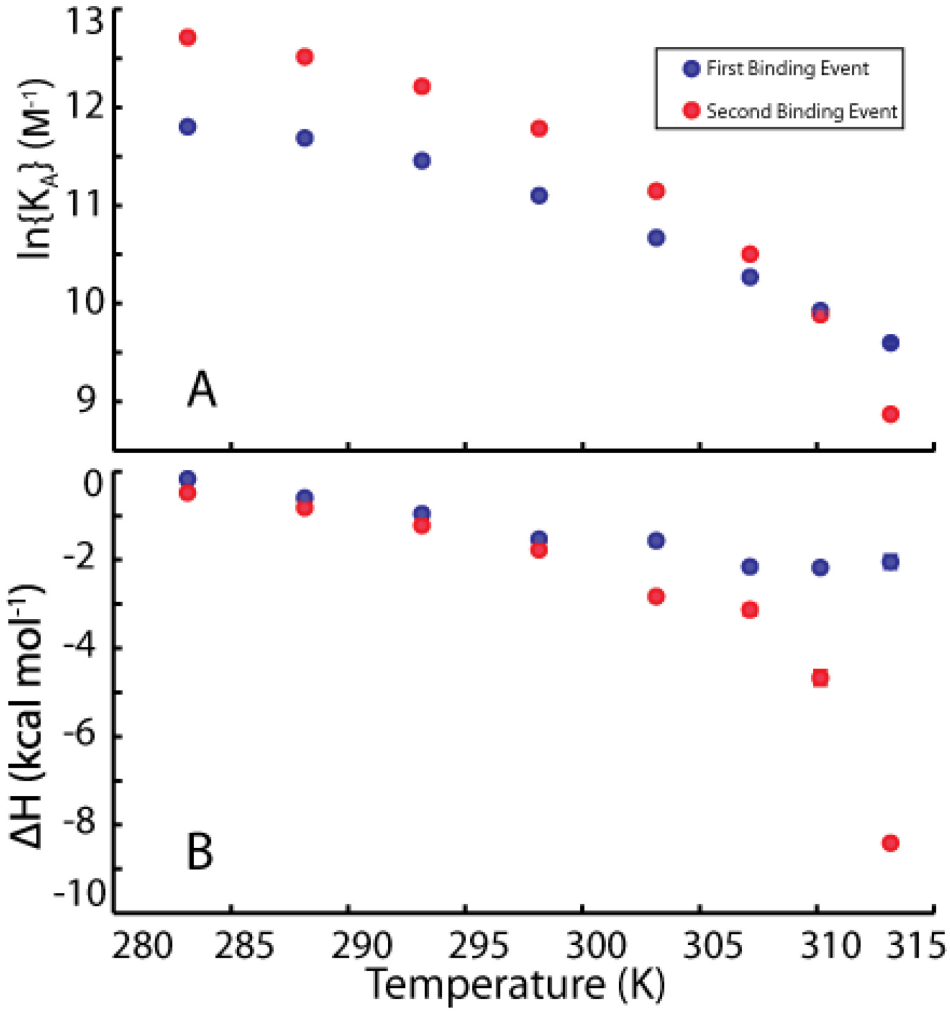

Fig. 4.3: Binding parameters obtained from the *van 't* Hoff global fit of ITC isotherms of AcCoA binding to AAC(6')-Ii. This gave A) association constants of both the first (blue dot) and second (red dot) binding event and B) enthalpies of binding. Error is given for all values but most uncertainty is smaller than data points shown.

In many systems, the binding enthalpy depends linearly on temperature with a slope equal to the difference in heat capacity between the bound and free forms. Much like the mutant AAC(6')-Ii W164A explained in Chapter 3, the wild type enzyme undergoes a temperature dependent change in heat capacity. For

AAC(6')-Ii, the binding enthalpies for the first and second molecules of AcCoA (ΔH_{A1}^{app}, ΔH_{A2}^{app}) exhibit curvature above about 30ºC. ΔH_{A1}^{app} deviates slightly upwards, while ΔH_{A2}^{app} exhibits a sharp decrease. Curved enthalpy profiles of this sort are characteristic of systems that populate both an active free form (**F**) and an inactive partly unfolded or fully unfolded form (**U**) that is higher in enthalpy, within the temperature range studied.[150,179] At low temperatures (Fig. 4.3 A,B), almost all protein molecules will be folded in the active **F** state, and ITC detects the intrinsic heat of binding, i.e. the difference in enthalpy between the bound (**B**) and **F** states. At high temperatures, free proteins populate the inactive **U** state. When ligand is added, the proteins must both fold and bind (**U**→**F**→**B**) and ΔH_{A}^{app} contains contributions from both folding and the intrinsic binding enthalpy. The curvature observed in the enthalpy vs temperature plot is different between the first and second binding event. This suggests that the folding events are different between each of the binding events. Shown below, section **4.6**, is the curvature in both the ΔH_{A1}^{app} and ΔH_{A2}^{app} profiles quantitatively explained by a model involving multiple states with coupled partial unfolding of the two enzyme subunits.

4.3 Circular Dichroism spectroscopy.

As described in Chapter 3 for mutant AAC(6')-Ii, the CD spectrum of wild type AAC(6')-Ii was monitored at 222 nm, from 0.1 to 71 ºC in the absence of AcCoA in buffer conditions which match the ITC titrations (25 mM HEPES, 2 mM EDTA, pH 7.5). The molar ellipticities ([Θ]) of both alpha-helices and beta-sheets are large and negative,[148,180] while those of unstructured polypeptides are close to zero or slightly positive at this wavelength.[148,180-181] The CD data show a sigmoidal decrease in the absolute molar ellipticity from about 35 to 45 ºC (Fig. 4.4). Curvature of the ITC-derived binding enthalpies is observed within the same temperature range. These data are thus consistent with an endothermic transition from the native free **F** state to a partly or fully unfolded **U** state that is unable to bind AcCoA, at around 40ºC. The NMR experiments are performed in 100 mM sodium phosphate ($NaPO_4$), pH 6.5, so these conditions were tested. The stability of the protein in these conditions was shown to increase the melting temperature by ~6 ºC. To test if this effect was from the different buffer salts, or higher salt concentrations the [Θ] of AAC(6')-Ii monitored in HEPES buffer with 150 mM NaCl. The increased salt concentration increased the melting temperature by ~6 ºC, shown in Fig. 4.4. This confirms that AAC(6')-Ii is stabilized by increased salt concentration.

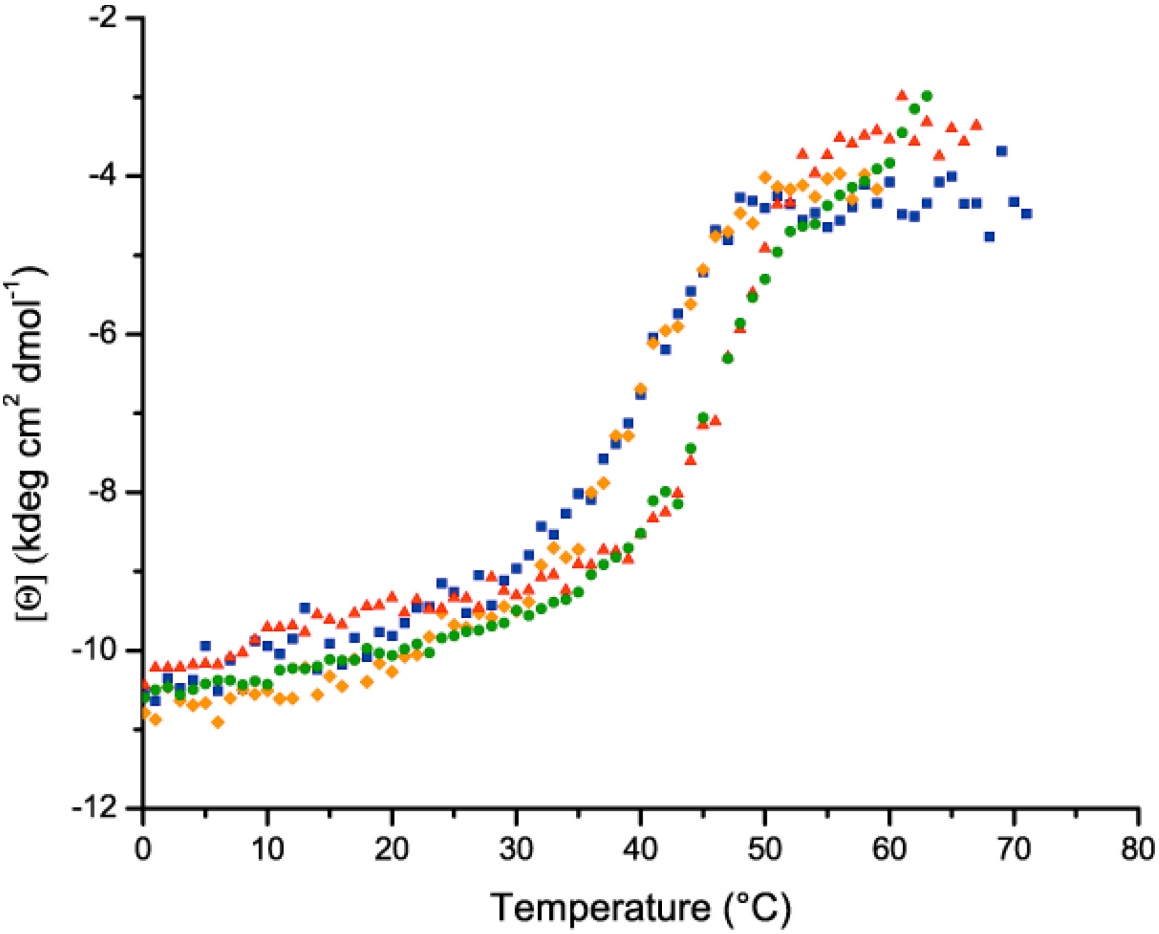

Fig. 4.4: Change of molar ellipticity ([Θ]) of AAC(6')-Ii at 222 nm with increasing temperature. Several conditions tested to observe change in T_m: ITC buffer conditions, (25 mM HEPES, 2 mM EDTA, pH 7.5), [AAC(6')-Ii] = 15 μM (■), [AAC(6')-Ii] = 45 μM (◆), ITC buffer with 150 mM NaCl, [AAC(6')-Ii] = 15 μM (▲), and NMR buffer conditions (100 mM $NaPO_4$, 2 mM EDTA, pH 7.5), [AAC(6')-Ii] = 15 μM (●).

We investigated whether the AAC(6')-Ii dimer fully dissociates when subunits are in the **U** state by repeating the CD experiments with the enzyme concentration reduced by about a factor of three. If unfolding and dissociation are concurrent, then lowering the concentration by a factor of 3 would be expected to

reduce the melting temperature by approximately $\frac{RT_U{}^2 \ln 3}{\Delta H_U}$, where ΔH_U is the enthalpy of the transition at the midpoint temperature, T_U. Using the values obtained from the joint ITC/CD fitting described below, this predicts a reduction in the midpoint temperature of 2.7ºC. However, the two CD traces are nearly super imposable and yield midpoints that differ by only about 0.1ºC, shown in Fig. 4.4. Therefore, the transition to the **U** state does not involve the complete loss of structure and dissociation of the subunits, but rather involves partial unfolding that leaves the dimer intact. This is supported by the observations that the enzyme elutes from size-exclusion chromatographic columns as a dimer, even in dilute solutions, and that binding cooperativity is not affected by protein concentration, as shown in Chapter 2.[55] From CD we observe that the enzyme undergoes a conformational change beginning around 30°C. This is the same temperature range which we observe the nonlinear dependence of binding enthalpy, and suggests that it is a folding event which is linked to binding.

4.4 Nuclear Magnetic Resonance spectroscopy.

4.4.1 Structural assignment of spectra

NMR is an ideal technique to study structural changes upon binding, and can detail structural information of partially saturated macromolecules. Two dimensional $^{1}H/^{15}N$ NMR correlation spectra are can provide information about

backbone structure of the protein. The backbone of proteins contains a series of amino acids linked together by amide bonds, and each non-proline residue contains an N-H bond. Therefore, information of the chemical environment can be gained for almost every amino acid in a protein. Two-dimensional $^{1}H/^{15}N$ heteronuclear single quantum correlation (HSQC) NMR experiments of AAC(6')-Ii in the free (apo) and ligand-saturated (holo) forms provide evidence that large structural and dynamical changes accompany AcCoA binding (Fig. 4.5 and Fig. 4.6). This confirms that the enzyme undergoes a conformational change linked to binding. The apo-spectrum contains only about 137 distinguishable backbone amide peaks, 60 of which are baseline-separated, while 172 signals are expected (Fig. 4.5a). The remainder of the signals are either located in a highly overlapped region in the center of the spectrum, or are absent altogether, possibly due to dynamical broadening or rapid hydrogen exchange with water. In contrast to the free form, the spectrum of the AcCoA-saturated enzyme is typical of a folded globular protein, containing about 166 well-resolved backbone amide resonances, 89 of which are baseline-separated (Fig. 4.6a). This suggests that in the absence of AcCoA, much of the protein is highly mobile or partially disordered, while a few ordered regions give rise to a number of well-dispersed signals. AcCoA binding to AAC(6')-Ii occurs on a slow timescale (ms-s), so both the apo and holo peaks were present at the same time under partially saturating

conditions. As a result, it was not possible to assign the NMR signals of the apo enzyme directly. Nevertheless, we were able to transfer 32 assignments from the holo to the apo spectrum through two methods. First, it was assumed that peaks which are largely superimposed between the apo and the holo state are from residues which maintain a similar chemical environment between the apo and holo states. Second, a 2D exchange spectroscopy (EXSY) experiment[182] was used to link together peaks between the apo and holo state in a partially saturated sample. If a residue is exchanging between two chemical environments, then there are two separate NMR signals. In these 2D NMR experiments, magnetization is transferred from the ^{15}N to the ^{1}H during a period known as the mixing time. The EXSY experiment adds a delay after the magnetization transfer. If a residue is exchanging on a timescale similar or faster than the delay time, then cross peaks appear for these two signals. In a partially saturated sample, the protein exchanges between the apo and holo states, so through this experiment several apo and holo signals developed crosspeaks (Appendix Figure A.3). From these crosspeaks, several apo peaks were assigned. On average, one in every 6 residues in the apo spectrum of AAC(6')-Ii was thus assigned by either superimposed apo and holo peaks or through EXSY crosspeaks. Therefore, it is significant that a stretch of about 46 residues, from 105 to 150, gives rise to no assigned peaks (Fig. 4.5 and Fig. 4.7 (red)). This

region is thus expected to undergo extensive dynamical broadening in the free form of the enzyme. The NMR measurements were performed under stabilizing conditions of higher salt so the free subunits are almost entirely in the **F** state. The **U** state, which predominates at higher temperatures, is presumably even less structured.

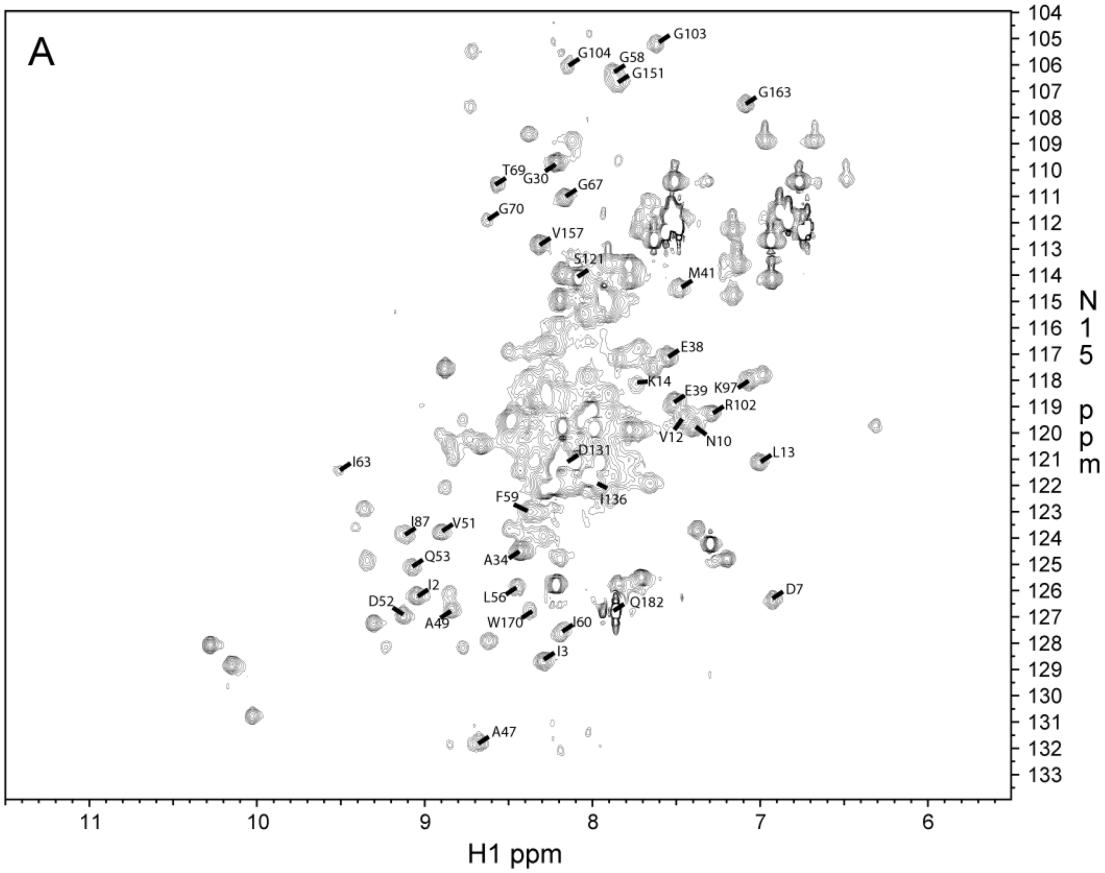

B

```
1           11          21          31          41          51          61
MIISEFDRNN PVLKDQLSDL LRLTWPEEYG DSSAEEVEEM MNPERIAVAA VDQDELVGFI GAIPQYGITG
71          81          91         101         111         121         131
WELHPLVVES SRRKNQIGTR LVNYLEKEVA SRGGITIYLG TDDLDHGTTL SQTDLYEHTF DKVASIQNLR
141         151         161         171         181
EHPYEFYEKL GYKIVGVLPN ANGWDKPDIW MAKTIIPRPD SQ
```

Fig. 4.5: (A) Assigned AAC(6')-Ii NMR spectra in the apo state. (B) The primary amino acid sequence of assigned amino acids given by underlined bold typeface.

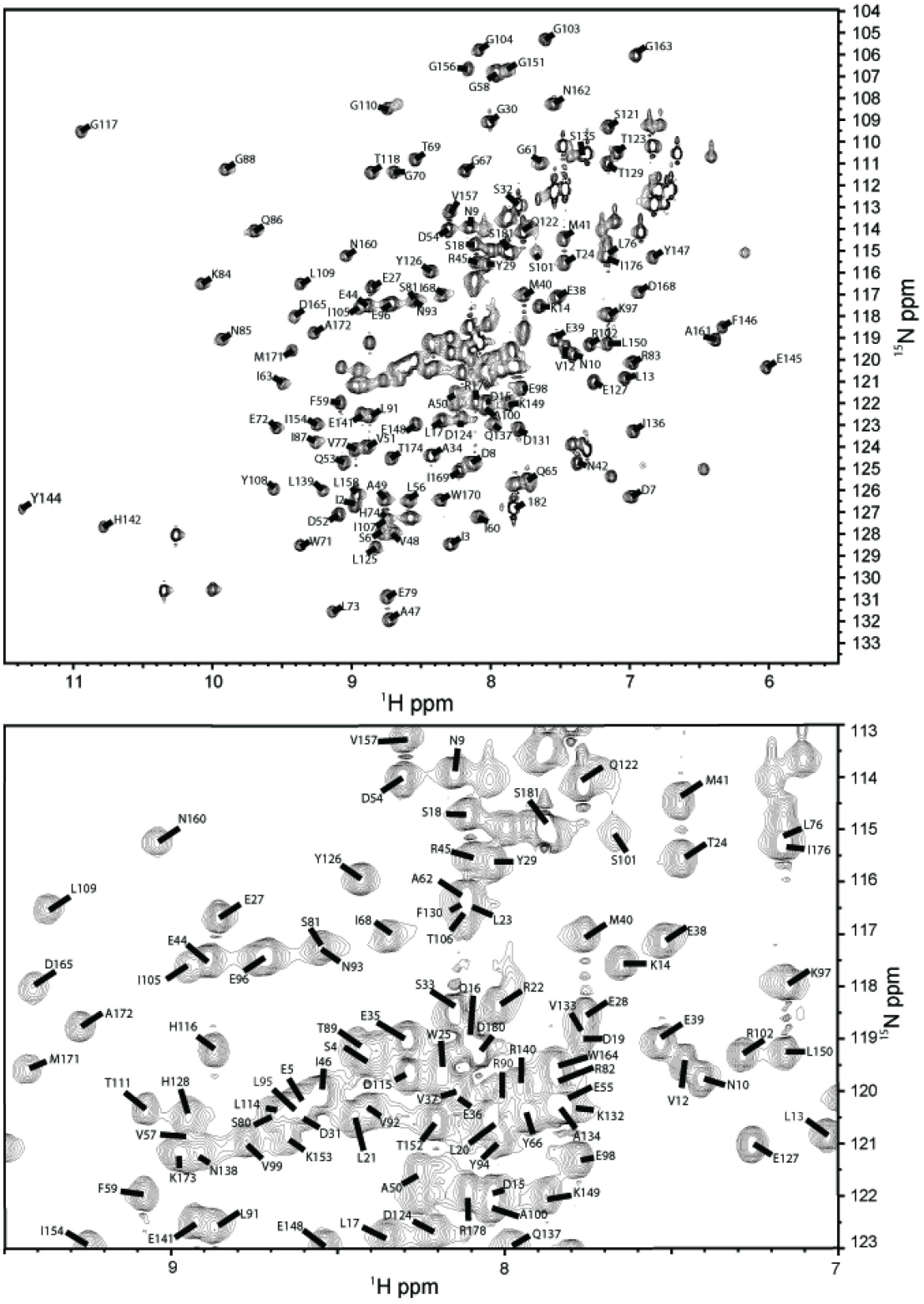

Fig. 4.6: Assigned AAC(6')-Ii NMR spectra produced by AcCoA binding (A) with a enlargement of the central region (B).

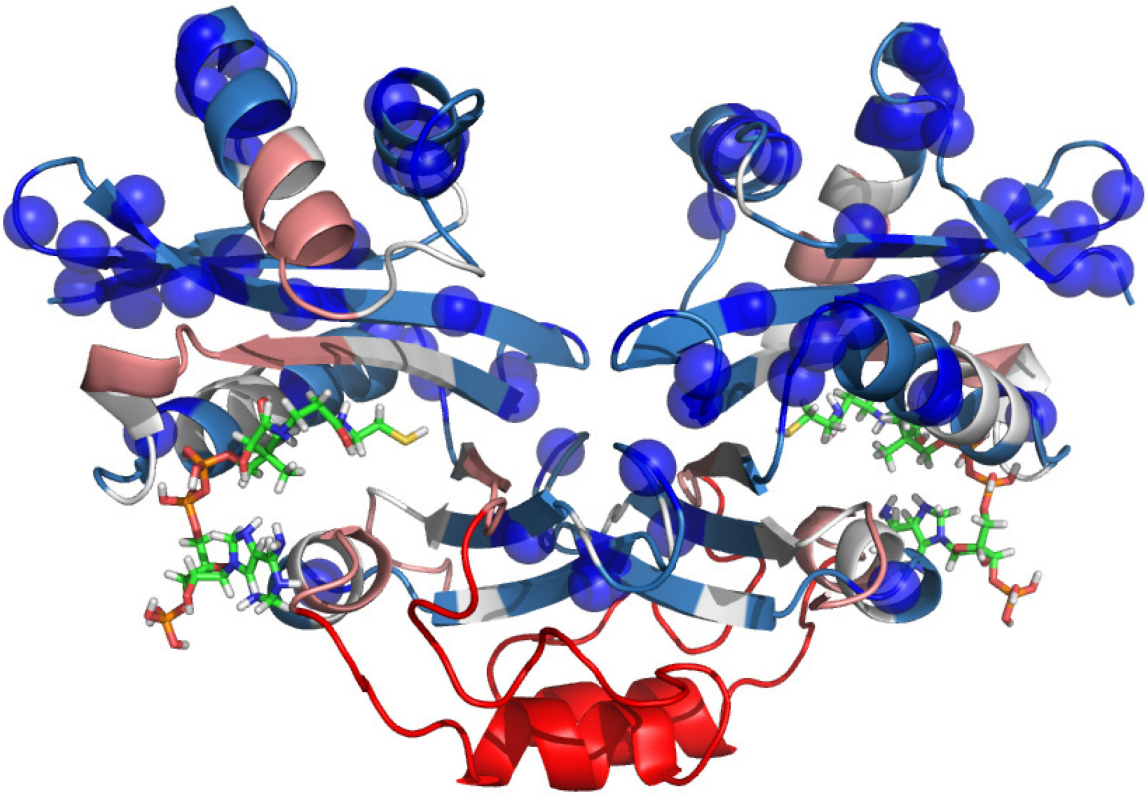

Fig. 4.7: X-ray crystal structure of the enzyme (PDB 2A4N[176]) bound to CoA (sticks) with blue spheres indicating the locations of residues with assigned cross-peaks in apo spectra. The backbone is color-coded according to the distance in the 1º sequence (n) from the nearest assigned residue according to $1 \leq n \leq 2$ (light blue), $3 \leq n \leq 5$ (white), $6 \leq n \leq 10$ (pink), $n > 10$ (red)

Information on the conformational transition from the active free (**F**) to the bound (**B**) states can be obtained from a comparison of the apo and holo spectra. Several of the well-resolved apo-peaks change their chemical shift upon addition of AcCoA (for example Leu56, located 15 Å from the active site). This strongly suggests that the free enzyme adopts a distinctly different configuration than that of the bound enzyme. It is unlikely that dynamical broadening in the unbound

enzyme is due to excursions between the **F** and **B** conformations in the absence of AcCoA. Millisecond-timescale exchange between the **F** and **B** conformation would preferentially broaden signals whose chemical shifts change the most upon AcCoA binding. However, this is not observed. We therefore conclude that the population of **B**-type conformations in the absence of AcCoA is below our detection limit (≈1%). As discussed above, only a relatively small number of spectral assignments could be obtained for the unbound enzyme. Thus, in order to map ligand-induced changes onto the protein structure, we calculated minimum chemical shift differences ($\Delta\delta_{app}$),[183] which are defined as the distance between each holo-peak and the nearest signal in the apo-spectrum. All residues with large values of $\Delta\delta_{app}$ either have very different chemical shifts in the free and bound forms, or are broadened beyond detection in the free form of the protein. Large values of $\Delta\delta_{app}$ are obtained throughout the protein, notably including residues located at the interface between the two subunits and near the bound AcCoA (Fig. 4.8). This suggests that binding AcCoA leads to remodelling of subunit interactions, and provides some insight into the mechanism for allosteric communication between the two active sites, as discussed below.

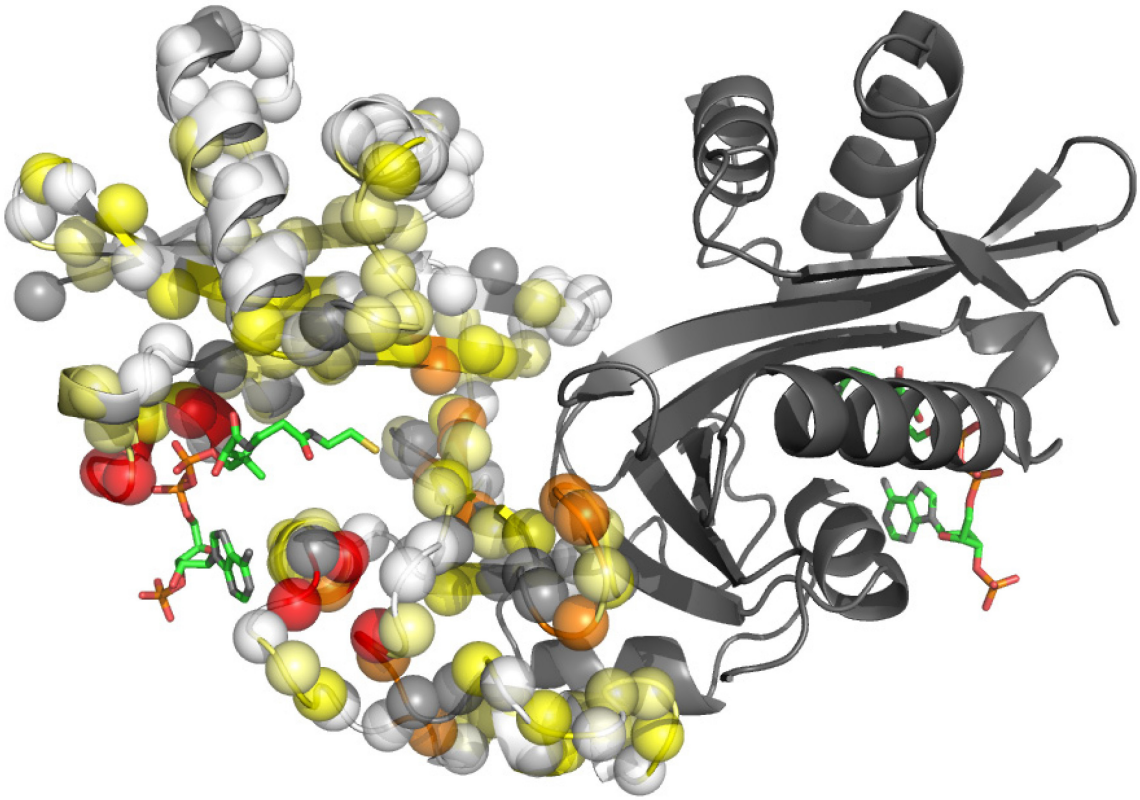

Fig. 4.8: Apparent minimal chemical shift differences ($\Delta\delta_{app} = \sqrt{\left(10 \cdot \Delta\delta_{app}^{1H}\right)^2 + \left(\Delta\delta_{app}^{15N}\right)^2}$) between the free and bound states, mapped onto the X-ray crystal structure (PDB 2A4N[176]). Backbone amide nitrogen atoms are indicated with spheres for one subunit of the dimer and colored according to $\Delta\delta_{app}$<0.5 ppm (white), 0.5≤$\Delta\delta_{app}$<1 (light yellow), 1≤$\Delta\delta_{app}$<2 (yellow), 2≤$\Delta\delta_{app}$<4 (orange), 4≤$\Delta\delta_{app}$ (red). Unassigned residues, including prolines, are indicated with gray spheres.

4.4.2 HSQC NMR titration

A series of two-dimensional protein NMR spectra was recorded as AcCoA was titrated into a sample of AAC(6')-Ii (Appendix Figure A.4). In what follows, apo and holo are used to describe peaks appearing in NMR spectra of the

AcCoA-free and AcCoA-saturated protein, and 0-bound, 1-bound, and 2-bound to describe the various ligated states of the enzyme. Binding occurs slowly on the NMR chemical shift timescale, so both apo and holo peaks are simultaneously visible in spectra collected midway through the titration when the enzyme is only partially saturated. The expected fraction of enzyme in the 0-bound (f_0), 1-bound (f_1), and 2-bound (f_2) forms may be calculated based on the known concentrations of AcCoA used in the titration and the binding parameters determined by ITC (Fig. 4.9a). The value of f_1 is predicted to increase to about 30% at partial AcCoA saturation, before decreasing at higher ligand concentrations. Notably, we do not observe any signals in the spectra that follow this pattern of intensities. We conclude that all signals from the 1-bound form either coincide with those of the 0-bound or 2-bound states (i.e. contribute to the apo and holo peaks or are located in overlapped regions) or are dynamically broadened beyond detection. The exchange between these two states occurs at a slow timescale (~seconds). Millisecond-timescale exchange between **F**-type and **B**-type configurations would preferentially broaden signals whose chemical shifts change the most upon AcCoA binding. In order to discriminate between these two possibilities on a peak-by-peak basis, we developed a joint analysis of the NMR and ITC data. The intensity profile of each well-resolved apo and holo peak was fitted using the sets of ITC-derived f_0, f_1, and f_2 values, adjusting only

the relative contribution of the 1-bound state to the apo or holo peak as follows: the initial intensity of each apo peak was normalized to 2, and the final intensity of each holo peak was normalized to 2. Peak intensities throughout the titration were calculated as $I_{tot}^{apo} = 2 \times f_0 + f_1 I_1^{apo}$ and $I_{tot}^{holo} = f_1 I_1^{holo} + 2 \times f_2$. The values of I_1^{apo} and I_1^{holo} were optimized for each apo and holo peak, respectively. Excellent agreement was obtained with all NMR titration data (Fig. 4.9b and Appendix Figure A.5-8). The value of I_1^{apo} or I_1^{holo} thus quantifies the contribution of the 1-bound form to each signal, relative to that of a single subunit of the 0-bound or 2-bound form, respectively. The 62 values of I_1^{holo} cluster about a value of 1 (Fig. 4.9c). This strongly suggests that a single subunit of the 1-bound enzyme resembles those of the 2-bound state, and produces a set of signals coincident with the holo spectrum. The 10 values of I_1^{apo} are more heterogeneous, ranging from 0 to 1. The presence of five peaks with I_1^{apo} significantly greater than zero suggests that the unbound subunit in the 1-bound enzyme may somewhat resemble those of the 0-bound form, and produces some signals coincident with the apo spectrum. The five values of I_1^{apo} close to zero could result from increased dynamical broadening, hydrogen exchange with solvent, or movement of peaks to overlapped regions of the spectrum.

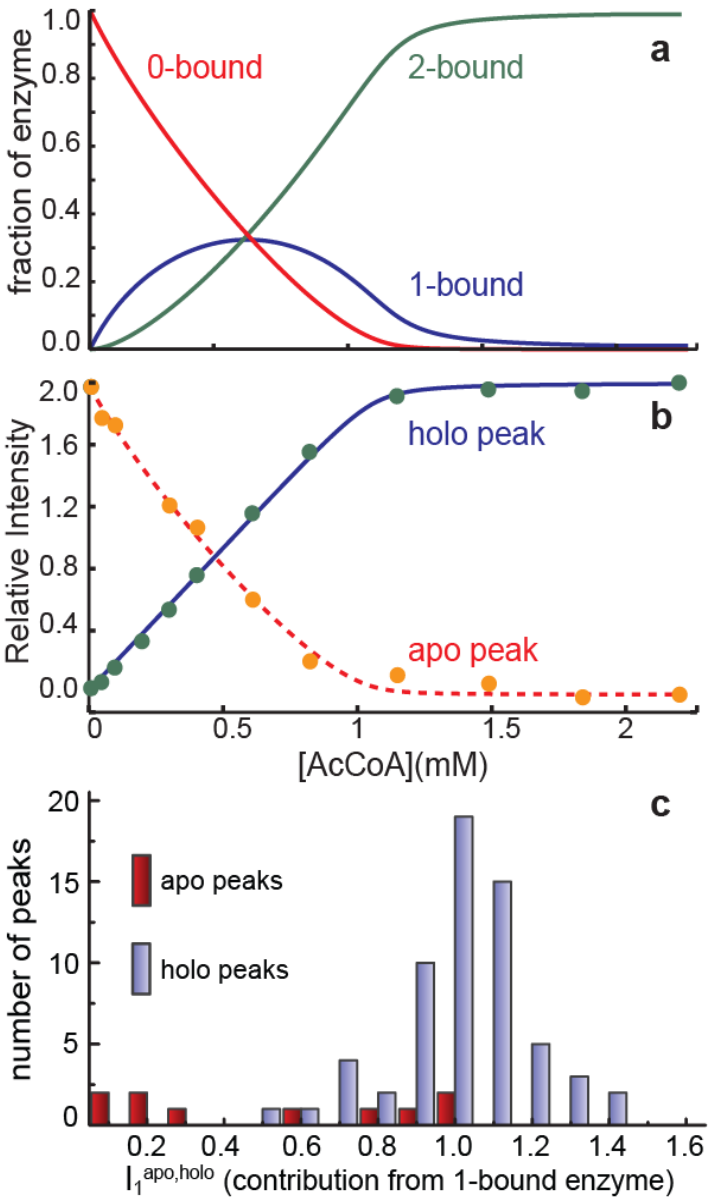

Fig. 4.9: Analysis of NMR titration data of AAC(6')-Ii with AcCoA. **(a)** Fraction of the enzyme in the 0-bound (red), 1-bound (blue), and 2-bound (green) states determined by ITC. **(b)** Intensities of the apo (yellow points, dashed red line) and holo(green points, solid blue line) peaks for L56 as a function of [AcCoA]. The intensities were analyzed to extract the relative contribution of the 1-bound enzyme to the signals ($I_1^{apo,holo}$) as described in the text. The lines correspond to the optimized theoretical intensities. **(c)** Histograms of the relative contribution of the 1-bound enzyme to apo (I_1^{apo}) and holo (I_1^{holo}) peaks in titrations of AAC(6')-Ii with AcCoA.

The relaxation rate of the transverse magnetization, known as R_2, is dependent on the relative dynamics of the nucleus studied. Protein with increased large scale motions in the ms timescale may have a higher R_2. R_2 values were measured for the protein in different ligated states: free, partially bound, and fully saturated. The apo state has elevated R_2s compared to the partially and fully saturated protein. This is likely due to the unbound protein rapidly sampling many different conformational states at ms-μs. This exchange causes dephasing of the transverse magnetisation and leads to exchange broadening in the signals and increases the relaxation rates. Meanwhile the bound subunit adopts a specific conformation reducing its R_2s by eliminating the exchange broadening. The partially saturated protein has slightly elevated R_2s for the holo signals compared to fully saturated AAC(6')-Ii. This increased relaxation is likely due to the protein in the 1-bound state has more dynamics at the ms timescale compared to that of the 2-bound saturated enzyme. Due to the lack of unequivocal data, no specific model is proposed for the unbound subunit of the 1-bound enzyme, and it will be referred to as the **F'** state, to distinguish it from the **F** subunits of the 0-bound state.

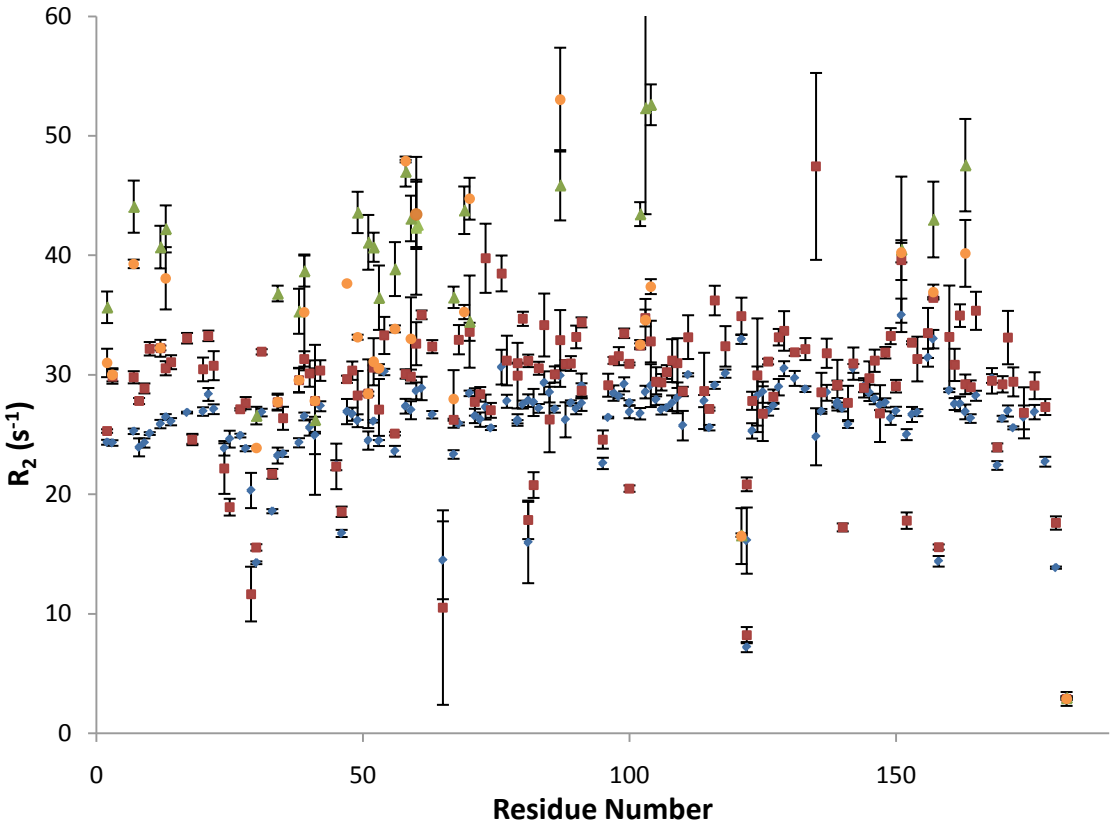

Fig. 4.10: R_2 values of each amino acid at different saturation states: Free protein apo peaks (green triangles), partially saturated apo peaks (yellow circles), partially saturated holo peaks (red square), and saturated (blue diamond).

The titration intensity analysis provides a basis for discriminating between the classical KNF[161] and MWC[158] paradigms (Fig. 4.1a,b). The KNF model predicts that the 1-bound enzyme contains one **B**-type subunit and one **F**-type subunit. Values of I_1^{apo} and I_1^{holo} should thus both be close to 1. This corresponds closely to what is observed experimentally, although some values of I_1^{apo} are smaller. In contrast, the MWC model predicts that the 1-bound enzyme contains two **B**-type subunits and no **F**-type subunits. Values of I_1^{apo} should be 0,

while values of I_1^{holo} should be close to 2, this is not observed. Given the large conformational changes exhibited by AAC(6')-Ii, it is of interest to understand the binding reaction pathways, or the sequences of events that occur as AcCoA is taken up by the enzyme. This process has historically been described by an "induced-fit" model, in which ligands bind weakly to **F**-type molecules, which subsequently convert to the tightly-bound **B** form.[115] More recent work has focused on a "conformational selection" model, in which ligands bind directly to a small, pre-existing population of unbound, high-affinity **B**-type molecules.[184-185] It has been noted that the conformational selection and MWC models are similar, since both models invoke small pre-existing populations of unbound **B**-type molecules.[186] As well, the induced fit and KNF paradigms are similar, and KNF is sometimes referred to as an "induced-fit" model.[62] However, our identification of a KNF-type allosteric mechanism in AAC(6')-Ii does not necessarily imply that ligands are taken up through an induced-fit pathway. The KNF paradigm describes binding purely in terms of thermodynamics, and ligands can be taken up by either induced fit or conformational selection pathways.[161] The contributions of the two pathways are governed by the microscopic rate constants for binding and conformational transitions[184,186-188] and also by protein and ligand concentrations.[188] Thus it is quite challenging to determine the extent to which a particular system follows the conformational selection or induced-fit

binding pathway. We cannot confidently assign either model to AAC(6')-Ii, given the data at hand. Even though we do not observe any **F** to **B** transition in the absence of AcCoA, it does not rule out the **B** state being present at very minor concentrations. Discriminating between the KNF and MWC allosteric models is more straightforward than identifying the binding pathway. According to the MWC model, the 1-bound enzyme exists in a **BB**-type conformation (Fig. 4.1a), while according to the KNF model, the 1-bound enzyme exists in a **BF**-type conformation (Fig. 4.1b), irrespective of ligand concentration or the rates of binding or conformational transitions. Based on the NMR titration data and this criterion, we can confidently assign a KNF-type model to the interaction of AcCoA with native AAC(6')-Ii.

4.5 Deriving equations.

4.5.1 Concentration dependent melting of dimers

If the dimer dissociates when AAC(6')-Ii is in the **U** state then there will be a concentration dependent effect on the melting temperature. The dissociation of the dimers (K_{D}) is given by

$$K_D = \frac{[\mathrm{M}]^2}{[\mathrm{D}]} \qquad 4.3$$

where [M] and [D] are the concentration of the protein as a monomer and dimer respectively and at the T_{m}

$$\mathrm{M} = 2\mathrm{D} \tag{4.4}$$

substituting 4.4 into 4.3 gives

$$K_{\mathrm{D}} = \frac{4[\mathrm{D}]^2}{[\mathrm{D}]} = 4[\mathrm{D}] \tag{4.5}$$

and the total protein concentration $[\mathrm{P}]_{\mathrm{T}}$ is given by

$$[\mathrm{P}]_T = \mathrm{M} + 2\mathrm{D}, \tag{4.6}$$

and substituting 4.4 and 4.5 into 4.6 gives

$$[\mathrm{P}]_T = \frac{K_{\mathrm{D}}}{2} + \frac{K_{\mathrm{D}}}{2} = K_{\mathrm{D}} \tag{4.7}$$

If the concentration is changed by a factor of Z then

$$[\mathrm{P}_Z] = Z[\mathrm{P}_I] = K_Z = \mathrm{Z}K_I \tag{4.8}$$

where $[\mathrm{P}_I]$, K_I, $[\mathrm{P}_Z]$ and K_Z are the protein concentration and dissociation constant at the initial and final concentration respectively.

If the difference in melting temperatures is only a few degrees K then

$$T_I \approx T_Z, \tag{4.9}$$

so we can express 4.8 as

$$-\mathrm{R}T_{\mathrm{m},Z}\ln\{K_Z\} = -\mathrm{R}T_{\mathrm{m},I}\ln\{ZK_I\} = -\mathrm{R}T_{\mathrm{m},I}\ln\{Z\} - \mathrm{R}T_{\mathrm{m},I}\ln\{K_I\} \tag{4.10}$$

where $T_{\mathrm{m},I}$ and $T_{\mathrm{m},Z}$ are the melting temperatures at the respective concentrations. We know that

$$-RT\ln\{K\} = \Delta H - T\Delta S, \tag{4.11}$$

so 4.11 can be substituted into 4.10 to give

$$\Delta H - T_{\mathrm{m,I}}\Delta S = -\mathrm{R}T_{\mathrm{m},Z}\ln\{Z\} + \Delta H - T_{\mathrm{m},Z}\Delta S, \tag{4.12}$$

and simplified to

$$(T_Z - T_I)\Delta S = -\mathrm{R}T_{\mathrm{m},Z}\ln\{Z\} \quad 4.13$$

rearranged to give

$$\Delta T = \frac{\mathrm{R}T_{\mathrm{m},Z}\ln\{Z\}}{\Delta S} \quad 4.14$$

at T_{m}

$$\Delta H = T\Delta S \quad 4.15$$

so substituting 4.15 into 4.13 we obtain

$$\Delta T = \frac{\mathrm{R}{T_{\mathrm{m},Z}}^2\ln\{Z\}}{\Delta H} \quad 4.16$$

4.5.2 Allosteric model

The experimentally observable parameters, which comprise the apparent binding affinities and enthalpies for the first and second molecules of AcCoA as a function of temperature (K_{A1}^{app}, $\Delta H_{\mathrm{A1}}^{app}$, K_{A2}^{app}, $\Delta H_{\mathrm{A2}}^{app}$), were re-cast in terms of microscopic model parameters, which describe 4 thermodynamic transitions: binding of the first and second molecules of AcCoA to the native enzyme and subunit melting in the 0-bound and 1-bound forms.

The microscopic binding constants for the first and second binding event of AcCoA to AAC(6')-Ii are defined as

$$K_{A1} = \frac{[\mathbf{BF}']}{[\mathbf{FF}][\mathbf{X}]} \quad 4.17$$

and

$$K_{A2} = \frac{[\mathbf{BB}]}{[\mathbf{BF'}][\mathbf{X}]} = \frac{[\mathbf{BB}]}{[\mathbf{F'B}][\mathbf{X}]}, \quad 4.18$$

where [**X**] is the concentration of free ligand. The equilibrium constant for the partial unfolding of the 0-bound and 1-bound state is given by

$$K_{U0} = \frac{[\mathbf{UF}]}{[\mathbf{FF}]} = \frac{[\mathbf{FU}]}{[\mathbf{FF}]} = \frac{[\mathbf{UU}]}{[\mathbf{FU}]} = \frac{[\mathbf{UF}]}{[\mathbf{UF}]}, \quad 4.19$$

and

$$K_{U1} = \frac{[\mathbf{U'B}]}{[\mathbf{F'B}]} = \frac{[\mathbf{FU'}]}{[\mathbf{FB'}]}, \quad 4.20$$

We denote the total concentrations of protein (i.e. all native and partially denatured forms) that are unbound, bound in the first subunit, bound in the second subunit, and fully bound with [**PP**], [**XPP**], [**PPX**], and [**XPPX**], respectively. Using these definitions and applying eq 4.17-4.20 we obtain

$$[\mathbf{PP}] = [\mathbf{FF}] + [\mathbf{UF}] + [\mathbf{FU}] + [\mathbf{UU}] = [\mathbf{FF}](1 + 2K_{U0} + K_{U0}^2) = [\mathbf{FF}](1 + K_{U0})^2 \quad 4.21$$

$$[\mathbf{XPP}] = [\mathbf{BF'}] + [\mathbf{F'B}] = [\mathbf{BF'}] + K_{U1}[\mathbf{BF'}] = K_{A1}[\mathbf{FF}][\mathbf{X}](1 + K_{U1}) \quad 4.22$$

$$[\mathbf{PPX}] = [\mathbf{F'B}] + [\mathbf{BF'}] = [\mathbf{F'B}] + K_{U1}[\mathbf{F'B}] = K_{A1}[\mathbf{FF}][\mathbf{X}](1 + K_{U1}) \quad 4.23$$

$$[\mathbf{XPPX}] = [\mathbf{FF}] = K_{A2}[\mathbf{BF'}][\mathbf{X}] = K_{A2}[\mathbf{F'B}][\mathbf{X}] = K_{A1}K_{A2}[\mathbf{FF}][\mathbf{X}]^2 \quad 4.24$$

The apparent equilibrium association constants for the first and second molecules of AcCoA are then given by the expressions

$$K_{A1}^{app} = \frac{[\mathbf{XPP}]}{[\mathbf{PP}][\mathbf{X}]} = \frac{[\mathbf{PPX}]}{[\mathbf{PP}][\mathbf{X}]} = \frac{K_{A1}[\mathbf{FF}][\mathbf{X}](1 + K_{U1})}{[\mathbf{FF}](1 + K_{U0})^2[\mathbf{X}]} = K_{\mathrm{A1}}\frac{(1 + K_{\mathrm{U1}})}{(1 + K_{\mathrm{U0}})^2} \quad 4.25$$

and

$$K_{A2}^{app} = \frac{[\mathbf{XPPX}]}{[\mathbf{XPP}][\mathbf{X}]} = \frac{[\mathbf{XPPX}]}{[\mathbf{PPX}][\mathbf{X}]} = \frac{K_{A1}K_{A2}[\mathbf{FF}][\mathbf{X}]^2}{K_{A1}[\mathbf{FF}][\mathbf{X}](1 + K_{U1})[\mathbf{X}]} = K_{\mathrm{A2}}\frac{1}{(1 + K_{\mathrm{U1}})} \quad 4.26$$

In Eq. 4.25, the apparent affinity for the first molecule of AcCoA (K_{A1}^{app}) in the absence of unfolding (K_{U0}, K_{U1}<<1) is equal to the intrinsic affinity of the native protein (K_{A1}), as expected. Partial unfolding in the 0-bound state (increasing K_{U0}) leads to a decrease in the apparent affinity, since the protein must undergo energetically-unfavorable folding in order to bind. Somewhat counterintuitively, unfolding of the unbound subunit in the 1-bound enzyme (increasing K_{U1}) leads to an increase in the apparent affinity for the first AcCoA molecule. This can be explained in terms of a hypothetical system where K_{U0}<<1<<K_{U1}. In this case, the 0-bound enzyme is almost entirely in the **FF** state, while the 1-bound enzyme is almost entirely in the **BU'** state. Binding of the first molecule of AcCoA is accompanied by unfolding of the unbound subunit, which helps to drive the reaction forward. In Eq. 4.26, partial unfolding of the unbound subunit in the 1-bound state (increasing K_{U1}) leads to a decrease in the apparent affinity for the second molecule of AcCoA, as expected. The average enthalpy for the 0-bound enzyme is given by,

$$H_{PP} = H_{FF} + \frac{2K_{U0}}{1 + K_{U0}} \Delta H_{U0} \qquad 4.27$$

where H_{FF} is the enthalpy of the native enzyme, ΔH_{U0} is the change in enthalpy upon partial denaturation of a single subunit, K_{U0}/(1+K_{U0}) is the fraction of subunits that are partially denatured, and the factor of 2 accounts for the fact that

both subunits of the 0-bound state can undergo partial denaturation. The average enthalpy of the 1-bound enzyme is given by

$$H_{XPP} = H_{PPX} = H_{F`B} + \frac{K_{U1}}{1+K_{U1}}\Delta H_{U1} = H_{BF'} + \frac{K_{U1}}{1+K_{U1}}\Delta H_{U1} \quad 4.28$$

where $H_{BF'} = H_{F'B}$ is the enthalpy of the native 1-bound state, ΔH_{U1} is the change in enthalpy upon partial denaturation of the unbound subunit, and $K_{U1}/(1+K_{U1})$ is the fraction of unbound subunits that are partially denatured. The enthalpy of the 2-bound state is denoted by

$$H_{XPPX} = H_{BB}. \quad 4.29$$

The intrinsic binding enthalpies for the first and second binding event are given by

$$\Delta H_{A1} = H_{BF'} - H_{FF} = H_{F'B} - H_{FF} \quad 4.30$$

and

$$\Delta H_{A2} = H_{BB} - H_{BF'} = H_{BB} - H_{F'B}. \quad 4.31$$

Combining eq 4.27, 4.28 and 4.30 gives the enthalpy for the first binding event, given as

$$\Delta H_{A1}^{app} = H_{PPX} - H_{PP} = H_{XPP} - H_{PP} = \Delta H_{A1} + \Delta H_{U1}\frac{K_{U1}}{1+K_{U1}} - \Delta H_{U0}\frac{2K_{U0}}{1+K_{U0}} \quad 4.32$$

and

$$\Delta H_{A2}^{app} = H_{XPPX} - H_{PPX} = H_{XPPX} - H_{XPP} = \Delta H_{A2} - \Delta H_{U1}\frac{K_{U1}}{1+K_{U1}}, \quad 4.33$$

Each of these transitions is associated with 3 parameters: an equilibrium constant (K') and enthalpy change ($\Delta H'$) at an arbitrary reference temperature

(T') and the change in heat capacity (ΔC_p). The temperature dependences of microscopic equilibrium constants and enthalpies are given by

$$K\{T\} = K'\exp\left\{\frac{\Delta \mathrm{H}'}{\mathrm{R}}\left(\frac{1}{\mathrm{T}'}-\frac{1}{\mathrm{T}}\right)+\frac{\Delta \mathrm{C_p}}{\mathrm{R}}\left(\ln\left(\frac{T}{T'}\right)+\frac{T'}{T}-1\right)\right\}, \quad 4.34$$

and

$$\Delta H\{T\} = \Delta H' + \Delta C_p(T - T'), \quad 4.35$$

The affinity and enthalpy profiles were relatively insensitive to the choices of $\Delta C_{p,\mathrm{U0}}$ and $\Delta C_{p,\mathrm{U1}}$. Therefore both parameters were fixed equal to the value we have previously determined for a monomeric mutant of AAC(6')-Ii in Chapter 3, 2.1 kcal mol^{-1} K^{-1}. The molar ellipticity of the protein was fitted as the population-weighted average of those of the **F** and **U** states, which were assumed to be linear functions of temperature, according to the expression

$$[\Theta]\{T\} = \frac{1}{1+K_{U0}}\left([\Theta]'_F + m_F \times (T - T')\right) + \frac{K_{U0}}{1+K_{Uo}}\left([\Theta]'_U + m_U \times (T - T')\right) \quad 4.36$$

where $[\Theta]'_{\mathrm{F}}$ and $[\Theta]'_{\mathrm{U}}$ are the molar ellipticities of the **F** and **U** states at T' and m_F and m_U are the corresponding temperature dependences. Fourteen parameters (K'_{A1}, $\Delta H'_{\mathrm{A1}}$, $\Delta C_{p,\mathrm{A1}}$, K'_{A2}, $\Delta H'_{\mathrm{A2}}$, $\Delta C_{p,\mathrm{A2}}$, K'_{U0}, $\Delta H'_{\mathrm{U0}}$, K'_{U1}, $\Delta H'_{\mathrm{U1}}$, $[\Theta]'_{\mathrm{F}}$, m_{F}, $[\Theta]'_{\mathrm{U}}$, m_{U}) were adjusted to minimize the residual function

$$\mathrm{RSS} = \sum\left(\frac{\ln\{K^{app}_{\mathrm{A1,2}}\}_{\mathrm{exp}} - \ln\{K^{app}_{\mathrm{A1,2}}\}_{\mathrm{calc}}}{\ln\{K^{app}_{\mathrm{A1,2}}\}_{\mathrm{exp}}}\right)^2 + \sum\left(\frac{\{\Delta H^{app}_{\mathrm{A1,2}}\}_{\mathrm{exp}} - \{\Delta H^{app}_{\mathrm{A1,2}}\}_{\mathrm{calc}}}{\{\Delta \mathrm{H}^{app}_{\mathrm{A1,2}}\}_{\mathrm{exp}}}\right)^2 + \sum\left(\frac{[\Theta]_{\mathrm{exp}} - [\Theta]_{\mathrm{calc}}}{[\Theta]_{\mathrm{exp}}}\right)^2, \quad 4.37$$

where the sums run over all data points.

4.5.3 Calculating theoretical ITC isotherms

As was explained in Chapter 2, given the apparent association constants (K_{A1}^{app} and K_{A2}^{app}) and enthalpies (ΔH_{A1}^{app} and ΔH_{A2}^{app}) for binding of the first and second molecules of AcCoA to AAC(6')-Ii, the initial concentrations of enzyme ($[P]_0$), and ligand ($[X]_0$), and the working volume of the cell (V_0), a theoretical ITC isotherm can be calculated. The heat released or absorbed (ΔQ) for injection i is dependent on the fraction of protein singly (f_1) and doubly (f_2) bound.

4.5.4 Calculating fractions of AAC(6')-Ii in the 0-bound, 1-bound, and 2-bound states

Given the apparent association constants (K_{A1}^{app} and K_{A2}^{app}) for binding of the first and second molecules of AcCoA to AAC(6')-Ii as well as the total concentration of enzyme ($[P]_T$) and AcCoA ($[X]_T$), the fractions of protein in the 0-bound, 1-bound, and 2-bound states (f_0, f_1, f_2) can be determined by

$$f_1 = \frac{2K_{A1}^{app}[X]}{1 + 2K_{A1}^{app} \cdot [X] + K_{A1}^{app} \cdot K_{A2}^{app} \cdot [X]^2}, \quad 4.38$$

and

$$f_2 = \frac{K_{A1}^{app} \cdot K_{A2}^{app} \cdot [X]^2}{1 + 2K_{A1}^{app} \cdot [X] + K_{A1}^{app} \cdot K_{K2}^{app} \cdot [X]^2}. \quad 4.39$$

Chapter 2 describes the expressions used to determine the concentration of free AcCoA ([X]) throughout the titration.

4.5.5 Global Fitting of ITC isotherms

Each ITC isotherm can be fit individually to five adjustable parameters: the apparent association constants (K_{A1}^{app} and K_{A2}^{app}) and enthalpies (ΔH_{A1}^{app} and ΔH_{A2}^{app}) for binding of the first and second molecules of AcCoA to AAC(6')-Ii, and the initial enzyme concentration ($[P]_0$). Individual fits of the entire 28-isotherm dataset therefore contain a total of 140 adjustable parameters. Through globally fitting the isotherms to a single set of binding parameters the number of adjustable parameters can be reduced to 46. Chapter 3 showed that the accuracy of the fits can be improved by using the *van't* Hoff global fitting scheme that makes no assumption regarding the underlying allosteric mechanism. In this approach, the van 't Hoff expression,

$$\frac{\partial \ln\{K_{A1,2}^{app}\}}{\partial T} = \frac{\Delta H_{A1,2}^{app}}{RT^2}, \qquad 4.40$$

is used to constrain the values of $\Delta H_{A1,2}^{app}$ and $K_{A1,2}^{app}$ within the global fits. The binding enthalpies, $\Delta H_{A1,2}^{app}$, are optimized at each experimental temperature (T_j), while association constants are fitted only at a single temperature (T_0). The remaining $K_{A1,2}^{app}$ values are obtained from the set of $\Delta H_{A1,2}^{app}(T_j)$ and the integrated form of Eq 4.40.

$$\ln\{K_{A1,2}^{app}(T_j)\} = \ln\{K_{A1,2}^{app}(T_0)\} + \frac{1}{R}\int_{T_0}^{T_j} \frac{\Delta H_{A1,2}^{app}(T)}{T^2}\, dT. \quad 4.41$$

The last term in Eq 4.41 is evaluated by trapezoidal numerical integration, in which the function $\Delta H_{A1,2}{}^{app}(T)/T^2$ is approximated by a series of straight lines connecting the experimental $\Delta H_{A1,2}{}^{app}(T_j)/T_j{}^2$ points, leading to the expression:

$$\ln\{K_{A1,2}^{app}(T_j)\} = \ln\{K_{A1,2}^{app}(T_0)\} + \sum_{i=1}^{j} \frac{T_i}{2R}\left(\frac{\Delta H_{A1,2}^{app}}{(T_{i-1})^2} + \frac{\Delta H_{A1,2}^{app}(T_i)}{(T_i)^2}\right) \quad 4.42$$

In this approach, 28 values of $[P]_0$ are optimized (one for each isotherm), 8 values of $\Delta H_{A1}{}^{app}$ and $\Delta H_{A2}{}^{app}$ are optimized (one pair of enthalpies for each temperature), and only a single value of $K_{A1}^{app}(T_0)$ and a single value of $K_{A2}^{app}(T_0)$ are fitted, at a reference temperature T_0. The values of $K_{A1}^{app}(T_j)$ and $K_{A2}^{app}(T_j)$at the remaining seven temperatures are obtained using Eq 4.42. The 46 adjustable parameters were varied to minimize the residual sum of squared deviations,

$$\mathrm{RSS} = \sum_i \left(\Delta Q(i)_{calc} - \Delta Q(i)_{exp}\right)^2, \quad 4.43$$

where the sum runs over all injection heats in all ITC experiments. The $\Delta Q(i)_{calc}$ values were calculated from the 46 adjustable parameters by computing 1) the 14 association constants at the seven remaining temperatures using Eq 4.42; 2) the total amounts of enzyme and ligand at each point of each isotherm using; 3) the concentrations of free ligand at each point of each isotherm; 4) the fractions of 0-bound, 1-bound, and 2-bound states (f_0, f_1, and f_2) at each point of each

isotherm using Eq 4.38 and 4.39; 5) the heat released during each injection (ΔQ(i)).

4.5.6 Error Calculations

Uncertainties in the parameters extracted from the global fit were determined using the covariance matrix similarly described in Chapter 2, given by:[131-132]

$$\hat{V} = \frac{RSS}{DF}\left(\hat{X}\hat{W}\hat{X}\right)^{-1} \quad 4.44$$

where $\hat{X}$ is a matrix of the first derivatives of the differences between the 756 calculated and experimental injection heats, $\Delta\Delta Q(i) = \Delta Q(i)_{calc} - \Delta Q(i)_{exp}$, with respect to each of the 46 adjustable parameters, $A_{1..46}$, evaluated numerically at the values of the optimized binding parameters:

$$X = \begin{bmatrix} \frac{\partial \Delta\Delta Q(1)}{\partial A_1} & \cdots & \frac{\partial \Delta\Delta Q(756)}{\partial A_1} \\ \vdots & \ddots & \vdots \\ \frac{\partial \Delta\Delta Q(1)}{\partial A_{46}} & \cdots & \frac{\partial \Delta\Delta Q(756)}{\partial A_{46}} \end{bmatrix}, \quad 4.45$$

$\hat{W}$ is a 756x756 diagonal matrix of the fitting weights for all data points (all equal to 1), RSS is the sum of the residual squares (Eq 4.43) and *DF* is the degrees of freedom for the fit (710). The diagonal elements in $\hat{V}$ are the variances of the optimized binding parameters, while the off-diagonal elements describe correlations between the errors of the extracted parameters.

The uncertainties in those affinity constants obtained by trapezoidal integration ($K_{A1,2}^{app}(T_1..T_7)$; Eq 4.42 and in the parameters extracted from fits of the allosteric model were computed from the covariance matrix using a Monte Carlo approach. 10^4 sets of 18 binding parameters, $A_{1..18}$, comprising the apparent affinities at the reference temperature, $K_{A1,2}^{app}(T_0)$, and apparent enthalpies at all temperatures, $\Delta H_{A1,2}^{app}(T_0..T_7)$, were generated with the appropriate distributions of random errors according to:[189]

$$\begin{bmatrix} A_1^{MC} \\ \vdots \\ A_{18}^{MC} \end{bmatrix} = \begin{bmatrix} A_1^{exp} \\ \vdots \\ A_{18}^{exp} \end{bmatrix} + \hat{L} \begin{bmatrix} \varepsilon_1 \\ \vdots \\ \varepsilon_{18} \end{bmatrix} \quad 4.46$$

where ε_i are random numbers distributed with means of 0 and a standard deviations of 1. $\hat{L}$ is the lower triangular matrix from Cholesky decomposition satisfying

$$\hat{V}' = \hat{L}\hat{L}' \quad 4.47$$

where $\hat{L}^T$ is the transpose of $\hat{L}$, and $\widehat{V}'$ corresponds to the portion of the covariance matrix describing uncertainties in the affinities and enthalpies (i.e. omitting portions related to uncertainties in fitted $[P]_0$ values). The 10^4 sets of Monte-Carlo binding parameters were used to generate 10^4 sets of 14 affinity constants ($K_{A1,2}^{app}(T_1..T_7)$) with Eq 4.42. The standard deviations in the values were taken as the experimental uncertainties. The allosteric model described in the text was fitted to the 10^4 Monte Carlo datasets (including affinity constants obtained by trapezoidal integration), yielding 10^4 sets of model parameters (K_{A1},

ΔH_{A1}, $\Delta C_{p,A1}$, K_{A2}, ΔH_{A2}, $\Delta C_{p,A2}$, K_{U0}, ΔH_{U0}, K_{U1}, ΔH_{U1}). The standard deviations in the parameters were taken as the experimental uncertainties.

4.6 Thermodynamic Description of Allostery.

Temperature-dependent allostery in AAC(6')-Ii can be explained by a model comprising a hybrid of the KNF and HT paradigms (Fig. 4.12). The ITC, CD, and NMR data indicate that each subunit of the enzyme can exist in at least 3 (likely more) distinct conformational states. Disordered conformations are increasingly prominent as the temperature is raised, although a dimeric form is retained. We have represented this as the transition of each subunit from a native free (**F**) form to a partially unfolded (**U**) form. The free enzyme can therefore exist as a mixture of **FF**, **FU**, **UF**, and **UU** states. Under conditions where the enzyme is entirely in the **FF** state, subunits undergo a large conformational change when AcCoA is bound (we assume that this conformational change does not occur to a significant extent in the absence of AcCoA, as discussed above). This can be represented as transitions from the **F** state to a bound (**B**) state. Under stabilizing conditions, the 1-bound enzyme contains one subunit in the **B** form, and another that somewhat resembles the 0-bound state, i.e. **BF'** and **F'B.** The free subunit (**F'**) also melts, since the temperature profile of ΔH_{A2}^{app} is curved. For the sake of generality, we will refer

to the unfolded subunit in the 1-bound enzyme as **U'** to distinguish it from unfolded subunits of the 0-bound enzyme. Therefore a full description of the 1-bound enzyme includes the states **BF'**, **BU'**, **F'B**, and **U'B**. The 2-bound enzyme exists simply as **BB**. The ITC data show that the thermal unfolding transition depends upon the conformational state of the adjacent subunit (i.e. **FF**$\rightarrow$**FU** $\neq$ **BF'**$\rightarrow$**BU'**). This conclusion is based on a simple calculation, equations 4.31 and 4.32, showing that if the thermal transition of each subunit were unaffected by its neighbor, both ΔH_{A1}^{app} and ΔH_{A2}^{app} would exhibit identical curvature, which is not the case (Fig. 4.11b). We therefore employed a model in which all thermal transitions of the 0-bound state are thermodynamically equivalent and the thermal transitions of the 1-bound state are different. The assumption that subunits partially unfold independently in the 0-bound enzyme (**FF**$\rightarrow$**FU** = **UF**$\rightarrow$**UU**) is almost certainly an over-simplification. However, a more realistic description of subunit unfolding would require additional adjustable parameters. This simple model provides excellent agreement with the data (see below). Any additional folding parameters would therefore be ill-defined by the data. The parameters extracted using this simple model provide effective measures of subunit unfolding, even though the process is likely more complex in reality.

Temperature-dependent allostery in this protein is thus described by 12 microscopic thermodynamic parameters. Equilibrium constants, enthalpy and

heat capacity changes are associated with the first (**FF**→**F'B**, **FF**→**BF'**) and second (**F'B**→**BB**, **BF'**→**BB**) binding events, as well as thermal transitions in the 0-bound (**FF**→**FU**, **FF**→**UF**, **FU**→**UU**, **UF**→**UU**) and 1-bound states (**BF'**→**BU'**, **F'B**→**U'B**). In addition, the linear CD baselines of the **F** and **U** states are each described by two parameters (slopes and vertical positions). These parameters were fitted to the combined ITC and CD dataset, as reported in Table 4.2. The lines in Fig. 4.11 are derived from these optimized thermodynamic parameters, and show excellent agreement between the model and all experimental data, even capturing the slight upward curvature of ΔH_{A1}^{app}.

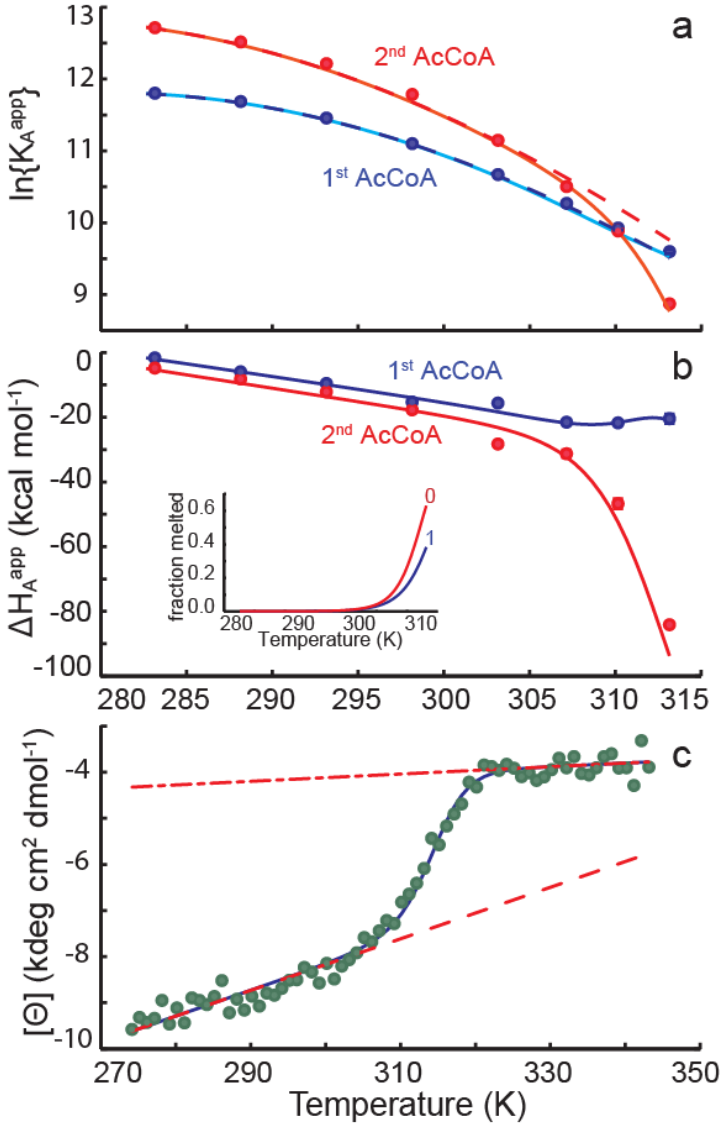

Fig. 4.11: Temperature dependence of AAC(6')-Ii binding thermodynamics and secondary structure. **(a)** Equilibrium association constants for the first and second molecules of AcCoA, plotted as a function of temperature. Solid lines correspond to the best fit obtained with Eqs. 4.17 to 4.37. Dashed lines indicate the predicted affinities in the absence of thermal melting of the subunits. **(b)** Binding enthalpies of the first and second molecules of AcCoA. Inset shows the fraction of free subunits that are melted in the 0-bound and 1-bound forms. **(c)** Molar ellipticity (222 nm) of AAC(6')-Ii as a function of temperature. Dashed and dash-dot lines correspond to the pre- and post-transition baselines, respectively.

Table 4.2: Thermodynamic parameters describing allostery in AAC(6')-Ii binding AcCoA at 37°C

K'_{A1} ($\times 10^4$ M^{-1})[a]	2.1	±0.1	$\Delta H'_{U0}$ (kcal mol^{-1})[k]	-71	±7
K'_{A2} ($\times 10^4$ M^{-1})[b]	2.8	±0.1	$\Delta H'_{U1}$ (kcal mol^{-1})[l]	-93	±6
K'_{U0}[c]	0.20	±0.06	$\Delta C_{p,A1}$ (cal mol^{-1} K^{-1})[m]	-790	±40
K'_{U1}[d]	0.38	±0.07	$\Delta C_{p,A2}$ (cal mol^{-1} K^{-1})[n]	-820	±30
$\Delta G'_{A1}$ (kcal mol^{-1})[e]	-6.13	±0.03	$\Delta C_{p,U0}$ (cal mol^{-1} K^{-1})[o]	2100	NA
$\Delta G'_{A2}$ (kcal mol^{-1})[f]	-6.32	±0.02	$\Delta C_{p,U1}$ (cal mol^{-1} K^{-1})[o]	2100	NA
$\Delta G'_{U0}$ (kcal mol^{-1})[g]	1.0	±0.2	$[\Theta]'_F$ (deg cm^2 $dmol^{-1}$)[p]	-7600	±200
$\Delta G'_{U1}$ (kcal mol^{-1})[h]	0.6	±0.1	$[\Theta]'_U$ (deg cm^2 $dmol^{-1}$)[q]	-4040	±20
$\Delta H'_{A1}$ (kcal mol^{-1})[i]	-22.9	±0.8	m_F (deg cm^2 $dmol^{-1}$ K^{-1})[r]	54	±3
$\Delta H'_{A2}$ (kcal mol^{-1})[j]	-28.1	±0.8	m_U (deg cm^2 $dmol^{-1}$ K^{-1})[s]	8	±2

T'=37ºC

[a]Equilibrium association constant for the native (non-melted) enzyme and the first AcCoA molecule

[b]Equilibrium association constant for the native (non- melted) enzyme and the second AcCoA molecule

[c]Equilibrium constant for subunit melting in the 0-bound enzyme

[d]Equilibrium constant for melting of the unbound subunit in the 1-bound enzyme

[e]Free energy change upon binding of one molecule of AcCoA to the native (non- melted) 0-bound enzyme

[f]Free energy change upon binding of one molecule of AcCoA to the native (non- melted) 1-bound enzyme

[g]Free energy change upon melting of a single subunit in the 0-bound enzyme

[h]Free energy change upon melting of the unbound subunit in the 1-bound enzyme

[i]Enthalpy change upon binding of one molecule of AcCoA to the native (non- melted) 0-bound enzyme

[j]Enthalpy change upon binding of one molecule of AcCoA to the native (non- melted) 1-bound enzyme

[k]Enthalpy change upon melting of a single subunit in the 0-bound enzyme

[l]Enthalpy change upon melting of the unbound subunit in the 1-bound enzyme

[m]Heat capacity change upon binding of one molecule of AcCoA to the native (non- melted) 0-bound enzyme

[n]Heat capacity change upon binding of one molecule of AcCoA to the native (non- melted) 1-bound enzyme

[o]Heat capacity change upon subunit melting. These values were fixed at the value obtained for a monomeric mutant of AAC(6')-Ii

[p]CD molar ellipticity of a native (non- melted) subunit

[q]CD molar ellipticity of a melted subunit

[r]Temperature dependence of the molar ellipticity of a native subunit

[s]Temperature dependence of the molar ellipticity of a melted subunit

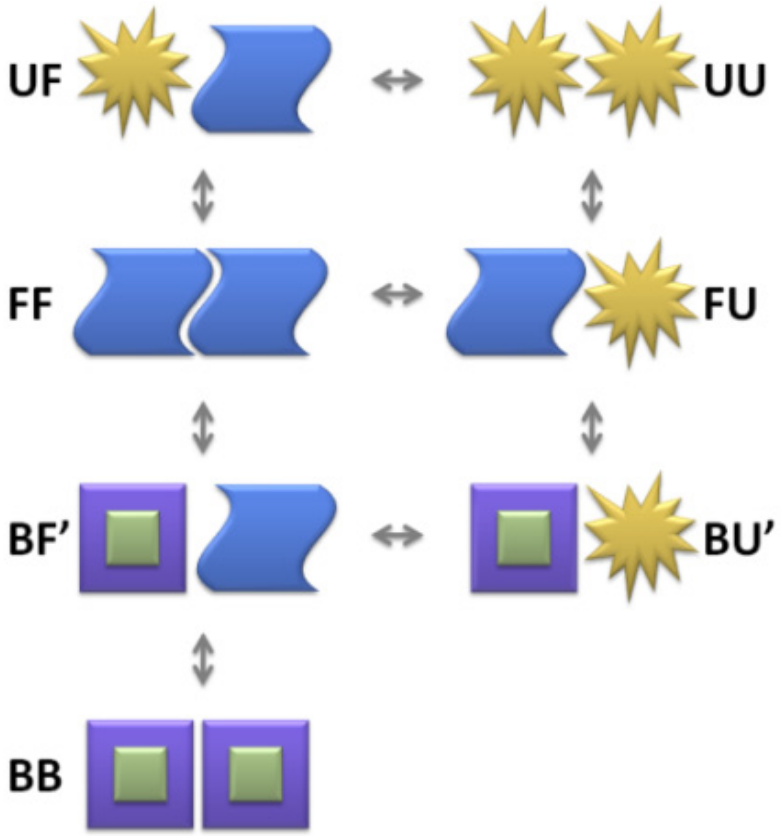

Fig. 4.12: Schematic representation of the allosteric binding model. **B** corresponds to the bound state. **F(F')** and **U(U')** correspond to the free folded and partially unfolded states that are adjacent to a free (bound) subunit, respectively. Transitions involving the symmetry-related **F'B** and **U'B** states are not shown.

4.7 Discussion

The energy of AAC(6')-Ii binding to AcCoA can be separated into two distinct contributions, based on the parameters extracted in the global fit of ITC and CD data (Fig. 4.11 and Table 4.2). The first component corresponds to the intrinsic binding affinity of the native dimer for AcCoA, while the second arises from partial unfolding of the subunits. In order to address the first component, the

intrinsic ability of the dimer to bind AcCoA in the absence of **F**→**U** and **F'**→**U'** transitions can be predicted based on the model parameters, even for temperatures where the **U** and **U'** states are prevalent (dashed lines in Fig. 4.11a). The calculations show that the dimer binds with inherently positive cooperativity across the entire temperature range studied, although the intrinsic positive cooperativity should disappear at about 48ºC due to the temperature dependences of K_{A1} and K_{A2}. According to the NMR data, when the 0-bound enzyme binds a single molecule of AcCoA, a single subunit converts from the **F** to the **B** state. This is consistent with a classical KNF explanation of allostery.[161] We hypothesize that binding of the first ligand (**FF**→**BF'**) is opposed by disruption of the **FF** interface, while binding of the second (**BF'**→**BB**) is promoted by formation of the **BB** interface; the symmetry of the **FF** and **BB** interfaces likely make them more stable than the **F'B** interface of the 1-bound state.[190]

The low intensities of some NMR signals for the free subunit in the 1-bound enzyme (**F'**) suggest that it may undergo additional dynamics beyond those already present in the **F** state. In fact, modulation of protein dynamics can provide a powerful driving force for protein allostery.[168-170] It is possible that the intrinsic positive cooperativity of the AAC(6')-Ii dimer derives from a combination of these two effects. This idea is supported by the extracted thermodynamic parameters (Table 4.2). Compared to binding the first molecule of AcCoA,

binding the second is enthalpically more favorable ($\Delta\Delta H_A$=-3.4 kcal mol^{-1} at 10ºC), consistent with the formation of additional contacts, and entropically less favorable ($\Delta\Delta S_A$=-10 cal mol^{-1} K^{-1} at 10ºC), consistent with the dampening of internal motions.

The unbound subunits undergo partial unfolding as the temperature is raised. The process is endothermic and entropically favored as would be expected, ΔH_U = 71, 93 kcal mol^{-1} and ΔS_U = 230, 300 cal mol^{-1} K^{-1} at 37ºC in the 0-bound and 1-bound states, respectively. The model used makes the assumption that each subunit folds and unfolds independently of the second subunit so that **FF**→**FU** is equivalent to **UF**→**UU**. However, the ligation state of the enzyme alters the stability of the subunits, and the model predicts that subunits are slightly more stable in the context of the 0-bound compared, **FF**, then the 1-bound state, **BF'**, with melting temperatures of 41.2 for **FF**→**FU** and 39.0 ºC for **BF'**→**BU'**. At 37ºC, K_{U0}=[**FU**]/[**FF**]=0.20, while K_{U1}=[**BU'**]/[**BF'**]=0.38. This difference in stability may be related to disruption of the symmetrical **FF** subunit interface when the first AcCoA molecule is bound. At higher temperatures, this destabilization leads to partial unfolding of the unbound subunit of the 1-bound enzyme (**BF'**→**BU'**), with a concomitant reduction in affinity for the second AcCoA molecule (K_{A2}^{app}) and a shift towards negative cooperativity. At lower temperatures, the unbound subunit is sufficiently stable to

remain in the active (**F'**) state, and the intrinsic positive cooperativity of the native dimer dominates. This effect represents a modification of the HT (coupled folding and binding) model of allostery (Fig. 4.1c).[166] In the HT model, ligand-induced folding of one subunit alters the folding equilibrium of the adjacent subunit. In AAC(6')-Ii, each subunit can adopt at least three distinct conformational states, and it is largely the **F** to **B** transition that modulates partial unfolding of the adjacent subunit.

The modulation of folding/unfolding equilibria is emerging as a sensitive and versatile mechanism for connecting distant sites in proteins.[167,191-193] In AAC(6'), ligand binding in one subunit triggers a change in the subunit interface that promotes partial unfolding of adjacent subunit, conveying a homotropic allosteric signal and modulating ligand binding. An important consequence of the HT model, and folding-mediated allostery in general, is that control of cooperativity can be shared by many or most residues in a protein, even those located far from subunit interfaces or the active sites themselves, provided that these residues influence subunit stability.[166] This view of allostery as a decentralized process contrasts sharply with other studies in which it has been explained in terms of specific networks of relatively small numbers of interacting residues.[96,171] In AAC(6')-Ii, a negatively cooperative HT mechanism opposes the intrinsic positive (KNF) cooperativity of the native dimer. To our knowledge, this

is the first reported observation of such an intertwined phenomenon. Interestingly, the presence of these competing allosteric mechanisms leads to additional properties beyond those of either the KNF or HT models alone. In the original HT model, the type of the cooperativity (positive or negative) is specified entirely by whether the interaction between the folded domains is favorable (positive) or unfavorable (negative) with the strength of cooperativity modulated by the stability of the domains.[166] In the hybrid KNF-HT mechanism exhibited by AAC(6')-Ii, both the sign and the magnitude of cooperativity can be modulated simply by changing the stability of the subunits. Allostery in such systems can be defined by three parameters: the intrinsic cooperativity coefficient of the native dimer, $\alpha_{int}=K_{A2}/K_{A1}$,[194] the equilibrium constant for melting in the 0-bound state, K_{U0}, and the ratio of melting equilibrium constants in the 1-bound and 0-bound forms, $\varphi=K_{U1}/K_{U0}$. The apparent cooperativity is then given by the expression:

$$\alpha_{app} = \alpha_{int}(1 + K_{U0})^2/(1 + \varphi K_{UO})^2. \quad 4.48$$

Even if both α_{int} and φ remain constant, the apparent cooperativity can vary from positive ($\alpha_{app}>1$) to negative ($\alpha_{app}<1$) depending only on the intrinsic tendency of the subunits to partially unfold, K_{U0}. At 37ºC, global fits of AAC(6')-Ii data give an intrinsic cooperativity coefficient, $\alpha_{int}=1.3$, and a ratio of thermal melting constants, $\varphi=1.9$. Cooperativity can therefore vary between weakly positive ($\alpha_{app}\approx1.3$) to weakly negative ($\alpha_{app}\approx0.36$) for $K_{U0}<<1$ and $K_{U0}>>1$, respectively

(Fig. 4.13a). Interestingly, dynamic range of up to six orders of magnitude in α_{app} can be achieved if K_{U0} varies between 10^{-4} to 10^{2} and $\alpha_{int}=\phi=1024$ (Fig. 4.13b). Several important lessons can be drawn from AAC(6')-Ii as a model system. It represents one of the clearest examples to date of a system following the HT coupled folding/binding allosteric model. It provides proof-of-principle for competition between simultaneous positive and negative cooperative mechanisms, and suggests a scenario in which the sign of cooperativity can be modulated simply by altering subunit stability. Finally, aspects of the approach we took to characterize this enzyme have the potential to be quite useful in future studies of allostery. The *van 't* Hoff global fitting approach, which was described in Chapter 3, significantly reduces the scatter in the extracted ΔH_A^{app} and K_A^{app} values obtained for the variable-temperature ITC data, and permits definitive characterization of coupled folding and binding (fits using non-global methods are shown in Appendix Figure A.9). Simultaneous analyses of variable-temperature ITC and CD data have been performed previously,[179] but to our knowledge this the first application of this method to study homotropic allostery. In addition, the combined analysis of ITC and NMR titration facilitates characterization of the spectral properties of the 1-bound protein, even though its signals are not directly distinguishable. A new form of allosteric regulation has been identified in AAC(6')-Ii by applying calorimetric and high-resolution spectroscopic techniques

in concert. It seems likely that similar superpositions of MWC, KNF, and HT allosteric mechanisms will be observed in additional systems as more studies are performed using this sort of approach.

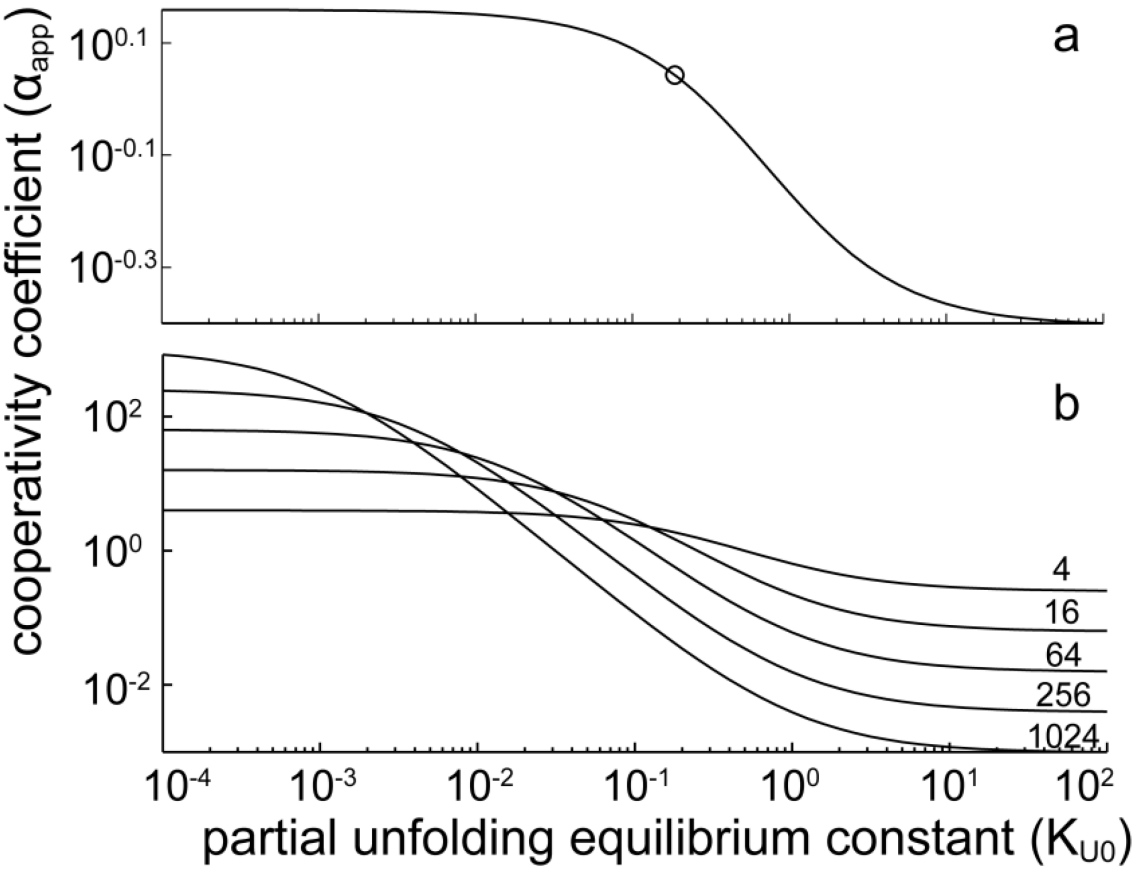

Fig. 4.13: Dependence of the apparent cooperativity coefficient (α_{app}) on subunit instability (K_{U0}=[**UF**]/[**FF**]) calculated using Eq. 4.48 and **(a)** the intrinsic cooperativity coefficient (α_{int}=1.3) and ratio of melting equilibrium constants constants (φ=1.9) determined for AAC(6')-Ii at 37ºC. The circle corresponds to the K_{U0} value obtained for AAC(6')-Ii at 37ºC (0.2). **(b)** Hypothetical proteins in which α_{int}=φ=4,16,64,256,1024..

5. Binding of paromomycin to aminoglycoside *N*-6'-acetyltransferase-Ii

5.0 Preface

As previously explained in the earlier chapters, isothermal titration calorimetry (ITC) is used to study the thermodynamics of molecular interactions through the direct measurement of heat released or absorbed. The previous chapters focused on the interactions of aminoglycoside *N*-6'-acetyltrasferase-Ii (AAC(6')-Ii with acetyl coenzyme A (AcCoA). Allostery was shown to affect the binding of AcCoA in the two active sites of AAC(6')-Ii.[62,66-67] Unlike the previous chapters, the ligand of interest in this chapter is the aminoglycoside. As explained in Chapter 1, AAC(6')-Ii undergoes a bi-bi sequential ordered mechanism first binding AcCoA followed by the aminoglycoside. However, aminoglycosides are also known to bind to AAC(6')-Ii in the absence of AcCoA.[45] However, to date there has been no successful attempt to crystallize AAC(6')-Ii with aminoglycosides bound. The only structural information available for aminoglycoside binding is from crystal structures of aminoglycosides chemically linked to a CoA molecule binding to AAC(6')-Ii. Methodologies described in Chapters 3 and 4 are used here to develop an allosteric model for the binding of aminoglycosides to AAC(6')-Ii. Data from ITC, nuclear magnetic resonance and circular dichroism spectroscopy experiments with AAC(6')-Ii in the presence of the aminoglycoside paromomycin suggests a different allosteric mechanism compared to the interaction of this enzyme with AcCoA. The work presented in

this chapter was performed by myself under the guidance of Dr. Karine Auclair and Dr. Anthony Mittermaier.

5.1 Introduction

AAC(6')-Ii consists of two identical subunits. Free in solution, the two subunits of the homodimer are in equilibrium between a binding competent folded (**F**) state and a binding incompetent partially unfolded (**U**) state. This equilibrium is temperature dependent and more protein populates the **U** state as the temperature is increased. When a subunit binds AcCoA it undergoes a conformational change from the **F** state to a bound (**B**) state to form a **FB** complex. The second subunit can bind an aminoglycoside and will form a **BB** complex. The two subunits interact with each other and prefer to be symmetric. This favours the enzyme to adopt either a **FF** or a **BB** conformation. The second binding event is thus favoured over the first binding event, giving rise to positive cooperativity. This follows the Koshland-Némethy-Filmer (KNF) model in which individual subunits fold from a free to a bound conformation and cooperativity results from the inter-subunit interactions,[64] shown in Fig. 4.11. Additionally, the unbound subunit of proteins in the **FB** state is destabilized due to the disruption of the interactions between the two subunits. The **FB** state will then unfold into the **UB** state at a lower temperature compared to free subunits in the **FF** state.

The increased prevalence of the **U** species creates negative cooperativity. This folding/unfolding equilibrium is reminiscent of the Hilser-Thompson model[88] (HT) explained in detail in Chapters 1 and 4. A detailed description of AcCoA binding to AAC(6')-Ii is found in section **4.6** of Chapter 4.

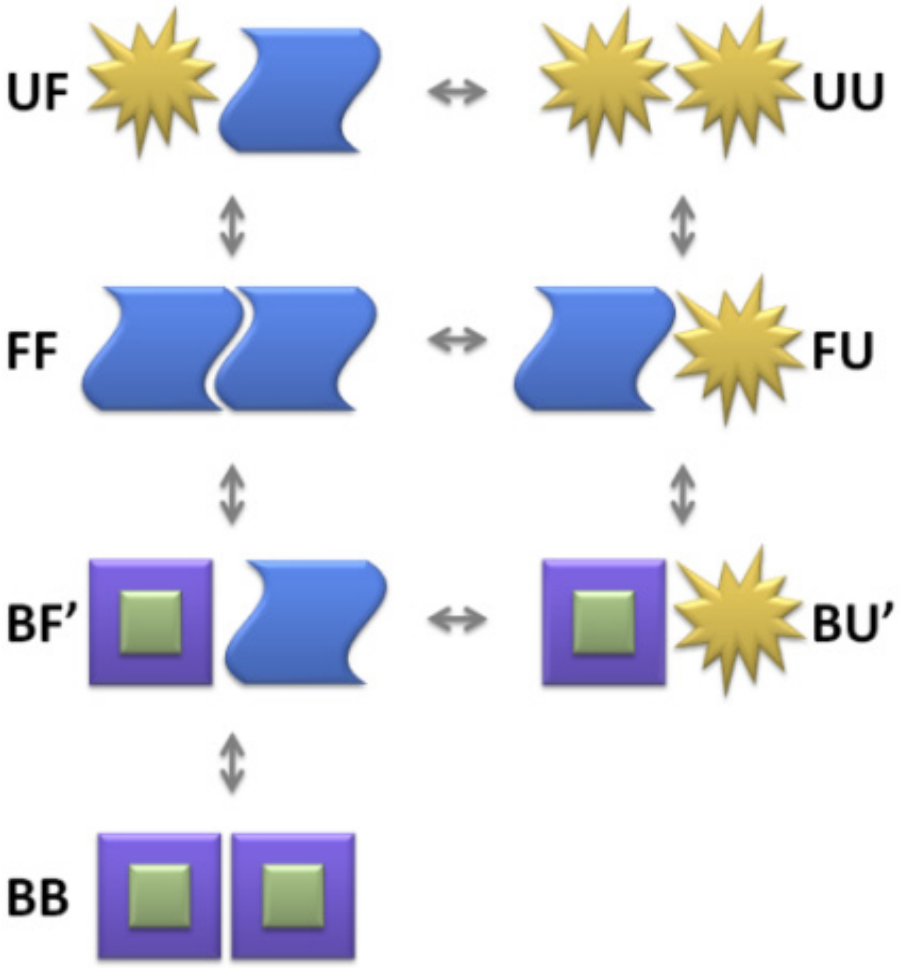

Fig. 5.1: Schematic representation of the allosteric binding model. **B** corresponds to the bound state. **F**(**F'**) and **U(U')** correspond to the free folded and partially unfolded states that are adjacent to a free (bound) subunit, respectively. Transitions involving the symmetry-related **F'B** and **U'B** states are not shown.

This chapter focuses on the interaction of AAC(6')-Ii with its other ligand, the aminoglycoside. AAC(6')-Ii is known to undergo a bi-bi sequential ordered catalytic mechanism with AcCoA binding initially followed by the aminoglycoside.[45] However, aminoglycosides can to bind to AAC(6')-Ii in the absence of AcCoA and produce an unproductive complex.[45] This complex must dissociate for AcCoA to bind and the enzyme reaction to occur. The aminoglycoside bound AAC(6')-Ii will be referred to as the unproductive complex and NMR signals which correspond to this complex will be referred to as unproductive peaks. Previously, Draker *et al.* have reported that aminoglycosides bind to AAC(6')-Ii in a cooperative manner. Preliminary ITC studies and kinetic studies showed that the wild type enzyme binds aminoglycosides with two non equivalent binding sites. Additionally, the kinetic studies showed mixed and partial inhibition of dead-end inhibitors which suggests cooperativity between the two sites.[45] The cooperativity observed was believed to be from the two subunits of the AAC(6')-Ii dimer interacting, as the cooperativity is not observed with the monomeric mutant variant AAC(6')-Ii W164A.[45]

Chapter 3 and 4 showed that binding enthalpy (ΔH_A) and binding constants (K_A) are linked through the *van 't* Hoff relation given as,

$$\frac{\partial \ln\{K_A\}}{\partial T} = \frac{\Delta H_A}{RT^2} \qquad 5.1$$

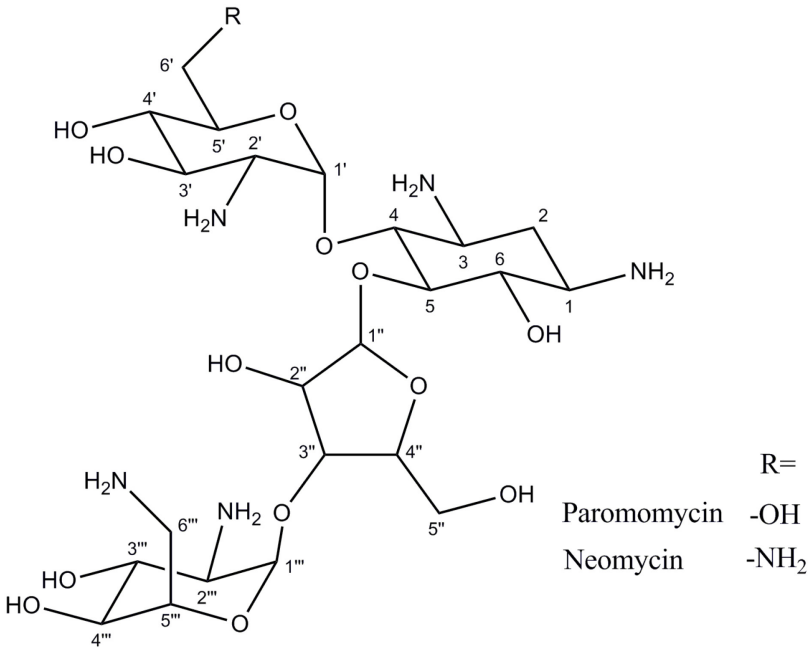

Fig. 5.2: Structure of the aminoglycosides paromomycin and neomycin.[195]

This relation can be used as a restraint for a variable T dataset and increase the accuracy in extracted phenomenological (macroscopic) binding parameters. These binding parameters can then be fit to a mechanistic (microscopic) model to describe the molecular events involved in binding. The work described in this chapter employs the methods detailed in Chapters 3 and 4 to study the binding of an aminoglycoside (paromomycin, Fig. 5.2) to AAC(6')-Ii. Paromomycin consists of a 4,5 disubstituted deoxystreptamine ring. Unlike most aminoglycosides, the 6' position consists of a hydroxyl group instead of an amine.[195] As a result, paromomycin is not acetylated by AAC(6')-Ii, and it is a competitive inhibitor.[45] Neomycin is the corresponding aminoglycoside containing a 6'-NH_2.

Paromomycin is an ideal probe, as future studies can be performed with paromomycin in the presence of AcCoA which would form the ternary complex without undergoing the acetyl transfer reaction. This will allow information on the ternary state to be obtained, by comparison with data on the unproductive complex studied in this chapter.

5.2 Isothermal titration calorimetry

Neomycin binding to AAC(6')-Ii was first compared to paromomycin binding AAC(6')-Ii. This verifies that substitution of the 6' amine of the aminoglycoside substrate with a hydroxyl group does not alter the binding mechanism. The resulting isotherms (Fig. 5.3) were fit to a 2-site sequential binding model. The values obtained for both fits are given in Table 5.1. The binding parameters obtained for neomycin and paromomycin are very similar with all values having less than 2-fold difference. The differences observed are unsurprising as it has been previously reported that different aminoglycosides can have a K_m up to 5-fold different from one another.[45] The isotherms of aminoglycosides binding to AAC(6')-Ii were also compared to that of AcCoA (Fig. 5.3C). It is immediately apparent that the binding of aminoglycosides differ from that of AcCoA.

Table 5.1: Binding parameters of individual fits of paromomycin and neomycin binding to AAC(6')-Ii

Aminoglycoside	K_{A1} (M^{-1})	ΔH_1 (kcal M^{-1})	K_{A2} (M^{-1})	ΔH_2(kcal M^{-1})
Paromomycin	3 ± 2 x 10^6	-22 ± 1	9 ± 2 x 10^6	-9 ± 1
Neomycin	2 ± 1 x 10^6	-22 ± 1	6 ± 1 x 10^6	-5 ± 1

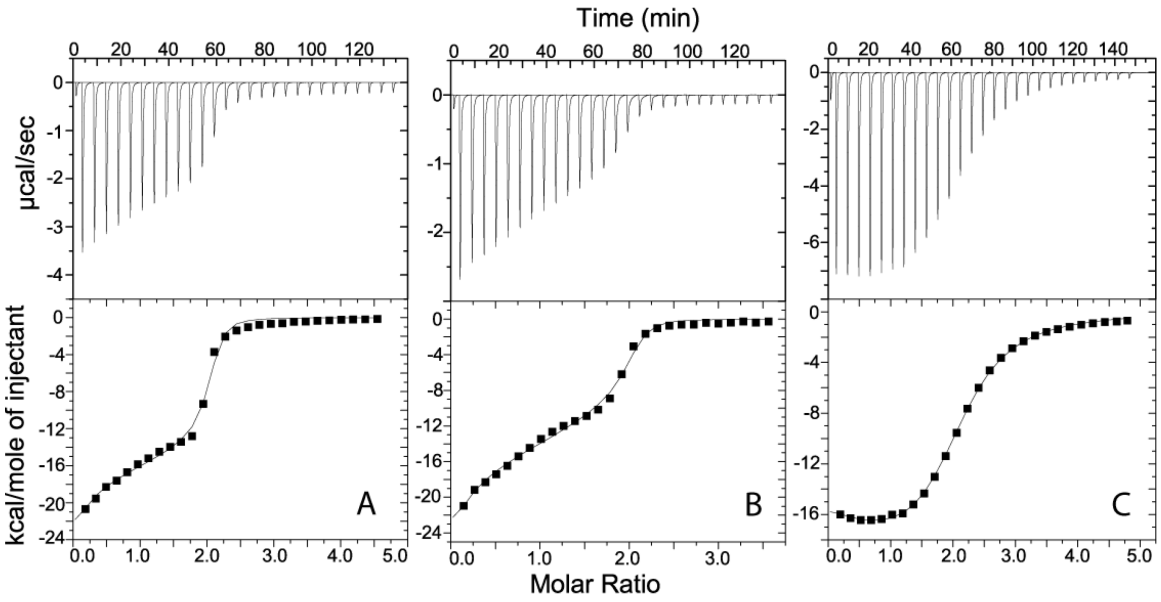

Fig. 5.3 Comparing isotherms of paromomycin (A), neomycin (B), and AcCoA binding to AAC(6')-Ii at 25°C.

The unproductive complex (i.e. that of AAC(6')-paromomycin) was next studied with ITC experiments performed in triplicates at 3-5°C intervals between 5 - 46 ºC (Appendix Figure A.10). Paromomycin was titrated into a solution of AAC(6')-Ii for a total of 33 ITC experiments. All the isotherms were fit together using the *van 't* Hoff global fit described in Chapter 3 to obtain the phenomenological binding parameters for the apparent binding enthalpies (ΔH_{A1}^{app}

and ΔH_{A2}^{app}) and association constants (K_{A1}^{app} and K_{A2}^{app}) of binding the first and second molecule of paromomycin to AAC(6')-Ii. The isotherms with the predicted fits are shown in Fig. 5.4 with the thermodynamic binding parameters shown in Fig. 5.5 and Table 5.2:. Again the *van 't* Hoff global fitting approach gives good agreement with the experimental data at all temperatures.

Table 5.2: ITC derived association constants and enthalpies for paromomycin binding to AAC(6')-Ii

Temperature (°C)	ΔH_{A1}^{app} (kcal)		ΔH_{A2}^{app} (kcal)		K_{A1}^{app} (x10^7 M^{-1})		K_{A2}^{app} (x10^7 M^{-1})	
5	6.9	±0.3	-3.4	±0.3	9.7	±0.5	14.6	±0.3
10	3.7	±0.2	-5.6	±0.2	11.5	±0.6	12.6	±0.3
15	-4.3	±0.2	-6.7	±0.2	11.4	±0.6	10.4	±0.2
20	-12.4	±0.2	-8.6	±0.3	8.9	±0.4	8.3	±0.2
25	-23.2	±0.3	-11.4	±0.3	5.3	±0.3	6.2	±0.1
30	-32.3	±0.3	-11.1	±0.4	2.5	±0.1	4.57	±0.07
34	-43.3	±0.4	-17.6	±0.4	1.09	±0.06	3.35	±0.05
37	-62.5	±0.6	-22.3	±0.7	0.47	±0.03	2.45	±0.04
40	-74.5	±0.8	-36.1	±0.9	0.16	±0.01	1.56	±0.04
43	-82	±1	-57	±1	0.049	±0.004	0.76	±0.03
46	-94	±1	-92	±1	0.0132	±0.001	0.25	±0.01

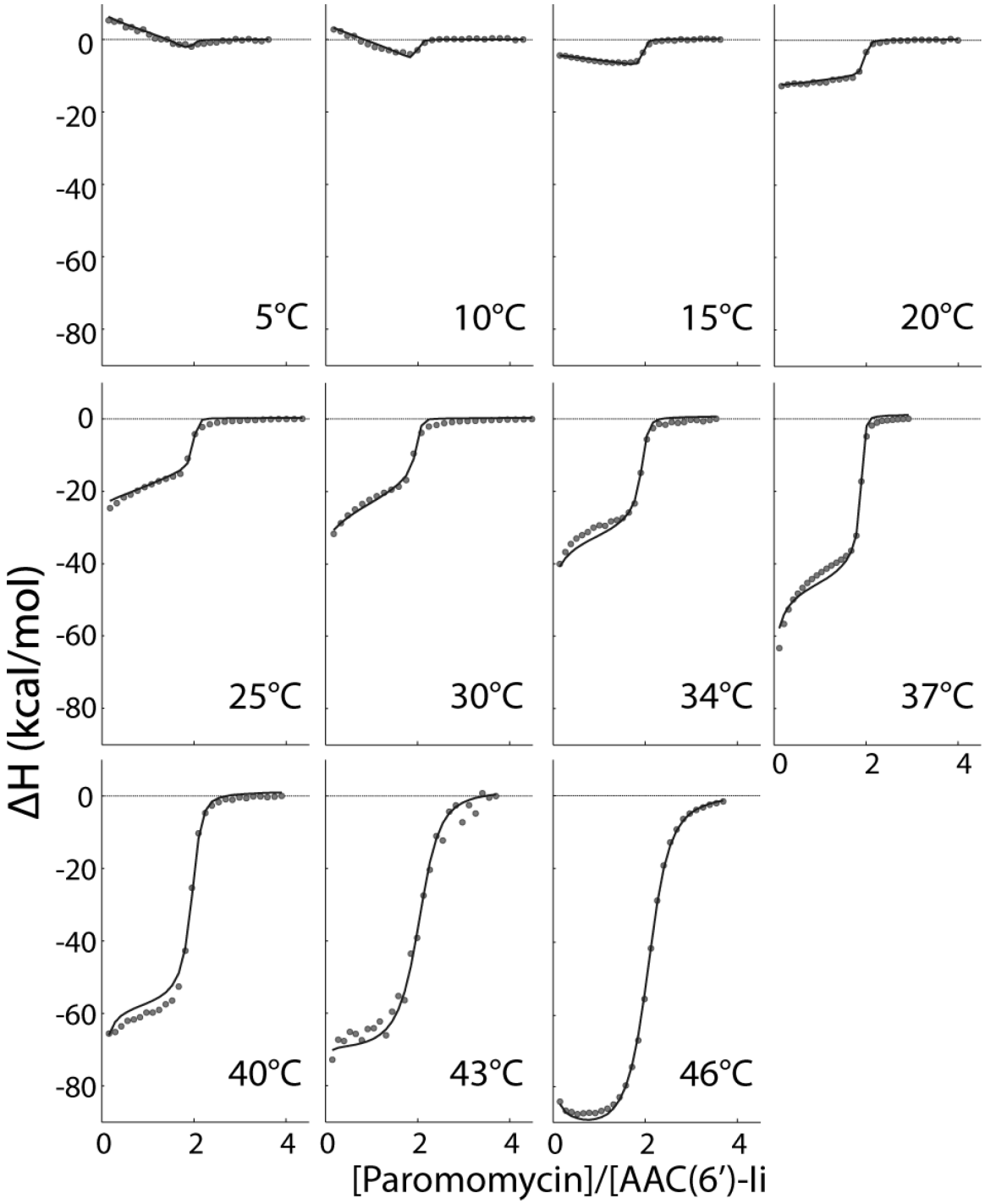

Fig. 5.4 ITC isotherms of paromomycin binding to AAC(6')-Ii at 5, 10, 15, 20, 25, 30, 34, 37, 40, 43, and 46°C. The experimental data (circles) is fit using the *van 't* Hoff global approach (line).

The ITC data suggest that the underlying mechanism of binding of aminoglycosides to AAC(6')-Ii to form the unproductive complex may differ from AcCoA binding to AAC(6')-Ii to form the holo complex. At all temperatures the isotherms obtained for paromomycin binding to AAC(6')-Ii differ greatly from isotherms obtained for AcCoA binding to the same enzyme. Chapter 4 describes the temperature dependence of binding enthalpy (ΔH_A) and association constants (K_A) of AcCoA binding to AAC(6')-Ii. AcCoA was shown to bind to AAC(6')-Ii with positive cooperativity ($K_{A1}^{app} < K_{A2}^{app}$) at lower temperatures, but the cooperativity decreases and switches to negative cooperativity ($K_{A1}^{app} > K_{A2}^{app}$) when the temperature is increased. Additionally above 30ºC the change in heat capacity (ΔC_p) between the free and bound state of AAC(6')-Ii increases greatly due to the thermal unfolding of AAC(6')-Ii. However, in the case of paromomycin binding to AAC(6')-Ii, the negative cooperativity appears to occur at ~15-20°C with positive cooperativity increasing below and above these temperatures. Additionally, the binding is endothermic at low temperatures (5°-10° C) for the first event (ΔH_1^{app}), but as temperature increases, it becomes exothermic and increasingly negative. The heat capacity (ΔC_p) is determined from the temperature dependence of enthalpy. For the first binding event the ΔC_p is quite large, ~1.3 kcal mol^{-1} K^{-1}, compared to 0.79 kcal mol^{-1} K^{-1} for the first binding event with AcCoA. This suggests a greater change in protein structure during

the first binding event of paromomycin compared to the first binding event of AcCoA. However, the change in ΔC_p with paromomycin binding follows the same trend as AcCoA. At lower temperatures the ΔC_p is constant but becomes increasingly negative at temperatures above 30ºC. This suggests that AAC(6')-Ii undergoes a similar linked folding and binding event with paromomycin. The phenomenological parameters obtained through the *van 't* Hoff global fit was fit to the same linked folding and binding model used for AcCoA binding to AAC(6')-Ii explained in Chapter 3.

5.3 Coupled folding and binding

Even though the temperature dependence of thermodynamic parameters describing the binding of paromomycin to AAC(6')-Ii differs from those of AcCoA there are some similarities. The value of ΔH_A decreases slowly as T° increases from 5 to 30°C for the first binding event and remains roughly constant for the second binding event from 5-30ºC. Above this temperature the ΔC_p (slope of ΔH vs T°) increases greatly and the temperature dependence of ΔH_A becomes strongly curvilinear. As this behaviour is similar to that of AcCoA binding to AAC(6')-Ii, it is likely explained by the thermal denaturation of AAC(6')-Ii. The phenomenological binding parameters were fit to a linked folding and binding model similar to that described in Chapters 3 and 4 which consist of a folded

state (**F**) and an unfolded state (**U**). Chapter 4 describes a model in which both subunits of the homo-dimeric enzyme are able to convert between the **F** and **U** state independently of the other subunit. This allows the protein to be in the following states: **FF**, **FU**, **UF**, and **UU**. Here again, our results suggest that only subunits in the **F** state can bind paromomycin, and for a subunit in the **U** state to bind paromomycin, it must first fold to the **F** state. Microscopic binding parameters for the linked folding and binding event were obtained through experimentally observed parameters, ΔH_{A1}^{app}, ΔH_{A2}^{app}, K_{A1}^{app} and K_{A1}^{app}. In this model used to explain folding and binding each monomer is able to fold and unfold. So for each monomer to bind ligand it undergoes the following

$$U + L \underset{}{\overset{K_F, \Delta H_F, \Delta C_{p,F}}{\longleftrightarrow}} F + L \underset{}{\overset{K_B, \Delta H_B, \Delta C_{p,B}}{\longleftrightarrow}} FL$$

ΔH_F, ΔH_B and $\Delta C_{p,F}$, $\Delta C_{p,B}$, are the changes in enthalpy and heat capacity for the folding and binding steps, while K_F = [**F**]/[**U**] and K_B = [**F**L]/([**F**][L]) are equilibrium constants.

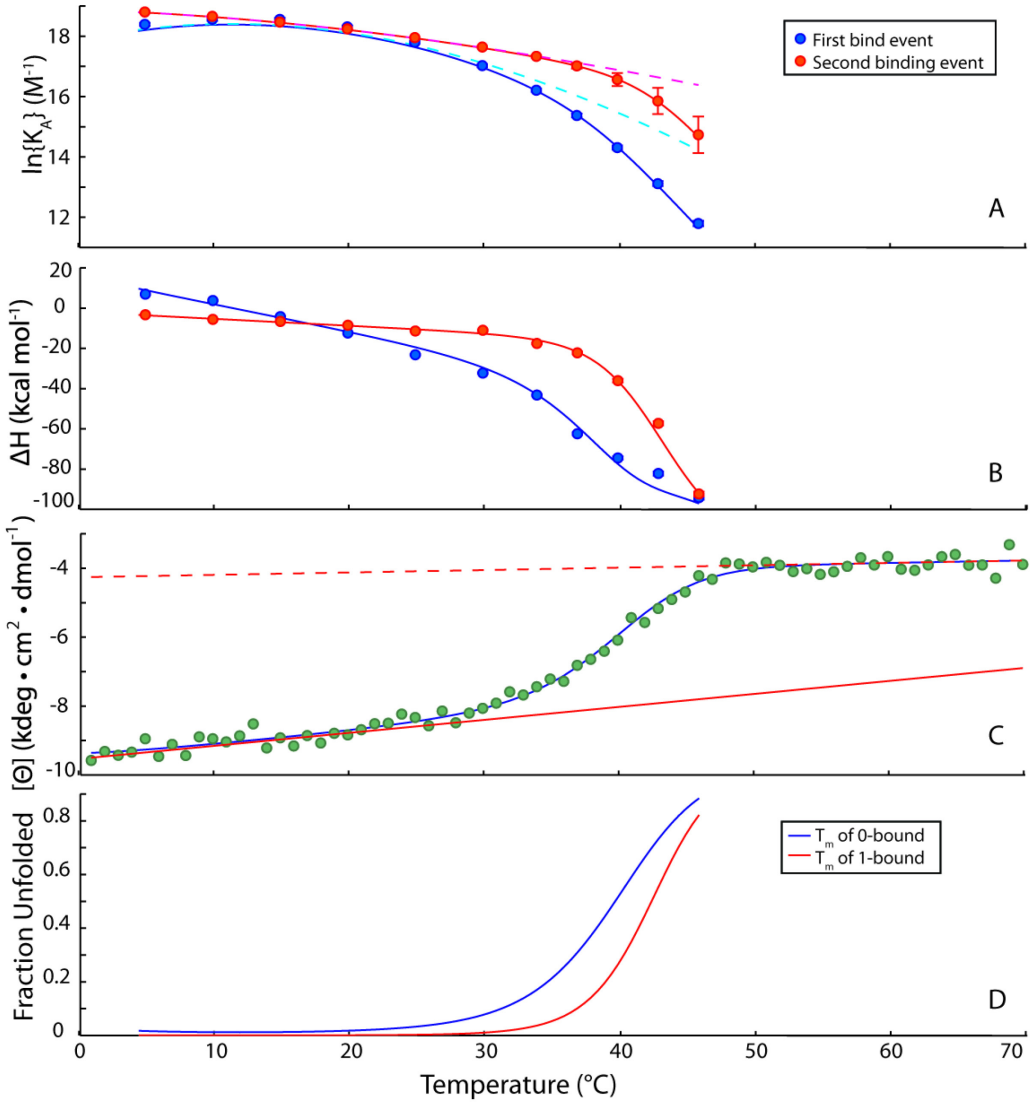

Fig. 5.5: *van 't* Hoff global fit (circles) of different binding parameters, K_A (**A**) and ΔH (**B**) for the first (blue) and second (red) binding events. The apparent binding constants where fit to a temperature dependent unfolding event (solid lines in **A** and **B**). Dashed lines in **A** predict the affinity constants in absence of thermal melting. **The F↔U** equilibrium was studied by monitoring molar ellipticity (**C**) at 222 nm. The folded and unfolded baselines are given by solid and dashed red line respectively. The fraction of unbound subunits unfolded (**D**) shows that the free subunits in the 1-bound state are more stable then the subunits in the 0-bound state.

Circular dichroism (CD) was again used to determine the relative population of AAC(6')-Ii in the **U** and **F** state (Fig. 5.5C). CD spectroscopy can measure the change in protein secondary structure through monitoring of molar ellipticity. Proteins rotate the plane of polarized light depending on their secondary structure. As before (section **4.3**), a wavelength of 222 nm was monitored at increasing temperatures to evaluate the change in secondary structure from a folded (alpha helices and beta sheets) to an unfolded state (random coil). The CD results from 0.1-71 ºC in the absence of ligand are shown on 5.5C. At low temperatures the molar ellipticity is around -9000 deg cm^2 $dmol^{-1}$ and sigmoidally approaches 0 as the temperature increases. The molar ellipticity ([Θ]) can be fit to a population weight average of the **F** and **U** state as was explained in Chapter 4, section **4.5.2**. The thermodynamic contributions from both folding and binding cannot be deconvoluted through ITC alone.[102] The use of CD spectroscopy allows the separate monitoring of the folding event, so through fitting together the apparent enthalpies, apparent association, and molar ellipticity we can obtain the thermodynamic parameters of both binding and folding events. The best fit values are given on Fig. 5.5 and Table 5.3.

.

Table 5.3: Thermodynamic parameters describing allostery in AAC(6')-Ii binding paromomycin at 37°C

K'_{A1} ($\times 10^7$ M^{-1})[a]	1.03	±0.08	$\Delta S'_{A1}$ (cal mol^{-1})[m]	-74	±3
K'_{A2} ($\times 10^7$ M^{-1})[b]	2.8	±0.2	$\Delta S'_{A2}$ (cal mol^{-1})[n]	-12	±3
K'_{U0}[c]	0.448	±0.03	$\Delta S'_{S0}$ (cal mol^{-1})[o]	-167	±3
K'_{U1}[d]	0.112	±0.06	$\Delta S'_{S1}$ (cal mol^{-1})[p]	-230	±70
$\Delta G'_{A1}$ (kcal mol^{-1})[e]	-9.9	±0.8	$\Delta C_{p,A1}$ (cal mol^{-1} K^{-1})[q]	-1310	±40
$\Delta G'_{A2}$ (kcal mol^{-1})[f]	-10.6	±0.8	$\Delta C_{p,A2}$ (cal mol^{-1} K^{-1})[r]	-341	±40
$\Delta G'_{U0}$ (kcal mol^{-1})[g]	0.49	±0.03	$\Delta C_{p,U0}$ (cal mol^{-1} K^{-1})[s]	2100	NA
$\Delta G'_{U1}$ (kcal mol^{-1})[h]	1.4	±0.7	$\Delta C_{p,U1}$ (cal mol^{-1} K^{-1})[s]	2100	NA
$\Delta H'_{A1}$ (kcal mol^{-1})[i]	-32.9	±0.9	$[\Theta]'_F$ (deg cm^2 $dmol^{-1}$)[t]	-8000	±200
$\Delta H'_{A2}$ (kcal mol^{-1})[j]	-14.40	±0.8	$[\Theta]'_U$ (deg cm^2 $dmol^{-1}$)[u]	-4010	±40
$\Delta H'_{U0}$ (kcal mol^{-1})[k]	-52.5	±0.8	m_F (deg cm^2 $dmol^{-1}$ K^{-1})[v]	38	±3
$\Delta H'_{U1}$ (kcal mol^{-1})[l]	-70	±20	m_U (deg cm^2 $dmol^{-1}$ K^{-1})[w]	7	±2

T′=37°C

[a, b]Association constant for the native (non-melted) enzyme for the first and second Paromomycin molecule

[c]Equilibrium constant for subunit melting in the 0-bound enzyme

[d]Equilibrium constant for melting of the unbound subunit in the 1-bound enzyme

[e, f]Free energy change upon binding of paromomycin to the native (non- melted) 0-bound enzyme and 1-bound enzyme

[g]Free energy change upon melting of a single subunit in the 0-bound enzyme

[h]Free energy change upon melting of the unbound subunit in the 1-bound enzyme

[i, j]Enthalpy change upon binding of paromomycin to the native (non- melted) 0-bound and 1-bound enzyme

[k, l]Enthalpy change upon melting of a single subunit in the 0-bound enzyme and 1-bound enzyme

[m, n]Entropy change upon binding of paromomycin to the native (non- melted) 0-bound and 1-bound enzyme

[o, p]Entropy change upon melting of a single subunit in the 0-bound enzyme and 1-bound enzyme

[q, r]Heat capacity change upon binding of paromomycin to the native (non- melted) 0-bound and 1-bound enzyme

[s]Heat capacity change upon subunit melting. These values were fixed at the value obtained for a monomeric mutant of AAC(6')-Ii

[t, u]CD molar ellipticity of a native (non- melted) subunit and melted subunit repectively

[v, w]Temperature dependence of the molar ellipticity of a native subunit and melted subunit respectively

The physical parameters derived from studies of paromomycin binding to AAC(6')-Ii differ greatly from those of AcCoA. The intrinsic affinity constants (K_{A1} and K_{A2}) are much higher for paromomycin compared to AcCoA, 10^7 vs 10^4 M^{-1} (at 37°C). Additionally, at all temperatures studied the model predicts paromomycin binds AAC(6')-Ii with positive cooperativity (Fig. 5.5A and Fig. 5.5). Unlike with AcCoA, the cooperativity of paromomycin binding AAC(6')-Ii increases below and above ~18°C. As established in Chapter 4, the unbound subunits of the enzyme undergo partial unfolding. Thus the model described in Chapter 4 where each subunit can unfold independently of the second subunit still holds (**FF**→**FU** is equivalent to **UF**→**UU**), but unlike with AcCoA, binding of paromomycin appears to stabilize the unbound subunit of the 1-bound species. As a result, the T_m of the unbound subunit increases from 313 K to 315.5 K upon the first binding event. In contrast, binding of AcCoA was found to destabilize the unbound subunit and decrease the T_m by 2 K. The binding enthalpies (ΔH_{A1} and ΔH_{A2}) also differ for paromomycin and AcCoA. During AcCoA binding to AAC(6')-Ii all binding events are exothermic with the second binding event being more exothermic then the first one (5-40°C). However, during formation of the paromomycin-AAC(6')-Ii complex, the first binding event is endothermic at lower temperatures (6.9 kcal M^{-1} K^{-1} at 5 °C), but becomes exothermic with increasing temperature (Fig. 5.5B). The first binding event begins more endothermic then

the second binding event but at around 15°C the first binding event becomes more exothermic. This is explained by the change in heat capacity of binding ($\Delta C_{p,A}$), which is much larger for the first than for the second binding events (-1.3 to -0.34 kcal mol^{-1} K^{-1} respectively). Interestingly, the $\Delta C_{p,A1}$ for paromomycin is much higher than the $\Delta C_{p,A1}$ for AcCoA, -1.3 to -0.79 kcal mol^{-1} K^{-1} respectively. It is believed that the change in heat capacity in proteins is dependent on the changes of exposure of hydrophobic residues to water.[196-197] This suggests that when AAC(6')-Ii binds the first paromomycin it buries more hydrophobic residues compared to when AAC(6')-Ii binds the first AcCoA. Meanwhile, the second binding event for paromomycin has a lower $\Delta C_{p,A2}$ than AcCoA, -0.34 versus -0.82 kcal mol^{-1} K^{-1}. Therefore, the event which buries the hydrophobic surface for paromomycin binding occurs mostly during the first binding event. This suggests that the conformational changes which occur when paromomycin binds AAC(6')-Ii are different from AcCoA binding AAC(6')-Ii, and supports the MWC folding model. To gain information about the structural changes which occur during binding of aminoglycosides to AAC(6')-Ii NMR experiments were performed.

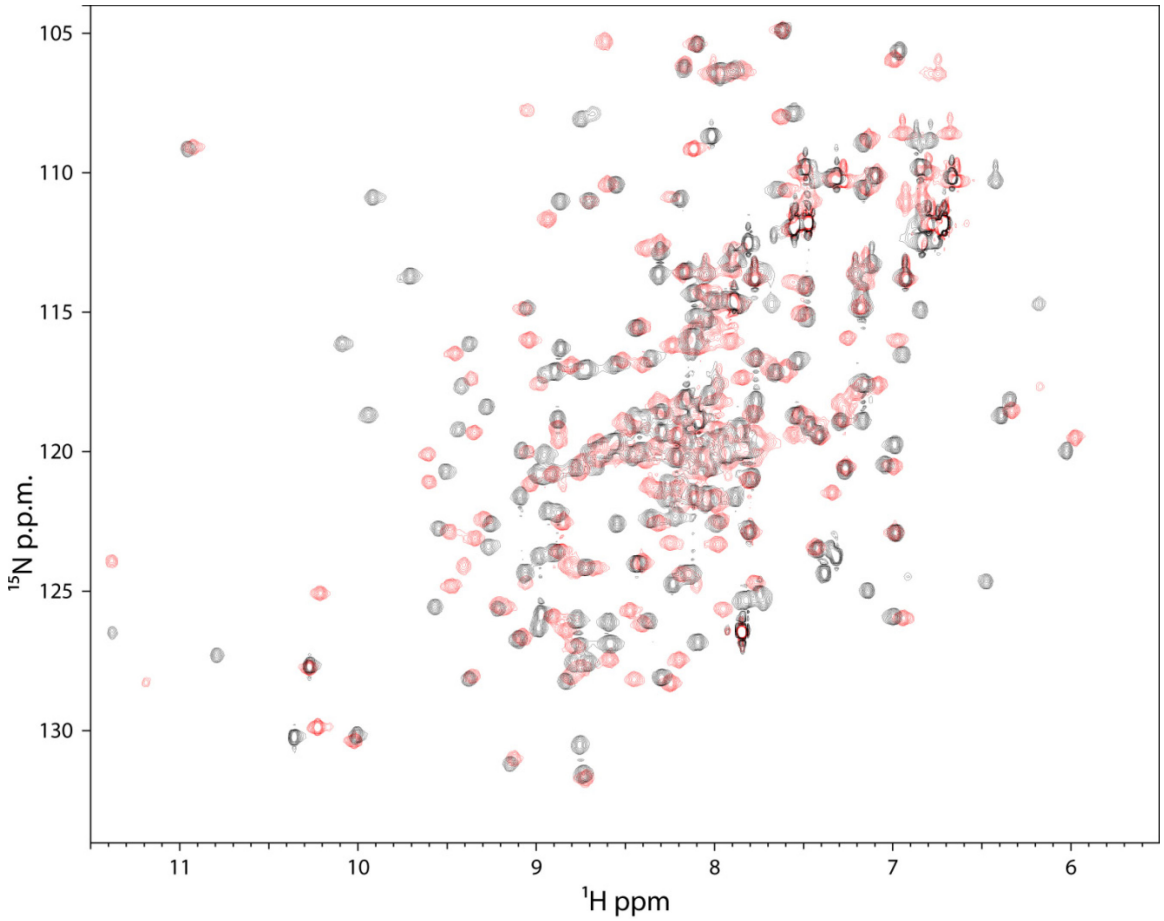

Fig. 5.6: Overlay of NMR spectra of AAC(6')-Ii saturated with AcCoA (Black) or paromomycin (red) at pH 6.5, 100 mM sodium phosphate.

5.4 Nuclear magnetic resonance spectroscopy

5.4.1 Paromomycin titration

Two dimensional ^{1}H-^{15}N single quantum coherence correlation (2D-HSQC) spectra of the free (apo) and the paromomycin-saturated (unproductive complex) forms of AAC(6')-Ii were obtained in 100 mM sodium phosphate at pH 6.5. These spectra suggest that large conformational and dynamic change occur upon paromomycin binding AAC(6')-Ii. The spectrum of the unproductive

complex contain 164 well-resolved backbone amide resonances, with 77 baseline separated. This is comparable to the AcCoA-AAC(6')-Ii complex which has 166 peaks with 89 baseline separated in the same conditions. While many peaks for both spectra are similar, many peaks also differ (Fig. 5.6). This suggests that the two bound states adopt different confirmations.

A series of HSQC spectra were also obtained at increasing paromomycin concentration in the presence of ^{15}N enriched AAC(6')-Ii (Appendix Figure A.11). A total of 15 spectra were obtained at 0, 0.025, 0.05, 0.1, 0.2, 0.3, 0.4, 0.5, 0.6, 0.8, 1.0, 1.25, 1.50, 1.75, and 2.0 mM of paromomycin, in the presence of 600 μM of AAC(6')-Ii in 25 mM HEPES, 2 mM EDTA, pH 7.5. This buffer was chosen because the binding constants obtained with ITC at pH 6.5 differed greatly from those at pH 7.5. Some peaks disappeared as the pH was increased which is likely due to proton exchange with the solvent at higher pH. As demostrated for AcCoA, NMR signals corresponding to the free and paromomycin-bound enzyme are in the slow exchange NMR regime (>>ms) and are simultaneously present in partially saturated samples. The maximum intensity observed for all peaks is around the saturation point of the enzyme (~600 μM paromomycin added to 600 μM AAC(6')-Ii). After this point the intensity for every peak decreases linearly with increasing concentration of paromomycin. Paromomycin is a polycationic molecule, and AAC(6')-Ii is negatively charged at pH 7.5 with a pI ≈ 4.6. This

may cause some non specific charge interactions of AAC(6')-Ii to the excess aminoglycosides and may alter the tumbling time of AAC(6')-Ii in solution. This in turn would broaden the NMR peaks and decrease their overall intensity. Additionally, many of the bound peaks migrate a small amount throughout the titration, but once the enzyme is saturated the peaks remain at the same chemical shift. Therefore, the change in chemical shift is due to the shift in population from the 1-bound to the 2-bound state, and not from random non specific interactions of paromomycin with AAC(6')-Ii. The intensities of the peaks were monitored throughout the titration. Unlike the titration of AcCoA, the bound peaks did not appear concertedly, shown in Fig. 5.8b. Some peaks appear very early, while others peaks have no measureable intensity well into the titration. From ITC measurements, we can determine the relative population of each state at all points throughout the titration. In a slow exchange model the population in a given state dictates the relative intensities of a peak. However, several of peak intensities are lower than expected throughout the titration to fit this model. Additionally, several chemical shifts migrate as the titration progresses. This suggests that there may be different dynamics between the binding of the first and second molecule of paromomycin to AAC(6')-Ii. Chapter 1 described the effects of dynamics on different NMR timescales. Some additional dynamics may occur in the intermediate or fast time regime. In intermediate exchange

models, the observed intensity can be suppressed through additional relaxation processes such as conformational exchange. Therefore the relative observed peak intensities may not correlate to the population of each state.

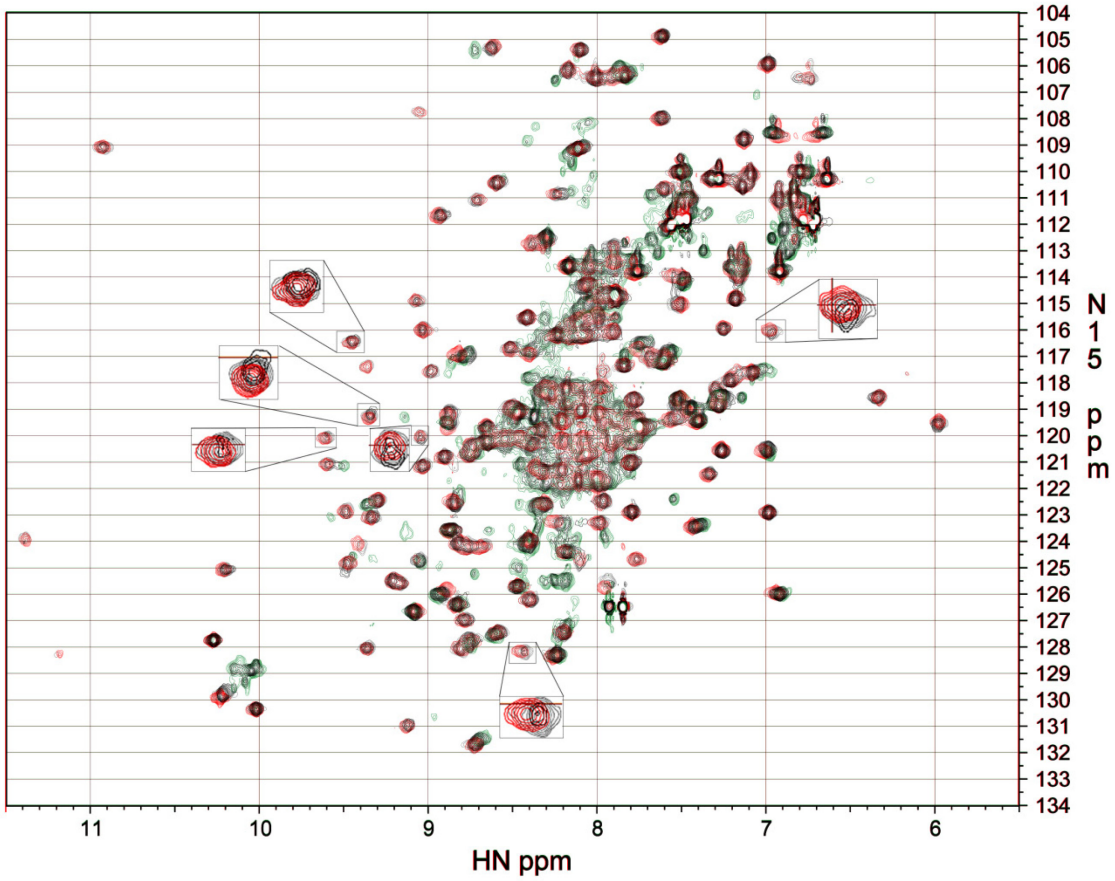

Fig. 5.7 Overlay of AAC(6')-Ii titration with paromomycin at 0 (green), 0.2 (black), 0.4 (grey) and 0.8 (red) mM. Several peaks have been expanded to show their migration at increased concentration of paromomycin

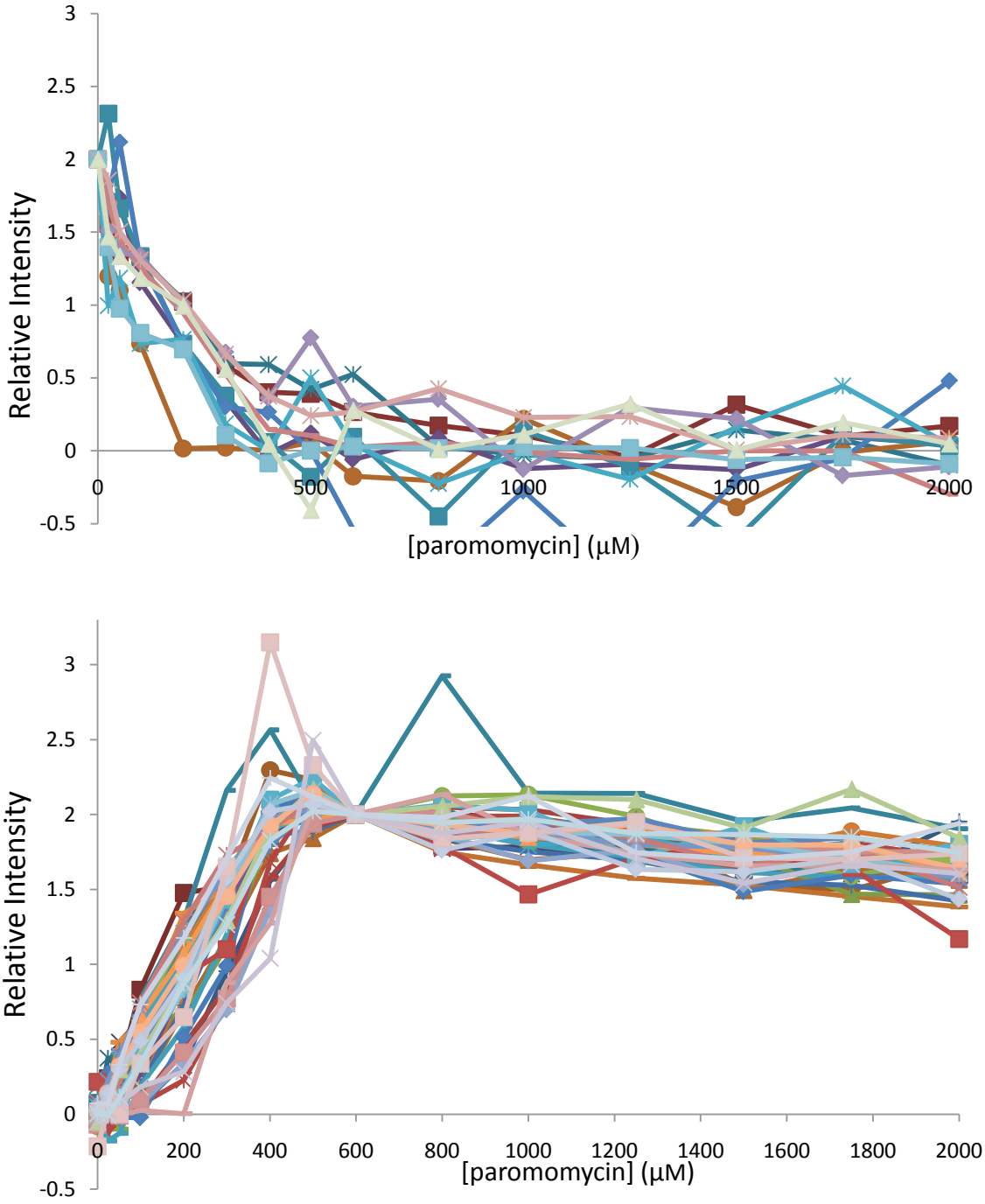

Fig. 5.8: Change of peak intensity with increasing concentrations of paromomycin. (A) Peaks corresponding to the apo state with all peak intensity normalized to 2 at 0 μM of paromomycin. (B) Peaks referring to the unproductive complex. All intensities were normalized to 2 at 600 μM of paromomycin.

A possible model to explain these is as follows (Fig. 5.10). Large conformational changes are likely responsible for the slow kinetics. The first binding event occurs under the slow time regime, likely due to a large scale conformational change and ordering. As the conformational changes have already occurred the second binding event occurs on the fast timescale with changes in the protein occurring only locally at the active site. Aminoglycosides are polycationic molecules and will greatly change the chemical environment in the area around them. As the concentration of paromomycin increases, the lifetime in the free state decreases, but the lifetime of the bound complex does not change. This is because k_{on} is a second order rate constant, and the average lifetime of the free state will be $1/(k_{\text{on}}[\text{Amg}])$, while k_{off} is a first order rate constant with the lifetime of the bound complex independent of ligand concentration. This causes the NMR signals to migrate from the 1-bound chemical shift to the 2-bound shift as the titration progresses. A fast exchange model can take this behaviour into account and fit the observed experimental intensities.

5.4.2 Fast Exchange Fit

This model explains the suppressed peak intensity through fast exchange between two different states (1-bound and 2-bound). In the 1-bound state, one

subunit is bound to paromomycin (**B**) and one subunit is free with a similar structure to the bound subunit, but has some peaks with different chemical shifts (**B'**). In the 2-bound state both subunits are bound to paromomycin (**BB**). The relative population of each state to each other (1-bound and 2-bound) is given by

$$pB' = \frac{0.5 \cdot f_1}{(f_1 + f_2)} \quad 5.2$$

$$pB = \frac{(0.5 \cdot f_1 + f_2)}{(f_1 + f_2)} \quad 5.3$$

where f_1 and f_2 are population of the 1-bound and 2-bound states to all protein (apo, 1-bound, 2-bound) respectively. The population of each state is known from the binding constants determined through ITC. Both the exchange rate (k_{ex}) and the difference in chemical shift (Δω) between the two different states affect the peak intensity. As both are unknown, both are combined into a single correction term (L) and the change of intensity is given by

$$FF = e^{\frac{-L \cdot pB' \cdot pB}{1 + pB'/pB}} \quad 5.4$$

where FF is the correction factor for the peak intensities. The Δω is unknown, and some peaks may have identical chemical shift in all states. Therefore it is possible that f_1 and f_2 give identical intensities. So the observed intensity (I_0) for each peak is given by

$$I_0 = FF \cdot I \cdot f_1 + FF \cdot 2 \cdot f_2.$$

5.5

where I is relative contribution of signal from the 1-bound state to the peaks corresponding to the **B** state.

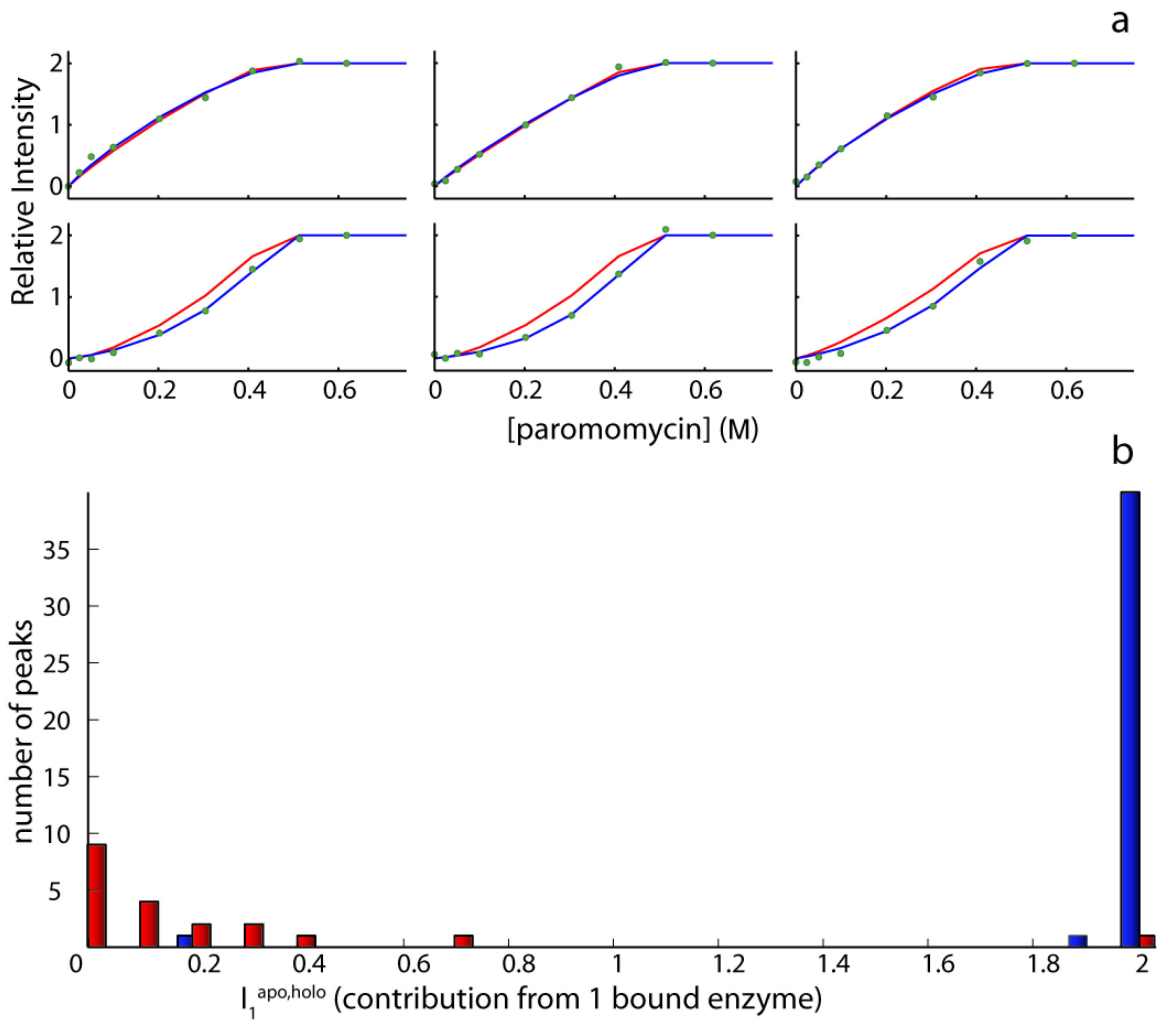

Fig. 5.9: (a) Experimental intensities (green circle) fit to a slow exchange (red line) and fast exchange (blue line). (**b**) Histograms of the relative contribution of the 1-bound enzyme to apo (I_1^{apo}) and holo (I_1^{holo}) peaks in titrations of AAC(6')-Ii with AcCoA.

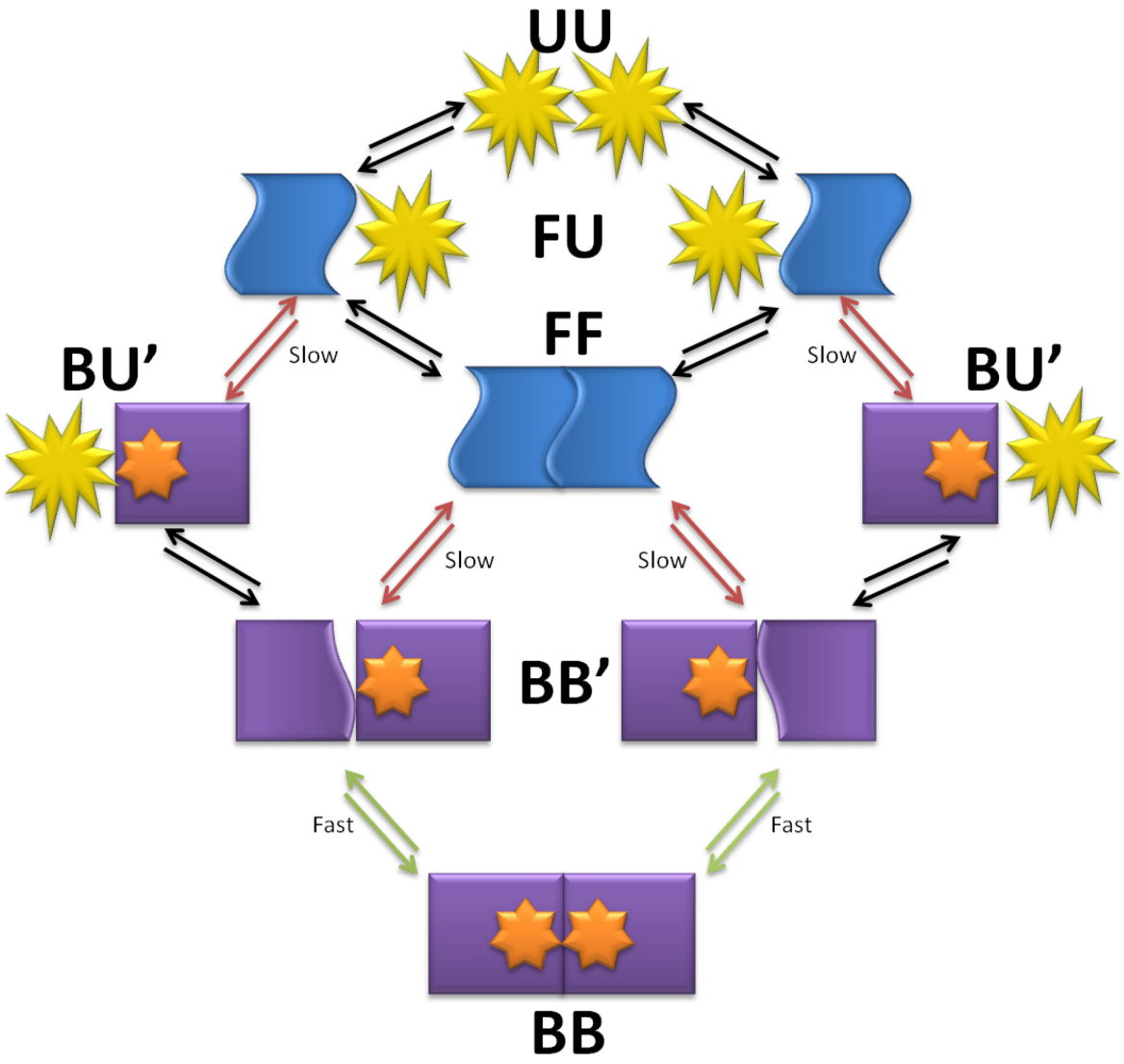

Fig. 5.10: Schematic representation of allosteric binding model of AAC(6')-Ii with aminoglycosides. **B (B')** corresponds to the bound state conformation with an aminoglycoside bound (unbound). **F** and **U(U')** correspond to the free folded and partially unfolded states that are adjacent to a free (bound) subunit, respectively The first binding event occurs under the slow exchange regime (red arrows). The second binding event occurs through fast exchange (green arrows).

This correction factor was used to refit the peak intensities measured throughout the titration with paromomycin. This exchange model fit the experimental with better agreement (Fig. 5.9A and Appendix Figure A.12). As can be seen the slow exchange model shows good agreement with peaks that appear rapidly, but deviates from the experimental data for peaks which appear slowly. Meanwhile, the fast exchange model fits all peaks with good agreement. The values for I_1^{apo} and I_1^{bound} where optimized for each peak for both the apo and bound state. The I_1^{apo} and I_1^{bound} correspond to the contribution of intensity of the 1-bound state to each signal relative to that of the 0-bound or 2-bound state respectively. The values for I_1^{apo} cluster around 0 while the I_1^{bound} cluster around 2. This strongly suggests that both subunits of AAC(6')-Ii 1-bound to paromomycin undergo a conformational change to that of bound conformation. This conformational change fits the MWC model.

5.5 Discussion

The global fit of CD and ITC data show that binding of paromomycin to AAC(6')-Ii has many similarities to that of AcCoA binding to AAC(6')-Ii. There are two distinct contributions affecting the K_A^{app} and ΔH_A^{app} of binding. The first contribution corresponds to the intrinsic affinity for paromomycin to the AAC(6')-Ii active site. NMR results suggest that binding of paromomycin at one subunit

induces a structural change across the whole protein, thus the free subunit in the 1-bound species has a similar structure to the bound subunit, and is referred to as **B'**. This is reminiscent of the MWC binding model and paromomycin binding at one subunit may stabilize the free subunit (**FF**→**BB'**). This leads to positive cooperativity at temperatures above 20°C. The second binding event occurs over a fast timescale as very little structural change occurs in the protein during the binding and release of the second aminoglycoside molecule. However, some peaks undergo a large chemical shift during the second binding event and cause the reduction of peak intensity when the AAC(6')-Ii is partially saturated with paromomycin. Large shifts in chemical exchange may be due to the aminoglycoside changing the local chemical environment in the active site when it binds. This may reduce the observed intensity of these peaks, and their intensity may appear to be much lower then would be expected throughout the titration. To confirm this idea the ^{1}H-^{15}N HSQC spectra needs to be assigned to determine which amino acids undergo the largest change in chemical environment. The second contribution in paromomycin binding to AAC(6')-Ii is a linked folding and binding (**U**→**F**→**B**) event which is reminiscent to the HT model. This contribution is similar to that of AcCoA binding to AAC(6')-Ii. The unbound subunits undergo a partial unfolding as temperature is raised. This process is entropically driven. As explained in Chapter 4, when AcCoA binds and forms the

1-bound complex with AAC(6')-Ii the unbound subunit is destabilized and melts at a lower temperature relative to the unbound subunits in the 0-bound state. When paromomycin binds however, the unbound subunit appears to be stabilized and form a structure similar to a bound subunit, as explained above. In Chapter 4, inter-subunit interactions were invoked to explain the cooperativity observed. These interactions can either increase or decrease the stability of the subunits and are dependent on whether the two subunits fold synchronously. In the case of AcCoA binding, AAC(6')-Ii follows the KNF folding model and only a single subunit folds to the **B** state. This disrupts the interactions of the subunits and the free subunit is destabilized. This causes the proportion of unbound subunits in the 1-bound state to be in the binding incompetent **U** conformation to be higher than the proportion of unbound subunits in the 0-bound state, and reduces the binding the second molecule of AcCoA. As the temperature increases this effect becomes more profound as more 1-bound free subunits shift into the **U** state. The observed effect is the apparent cooperativity of binding AcCoA switches from positive to negative as temperature increases. However, in the case of paromomycin, as detailed in this chapter, AAC(6')-Ii appears to follows MWC folding model and the entire protein folds into the **B** state. This concerted folding stabilizes the free subunit as the T_m increases from 40 to 42.5 °C. This is explained by the 1-bound free subunit favours the competent fold compared to

the 0-bound enzyme. This stabilization has the effect of increasing the cooperativity. The unbound subunit can still melt (**BB'**→**BU**) but this occurs at a higher temperature relative to the 0 bound complex (**FF**→**FU**). The reason for the apparent disparity between AcCoA binding and paromomycin binding is unknown. The results described here need to be confirmed with additional experiments. However the ability of AAC(6')-Ii to behave differently with respect to each of its substrates may help to explain how AAC(6')-Ii has the ability to form an unproductive complex with one of its substrates.

6. Scientific Contributions

6.0 Preface

This thesis has three distinct contributions toward science. The first is expanding the current protocol for the analysis of isothermal titration calorimetery (ITC) data sets alone or in conjunction with additional spectroscopic data. Second is increasing the understanding of the mechanisms of protein allostery. Finally, this thesis has helped to understand the specific mechanism used by aminoglycoside *N*-6'-acetyltransferase-Ii (AAC(6')-Ii) to bind its substrates.

6.1 Contributions to isothermal titration calorimetry

ITC is a rapidly expanding technique. As the sensitivity of the instruments increases, more complex systems can be studied. However, understanding the underlying mechanistic details of these systems is complicated. Chapter 2 showed that multiple binding models can often fit identical experimental data with equal agreement. Chapter 2 described one method to overcome this limitation. By altering the concentration of the protein in the sample cell over several experiments one will observe a series of different isotherms. How these isotherms change over a concentration range is dependent upon the mechanism which the ligand binding follows. Therefore by globally fitting the data set to a single set of binding parameters the correct binding model can be identified. This work expands upon previous techniques which also approaches this problem.[124,126]

Often ligand binding in proteins is coupled with additional physical events, such as conformational changes or dimerization. These events have distinct thermodynamic contributions to the system studied. ITC measures all events with non-zero ΔH which are linked to binding, so a component of the heat measured will be from these coupled events. Previously reported methods entail multiple ITC experiments at different temperatures to deconvolute the thermodynamic parameters of coupled events.[102,191] Ladbury and coworkers described a method to combine circular dichroism with ITC data. This allowed for the accurate determination of the folding/unfolding component of the heats measured by ITC.[102] Chapter 3, 4 and 5 built upon this technique. However, unlike the system described by Ladbury, AAC(6')-Ii contains multiple subunits which bind their ligands cooperatively.[45] This makes accurate determination of the enthalpies and association constants of the two binding events challenging because the thermodynamic parameters co-vary with each other. Globally fitting a set of isotherms to a set of parameters has been shown to reduce the variance of fitted parameters. The data sets however, must be related mathematically, which is not the case for variable-T data sets using standard phenomenological models. Chapter 3 introduced the *van 't* Hoff relationship as a constraint for fitting a variable temperature datasets. We are unaware of this relationship being used before with variable temperature ITC datasets and its use greatly reduces

the uncertainties in the phenomenological thermodynamic constants. This restraint was shown to be useful in Chapter 4 and 5 when determining the thermodynamic parameters for complex systems which would otherwise not be nearly as amenable to ITC analysis.

These parameters were then used with CD and NMR to obtain a mechanistic model to describe the binding of the ligands to AAC(6')-Ii. This allowed us to identify a linked folding event with binding. Although this strategy to identify events linked to binding takes foundation on Ladbury's method, our system is much more complex with 3-state binding and multiple unfolded states.

6.2 Contributions to protein allostery

Allostery has been of great interest has been of great interest for many years. [70-71] There have been several models proposed to explain allosteric cooperativity. This thesis shows that we were able to describe multiple separate allosteric mechanisms which affect the observed cooperativity of AAC(6')-Ii. Additionally, our results show that for this enzyme the allosteric mechanism is dependent on the ligand. We showed that when binding acetyl coenzyme A (AcCoA) AAC(6')-Ii undergoes folding as described by the Koshland-Némethy-Filmer (KNF) model with only a single subunit folding with each binding event. When aminoglycosides bind to AAC(6')-Ii however, both subunits folding upon

the first binding event as in the Monod-Wyman-Changeux (MWC) model. With both ligands, there is a thermal unfolding event affecting the observed cooperativity. This is the first report of coexisting allosteric effects in binding. Additionally, Chapter 4 describes how cooperativity can be fine tuned through the thermal unfolding event by adjusting the stability of the unbound subunits. This was shown through the results in Chapters 4 and 5. In Chapter 4 the thermal unfolding event contributed to negative cooperativity due to the 1-bound subunits being less stable than the 0 bound subunits. However, in Chapter 5 the thermal unfolding event contributed to positive cooperativity due to the 1-bound subunits being more stable than the 0-bound subunits.

6.3 Contributions to aminoglycoside *N*-6'-acetyltransferase Ii

AAC(6')-Ii belongs to the GCN5-related *N*-acetyltransferase (GNAT) super family of proteins. Its function as an antibiotic resistance-causing enzyme makes it an important target for understanding protein biophysics. There has been a large number of structural studies performed on AAC(6')-Ii.[46-48,198-199] There is however no crystal structure for the aminoglycoside-AAC(6')-Ii complex. Kinetic studies in conjunction with preliminary ITC experiments suggested that there is cooperativity between the two subunits.[45] In Chapter 2 and 5 we showed that AAC(6')-Ii binds to both of its ligands, AcCoA and aminoglycosides, with a 2-site

sequential model. This corrects previous reports which used a 2-site independent model to fit ITC data.[45] This cooperativity is only present in the dimer as Chapter 3 showed that binding of AcCoA to a monomeric mutant fit a 1-site binding model with no cooperativity. Through the strategy developed in Chapter 3, we have identified two allosteric processes which contribute to the observed cooperativity. First, AAC(6')-Ii undergoes a conformational change when interacting with ligands. Depending on whether AAC(6')-Ii binds AcCoA or an aminoglycoside, its subunit fold via a KNF or MWC model respectively. The reason for this is not understood but appear to connected to the differences in thermal stability of the free subunit in the 1-bound state. The thermal stability of the subunits is the second contribution to the observed cooperativity. When the AcCoA binds to AAC(6')-Ii a single subunits undergoes a conformational change and appears to destabilize the free subunit and results in cooperativity becoming negative with increasing temperature. On the other hand, when an aminoglycoside binds to AAC(6')-Ii both subunits undergo a conformational change. This appears to stabilize the free subunit which produces positive cooperativity with increasing temperature.

Some specific structural information was also extracted from the NMR peak assignments of the AAC(6')-Ii-AcCoA complex. These assignments were obtained from Oliver Baettig under the supervision of Dr. Albert Berghuis, with

the assistance of Dr. Tara Sprules. From these assignments it was possible to determine specific regions of the protein which undergo large conformational changes. Additionally, some of the peak assignments were also transferred to the apo NMR spectrum, which allowed identification of regions expected to be disordered when AAC(6')-Ii is unbound in solution.

6.4 List of publications

The following is the list of my publication throughout my Ph. D. in chronological order beginning with the most recent.

Freiburger, L. A., Mittermaier, A. K., Auclair, K. "Van't Hoff global analyses of variable temperature isothermal titration calorimetry" *Thermochimica Acta* (submitted)

Freiburger, L. A., Mittermaier, A. K., Auclair, K., "Collecting Variable-concentration Isothermal Titration Calorimetry Datasets in Order to Determine Binding Mechanisms" http://www.jove.com/details.stp?id=2529 doi: 10.3791/2529. *J Vis Exp*. **2011**, 50.

Freiburger, L. A. Baettig, O. M. Sprules, T. Berghuis, A. M. Auclair, K.; Mittermaier, A. K. "Competing allesteric mechanisms modulate substrate binding in a dimeric enzyme."*Nature: Structure and Molecular Biology* **2011**, 18, 288-294

Freiburger, L. A., Auclair, K. Mittermaier, A. K., "Elucidating protein binding mechanisms by variable-c ITC." *Chembiochem*. 2009, 14, 2871-3.

Magalhaes, M.L.B., Vetting, M.W., Gao, F., Freiburger, L., Auclair, K., Blanchard, J.S., " Kinetic and Structural Analysis of Bisubstrate Inhibition of the *Salmonella enterica* Aminoglycoside 6'-*N*-Acetyltransferase." *Biochemistry*, 2008, 47, 579-584

6.5 Future directions

Even though much has been learned about AAC(6')-Ii and its interactions with its substrates, there are still many more questions without an answer. There appear to be significant differences in AAC(6')-Ii behaviour upon binding of different ligands. In order to gain an idea of the differences in the structure, the NMR peak assignments must be obtained for aminoglycoside bound AAC(6')-Ii. This will allow residue by residue information for chemical shift differences and relaxation rates between the AcCoA- and aminoglycoside-bound AAC(6')-Ii complexes. In addition, specific regions involved in binding and folding can be identified. Since no structure is available for the aminoglycoside-AAC(6')-Ii complex, an NMR structure would be highly useful for comparison with the AcCoA-bound complex.

In its catalytic cycle, after binding AcCoA, AAC(6')-Ii must bind aminoglycoside to form a ternary complex. To properly understand the catalytic mechanism of AAC(6')-Ii the ternary complex must also be studied. The methodologies developed therein for studying the binary and unproductive complexes should prove instrumental in studies of the ternary complex. This information should highlight differences between the ternary and the unproductive complexes and provide a rational for why substrate binding is ordered for this enzyme.

Based on its fold, AAC(6')-Ii belongs to a large family of enzymes, the GCN5 related *N*-acetyltransferase (GNAT) super family.[46] This group of enzymes is important to a wide variety of biological functions. It would be interesting to see whether the behaviour of AAC(6')-Ii is unique to itself, or if other similar enzymes share its interesting behaviour. Structural information is available for two other AAC(6')s, AAC(6')-Ib and AAC(6')-Iy. Both of these isoforms appear to be homodimeric from their crystal structures, and have the potential for interesting allosteric behaviour. AAC(6')-Iy proceeds via a sequential random catalytic mechanism.[200] AAC(6')-Ib is the most prevalent isoform conferring clinically relevant aminoglycoside resistance.[1] Similarly to AAC(6')-Ii it uses a sequential ordered mechanism.[201] Additionally, this isoform has the ability to modify another structurally distinct family of antibiotics, that of

fluoroquinones.[201] Studying what allosteric effects occur when AAC(6')-Ib binds different ligands may have multiple implications.

The GNAT super family of enzymes is a large group of enzymes which contain a similar fold and is found in all domains of life. Even though the sequence homology is quite small (20-40%),[44] their structures are well conserved.[46] Through gaining a better understanding of the function of AAC(6')-Ii, a better understanding of this large class of enzymes may result.

7 Experimental

7.1 Reagents

The plasmids containing AAC(6')-Ii and the AAC(6')-Ii mutant were both generously provided by Dr. Gerry D. Wright, biochemistry and Biomedical Sciences, Master University, Canada. . The buffer and cell broth reagents were obtained from Fischer Scientific (Whitby, ON, Canada). The acetyl coenzyme A (AcCoA), paromomycin, ribostamycin, neomycin, and protease inhibitors were purchased from Sigma-Aldrich Canada (Oakville, ON, Canada). The Q-Sephorose Fast Flow and Superdex 75 chromatography resins were obtained from GE Healthcare. The activated affinity Affi-Gel 15 was purchased from Bio-Rad (Mississauga, ON). The Escherichia coli strain BL21(DE3) competent cells were obtained from Invitrogen (Carlsbad, CA). The $^{15}NH_4Cl$ was purchased from Isotech a subsidiary of Sigma-Aldrich (Oakville, ON, Canada).

7.2 Protein Purification

The purification procedure was obtained from previously reported procedure with some modifications to maximize yield and minimize the time required for purification.[44] Original work done by the Wright group cloned and sequence the *aac*(6')-Ii *Enterococcus faecium* CIP 54-32. This gene was inserted into a pET22b expression plasmid which carried an ampicillin resistance

gene. Additionally, the Wright group perform site directed mutagenesis to obtain the *aac*(6')-Ii W164A mutant gene.

7.2.1 Expression of AAC(6')-Ii

BL21(DE3) cells were transformed using the One Shot® protocol developed by invitrogen with a pET-22b(+) vector containing aac(6')-Ii gene. The cells were grown on a Luria-Bertani (LB) agar plate containing ampicillin (100 μM/mL). 3x10 mL of LB (NaCl 10 g/L, Trypton 10 g/L, yeast extract 5 g/L, amphicillin 100 mg/L, autoclaved) broth was inoculated from a single culture and grown overnight at 37ºC and shaken at 250 rpm. Each 10 mL culture was used to innoculate 1 L of LB to make a total of 10 L. The cell culture was grown at 37º C and shaken at 250 rpm until the OD_{600} reached 0.6. The culture was then induced using isopropyl-β-D-thiogalactoside (IPTG) (1 mM) and was grown at 37º C and shaken at 250 rpm for 5-6 hours. The cells were collected through centrifugation (5000 G at 20 min). The cell pellet was frozen and stored over night (-80ºC).

7.2.2 Expression of ^{15}N Labelled AAC(6')-Ii

7.2.2.1 Preparation of Minimal Media

10X M9 salts (Anhydrous Na_2HPO_4 60g/L, KH_2PO_4 30g/L, NaCl 5 g/L), $CaCl_2$ (0.1 M), $MgSO_4$ (1 M), and glucose (20% w/v) must all be autoclaved

separately. Thiamine (10 mg/mL), d-biotin (10 mg/mL), ampicillin (100 mg/mL), NH_4Cl (1 g/mL) were sterilized with of 0.2 µm seringe filter. The ingredients were combined (10X M9 salts 100 mL, $CaCl_2$ 1 mL, $MgSO_4$ 1 mL, glucose 15 mL, thiamine 1 mL, d-biotin 1 mL, ampicillin 1 mL, NH_4Cl 1 mL) and diluted to 1 L with double distilled water.

7.2.2.2 Expression of protein

The expression protocol for labelled proteins was taken from Marley *et al.*[202] The beginning of the expression matches unlabelled expression except only 4 L of LB was used. Once the cells reach an OD_{600} of 0.6 collect the cells through centrifugation (5000G for 20 min). Cells were resuspended in 1 L of minimal media and grown for 30-45 min at 37ºC and shaken at 250 rpm. Cells are again collected through centrifugation (5000G for 20 min) and resuspended in 1 L minimal media contain ^{15}N ammonium chloride. Cells were shaken at 37º C and 250 rpm for 30 to 45 min then induced with IPTG (1mM). The culture was grown for 5-6 hours then the cells were collected through centrifugation (5000G for 20 min). The Cell pellet was frozen and stored over night (-80ºC).

7.2.3 Purification of AAC(6')-Ii

The cell pellet was resuspended in lysis buffer (HEPES 25 mM, EDTA 2 mM, Leupeptin 0.05 mg/L, Aprotinin 0.5 mg/L, Bestatin 0.01 mM, Pepstatin A 0.05 mg/L, phenylmethanesulfonylfluoride 1 μM). After pellet was resuspended lysozyme was added (10 mg/g of cell pellet), and sat on ice for 30 min. The cells were further lyzed through sonification (8x15 s.). The suspension was centrifuged (18000 G for 20 min) and pellet was discarded. AAC(6')-Ii was then purified as previously described[44] with a Q-sepharose anion exchange column, an affinity column and a size exclusion column. The first column was a Q-Sepharose Fast Flow ion exchange with a bed volume of 75 mL with diameter of 26 mm. It was packed with 5 column volumes of HEPES buffer (25 mM HEPES, 2 mM EDTA, pH 7.5) at a rate of 3 mL min^{-1}. After loading the bacterial supernatant, the column was washed with HEPES buffer in a linear-stepwise manner of increasing NaCl with the following volume and concentration: 100 mL at 0 M, 200 mL at 0.2 M, 100 mL at 0.3 M, 200 mL at 0.4 M, and 200 mL at 1 M. Fractions containing AAC(6')-Ii were identified with SDS-PAGE 20% polyacrylamide gel. AAC(6')-Ii migrates as a monomer to an apparent MW of ~21 kDa. The collected fractions were dialysed overnight against 0 M NaCl HEPES buffer. The second column used was an Affi-Gel 15 paromomycin-coupled agarose affinity column and was performed following the dialyses. A

bed volume of 25 mL in a 16 mm column was packed at 2 mL min^{-1} with HEPES buffer (25 mM HEPES, 2 mM EDTA, pH 7.5). After the column affinity was loaded protein was eluted using 200 mL of HEPES buffer with NaCl (100 mM). This is done to remove an uncharacterized 42 kDa protein, LEE. AAC(6')-Ii was then eluted with HEPES buffer by linearly increasing the NaCl concentration to 1 M. Fractions containing AAC(6')-Ii were identified again with SDS-PAGE 20%. Collected fractions are concentrated to 8 mL with 10 kDa cut off centrifugal filtration units (millipore). The Size exclusion chromotography was performed with a hand-packed XK16 Superdex 75 column on an AKTA FPLC system and an elution buffer consisting of HEPES (25 mM, pH 7.5), EDTA (2 mM) and NaCl (1 M). The high salt is used to remove any compound which is bound to the protein throughout the purification. The purification was monitored through UV absorbance and only one major peak was observed which was at the predicted molecular weight of the dimer. The collected fractions were concentrated and dialysed against the appropriate buffer for the intended experiment. Protein concentrations were determined by spectroscopic absorbance measurements using a theoretical extinction coefficient of 33,920 $M^{-1}cm^{-1}$ at 280 nm (ExPASy Proteomics), and Lowry-Bradford assays.

7.2.4 Purification of AAC(6')-Ii W164A Mutant

The expression the mutant variant matched that of the wild type. The purification protocol was similar to the wild type with the following exceptions. The size exclusion chromatography was performed after the Q-sepharose anion exchange column. Two major peaks were observed and the second one was collected which corresponded to the molecular weight of the monomer. The protein was further purified be affinity chromatography as above, and the protein concentrations were determined in the same manner as the wild type.

7.3 ITC

7.3.1 ITC data collection

All ITC experiments were performed on a MicroCal VP-ITC isothermal titration calorimeter from MicroCal (North Hampton, MA, USA). Solutions of protein were extensively dialyzed against HEPES buffer (25 mM HEPES, 2 mM EDTA, pH 7.5) and the resulting solution was used to dissolve the ligand. All runs were performed with protein (5-200 μM) in the sample cell (1.4539 mL), and the ligand (0.1-4 mM) in the injection syringe. Titrations were performed at 43, 40, 37, 34, 30, 25, 20, 15, 10, and 5 ºC. Each titration comprise of an initial delay of 60 s, a first injection of 2 μL and a delay of 150 s, 26 injections of 10 μL each followed by 240-360 s delays, and a final injection of 10 μL followed by a delay of

300-600 s to ensure the system had reached the baseline between each injection. Blank runs were obtained by matching the experimental runs in the absence of protein. The blank heats were subtracted from the experimental heats and the first data point was removed due to the different injection and delay parameters.

7.3.2 ITC data analysis

All data analysis was performed using the equations described in the text with inhouse scripts using MATLAB (7.8.0.347 (R2009a), MathWorks).

7.3.3 Variable-c fitting procedure

In the case of the independent sites model, 7 and 12 parameters were optimized in the individual and global minimizations, respectively: the dissociation constant (K_{D1}, K_{D2}), binding enthalpy (ΔH_1, ΔH_2), and number (n_1 and n_2) of each type of site, and an offset (Q_0, equation 2.2) for each ITC titration. Note that the stoichiometric parameters, n_1 and n_2 also account for uncertainties in the protein concentration.[203] For the independent sites model, the following protocol was used:

1. Using the initial protein, $[P]_0$ and ligand $[X]_0$ concentrations together with the set of injection volumes, V_i, the calorimeter cell volume, V_c,

and Equations 2.3 and 2.4, calculate the total concentrations of protein, [P]T, and ligand, $[X]_T$, present in the calorimeter cell after each injection.

2. Select values of K_{D1}, K_{D2}, ΔH_1, ΔH_2, n_1, n_2 and Q_0.
3. Using $[P]_T$, $[X]_T$, K_{D1}, K_{D2}, n_1 and n_2, find the real positive root of Equation 2.7, to obtain the concentration of free ligand, [X], present after each injection.
4. Using $[X]$ and Equation 2.5, calculate the fractional saturation of type 1 and type 2 sites, Θ_1 and Θ_2.
5. Using $[P]_T$, n_1, n_2, Θ_1, Θ_2, ΔH_1, ΔH_2, and Equation 2.8, calculate the value of the heat function, Q, after each injection.
6. Use Q_0, Q and Equation 2.2 to calculate the theoretical ITC isotherm. Compute the sum of squared differences, RSS, between calculated and experimental ITC profiles according to Equation 2.16
7. For global fits, the sum runs over all data points. For individual fits, the sum runs over data at a single protein concentration.
8. Repeat steps 2 to 7, varying the values of the parameters in order to minimize RSS. In this study, the MATLAB simplex minimization scheme was used.

For the cooperative model, 6 and 11 parameters were optimized in the individual and global minimizations: the dissociation constants (K_{D1}, K_{D2}) and binding enthalpies (ΔH_1, ΔH_2) for the two sites, the initial protein concentration, $[P]_0$, as well as the offset, Q_0, for each titration. The following protocol was used:

1. Select values of K_{D1}, K_{D2}, ΔH_1, ΔH_2, $[P]_0$, and Q_0.
2. Using $[P]_0$ and $[X]_0$ together with the set of injection volumes, Vi, the calorimeter cell volume, V_c, and Equations 2.3 and 2.4, calculate the total concentrations of protein, $[P]_T$, and ligand, $[X]_T$, present in the calorimeter cell after each injection.
3. Using $[P]_T$, $[X]_T$, K_{D1}, and K_{D2} find the real positive root of Equation 2.14, to obtain the concentration of free ligand, $[X]$, present after each injection.
4. Using $[X]$ and Equations (10) and (11), calculate the fraction of protein in the singly and doubly bound states, f_1 and f_2.
5. Using $[P]_T$, ΔH_1, ΔH_2, and Equation (14), calculate the value of the heat function, Q, after each injection.
6. Use Q_0, Q and Equation 2.2 to calculate the theoretical ITC isotherm.
7. Compute the sum of squared differences, RSS, between calculated and experimental ITC profiles according to Equation 2.16
8. For global fits, the sum runs over all data points. For individual fits, the sum runs over data at a single protein concentration.

9. Repeat steps 1 to 7, varying the values of the parameters in order to minimize RSS. In this study, the MATLAB simplex minimization scheme was used.

7.4 Circular Dichroism.

CD measurements were performed on a Jasco J-810 spectrometer, using a 0.2 mm path length cuvette. Samples contained 25-80 μM protein with HEPES (25 mM), EDTA (2 mM) at pH 7.5, and NaCl (0 or 100 mM). Data were collected at temperatures between 0.1 to 70°C and wavelengths from 200 to 300 nm at scan rates of 50-200 nm/min in 0.5 nm increments with bandwidths of 1 nm. Each scan was performed three times then averaged. The final analysis was performed with two sets of thermal unfolding experiments. The first employed 1°C intervals with four minute equilibration times and the second employed 3-5°C intervals with 10 minute equilibration times.

7.5 NMR

NMR experiments were performed on Varian INOVA spectrometers equipped with either a high-sensitivity cold-probes or room temperature probe operating at 500 and 800 MHz ^{1}H Larmor frequencies. Spectra were collected for protein samples (0.6 to 1.5 mM) in sodium phosphate buffer(100 mM, pH 6.5)

containing EDTA (2mM), 2,2-dimethyl-2-silapentane-5-sulfonic acid (10 μM) and D_2O (10% v/v) at 37ºC. Spectra obtained under these conditions were significantly better resolved than those collected at lower temperatures and in 25 mM HEPES pH 7.5. Higher temperatures lead to more rapid rotational diffusion and sharper peaks, while lower pHs lead to slower chemical exchange of backbone hydrogens with the solvent and stronger signals for unprotected sites. Furthermore, the addition of 100 mM $NaPO_4$ raises the thermal melting temperature by about 7°C, consistent with salt stabilization of this enzyme, which has been observed previously.[204] Each spectra was collected with 64-80*(^{15}N)x512(^{1}H) point matrix and used 4-16 scans per transient. For spectra with ligand bound, 5 fold concentration of ligand was added to ensure the protein was completely saturated.

7.5.1 AcCoA titration

^{1}H/^{15}N HSQC spectra[205] were collected for AAC(6')-Ii with 0, 0.05, 0.1, 0.2, 0.3, 0.4, 0.6, 0.8, 1.1, 1.4, 1.7, 2.0 mM AcCoA. A sample of AAC(6')-Ii (580 μM, 910 μL) had AcCoA (20 mM) added with an analytical pipette between each spectra to a total of 100 μL. After each addition the sample was returned to the NMR and allowed to equilibrate for 15 min. After a ^{1}H/^{15}N HSQC spectra[205] was collected. ITC experiments were performed using both AAC(6')-Ii and AcCoA

from the same stock solution as the NMR experiments to determine the binding parameters of the given conditions.

7.5.2 Paromomcyin titration

$^{1}H/^{15}N$ HSQC spectra[205] were collected for AAC(6')-Ii with 0, 0.025, 0.05, 0.1, 0.2, 0.3, 0.4, 0.5, 0.6, 0.8, 1.0, 1.25, 1.5, 1.75, 2.0 mM paromomycin. A sample of AAC(6')-Ii (575 μM, 900 μL) had paromomycin (20 mM) added with an analytical pipette between each spectra to a total of 100 μL. After each addition the sample was returned to the NMR and allowed to equilibrate for 15 min. After a $^{1}H/^{15}N$ HSQC spectra[205] was collected.

7.5.3 EXSY spectra

EXSY spectra[182] were collected for a 50% AcCoA-saturated sample with mixing times of 500 and 1000 ms. To determine the 50% saturation point, a series have HSQCs were performed slowly increasing the concentration of AcCoA. The intensity of peaks which corresponded to the apo state was monitored until they reached 50% of their initial concentration. The presence of faint exchange cross-peaks in these spectra implies that dissociation rate constants are on the order of about 1 s^{-1}.

7.5.4 NMR data analysis

Peak intensities were quantified using the NMRPipe/NMRDraw[206] suite of software and were corrected for dilution of the sample caused by addition of ligand by multiplying each intensity by a factor of $(V_0+\Delta V_i)/V_0$, where V_0 is the initial sample volume and ΔV_i is the total volume of ligand added. In the titration analysis, only well-resolved signals from apo peaks that disappear at high ligand concentrations and holo peaks that are not present in the absence of ligand were considered. The data for each peak were normalized such that the initial intensity of each apo peak was 2 and the final intensity for each bound peak was 2. The ITC-derived binding constants for the first and second molecules of ligand were used together with the concentrations of ligand and enzyme to calculate the fractions of protein in the 0-bound, 1-bound and 2-bound states at each titration point (f_0, f_1, f_2). The intensities of apo and holo peaks were fitted using the series of f_0, f_1, and f_2 value. The contributions of the f_1 state to the apo and holo peaks was determined by adjusting values of I_1^{apo} and I_1^{holo} on a per-peak basis in order to maximize agreement between experimental and calculated intensities in a non-linear least-squares analysis using MATLAB (7.8.0.347 (R2009a), MathWorks). In these fits, the enzyme concentration was adjusted as single global variable in order to simultaneously optimize agreement for all apo and holo

peak intensity series, and was within 10 % of the initial concentration estimate based on A_{280} measurements.

References

1 Vakulenko, S. B. & Mobashery, S. Versatility of Aminoglycosides and Prospects for Their Future. *Clin. Microbiol. Rev.* **16**, 430-450, doi:10.1128/cmr.16.3.430-450.2003 (2003).

2 Hancock, R. E. W. Aminoglycoside uptake and mode of action—with special reference to streptomycin and gentamicin. *Journal of Antimicrobial Chemotherapy* **8**, 429-445, doi:10.1093/jac/8.6.429 (1981).

3 Kotra, L. P., Haddad, J. & Mobashery, S. Aminoglycosides: Perspectives on Mechanisms of Action and Resistance and Strategies to Counter Resistance. *Antimicrob. Agents Chemother.* **44**, 3249-3256, doi:10.1128/aac.44.12.3249-3256.2000 (2000).

4 Shakil, S., Khan, R., Zarrilli, R. & Khan, A. Aminoglycosides versus bacteria – a description of the action, resistance mechanism, and nosocomial battleground. *Journal of Biomedical Science* **15**, 5-14 (2008).

5 Miller, G. H. *et al.* The Most Frequent Aminoglycoside Resistance Mechanisms: Changes with Time and Geographic Area: A Reflection of Aminoglycoside Usage Patterns? *Clinical Infectious Diseases* **24**, S46-S62 (1997).

6 Pasteur, L. The Germ Theory and Its Applications to Medicine and Surgery. *Comptes rendus de l'Académie des Sciences* **lxxxvi**, 1037-1043 (1878).

7 Koch, R. *Die Ätiologie der Milzbrand-Krankheit, begründet auf die Entwicklungsgeschichte des Bacillus Anthracis [1876]*. (1910).

8 Ehrlich, P. Über den jetzigen Stand der Chemotherapie. *Berichte der deutschen chemischen Gesellschaft* **42**, 17-47, doi:10.1002/cber.19090420105 (1909).

9 Riethmiller, S. From Atoxyl to Salvarsan: Searching for the Magic Bullet. *Chemotherapy* **51**, 234-242 (2005).

10 Fleming, A. On the Antibacterial Action of Cultures of a Penicillium, with Special Reference to Their Use in the Isolation of B. influenzae. *British Journal of Experimental Pathology* **10**, 226-236 (1929).

11 Schatz, A. Streptomycin, a substance exhibiting antibiotic activity against gram-positive and gram-negative bacteria. *Proceedings of the Society for Experimental Biology and Medicine* **55**, 66 (1944).

12 Gould, I. M. Antibiotic resistance: the perfect storm. *International Journal of Antimicrobial Agents* **34**, S2-S5 (2009).

13 Zerikly, M. & Challis, G. L. Strategies for the Discovery of New Natural Products by Genome Mining. *ChemBioChem* **10**, 625-633 (2009).

14 Wright, G. D. The antibiotic resistome: the nexus of chemical and genetic diversity. *Nature Reviews Microbiology* **5**, 175-186, doi:10.1038/nrmicro1614 (2007).

15 Sefton, A. M. Mechanisms of Antimicrobial Resistance: Their Clinical Relevance in the New Millennium. *Drugs* **62**, 557-566 (2002).

16 Durante-Mangoni, E., Grammatikos, A., Utili, R. & Falagas, M. E. Do we still need the aminoglycosides? *International Journal of Antimicrobial Agents* **33**, 201-205 (2009).

17 Wright, G. D. & Thompson, P. R. Aminoglycoside phosphotransferases: proteins, structure, and mechanism. *Frontiers in Bioscience* **4**, D9-21 (1999).

18 Mingeot-Leclercq, M.-P., Glupczynski, Y. & Tulkens, P. M. Aminoglycosides: Activity and Resistance. *Antimicrob. Agents Chemother.* **43**, 727-737 (1999).

19 Carter, A. P. *et al.* Functional insights from the structure of the 30S ribosomal subunit and its interactions with antibiotics. *Nature* **407**, 340-348, doi:http://www.nature.com/nature/journal/v407/n6802/suppinfo/407340a0_S1.html (2000).

20 Fourmy, D., Recht, M. I., Blanchard, S. C. & Puglisi, J. D. Structure of the A Site of Escherichia coli 16S Ribosomal RNA Complexed with an Aminoglycoside Antibiotic. *Science* **274**, 1367-1371, doi:10.1126/science.274.5291.1367 (1996).

21 Fourmy, D., Yoshizawa, S. & Puglisi, J. D. Paromomycin binding induces a local conformational change in the A-site of 16 s rRNA. *Journal of Molecular Biology* **277**, 333-345 (1998).

22 Yoshizawa, S., Fourmy, D. & Puglisi, J. D. Structural origins of gentamicin antibiotic action. *EMBO J* **17**, 6437-6448 (1998).

23 Ogle, J. M. *et al.* Recognition of Cognate Transfer RNA by the 30S Ribosomal Subunit. *Science* **292**, 897-902, doi:10.1126/science.1060612 (2001).

24 Vicens, Q. & Westhof, E. Crystal Structure of Paromomycin Docked into the Eubacterial Ribosomal Decoding A Site. *Structure (London, England : 1993)* **9**, 647-658 (2001).

25 Vicens, Q. & Westhof, E. Crystal Structure of a Complex between the Aminoglycoside Tobramycin and an Oligonucleotide Containing the Ribosomal Decoding A Site. *Chemistry & Biology* **9**, 747-755 (2002).

26 Vicens, Q. & Westhof, E. Crystal Structure of Geneticin Bound to a Bacterial 16 S Ribosomal RNA A Site Oligonucleotide. *Journal of Molecular Biology* **326**, 1175-1188 (2003).

27 Fourmy, D., Recht, M. I. & Puglisi, J. D. Binding of neomycin-class aminoglycoside antibiotics to the A-site of 16 s rRNA. *Journal of Molecular Biology* **277**, 347-362 (1998).

28 Yoshizawa, S., Fourmy, D., Eason, R. G. & Puglisi, J. D. Sequence-Specific Recognition of the Major Groove of RNA by Deoxystreptamine†. *Biochemistry* **41**, 6263-6270, doi:10.1021/bi0121609 (2002).

29 François, B. *et al.* Crystal structures of complexes between aminoglycosides and decoding A site oligonucleotides: role of the number

of rings and positive charges in the specific binding leading to miscoding. *Nucleic Acids Research* **33**, 5677-5690, doi:10.1093/nar/gki862 (2005).

30 Yoshizawa, S., Fourmy, D. & Puglisi, J. D. Recognition of the Codon-Anticodon Helix by Ribosomal RNA. *Science* **285**, 1722-1725, doi:10.1126/science.285.5434.1722 (1999).

31 Kaul, M., Barbieri, C. M. & Pilch, D. S. Aminoglycoside-Induced Reduction in Nucleotide Mobility at the Ribosomal RNA A-Site as a Potentially Key Determinant of Antibacterial Activity. *Journal of the American Chemical Society* **128**, 1261-1271, doi:10.1021/ja056159z (2006).

32 Davis, B. D. Mechanism of bactericidal action of aminoglycosides. *Microbiology and molecular biology reviews* **51**, 341 (1987).

33 Magnet, S. & Blanchard, J. S. Molecular Insights into Aminoglycoside Action and Resistance. *Chemical Reviews* **105**, 477-498, doi:10.1021/cr0301088 (2004).

34 Recht, M. I., Douthwaite, S. & Puglisi, J. D. Basis for prokaryotic specificity of action of aminoglycoside antibiotics. *EMBO J* **18**, 3133-3138 (1999).

35 Fleming, A. in *Nobel Lectures, Physiology or Medicine 1942-1962* (Elsevier Publishing Company, 1964).

36 Demerec, M. Production of Staphylococcus Strains Resistant to Various Concentrations of Penicillin. *Proc. Natl. Acad. Sci. U.S.A.* **31**, 16-24 (1945).

37 Demerec, M. Origin of Bacterial Resistance to Antibiotics. *Journal of Bacteriology* **56**, 63-74 (1948).

38 Normark, B. H. & Normark, S. Evolution and spread of antibiotic resistance. *Journal of Internal Medicine* **252**, 91-106 (2002).

39 Shakya, T. & Wright, G. D. in *Aminoglycoside Antibiotics* (ed Dev P Arya) Ch. 3, 119-130 (John Wiley & Sons, Inc., 2007).

40 Shaw, K. J., Rather, P. N., Hare, R. S. & Miller, G. H. Molecular genetics of aminoglycoside resistance genes and familial relationships of the

aminoglycoside-modifying enzymes. *Microbiol. Mol. Biol. Rev.* **57**, 138-163 (1993).

41 Bush, K. & Miller, G. H. Bacterial enzymatic resistance: β-lactamases and aminoglycoside-modifying enzymes. *Current Opinion in Microbiology* **1**, 509-515 (1998).

42 Wright, G. D. Aminoglycoside-modifying enzymes. *Current Opinion in Microbiology* **2**, 499-503 (1999).

43 Costa, Y., Galimand, M., Leclercq, R., Duval, J. & Courvalin, P. Characterization of the chromosomal aac(6')-Ii gene specific for Enterococcus faecium. *Antimicrob. Agents Chemother.* **37**, 1896-1903, doi:10.1128/aac. (1993).

44 Wright, G. D. & Ladak, P. Overexpression and characterization of the chromosomal aminoglycoside 6'-N-acetyltransferase from Enterococcus faecium. *Antimicrob. Agents Chemother.* **41**, 956-960 (1997).

45 Draker, K., Northrop, D. B. & Wright, G. D. Kinetic Mechanism of the GCN5-Related Chromosomal Aminoglycoside Acetyltransferase AAC(6')-Ii from Enterococcus faecium: Evidence of Dimer Subunit Cooperativity. *Biochemistry* **42**, 6565-6574 (2003).

46 Wybenga-Groot, L. E., Draker, K.-a., Wright, G. D. & Berghuis, A. M. Crystal structure of an aminoglycoside 6'-N-acetyltransferase: defining the GCN5-related N-acetyltransferase superfamily fold. *Structure* **7**, 497-507 (1999).

47 Draker, K.-A. *Characterization of the Chromosomal Aminoglycoside 6'-N-Acetyltransferase from Enterococcus faecium* Ph. D thesis, McMaster, (2004).

48 Burk, D. L., Ghuman, N., Wybenga-Groot, L. E. & Berghuis, A. M. X-ray structure of the AAC(6')-Ii antibiotic resistance enzyme at 1.8 Å resolution; examination of oligomeric arrangements in GNAT superfamily members. *Protein Science* **12**, 426-437 (2003).

49 Burk, D. L., Xiong, B., Breitbach, C. & Berghuis, A. M. Structures of aminoglycoside acetyltransferase AAC(6')-Ii in a novel crystal form: structural and normal-mode analyses. *Acta Crystallographica Section D* **61**, 1273-1279, doi:doi:10.1107/S0907444905021487 (2005).

50 Neuwald, A. F. & Landsman, D. GCN5-related histone N-acetyltransferases belong to a diverse superfamily that includes the yeast SPT10 protein. *Trends in Biochemical Sciences* **22**, 154-155 (1997).

51 Siehl, D. L., Castle, L. A., Gorton, R. & Keenan, R. J. The Molecular Basis of Glyphosate Resistance by an Optimized Microbial Acetyltransferase. *Journal of Biological Chemistry* **282**, 11446-11455, doi:10.1074/jbc.M610267200 (2007).

52 Vetting, M. W., de Carvalho, L. P. S., Roderick, S. L. & Blanchard, J. S. A Novel Dimeric Structure of the RimL Nα-acetyltransferase from Salmonella typhimurium. *Journal of Biological Chemistry* **280**, 22108-22114, doi:10.1074/jbc.M502401200 (2005).

53 Peneff, C., Mengin-Lecreulx, D. & Bourne, Y. The Crystal Structures of Apo and Complexed Saccharomyces cerevisiae GNA1 Shed Light on the Catalytic Mechanism of an Amino-sugar N-Acetyltransferase. *Journal of Biological Chemistry* **276**, 16328-16334, doi:10.1074/jbc.M009988200 (2001).

54 Vetting, M. W. *et al.* Mechanistic and Structural Analysis of Aminoglycoside N-Acetyltransferase AAC(6')-Ib and Its Bifunctional, Fluoroquinolone-Active AAC(6')-Ib-cr Variant. *Biochemistry* **47**, 9825-9835, doi:doi:10.1021/bi800664x (2008).

55 Freiburger, L. A., Auclair, K. & Mittermaier, A. K. Elucidating Protein Binding Mechanisms by Variable-*c* ITC. *ChemBioChem* **10**, 2871-2873 (2009).

56 Leonardi, R., Zhang, Y.-M., Rock, C. O. & Jackowski, S. Coenzyme A: Back in action. *Progress in Lipid Research* **44**, 125-153 (2005).

57 Vallari, D. S., Jackowski, S. & Rock, C. O. Regulation of pantothenate kinase by coenzyme A and its thioesters. *Journal of Biological Chemistry* **262**, 2468-2471 (1987).

58 del Cardayré, S. B. & Davies, J. E. *Staphylococcus aureus* Coenzyme A Disulfide Reductase, a New Subfamily of Pyridine Nucleotide-Disulfide Oxidoreductase. *Journal of Biological Chemistry* **273**, 5752-5757, doi:10.1074/jbc.273.10.5752 (1998).

59 de Cabo, R. & Navas, P. "AcCoA"lade for Energy and Life Span. *Cell Metabolism* **9**, 305-306 (2009).

60 Steinberg, S. J., Morgenthaler, J., Heinzer, A. K., Smith, K. D. & Watkins, P. A. Very Long-chain Acyl-CoA Synthetases. *Journal of Biological Chemistry* **275**, 35162-35169, doi:10.1074/jbc.M006403200 (2000).

61 Mitchell, G. A. *et al.* Hereditary and acquired diseases of acyl-coenzyme A metabolism. *Molecular Genetics and Metabolism* **94**, 4-15 (2008).

62 Koshland, D. E. & Hamadani, K. Proteomics and Models for Enzyme Cooperativity. *Journal of Biological Chemistry* **277**, 46841-46844, doi:10.1074/jbc.R200014200 (2002).

63 Bohr, C., Hasselbalch, K. & Krogh, A. On the Influence of Carbonic Acid Tension on the Oxygen Uptake in the Blood. [machine translation]. *Centr.-Bl. f. Physiol.* **17**, 661-664 (1904).

64 Koshland, D. E., Némethy, G. & Filmer, D. Comparison of Experimental Binding Data and Theoretical Models in Proteins Containing Subunits. *Biochemistry* **5**, 365-385, doi:doi:10.1021/bi00865a047 (1966).

65 Monod, J., Wyman, J. & Changeux, J. P. On the Nature of Allosteric Transitions: A Plausible Model. *Journal of Molecular Biology* **19**, 88-118 (1965).

66 Cooper, A. & Dryden, D. T. F. Allostery without conformational change. *European Biophysics Journal* **11**, 103-109 (1984).

67 Tsai, C.-J., del Sol, A. & Nussinov, R. Allostery: Absence of a Change in Shape Does Not Imply that Allostery Is Not at Play. *Journal of Molecular Biology* **378**, 1-11 (2008).

68 Miyazawa, A., Fujiyoshi, Y. & Unwin, N. Structure and gating mechanism of the acetylcholine receptor pore. *Nature* **423**, 949-955, doi:http://www.nature.com/nature/journal/v423/n6943/suppinfo/nature01748_S1.html (2003).

69 Holman, G. D. An allosteric pore model for sugar transport in human erythrocytes. *Biochimica et Biophysica Acta (BBA) - Biomembranes* **599**, 202-213 (1980).

70 Monod, J. & Jacob, F. General Conclusions: Teleonomic Mechanisms in Cellular Metabolism, Growth, and Differentiation. *Cold Spring Harb Symp* **26**, 389-401 (1961).

71 Changeux, J.-P. The Feedback Control Mechanism of Biosynthetic L-Threonine Deaminase by L-Isoleucine. *Cold Spring Harb Symp Quant Biol* **26**, 313-318 (1961).

72 Perutz, M. F. Mechanisms of cooperativity and allosteric regulation in proteins. *Quarterly Reviews of Biophysics* **22**, 139-237, doi:doi:10.1017/S0033583500003826 (1989).

73 Fenton, A. W. Allostery: an illustrated definition for the `second secret of life'. *Trends in Biochemical Sciences* **33**, 420-425 (2008).

74 DeDecker, B. S. Allosteric drugs: thinking outside the active-site box. *Chemistry & Biology* **7**, R103-R107 (2000).

75 Foster, B. A., Coffey, H. A., Morin, M. J. & Rastinejad, F. Pharmacological Rescue of Mutant p53 Conformation and Function. *Science* **286**, 2507-2510, doi:10.1126/science.286.5449.2507 (1999).

76 McMillan, K. *et al.* Allosteric inhibitors of inducible nitric oxide synthase dimerization discovered via combinatorial chemistry. *Proceedings of the National Academy of Sciences of the United States of America* **97**, 1506-1511 (2000).

77 Schlessinger, J. Signal transduction by allosteric receptor oligomerization. *Trends in Biochemical Sciences* **13**, 443-447 (1988).

78 Qiang Cui, M. K. Allostery and cooperativity revisited. *Protein Science* **17**, 1295-1307 (2008).

79 Szabo, A. & Karplus, M. Analysis of cooperativity in hemoglobin. Valency hybrids, oxidation, and methemoglobin replacement reactions. *Biochemistry* **14**, 931-940 (1975).

80 Cori, G. T., Colowick, S. P. & Cori, C. F. The Action of Nucleotides in the Disruptive Phosphorylation of Glycogen. *Journal of Biological Chemistry* **123**, 381-389 (1938).

81 Koshland, D. E. The structural basis of negative cooperativity: receptors and enzymes. *Current Opinion in Structural Biology* **6**, 757-761 (1996).

82 Hill, A. V. The possible effects of the aggregation of the molecules of huemoglobin on its dissociation curves. *The Journal of Physiology* **40**, i-vii (1910).

83 Perutz, M. F. Stereochemistry of Cooperative Effects in Haemoglobin: Haem-Haem Interaction and the Problem of Allostery. *Nature* **228**, 726-734 (1970).

84 Hardy, J. A. & Wells, J. A. Searching for new allosteric sites in enzymes. *Current Opinion in Structural Biology* **14**, 706-715 (2004).

85 Gao, Z.-G. & Jacobson, K. A. Keynote review: Allosterism in membrane receptors. *Drug Discovery Today* **11**, 191-202 (2006).

86 Swain, J. F. & Gierasch, L. M. The changing landscape of protein allostery. *Current Opinion in Structural Biology* **16**, 102-108 (2006).

87 Pauling, L. The Oxygen Equilibrium of Hemoglobin and Its Structural Interpretation. *Proceedings of the National Academy of Sciences of the United States of America* **21**, 186-191 (1935).

88 Hilser, V. J. & Thompson, E. B. Intrinsic disorder as a mechanism to optimize allosteric coupling in proteins. *Proceedings of the National*

Academy of Sciences **104**, 8311-8315, doi:10.1073/pnas.0700329104 (2007).

89 Eaton, W. A., Henry, E. R., Hofrichter, J. & Mozzarelli, A. Is cooperative oxygen binding by hemoglobin really understood? *Nat Struct Mol Biol* **6**, 351-358 (1999).

90 Changeux, J.-P. & Edelstein, S. J. Allosteric Mechanisms of Signal Transduction. *Science* **308**, 1424-1428, doi:10.1126/science.1108595 (2005).

91 Koshland, D. E. The Key–Lock Theory and the Induced Fit Theory. *Angewandte Chemie International Edition in English* **33**, 2375-2378, doi:10.1002/anie.199423751 (1995).

92 Koshland, D. E. Application of a Theory of Enzyme Specificity to Protein Synthesis. *Proceedings of the National Academy of Sciences* **44**, 98-104 (1958).

93 Hammes, G. G., Chang, Y.-C. & Oas, T. G. Conformational selection or induced fit: A flux description of reaction mechanism. *Proceedings of the National Academy of Sciences* **106**, 13737-13741, doi:10.1073/pnas.0907195106 (2009).

94 Popovych, N., Sun, S., Ebright, R. H. & Kalodimos, C. G. Dynamically driven protein allostery. *Nat Struct Mol Biol* **13**, 831-838, doi:http://www.nature.com/nsmb/journal/v13/n9/suppinfo/nsmb1132_S1.html (2006).

95 Gandhi, P. S., Chen, Z., Mathews, F. S. & Di Cera, E. Structural identification of the pathway of long-range communication in an allosteric enzyme. *Proceedings of the National Academy of Sciences* **105**, 1832-1837, doi:10.1073/pnas.0710894105 (2008).

96 Lockless, S. W. & Ranganathan, R. Evolutionarily conserved pathways of energetic connectivity in protein families. *Science* **286**, 295-299 (1999).

97 Gunasekaran, K., Ma, B. & Nussinov, R. Is allostery an intrinsic property of *all* dynamic proteins? *Proteins: Structure, Function, and Bioinformatics* **57**, 433-443 (2004).

98 Perutz, M. F., Wilkinson, A. J., Paoli, M. & Dodson, G. G. The Stereochemical Mechanism of the Cooperative Effects in Hemoglobin Revisited. *Annual Review of Biophysics and Biomolecular Structure* **27**, 1-34, doi:doi:10.1146/annurev.biophys.27.1.1 (1998).

99 Holt, J. & Ackers, G. The pathway of allosteric control as revealed by hemoglobin intermediate states. *FASEB J.* **9**, 210-218 (1995).

100 Stevens, S. Y., Sanker, S., Kent, C. & Zuiderweg, E. R. P. Delineation of the allosteric mechanism of a cytidylyltransferase exhibiting negative cooperativity. *Nat Struct Mol Biol* **8**, 947-952 (2001).

101 Brown, A. Analysis of Cooperativity by Isothermal Titration Calorimetry. *International Journal of Molecular Sciences* **10**, 3457-3477 (2009).

102 Cliff, M. J., Williams, M. A., Brooke-Smith, J., Barford, D. & Ladbury, J. E. Molecular Recognition via Coupled Folding and Binding in a TPR Domain. *Journal of Molecular Biology* **346**, 717-732 (2005).

103 Baranauskienė, L., Petrikaitė, V., Matulienė, J. & Matulis, D. Titration Calorimetry Standards and the Precision of Isothermal Titration Calorimetry Data. *International Journal of Molecular Sciences* **10**, 2752-2762 (2009).

104 Freire, E., Mayorga, O. L. & Straume, M. Isothermal Titration Calorimetry. *Anal Chem* **62**, A950-A959 (1990).

105 Liang, Y. Applications of isothermal titration calorimetry in protein science. *Acta Biochim Biophys Sin* **40**, 565-576, doi:10.1111/j.1745-7270.2008.00437.x (2008).

106 Leavitt, S. & Freire, E. Direct measurement of protein binding energetics by isothermal titration calorimetry. *Current Opinion in Structural Biology* **11**, 560-566 (2001).

107 Barisas, B. G. & Gill, S. J. Micro-Calorimetry of Biological-Systems. *Annu Rev Phys Chem* **29**, 141-166 (1978).

108 Wiseman, T., Williston, S., Brandts, J. F. & Lin, L.-N. Rapid measurement of binding constants and heats of binding using a new titration calorimeter. *Analytical Biochemistry* **179**, 131-137 (1989).

109 Oksana Okhrimenko, I. J. A survey of the year 2006 literature on applications of isothermal titration calorimetry. *Journal of Molecular Recognition* **21**, 1-19 (2008).

110 Ababou, A. & Ladbury, J. E. Survey of the year 2005: literature on applications of isothermal titration calorimetry. *Journal of Molecular Recognition* **20**, 4-14 (2007).

111 Ababou, A. & Ladbury, J. E. Survey of the year 2004: literature on applications of isothermal titration calorimetry. *Journal of Molecular Recognition* **19**, 79-89 (2006).

112 Cliff, M. J., Gutierrez, A. & Ladbury, J. E. A survey of the year 2003 literature on applications of isothermal titration calorimetry. *Journal of Molecular Recognition* **17**, 513-523 (2004).

113 Cliff, M. J. & Ladbury, J. E. A survey of the year 2002 literature on applications of isothermal titration calorimetry. *Journal of Molecular Recognition* **16**, 383-391 (2003).

114 Bjelic, S. & Jelesarov, I. A survey of the year 2007 literature on applications of isothermal titration calorimetry. *Journal of Molecular Recognition* **21**, 289-312 (2008).

115 Koshland, D. E. Application of a theory of enzyme specificity to protein synthesis. *Proceedings of the National Academy of Sciences of the United States of America* **44**, 98-104 (1958).

116 Eftink, M. R., Anusiem, A. C. & Biltonen, R. L. Enthalpy-entropy compensation and heat capacity changes for protein-ligand interactions: general thermodynamic models and data for the binding of nucleotides to ribonuclease A. *Biochemistry* **22**, 3884-3896 (1983).

117 Prabhu, N. & Sharp, K. Heat capacity in proteins. *Annu. Rev. Phys. Chem.* **56**, 521 (2005).

118 McConnell, H. M. Reaction Rates by Nuclear Magnetic Resonance. *The Journal of Chemical Physics* **28**, 430-431 (1958).

119 Bain, A. D. Chemical Exchange in NMR. *Progress in Nuclear Magnetic Resonance Spectroscopy* **43**, 63-103, doi:10.1016/j.pnmrs.2003.08.001 (2004).

120 Feher, V. A., Baldwin, E. P. & Dahlquist, F. W. Access of ligands to cavities within the core of a protein is rapid. *Nat Struct Mol Biol* **3**, 516-521 (1996).

121 Palmer, A. G., Kroenke, C. D., Loria, J. P., Thomas L. James, V. D. & Uli, S. in *Methods in Enzymology* Vol. Volume 339 204-238 (Academic Press, 2001).

122 Capaldi, S. *et al.* The X-Ray Structure of Zebrafish (Danio rerio) Ileal Bile Acid-Binding Protein Reveals the Presence of Binding Sites on the Surface of the Protein Molecule. *Journal of Molecular Biology* **385**, 99-116 (2009).

123 Freire, E., Schön, A., VelazquezCampoy, A., Michael L. Johnson, J. M. H. & Gary, K. A. in *Methods in Enzymology* Vol. Volume 455 127-155 (Academic Press, 2009).

124 Houtman, J. C. D. *et al.* Studying multisite binary and ternary protein interactions by global analysis of isothermal titration calorimetry data in SEDPHAT: Application to adaptor protein complexes in cell signaling. *Protein Science* **16**, 30-42, doi:10.1110/ps.062558507 (2007).

125 Tsamaloukas, A., Szadkowska, H., Slotte, P. J. & Heerklotz, H. Interactions of Cholesterol with Lipid Membranes and Cyclodextrin Characterized by Calorimetry. *Biophysical Journal* **89**, 1109-1119 (2005).

126 Henzl, M. T., Larson, J. D. & Agah, S. Estimation of parvalbumin Ca2+- and Mg2+-binding constants by global least-squares analysis of

isothermal titration calorimetry data. *Analytical Biochemistry* **319**, 216-233 (2003).

127 MicroCal. *ITC Data Analysis in Origin®*. 7.0 edn, (MicroCal, 2004).

128 Burden, R. L. & Faires, J. D. *Numerical Analysis*. 7th edn, (Brooks/Cole, 2000).

129 Walpole, R. E., Myers, R. H. & Myers, S. L. *Probability and Statistics for Engineers and Scientists*. (Prentice Hall, 1998).

130 Press, W. H., Flannery, S. A. & Teukolsky, W. T. *Numerical Recipes in C*. (Cambridge University Press, 1988).

131 Tellinghuisen, J. A Monte Carlo Study of Precision, Bias, Inconsistency, and Non-Gaussian Distributions in Nonlinear Least Squares. *J. Phys. Chem.* **104**, 2834-2844 (2000).

132 Tellinghuisen, J. Statistical error in isothermal titration calorimetry: Variance function estimation from generalized least squares. *Analytical Biochemistry* **343**, 106-115 (2005).

133 Tellinghuisen, J. Isothermal titration calorimetry at very low c. *Analytical Biochemistry* **373**, 395-397, doi:10.1016/j.ab.2007.08.039 (2008).

134 Velazquez-Campoy, A., Ohtaka, H., Nezami, A., Muzammil, S. & Freire, E. Isothermal Titration Calorimetry. *Curr. Prot. Cell Biol.* **23**, 17.18.01-17.18.24 (2004).

135 Freire, E., Schon, A. & Velazquez-Campoy, A. Isothermal titration calorimetry: general formalism using binding polynomials. *Methods Enzymol* **455**, 127-155, doi:S0076-6879(08)04205-5 [pii]
10.1016/S0076-6879(08)04205-5 (2009).

136 Ha, J.-H., Spolar, R. S. & Record, M. T. Role of the hydrophobic effect in stability of site-specific protein-DNA complexes. *Journal of Molecular Biology* **209**, 801-816 (1989).

137 Prabhu, N. V. & Sharp, K. A. Heat capacity in proteins. *Annu. Rev. Phys. Chem.* **56**, 521-548, doi:10.1146/annurev.physchem.56.092503.141202 (2005).

138 Herman, P. & Lee, J. C. Functional Energetic Landscape in the Allosteric Regulation of Muscle Pyruvate Kinase. 1. Calorimetric Study. *Biochemistry* **48**, 9448-9455, doi:10.1021/bi900279x (2009).

139 Baker, B. M. & Murphy, K. P. Evaluation of linked protonation effects in protein binding reactions using isothermal titration calorimetry. *Biophysical Journal* **71**, 2049-2055 (1996).

140 Freiburger, L. A. *et al.* Competing allosteric mechanisms modulate substrate binding in a dimeric enzyme. *Nat Struct Mol Biol* **18**, 288-294, doi:http://www.nature.com/nsmb/journal/vaop/ncurrent/abs/nsmb.1978.html#supplementary-information (2011).

141 Tochtrop, G. P. *et al.* Energetics by NMR: Site-specific binding in a positively cooperative system. *Proceedings of the National Academy of Sciences of the United States of America* **99**, 1847-1852, doi:DOI 10.1073/pnas.012379199 (2002).

142 Schon, A. & Freire, E. Thermodynamics of intersubunit interactions in cholera-toxin upon binding to the oligosaccharide portion of its cell-surface receptor, ganglioside-gm1. *Biochemistry* **28**, 5019-5024 (1989).

143 Baker, B. M. & Murphy, K. P. Dissecting the energetics of a protein-protein interaction: the binding of ovomucoid third domain to elastase. *Journal of Molecular Biology* **268**, 557-569 (1997).

144 Armstrong, K. M. & Baker, B. M. A comprehensive calorimetric investigation of an entropically driven T cell receptor-peptide/major histocompatibility complex interaction. *Biophys J* **93**, 597-609, doi:10.1529/biophysj.107.104570 (2007).

145 Turner, D. C., Straume, M., Kasimova, M. R. & Gaber, B. P. Thermodynamics of Interaction of the Fusion-Inhibiting Peptide Z-D-Phe-L-Phe-Gly with Dioleoylphosphatidylcholine Vesicles: Direct Calorimetric Determination. *Biochemistry* **34**, 9517-9525, doi:10.1021/bi00029a028 (1995).

146 Jon, C. D. H. *et al.* Studying multisite binary and ternary protein interactions by global analysis of isothermal titration calorimetry data in SEDPHAT: Application to adaptor protein complexes in cell signaling. *Protein Science* **16**, 30-42 (2007).

147 Saxena, V. P. & Wetlaufe, D. B. New Basis for Interpreting Circular Dichroic Spectra of Proteins. *Proceedings of the National Academy of Sciences of the United States of America* **68**, 969-972 (1971).

148 Adler, A. J., Greenfield, N. J. & Fasman, G. D. Circular dichroism and optical rotatory dispersion of proteins and polypeptides. *Methods Enzymol* **27**, 675-735 (1973).

149 Uversky, V. N. Natively unfolded proteins: A point where biology waits for physics. *Protein Science* **11**, 739-756, doi:10.1110/ps.4210102 (2002).

150 Fisher, H. F., Colen, A. H. & Medary, R. T. Temperature-dependent ΔC_p^0 generated by a shift in equilibrium between macrostates of an enzyme. *Nature* **292**, 271-272 (1981).

151 Elwell, M. & Schellman, J. Phage-T4 lysozyme - physical-properties and reversible unfolding. *Biochimica Et Biophysica Acta* **386**, 309-323 (1975).

152 Kuhlman, B., Boice, J. A., Fairman, R. & Raleigh, D. P. Structure and stability of the N-terminal domain of the ribosomal protein L9: Evidence for rapid two-state folding. *Biochemistry* **37**, 1025-1032 (1998).

153 Beadle, B. M., Baase, W. A., Wilson, D. B., Gilkes, N. R. & Shoichet, B. K. Comparing the thermodynamic stabilities of a related thermophilic and mesophilic enzyme. *Biochemistry* **38**, 2570-2576 (1999).

154 Robertson, A. D. & Murphy, K. P. Protein Structure and the Energetics of Protein Stability. *Chemical Reviews* **97**, 1251-1268, doi:10.1021/cr960383c (1997).

155 Tellinghuisen, J. Optimizing Experimental Parameters in Isothermal Titration Calorimetry: Variable Volume Procedures. *The Journal of Physical Chemistry B* **111**, 11531-11537, doi:10.1021/jp074515p (2007).

156 Tellinghuisen, J. Optimizing experimental parameters in isothermal titration calorimetry. *Journal of Physical Chemistry B* **109**, 20027-20035, doi:10.1021/jp053550y (2005).

157 Perutz, M. F. Mechansism of cooperativity and allosteric regulation in proteins. *Q. Rev. Biophys.* **22**, 139-236 (1989).

158 Monod, J., Wyman, J. & Changeux, J. P. On nature of allosteric transitions - a plausible model. *J. Mol. Biol.* **12**, 88-118 (1965).

159 Fenton, A. W. Allostery: an illustrated definition for the 'second secret of life'. *Trends Biochem. Sci.* **33**, 420-425, doi:10.1016/j.tibs.2008.05.009 (2008).

160 DeDecker, B. S. Allosteric drugs: thinking outside the active-site box. *Chem. Biol.* **7**, R103-R107 (2000).

161 Koshland, D. E., Nemethy, G. & Filmer, D. Comparison of experimental binding data and theoretical models in proteins containing subunits. *Biochemistry* **5**, 365-385 (1966).

162 Perutz, M. F., Wilkinson, A. J., Paoli, M. & Dodson, G. G. The stereochemical mechanism of the cooperative effects in hemoglobin revisited. *Annu Rev Biophys Biomol Struct* **27**, 1-34 (1998).

163 Helmstaedt, K., Krappmann, S. & Braus, G. H. Allosteric regulation of catalytic activity: Escherichia coli aspartate transcarbamoylase versus yeast chorismate mutase. *Microbiol. Mol. Biol. Rev.* **65**, 404-421 (2001).

164 Cui, Q. & Karplus, M. Allostery and cooperativity revisited. *Protein Sci.* **17**, 1295-1307, doi:10.1110/ps.03259908 (2008).

165 Kern, D. & Zuiderweg, E. R. P. The role of dynamics in allosteric regulation. *Curr. Opin. Struct. Biol.* **13**, 748-757, doi:10.1016/j.sbi.2003.10.008 (2003).

166 Hilser, V. J. & Thompson, E. B. Intrinsic disorder as a mechanism to optimize allosteric coupling in proteins. *Proc. Natl. Acad. Sci. U.S.A.* **104**, 8311-8315, doi:10.1073/pnas.0700323104 (2007).

167 Reichheld, S. E., Yu, Z. & Davidson, A. R. The induction of folding cooperativity by ligand binding drives the allosteric response of tetracycline repressor. *Proc. Natl. Acad. Sci. U.S.A.* **106**, 22263-22268, doi:10.1073/pnas.0911566106 (2009).

168 Popovych, N., Sun, S. J., Ebright, R. H. & Kalodimos, C. G. Dynamically driven protein allostery. *Nat. Struct. Mol. Biol.* **13**, 831-838, doi:10.1038/nsmb1132 (2006).

169 Cooper, A. & Dryden, D. T. F. Allostery without conformational change - a plausible model. *Eur. Biophys. J.* **11**, 103-109 (1984).

170 Tzeng, S. R. & Kalodimos, C. G. Dynamic activation of an allosteric regulatory protein. *Nature* **462**, 368-U139, doi:10.1038/nature08560 (2009).

171 Gandhi, P. S., Chen, Z. W., Mathews, F. S. & Di Cera, E. Structural identification of the pathway of long-range communication in an allosteric enzyme. *Proc. Natl. Acad. Sci. U.S.A.* **105**, 1832-1837, doi:10.1073/pnas.0710894105 (2008).

172 Pan, H., Lee, J. C. & Hilser, V. J. Binding sites in Escherichia coli dihydrofolate reductase communicate by modulating the conformational ensemble. *Proceedings of the National Academy of Sciences of the United States of America* **97**, 12020-12025 (2000).

173 Volkman, B. F., Lipson, D., Wemmer, D. E. & Kern, D. Two-state allosteric behavior in a single-domain signaling protein. *Science* **291**, 2429-2433 (2001).

174 Gunasekaran, K., Ma, B. Y. & Nussinov, R. Is allostery an intrinsic property of all dynamic proteins? *Proteins* **57**, 433-443, doi:10.1002/prot.20232 (2004).

175 Clarkson, M. W., Gilmore, S. A., Edgell, M. H. & Lee, A. L. Dynamic coupling and allosteric behavior in a nonallosteric protein. *Biochemistry* **45**, 7693-7699, doi:10.1021/bi060652l (2006).

176 Burk, D. L., Xiong, B., Breitbach, C. & Berghuis, A. M. Structures of aminoglycoside acetyltransferase AAC(6 ')-Ii in a novel crystal form: structural and normal-mode analyses. *Acta Crystallogr. D Biol. Crystallogr.* **61**, 1273-1279 (2005).

177 Burk, D. L., Ghuman, N., Wybenga-Groot, L. E. & Berghuis, A. M. X-ray structure of the AAC(6 ')-Ii antibiotic resistance enzyme at 1.8 angstrom resolution; examination of oligomeric arrangements in GNAT superfamily members. *Protein Sci.* **12**, 426-437, doi:10.1110/ps.0233503 (2003).

178 Gao, F., Yan, X. X., Baettig, O. M., Berghuis, A. M. & Auclair, K. Regio- and chemoselective 6 '-N-derivatization of aminoglycosides: Bisubstrate inhibitors as probes to study aminoglycoside 6 '-N-acetyltransferases. *Angew. Chem. Int. Ed. Engl.* **44**, 6859-6862, doi:10.1002/anie.200501399 (2005).

179 Cliff, M. J., Williams, M. A., Brooke-Smith, J., Barford, D. & Ladbury, J. E. Molecular Recognition via Coupled Folding and Binding in a TPR Domain. *J. Mol. Biol.* **346**, 717-732 (2005).

180 Saxena, V. P. & D.B., W. New Basis for Interpreting Circular Dichroic Spectrao of Proteins. *Proc. Natl. Acad. Sci. U.S.A.* **68**, 969-972 (1971).

181 Uversky, V. N. Natively unfolded proteins: A point where biology waits for physics. *Protein Sci.* **11**, 739-756, doi:10.1110/ps.4210102 (2002).

182 Farrow, N. A., Zhang, O., Forman-Kay, J. D. & Kay, L. E. A heteronuclear correlation experiment for simultaneous determination of ^{15}N longitudinal decay and chemical exchange rates of systems in slow equilibrium. *J. Biomol. NMR* **4**, 727-734 (1994).

183 Farmer, B. T. Localizing the NADP(+) binding site on the MurB enzyme by NMR. *Nat. Struct. Biol.* **3**, 995-997 (1996).

184 Foote, J. & Milstein, C. Conformational isomerism and the diversity of antibodies. *Proceedings of the National Academy of Sciences of the United States of America* **91**, 10370-10374 (1994).

185 Tsai, C. J., Kumar, S., Ma, B. Y. & Nussinov, R. Folding funnels, binding funnels, and protein function. *Protein Science* **8**, 1181-1190 (1999).

186 Boehr, D. D., Nussinov, R. & Wright, P. E. The role of dynamic conformational ensembles in biomolecular recognition. *Nat. Chem. Biol.* **5**, 789-796, doi:10.1038/nchembio.232 (2009).

187 Bosshard, H. R. Molecular recognition by induced fit: How fit is the concept? *News in Physiological Sciences* **16**, 171-173 (2001).

188 Hammes, G. G., Chang, Y. C. & Oas, T. G. Conformational selection or induced fit: A flux description of reaction mechanism. *Proceedings of the National Academy of Sciences of the United States of America* **106**, 13737-13741, doi:10.1073/pnas.0907195106 (2009).

189 Amsler *et al.* 33. Monte Carlo Techniques. *Phys. Lett. B667* **1** (2008).

190 Goodsell, D. S. & Olson, A. J. Structural Symmetry and Protein Function. *Annual Review of Biophysics and Biomolecular Structure* **29**, 105-153, doi:doi:10.1146/annurev.biophys.29.1.105 (2000).

191 Keramisanou, D. *et al.* Disorder-order folding transitions underlie catalysis in the helicase motor of SecA. *Nature Structural & Molecular Biology* **13**, 594-602, doi:10.1038/nsmb1108 (2006).

192 Radley, T. L., Markowska, A. I., Bettinger, B. T., Ha, J. H. & Loh, S. N. Allosteric switching by mutually exclusive folding of protein domains. *Journal of Molecular Biology* **332**, 529-536, doi:10.1016/s0022-2836(03)00925-2 (2003).

193 Laine, O., Streaker, E. D., Nabavi, M., Fenselau, C. C. & Beckett, D. Allosteric signaling in the biotin repressor occurs via local folding coupled to global dampening of protein dynamics. *J. Mol. Biol.* **381**, 89-101, doi:10.1016/j.jmb.2008.05.018 (2008).

194 Ehlert, F. J. Estimation of the affinities of allosteric ligands using radioligand binding and pharmacological null methods. *Mol. Pharmacol.* **33**, 187-194 (1988).

195 Jana, S. & Deb, J. K. Molecular understanding of aminoglycoside action and resistance. *Applied Microbiology & Biotechnology* **70**, 140-150 (2006).

196 Loladze, V. V., Ermolenko, D. N. & Makhatadze, G. I. Heat capacity changes upon burial of polar and nonpolar groups in proteins. *Protein Science* **10**, 1343-1352 (2001).

197 Makhatadze, G. I., Clore, G. M. & Gronenborn, A. M. Solvent isotope effect and protein stability. *Nat Struct Mol Biol* **2**, 852-855 (1995).

198 Gao, F., Yan, X., Baettig, O. M., Berghuis, A. M. & Auclair, K. Regio- and Chemoselective 6′-N-Derivatization of Aminoglycosides: Bisubstrate Inhibitors as Probes To Study Aminoglycoside 6′-N-Acetyltransferases. *Angewandte Chemie International Edition* **44**, 6859-6862, doi:10.1002/anie.200501399 (2005).

199 Draker, K. A. & Wright, G. D. Molecular Mechanism of the Enterococcal Aminoglycoside 6'-N-Acetyltransferase': Role of GNAT-Conserved Residues in the Chemistry of Antibiotic Inactivation. *Biochemistry* **43**, 446-454 (2004).

200 Magalhaes, M. L. B. *et al.* Kinetic and Structural Analysis of Bisubstrate Inhibition of the Salmonella enterica Aminoglycoside 6'-N-Acetyltransferase. *Biochemistry* **47**, 579-584 (2008).

201 Vetting, M. W. *et al.* Mechanistic and Structural Analysis of Aminoglycoside N-Acetyltransferase AAC(6′)-Ib and Its Bifunctional, Fluoroquinolone-Active AAC(6′)-Ib-cr Variant†‡. *Biochemistry* **47**, 9825-9835, doi:10.1021/bi800664x (2008).

202 Marley, J., Lu, M. & Bracken, C. A method for efficient isotopic labeling of recombinant proteins. *Journal of Biomolecular NMR* **20**, 71-75 (2001).

203 Tellinghuisen, J. A study of statistical error in isothermal titration calorimetry. *Analytical Biochemistry* **321**, 79-88 (2003).

204 Freiburger, L. A., Auclair, K. & Mittermaier, A. K. Global analysis of variable temperature ITC data using a model-independent van ‘t Hoff constraint. *submitted* (2010).

205 Kay, L. E., Keifer, P. & Saarinen, T. Pure absorption gradient enhanced heteronuclear single quantum correlation spectroscopy with improved sensitivity. *J. Am. Chem. Soc.* **114**, 10663-10665 (1992).

206 Delaglio, F. *et al.* NMRPipe: a multidimensional spectral processing system based on UNIX pipes. *J. Biomol. NMR* **6**, 277-293 (1995).

Appendix

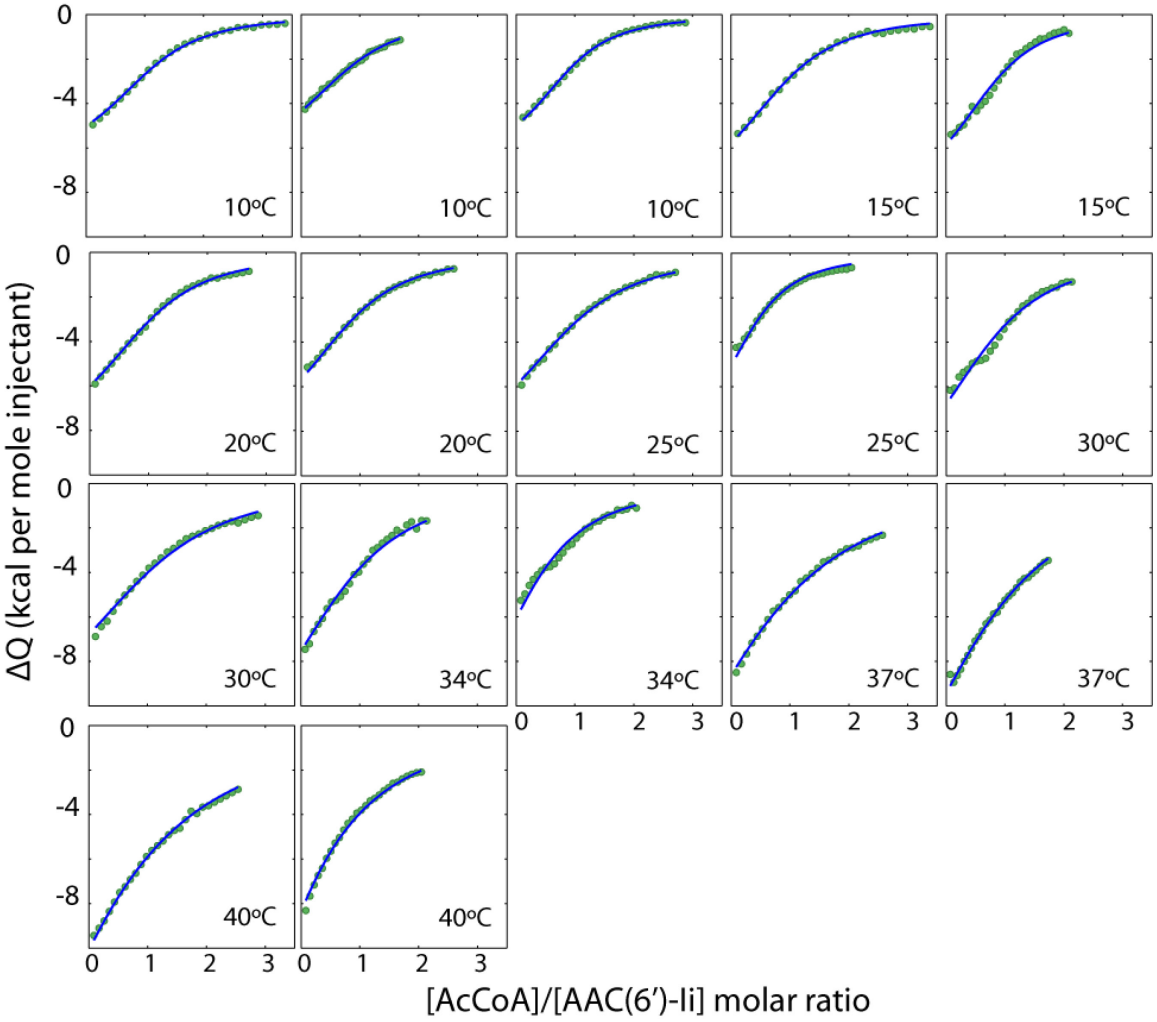

Figure A.1: Full variable temperature ITC dataset of AcCoA titrated into mutant AAC(6')-Ii W164A. Points correspond to experimental injection heats, while lines represent the best fit using a generalized global analysis.

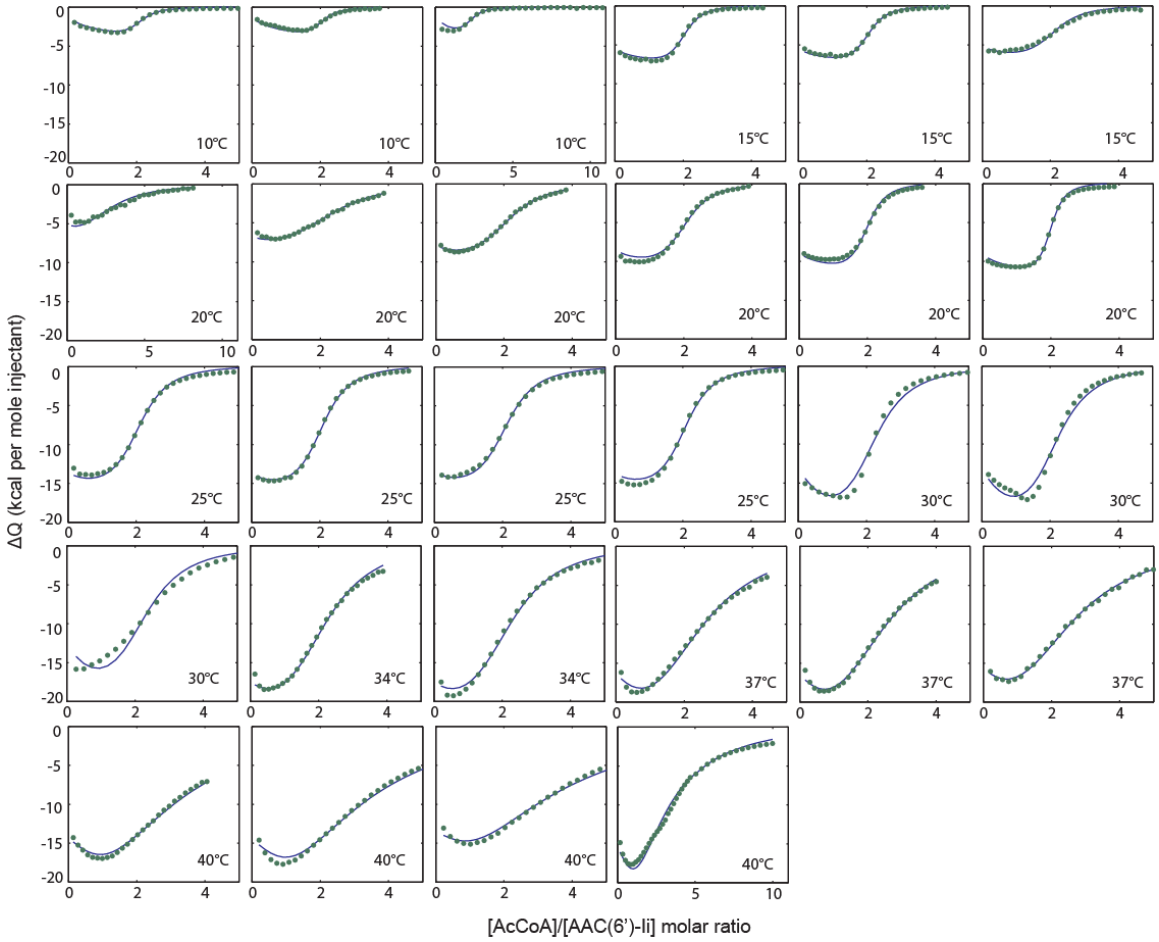

Figure A.2: Full variable temperature ITC dataset of AcCoA titrated into wild type AAC(6')-Ii. Points correspond to experimental injection heats, while lines represent the best fit using a generalized global analysis.

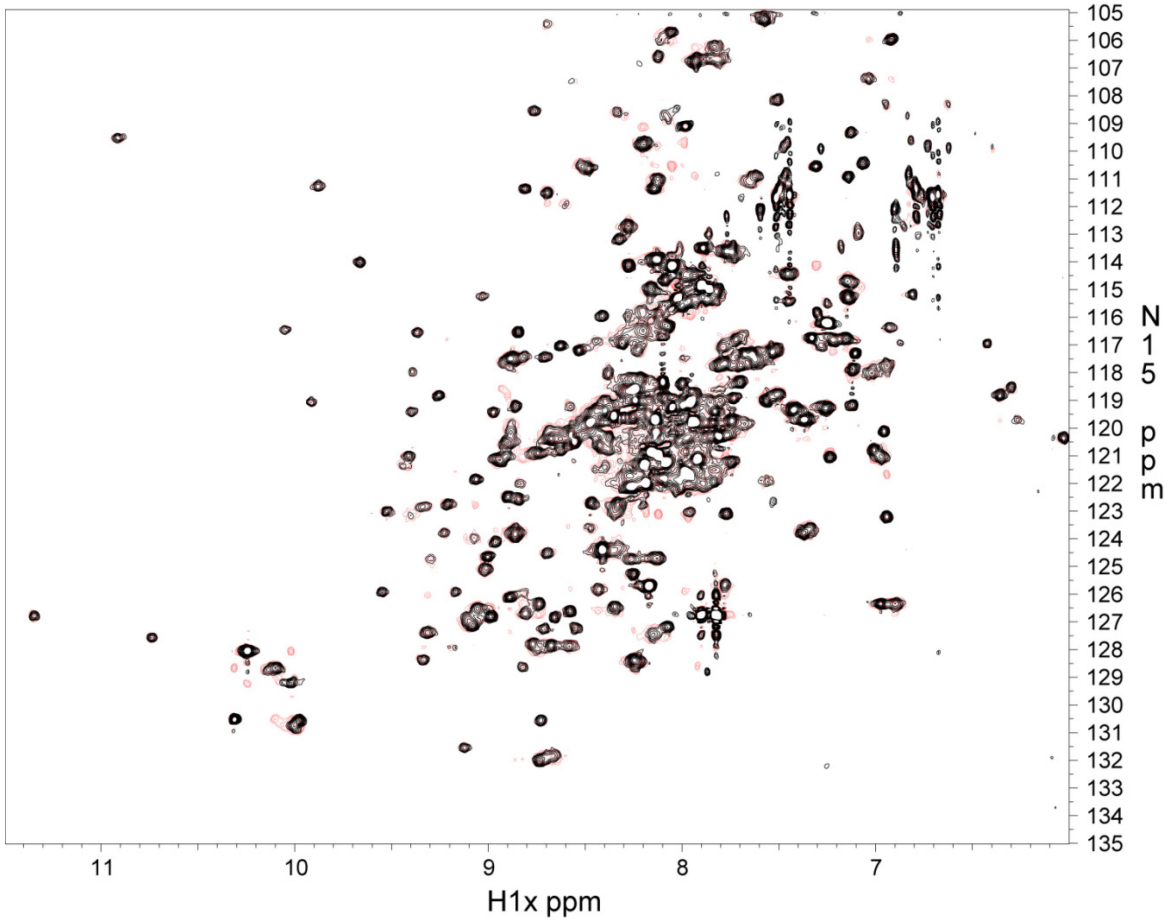

Figure A.3 EXSY spectra of AAC(6')-Ii partially bound to AcCoA in the presence of absence of a delay (black) and the presence of a 0.5 s (red) delay. Several red cross peaks can be observed between peaks corresponding to holo and apo states.

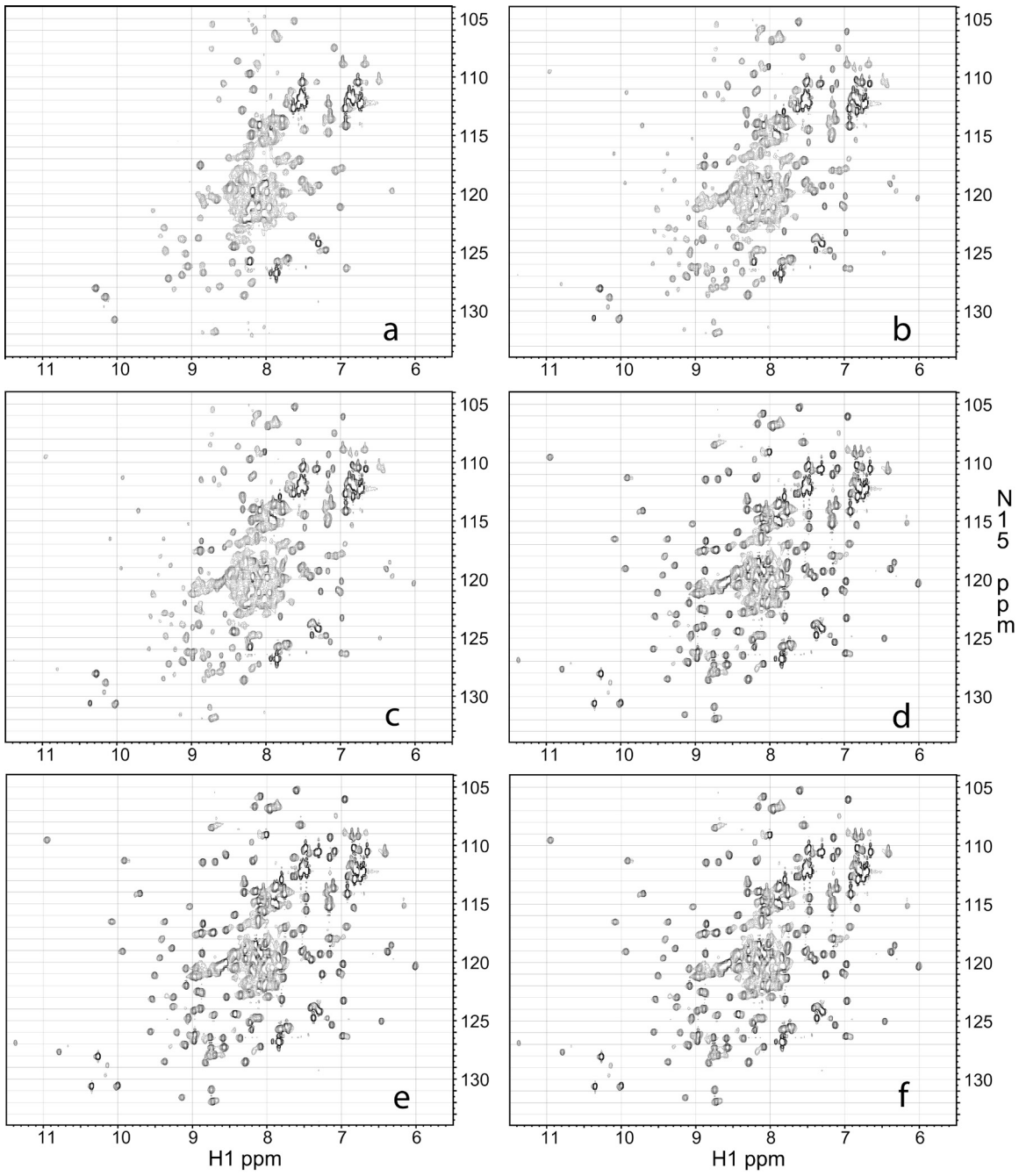

Figure A.4: Representative NMR titration data of AcCoA titration with AAC(6')-Ii at 37°C: $^{15}N/^{1}H$ HSQC spectra of AAC(6')-Ii samples containing **(a)** 0.0 **(b)** 0.1 **(c)** 0.3 **(d)** 0.6 **(e)** 1.1 **(f)** 1.7 mM AcCoA.

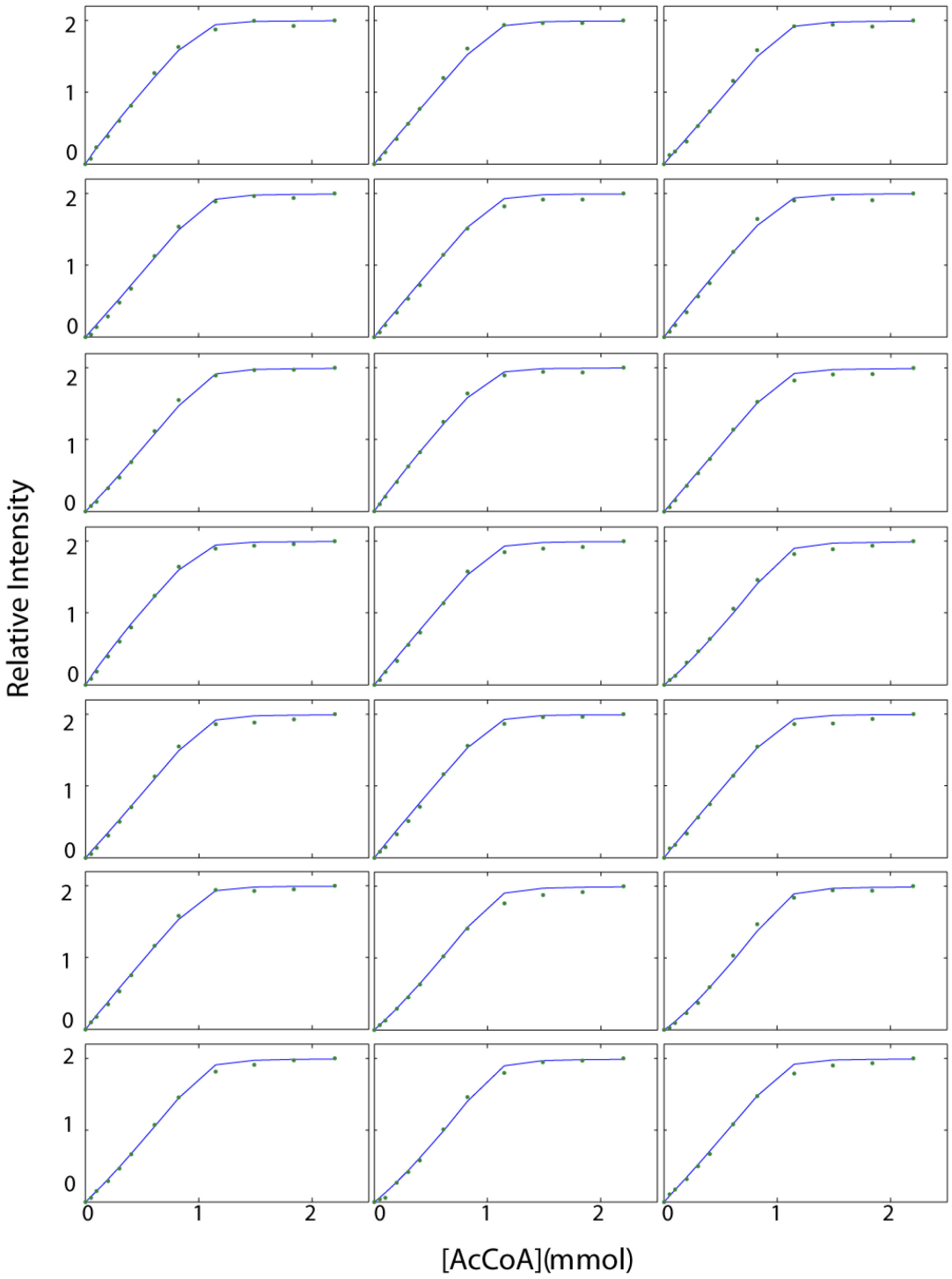

Figure A.5: Relative intensities of all well-resolved holo-peaks in $^{1}H/^{15}N$ NMR correlation spectra of AAC(6')-Ii determined as a function of AcCoA concentration. Lines correspond to the theoretical profiles with ITC-derived f_0, f_1, and f_2 series and individually-optimized values of I_1^{holo}, as described in the text

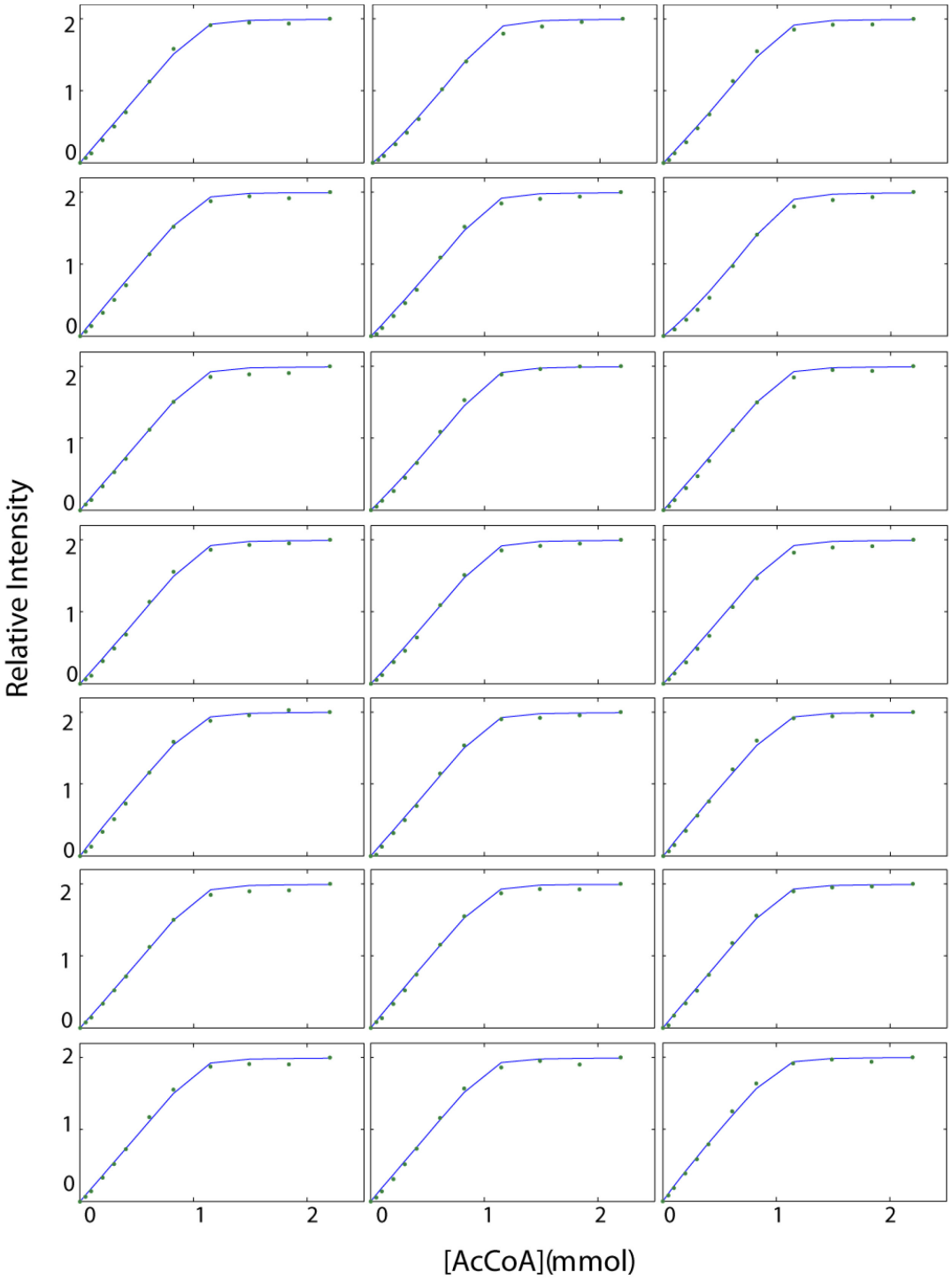

Figure A.6: Relative intensities of all well-resolved holo-peaks continued.

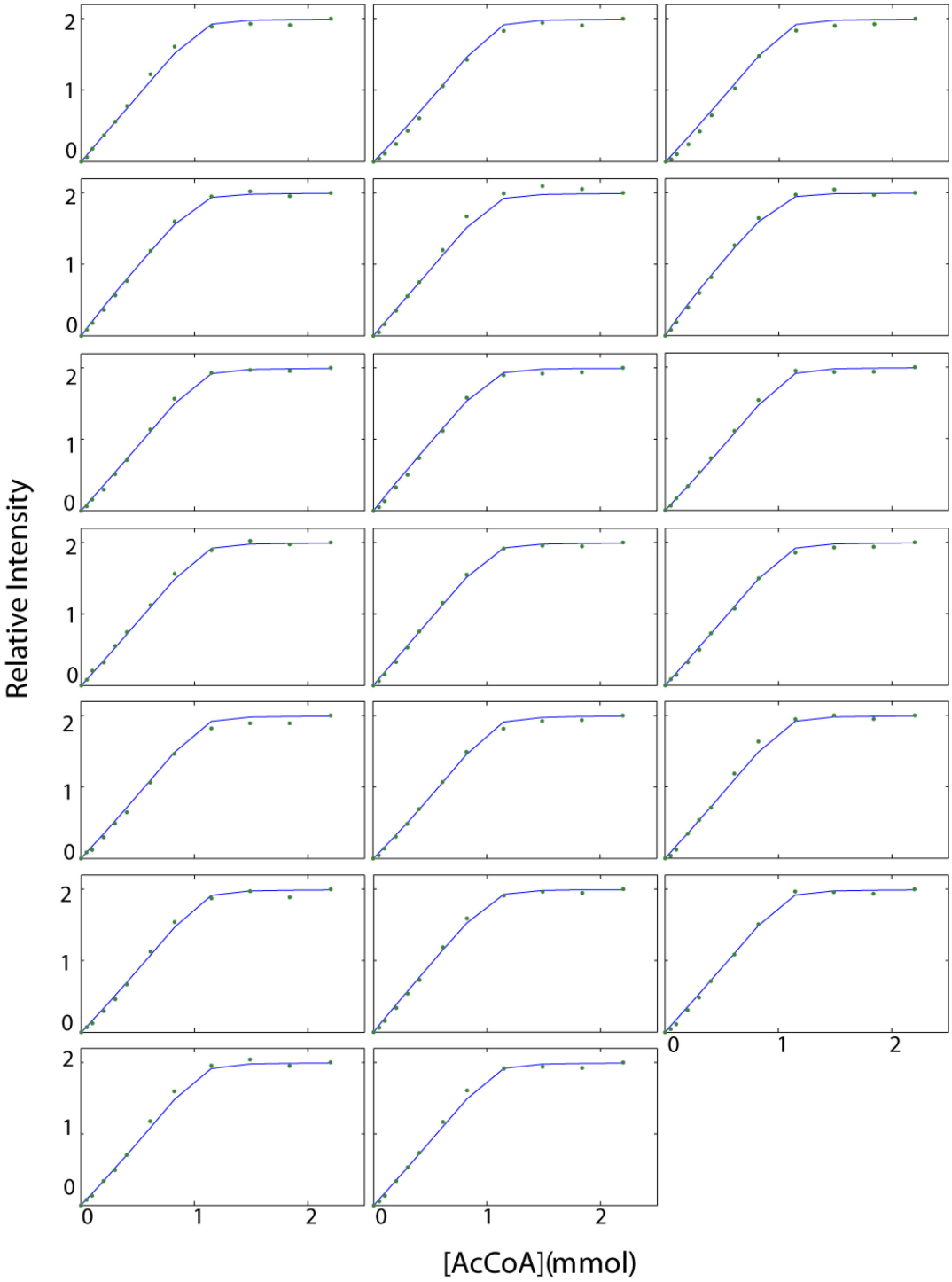

Figure A.7: Relative intensities of all well-resolved holo-peaks continued.

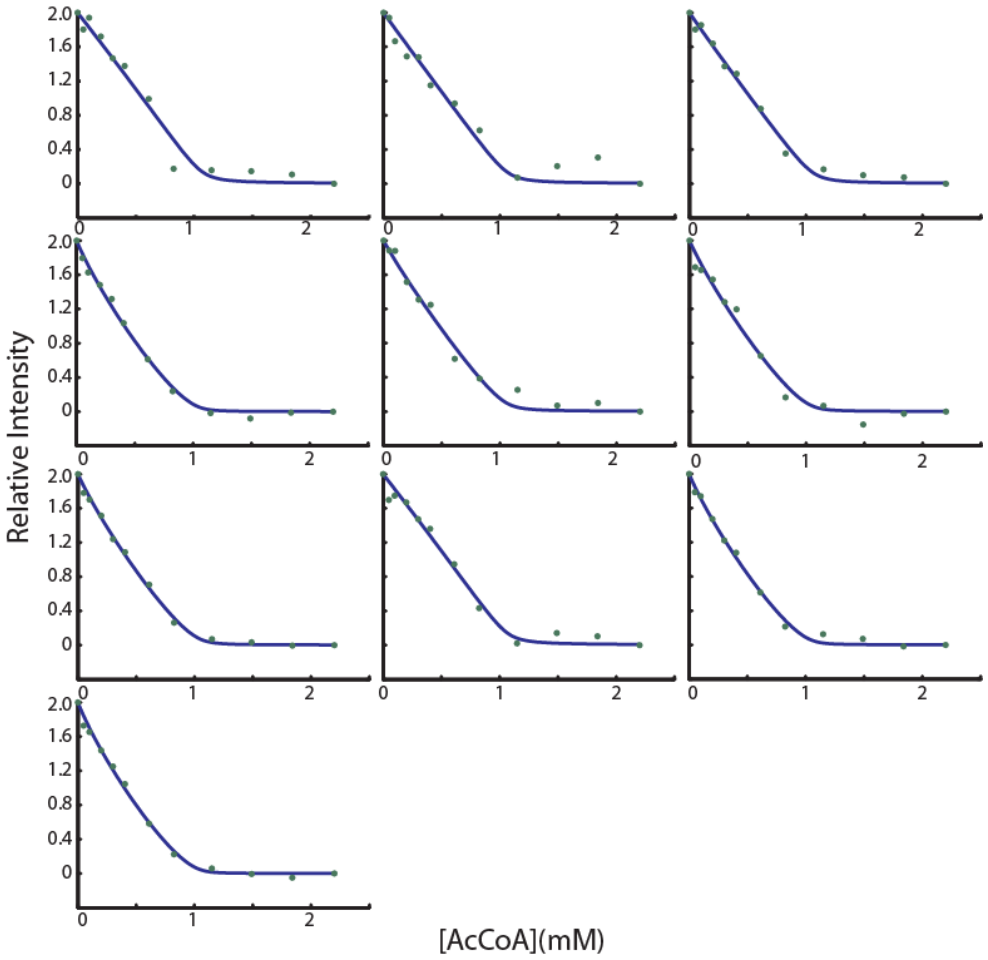

Figure A.8: Relative intensities of all well-resolved apo-peaks in $^{1}H/^{15}N$ NMR correlation spectra of AAC(6')-Ii determined as a function of AcCoA concentration. Lines correspond to the theoretical profiles with ITC-derived f_0, f_1, and f_2 series and individually-optimized values of I_1^{apo}, as described in the text.

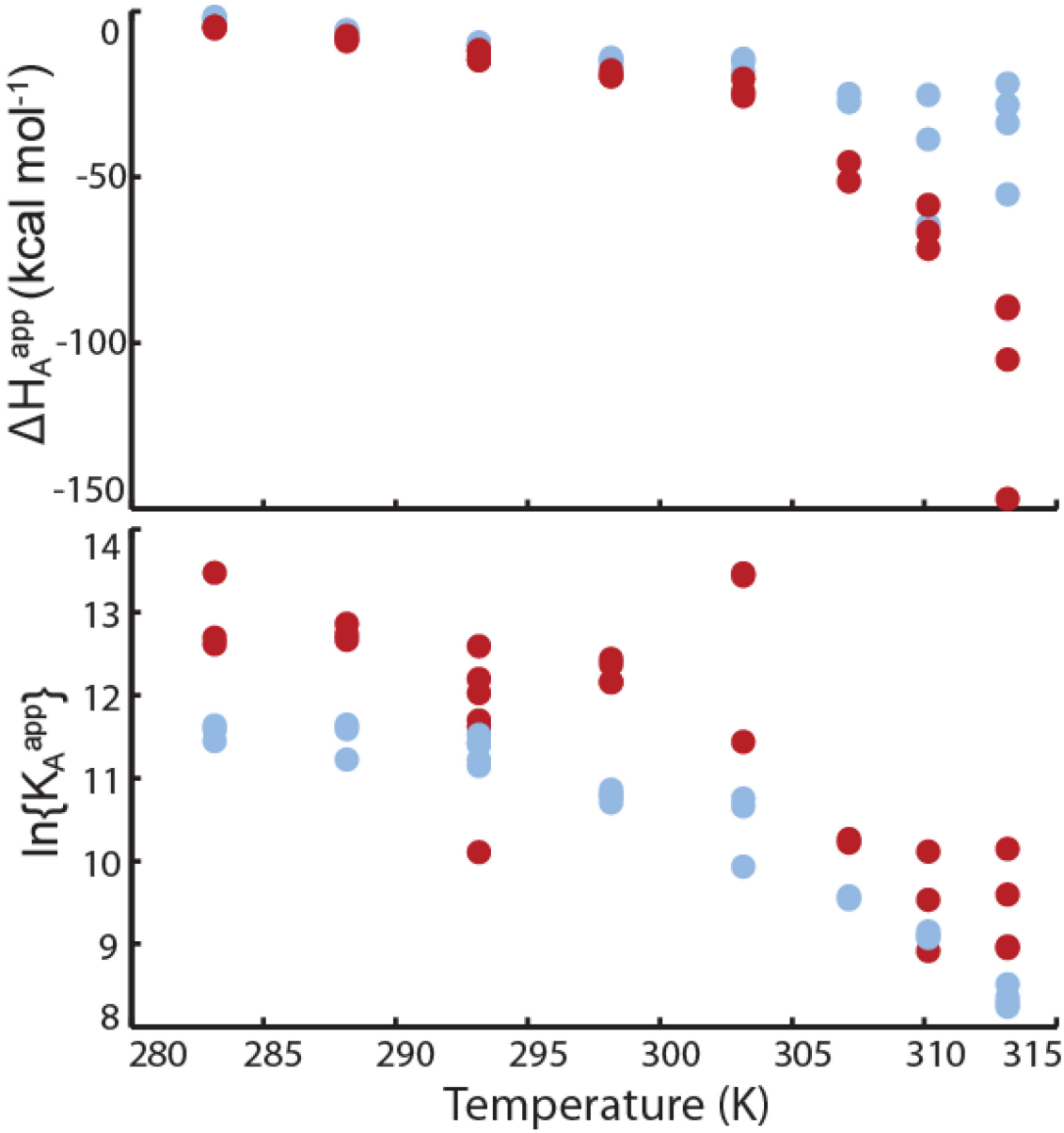

Figure A.9: Values of ΔH_A^{app} and K_A^{app} determined from independent (non-global) fits of individual ITC isotherms for binding of the first (light blue) and second (dark red) molecules of AcCoA to AAC(6')-Ii.

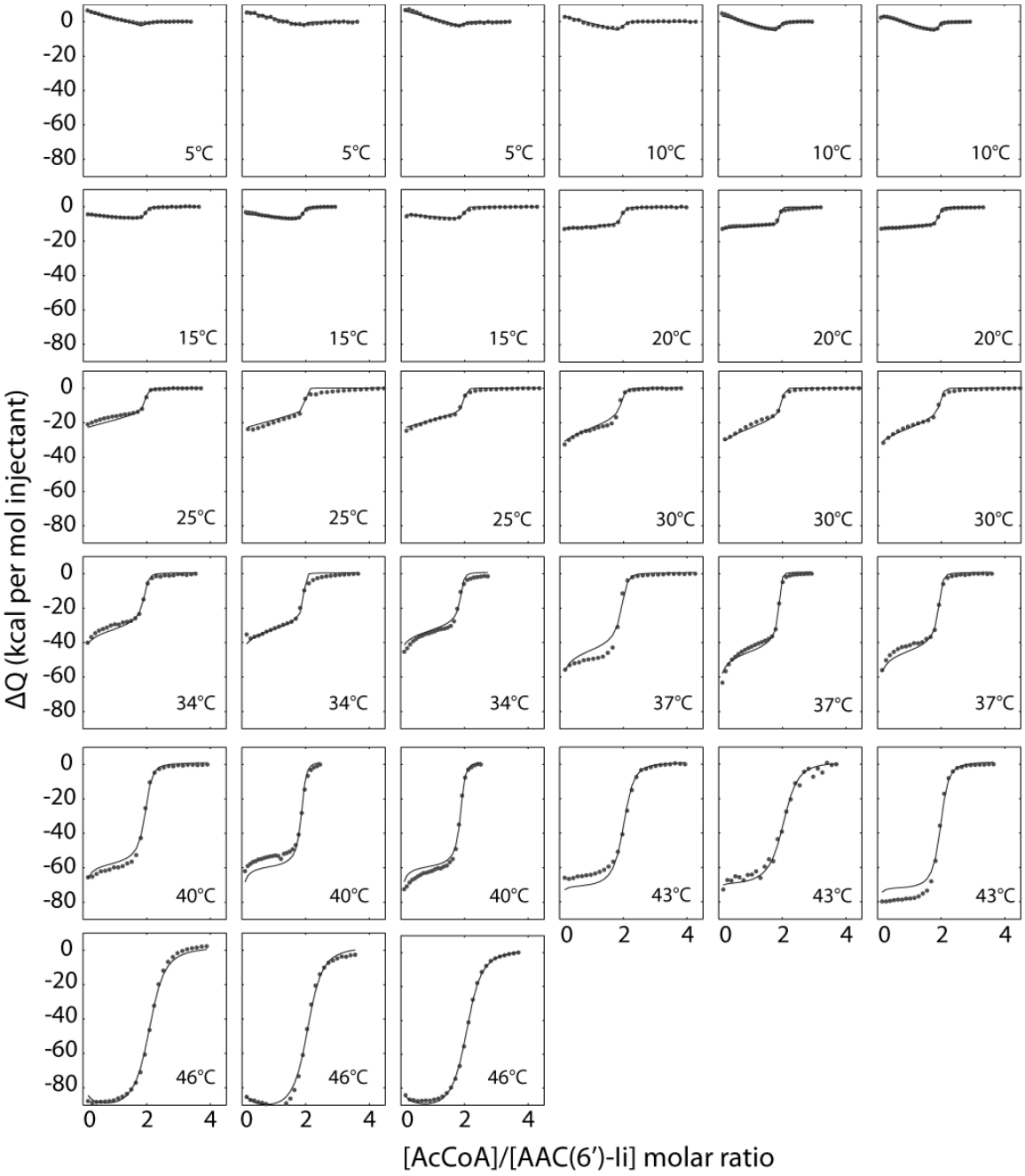

Figure A.10: Full variable temperature ITC dataset of paromomycin titrated into wild type AAC(6')-Ii. Points correspond to experimental injection heats, while lines represent the best fit using a generalized global analysis.

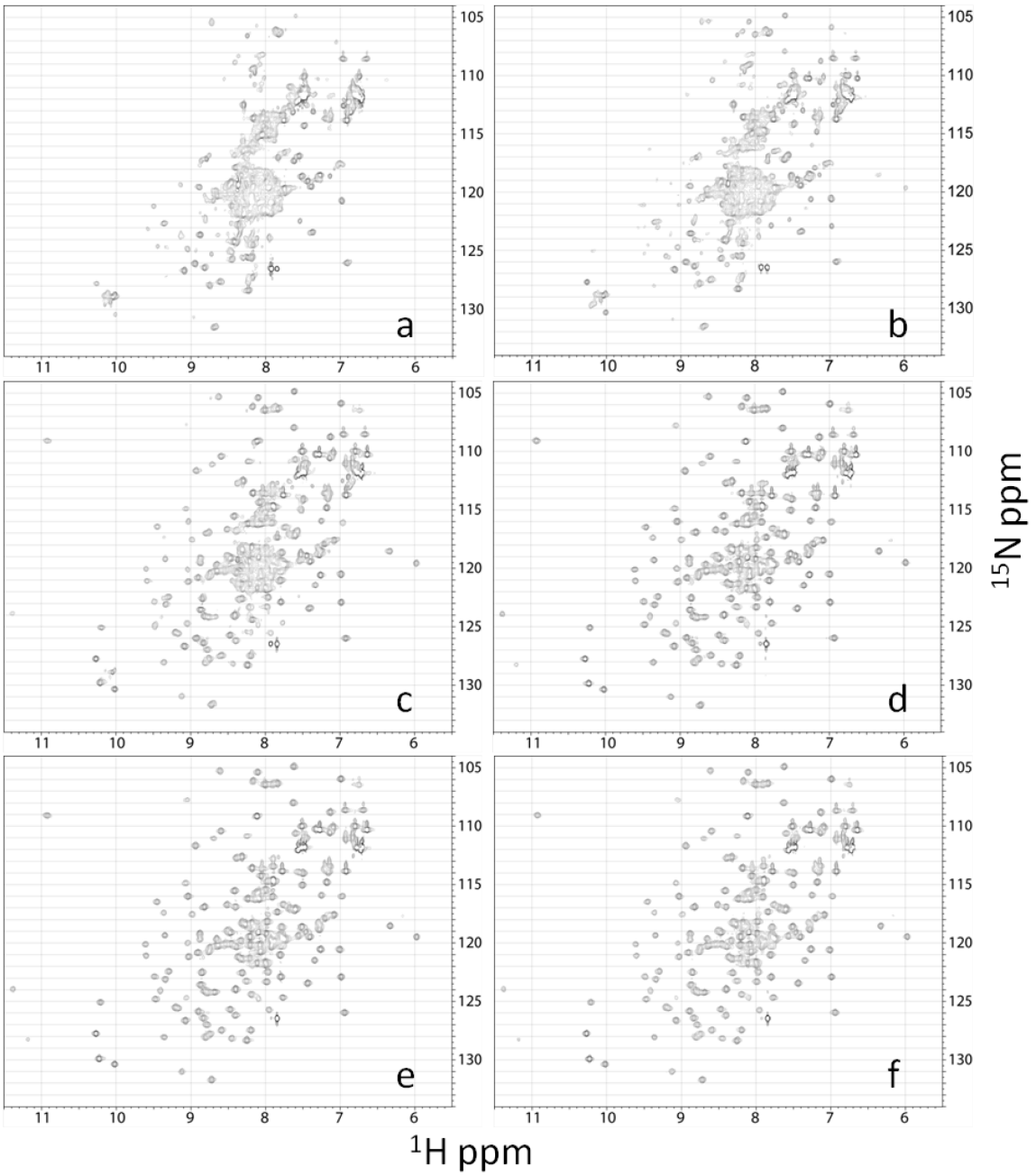

Figure A.11: Representative NMR titration data of AcCoA titration with paromomycin(6')-Ii at 37°C: ^{15}N/^{1}H HSQC spectra of AAC(6')-Ii samples containing **(a)** 0.0 **(b)** 0.1 **(c)** 0.3 **(d)** 0.6 **(e)** 1.25 **(f)** 2 mM paromomycin.

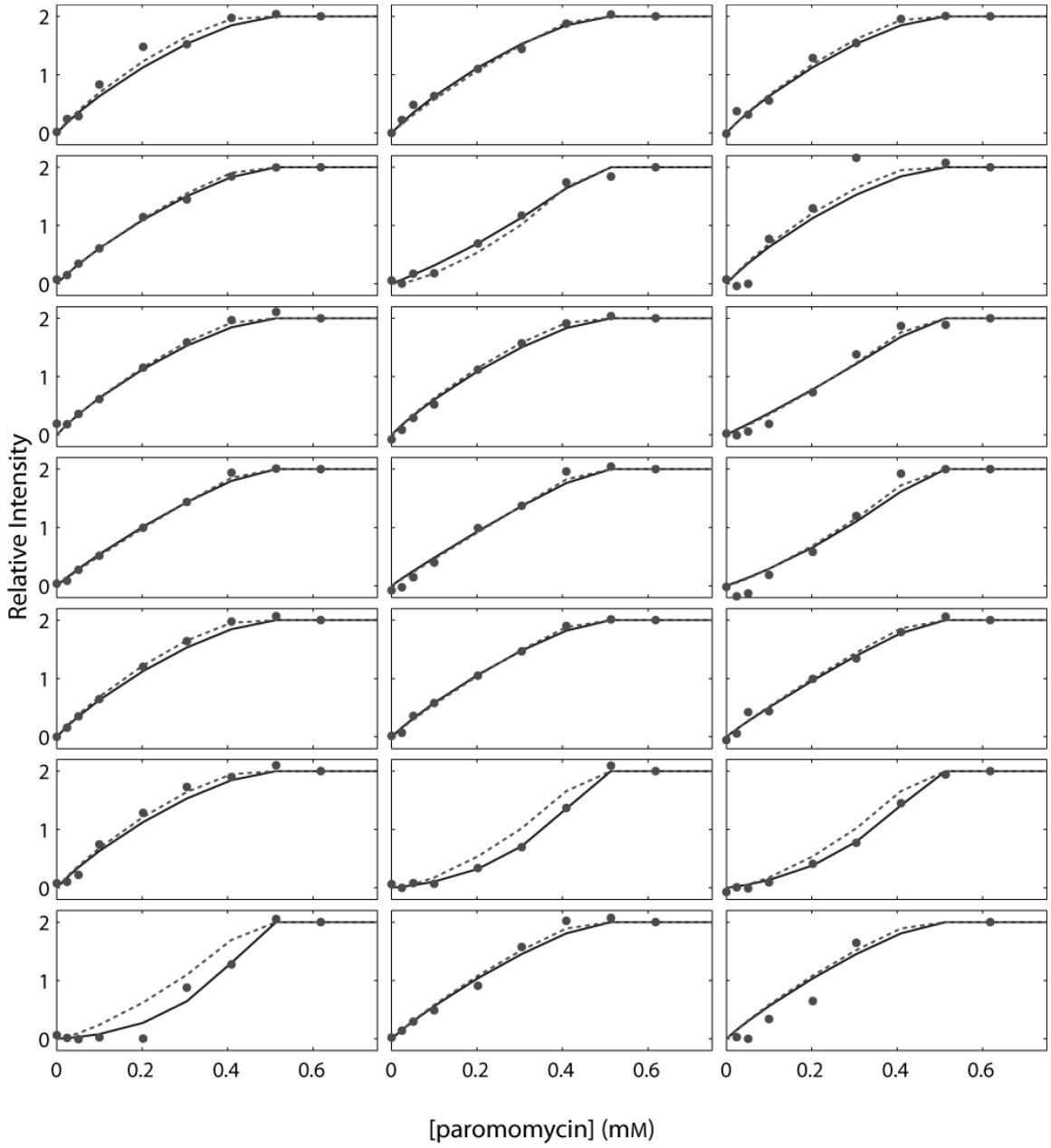

Figure A.12: Relative intensities of all well-resolved peaks for paromomycin titration in $^{1}H/^{15}N$ NMR correlation spectra of AAC(6')-Ii determined as a function of paromomycin concentration. Experimental data (dots) where fit to a slow exchange (dashed line) and fast exchange (solid line) model. The theoretical profiles with ITC-derived f_0, f_1, and f_2 series and individually-optimized values of I_1^{unprod}, as described in the text

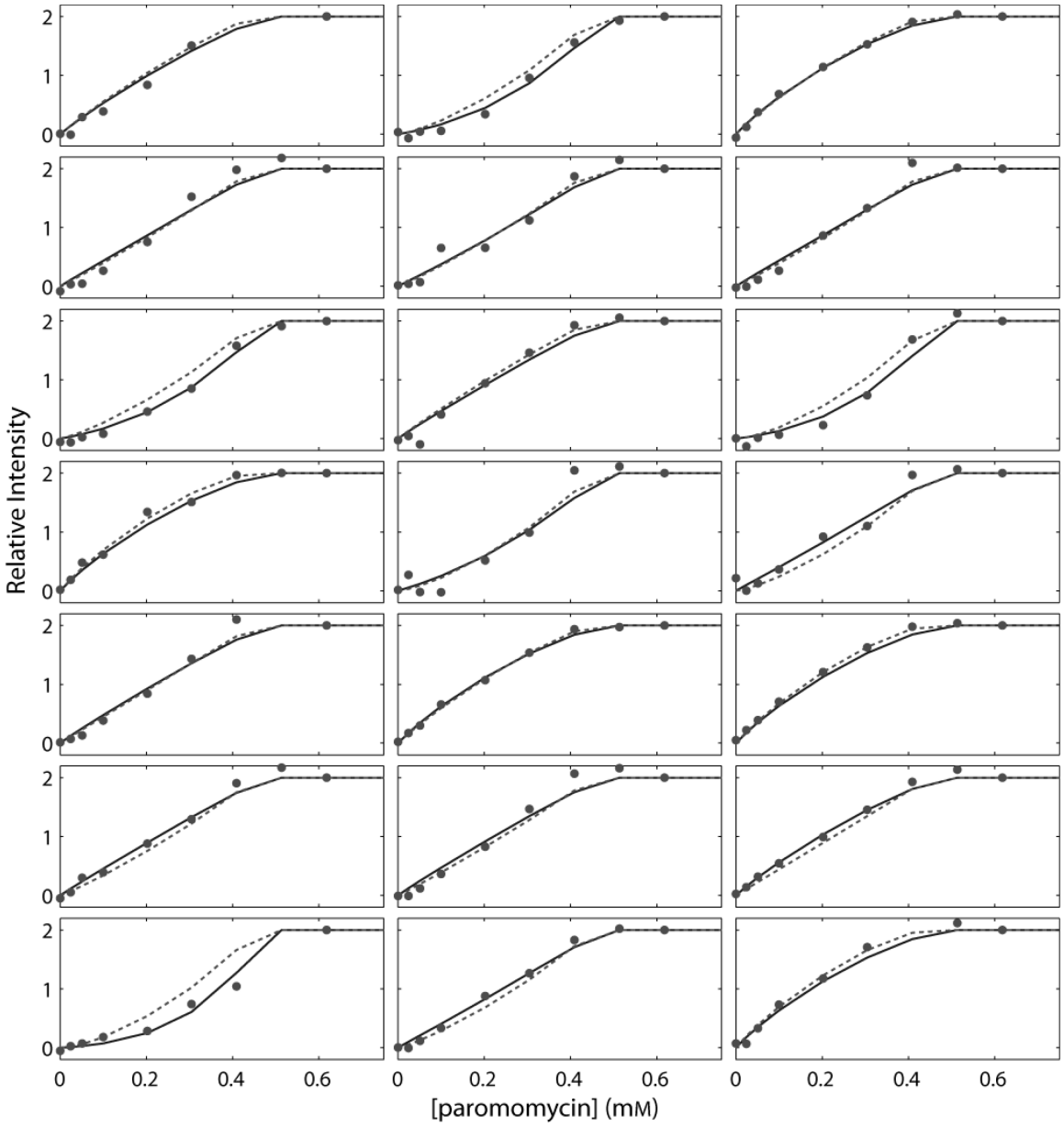

Figure A.13: Relative intensities of all well-resolved peaks for paromomycin titration continued

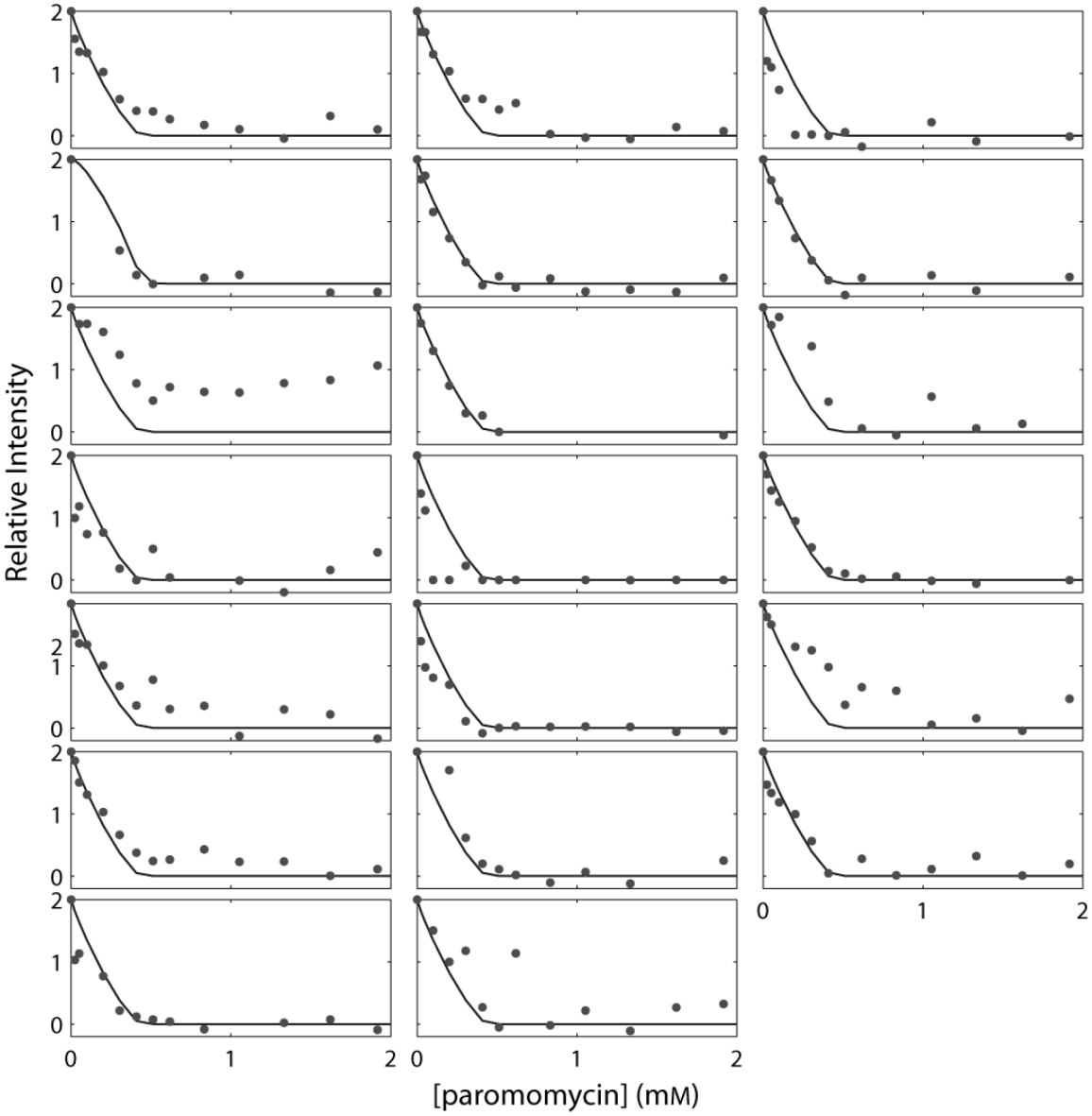

Figure A.14: Relative intensities of all well-resolved apo-peaks for paromomycin titration in $^{1}H/^{15}N$ NMR correlation spectra of AAC(6')-Ii determined as a function of paromomycin concentration. Lines correspond to the theoretical profiles with ITC-derived f_0, f_1, and f_2 series and individually-optimized values of I_1^{apo}, as described in the text.